

Physiologically based in silico modelling to examine DNA adduct formation by different food-borne α,β -unsaturated aldehydes at realistic low dietary exposure levels

Reiko Kiwamoto

Thesis committee

Promotor

Prof. Dr. I.M.C.M. Rietjens
Professor of Toxicology
Wageningen University

Co-promotor

Dr. A. Punt
Assistant Professor, Division of Toxicology
Wageningen University

Other members

Dr. J. van Benthem, National Institute of Public Health and the Environment (RIVM)
Prof. Dr. W.J.H. van Berkel, Wageningen University
Prof. Dr. B. Blaauboer, Utrecht University
Dr. S. Bosgra, TNO

This research was conducted under the auspices of the Graduate School VLAG (Advanced studies in Food Technology, Agrobiotechnology, Nutrition and Health Sciences).

Physiologically based in silico modelling to examine DNA
adduct formation by different food-borne α,β -unsaturated
aldehydes at realistic low dietary exposure levels

Reiko Kiwamoto

Thesis

submitted in fulfilment of the requirements for the degree of doctor
at Wageningen University

by the authority of the Rector Magnificus

Prof. Dr. M.J. Kropff.

in the presence of the

Thesis Committee appointed by the Academic Board

to be defended in public

on Wednesday 13 May 2015

at 11 a.m. in the Aula.

Reiko Kiwamoto

Physiologically based in silico modelling to examine DNA adduct formation by different food-borne α,β -unsaturated aldehydes at realistic low dietary exposure levels.

PhD thesis, Wageningen University, Wageningen, NL (2015)

With references, with summaries in Dutch and English

ISBN 978-94-6257-284-3

TABLE OF CONTENTS

Chapter 1	General introduction	7
Chapter 2	A physiologically based in silico model for <i>trans</i> -2-hexenal detoxification and DNA adduct formation in rat	31
Chapter 3	A physiologically based in silico model for <i>trans</i> -2-hexenal detoxification and DNA adduct formation in human including interindividual variation indicates efficient detoxification and a negligible genotoxicity risk	65
Chapter 4	An integrated QSAR-PBK/D modelling approach for predicting detoxification and DNA adduct formation of 18 acyclic food-borne α,β -unsaturated aldehydes	93
Chapter 5	Dose-dependent DNA adduct formation by cinnamaldehyde and other food-borne α,β -unsaturated aldehydes predicted by physiologically based in silico modelling	125
Chapter 6	General discussion and future perspectives	159
Chapter 7	Summary (English)	183
Appendices	Abbreviations	190
	Samenvatting	191
	Acknowledgement	194
	Carriculum vitae	197
	List of publications	198
	Overview of completed training activities	199



CHAPTER 1

General Introduction

1.1 Background

α,β -Unsaturated aldehydes are ubiquitously present in our surroundings, and human exposure occurs from endogenous sources as well as from exogenous sources including the diet. Various aldehydes are present in fruits, vegetables and beverages as natural constituents [1], and many of them are intentionally added as food flavouring agents because of their aromatic features. The structure of α,β -unsaturated aldehydes is characterized by the presence of a polarized carbon-oxygen double bond, and a double bond between carbons 2 and 3 (α and β) (Figure 1.1). Due to the electrophilic nature of the α,β -unsaturated aldehyde moiety, α,β -unsaturated aldehydes readily react with DNA via Michael addition [2]. This reactive nature of α,β -unsaturated aldehydes raises a food safety concern for genotoxicity. α,β -Unsaturated aldehydes have been shown to be positive in in vitro genotoxicity tests using bacteria or mammalian cell lines [3-5]. In vivo, DNA adduct formation in the liver has been detected when rats were orally exposed to high doses of *trans*-2-hexenal for a single time but not at doses lower than 50 mg/kg bw [6, 7]. Considering that DNA adduct formation was observed only at exposure levels that were four orders of magnitude higher than the estimated daily intake (EDI) of *trans*-2-hexenal when used as an added flavouring (1 $\mu\text{g}/\text{kg}$ bw/day), the relevance of DNA adduct formation observed in the rodent studies at high dose levels for the human situation remains to be established.

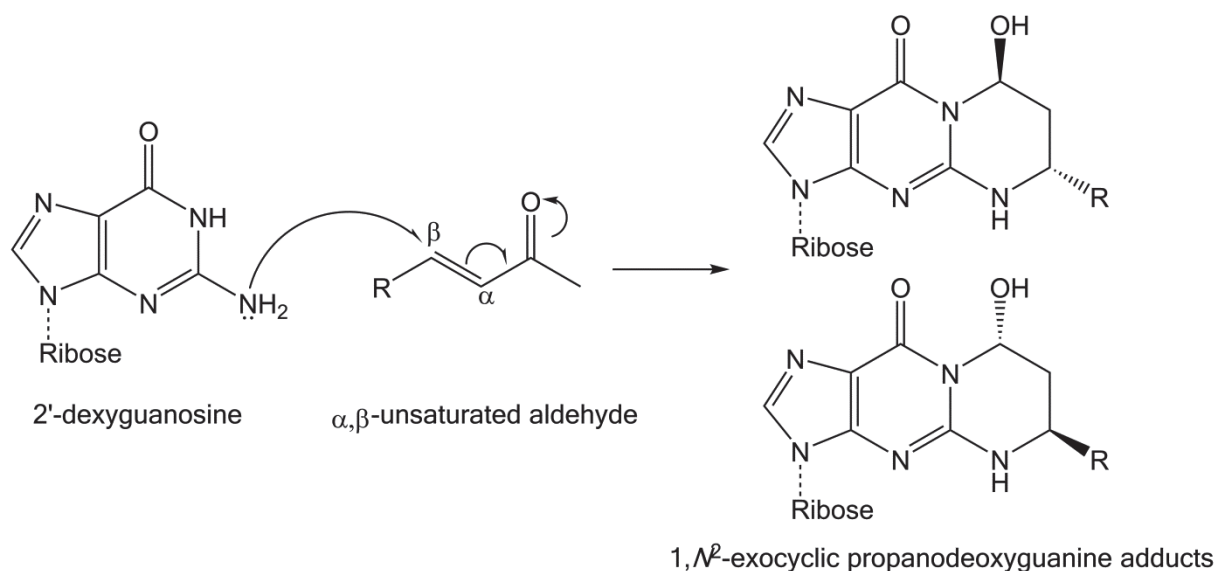


Figure 1.1 Michael addition of guanine to an α,β -unsaturated aldehyde [8]

The JECFA (Joint FAO/WHO Expert Committee on Food Additives) [9-11] and the Expert Panel of the FEMA (Flavor and Extract Manufacturers Association) [12, 13] considered that the use of α,β -unsaturated aldehydes as flavouring agents does not pose a significant risk because of low levels of use as added flavouring agents and possible rapid detoxification in vivo. For these reasons the FEMA Exert Panel affirmed that the α,β -unsaturated aldehydes are GRAS

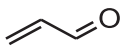
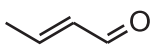
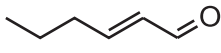
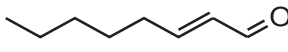
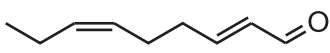
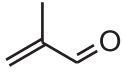
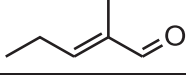
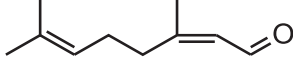
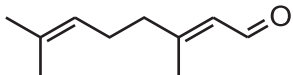
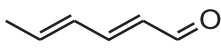
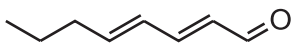
(Generally Recognized as Safe). In contrast, EFSA (European Food Safety Authority) considered the α,β -unsaturated aldehyde moiety to be an alert for genotoxicity and the safety cannot be established unless in vivo data become available to overrule concerns raised by positive in vitro genotoxicity data [14]. As a result the use of more than 70 α,β -unsaturated aldehydes and related compounds that are metabolized to α,β -unsaturated aldehyde as food flavouring agents is suspended in the EU since 2013. Data on their genotoxicity, especially in vivo, have been requested by EFSA. It can be questioned, however, whether low exposure levels, as a result of their use as flavourings, would lead to a safety concern. A significant adverse effect may not occur at low doses due to protection mechanisms such as detoxification of the genotoxic substance in vivo. For the safety evaluation of the α,β -unsaturated aldehydes insight in genotoxicity at low dietary doses needs to be obtained taking dose-dependent detoxification into account. However, measuring such adverse effects in vivo at low dose levels for large amount of compounds is practically not feasible. Therefore the objective of the research described in this PhD thesis was to quantitatively integrate detoxification kinetics, and define dose-dependent in vivo DNA adduct formation for a group of structurally related α,β -unsaturated aldehydes used as food flavourings by developing physiologically based in silico models. This should provide insight in the DNA adduct formation at low exposure levels relevant to realistic human dietary exposure, and generate data on in vivo DNA adduct formation that cannot be obtained by animal experiments.

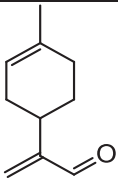
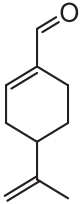
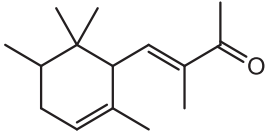
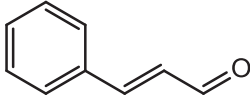
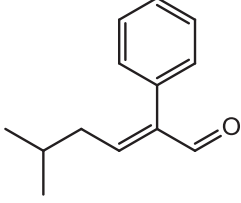
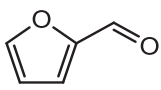
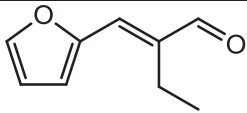
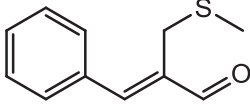
1.2 Structures of α,β -unsaturated aldehydes and exposure

Many α,β -unsaturated aldehydes are produced by plants as natural fungicides. For this reason these aldehydes are present in many foods and beverages of plant origin as natural constituents [1]. α,β -Unsaturated aldehydes are often volatile and give distinguished odours resembling different fruits, vegetables and herbs. For instance, *trans*-2-hexenal gives a fresh apple-like smell and is called “leaf aldehyde” (see Table 1.1 for the structure). *trans*-2-*cis*-6-Nonadienal gives a cucumber-like smell and *trans*-2-decenal gives an odour that is characteristic of coriander. Cinnamaldehyde gives the unique odor of cinnamon. Due to their aromatic features, many α,β -unsaturated aldehydes are intentionally added to a broad type of foods as flavouring agents. Some examples of α,β -unsaturated aldehydes that may be used as food flavouring agents are presented in Table 1.1. The examples are listed in accordance with the classification made by EFSA based on the structural similarity [14]. The highest dietary α,β -unsaturated aldehyde intake is reported to result from cinnamaldehyde: 59,000 $\mu\text{g/day/capita}$ in the US and 2,500 $\mu\text{g/day/capita}$ in Europe [9]. Among the aliphatic substances, the majority of the production has been attributed to 2-hexenal and its corresponding alcohol and acetate ester [10]. The estimated daily intakes of 2-hexenal as an added flavouring agent in Europe and the US are 791 and 409 $\mu\text{g/day/capita}$, respectively [9].

Exposure to α,β -unsaturated aldehydes also comes from other sources than the diet. 2-Propenal (acrolein) and 2-butenal (crotonaldehyde) for example are produced during combustion of organic materials and therefore found in all types of smoke including cigarette smoke and exhaust from engines [2, 10]. 2-Propenal is present at 25 – 140 $\mu\text{g}/\text{cigarette}$ in the gas phase of the smoke [2]. α,β -Unsaturated aldehydes are furthermore formed endogenously by lipid peroxidation of polyunsaturated fatty acids (PUFAs) [2, 15]. Lipid peroxidation, initiated by a free-radical chain reaction mechanism, yields lipid hydroperoxides as major initial reaction products. Subsequent decomposition of lipid hydroperoxides generates a number of degradation products including 2-propenal, 4-hydroxy-2-alkenals, and malondialdehyde [16].

Table 1.1 Examples of food-borne α,β -unsaturated aldehydes listed in accordance with the categories made by EFSA based on the structural similarity [14]

Description of the category		Name	Structure	Sources
Aliphatic	With or without additional non-conjugated double-bonds	2-propenal (acrolein)		red wine [1], tobacco smoke [2]
		2-butenal (crotonaldehyde)		red wine [1], tobacco smoke [2]
		<i>trans</i> -2-hexenal		banana [1], fig [17]
		<i>trans</i> -2-octenal		grape, orange [1]
		<i>trans</i> -2- <i>cis</i> -6-nonadienal		cucumber [18]
	2-alkylated aldehydes with or without additional double bonds	2-methylcrotonaldehyde		
		<i>trans</i> -2-methyl-2-pentenal		black tea [19]
	3-alkylated aldehydes with or without additional double bonds	citral (mixture of neral and geranial)		lime [1]
				
	Two or more conjugated double-bonds with or without additional non-conjugated double-bonds	<i>trans</i> -2- <i>trans</i> -4-hexadienal		fig [17], blueberry [20]
<i>trans</i> -2- <i>trans</i> -4-octadienal				

Alicyclic	α,β -unsaturation in side chain	p-mentha-1,8(10)-dien-9-al		
	α,β -unsaturation in ring/side chain	p-mentha-1,8-dien-7-al		
	more complex	2,6,6-trimethylcyclohexa-1,3-diene-1-carbaldehyde		
Cinnamyl derivatives and other aromatic alkyl substituted aldehydes	Cinnamyl aldehyde	<i>trans</i> -cinnamaldehyde		cassia (bark oil) [1]
	2-phenyl-2-alkenals	5-methyl-2-phenylhex-2-enal		
Heterocyclic	Furfural derivatives	Furfural		cacao, coffee, meat products [21]
	Furans with conjugation in side chain	Furfurylidene-2-butanal		
Others	Other sulphur containing substances	2-(Methylthiomethyl)-3-phenylpropenal		

1.3 ADME (absorption, distribution, metabolism and excretion)

α,β -Unsaturated aldehydes are rapidly absorbed, distributed, metabolized and excreted in urine, faeces and expired air. When male Wistar rats were exposed to 100 mg/kg bw of ^{14}C labelled *trans*-2-nonenal or *trans*-2-pentenal by gavage [22], both aldehydes entered the systemic circulation from the gastrointestinal (GI) tract, and were metabolized to yield C-3 mercapturic acids within 24 hours. Only trace amount of *trans*-2-nonenal or *trans*-2-pentenal were found in faeces [22]. In another study, male and female Sprague-Dawley rats were exposed to 2.5 or 15 mg/kg bw ^{14}C labelled 2-propenal by gavage [23]. Urine was the major excretion route

(40.6-63.4%) in all groups. Excretion in faeces increased from 14.8% to 28.4% in male and from 12.8% to 30.6% in female rats when the dose levels increased from 2.5 to 15 mg/kg bw, suggesting that at the higher dose level a higher proportion of 2-propenal reacted with food components already in the GI tract, ending up in faeces. More than 80% of 2-propenal was excreted via urine, faeces or expired air within 24 hours at both exposure doses. Sapienza et al. administered 5, 50 or 500 mg/kg bw ^{14}C -labelled cinnamaldehyde to male F344 rats by gavage [24]. More than 81% of the cinnamaldehyde was excreted in urine and 3.2-5.1% was excreted in faeces within 24 hours in all animal groups. In another study, male Fischer 344 (F344) rats were exposed to 5, 50 and 500 mg/kg bw of [^{14}C] citral via oral administration [25]. In all exposure groups, the majority of citral (76.7-93.7%) was excreted within 24 hours in the urine (47.9-63.4%), faeces (12.0-15.6%) or as CO_2 (10.4-16.6%). Altogether these in vivo studies indicate that α,β -unsaturated aldehydes are swiftly absorbed and excreted within 24 hours and that the principle route of excretion is via urine. The studies also indicate that the administered aldehydes may react with food residues in the GI tract resulting in excretion via faeces and a reduction in bioavailability.

As Figure 1.2 illustrates, α,β -unsaturated aldehydes are detoxified via three pathways: oxidation, conjugation with glutathione (GSH), and reduction.

Oxidation

α,β -Unsaturated aldehydes are oxidized by NAD^+ -dependent aldehyde dehydrogenases (ALDHs) to α,β -unsaturated carboxylic acids. In humans, ALDHs are present throughout the body including liver, lungs, kidneys, GI tract, heart, and in the brain [26]. Sixteen ALDH genes and three pseudogenes have been identified in the human genome [27], and this diversity enables oxidation of a wide variety of substrates with varying specificity of the aldehydes towards each ALDH isoenzyme [28]. Among the isoenzymes, ALDH I and ALDH II, which are mostly present in cytosol and mitochondrial matrix respectively, play a predominant role in the metabolism of linear aldehydes in the digestive tract [26, 29, 30]. The α,β -unsaturated carboxylic acids formed are further metabolized via β oxidation and the tricarboxylic acid (TCA) cycle to acetyl-CoA or propionyl-CoA, and are eventually excreted from the body as CO_2 or water [12].

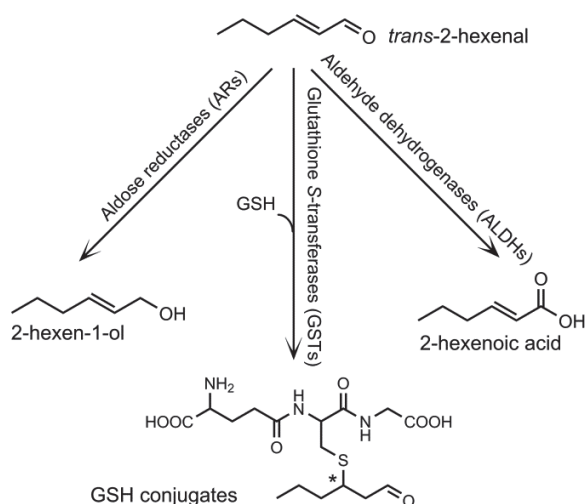


Figure 1.2 Metabolism of α,β -unsaturated aldehydes taking *trans*-2-hexenal as an example.

Conjugation with GSH

α,β -Unsaturated aldehydes react with GSH to form GSH conjugates via Michael addition. The carbon double bond between the α and β carbons connected to an electron-withdrawing aldehyde group results in a positively polarized β -carbon, which becomes a preferred site for an attack by soft nucleophiles such as GSH [31]. The reaction occurs spontaneously, but the reaction rate increases remarkably in the presence of a family of phase II enzymes, glutathione S-transferases (GSTs) [4]. GSTs are present in mitochondria and microsomes, but cytosolic GSTs represent the largest family of this group of enzymes [32]. Among different isoenzymes GST A4-4, a cytosolic GST, is recognized as one of the predominant enzymes responsible for the metabolism of 2-alkenals [33, 34]. The presence of GSH in cells is a prerequisite for the reaction, and depletion of GSH at high exposure levels hampers this pathway regardless of the GST kinetics. Following the conjugation with GSH, the aldehyde functional group is oxidized or reduced, and the metabolites are ultimately excreted in urine as corresponding mercapturic acids [35-37].

Reduction

The reduction of α,β -unsaturated aldehydes to α,β -unsaturated alcohols is catalysed by aldose reductases (ARs) such as AKR1B1, or closely related aldo-keto reductases such as AKR1B10 and AKR1C1 [38-40]. These enzymes are present in a variety of human tissues (e.g. intestine, liver, heart, kidney) and have broadly overlapping substrate specificity. The enzymes play an important role not only in the detoxification of exogenous compounds but also in cytokine-mediating signalling processes. For the latter reason many literature studies have focused on the features of ARs as a possible therapeutic target for different diseases such as diabetes and inflammatory diseases. Little is known about AR isoenzymes [41].

1.4 Genotoxicity and carcinogenicity of α,β -unsaturated aldehydes

The structure of α,β -unsaturated aldehydes is characterized by the presence of a polarized carbon-oxygen double bond, and a double bond between carbons 2 and 3 (α and β). Because of the difference in electronegativity between the oxygen and the carbon atom in the aldehyde group, the β -carbon becomes positively polarized and is the preferred site of nucleophilic attack [1, 42]. This electrophilic nature of the aldehydes enables them to interact with electron-rich macromolecules including DNA. The major DNA adducts formed by α,β -unsaturated aldehydes are 1, N^2 -hydroxypropano adducts of deoxyguanosine (Figure 1.1) [8]. Stereocenters are generated in the course of reaction leading to diastereomeric adducts.

- **Genotoxicity**

In vitro

In vitro results indicate genotoxicity and mutagenicity of α,β -unsaturated aldehydes. *trans*-2-Hexenal and crotonaldehyde react directly with calf thymus DNA resulting in the formation of 1, N^2 -propanodeoxyguanosine adducts. The formation of these DNA adducts was also observed in cells from the human lymphoblastoid Namalva cell line and in primary rat colon mucosa cells [3]. The aldehydes are mutagenic in bacteria [42-44] and in mammalian cells [45]. 2-Alkenals (2-pentenal, 2-hexenal, 2-heptenal, 2-octenal and 2-nonenal) were shown to be mutagenic in V79 Chinese hamster cells and the mutagenic potencies increased with increasing carbon chain length [46]. The aldehydes induce DNA single-strand breaks *in vitro* [4, 43]. 2-Propenal, 2-butenal and *trans*-2-hexenal induce DNA single strand breaks in human Namalva cells as well as in rat primary hepatocytes [4]. In addition, 2-butenal, *trans*-2-hexenal and *trans*-2-*cis*-6-nonadienal were reported to cause chromosomal aberrations, micronuclei and sister chromatid exchanges in human blood lymphocytes and Namalva cells [5]. Altogether these results support that α,β -unsaturated aldehydes are genotoxic as well as mutagenic in *in vitro* assays.

In vivo

In contrast to *in vitro* experiments, *in vivo* data on genotoxicity of α,β -unsaturated aldehydes are limited. The formation of DNA adducts *in vivo* has been reported for *trans*-2-hexenal and 2-butenal (crotonaldehyde) upon single oral administration of extremely high doses of the aldehydes [6, 7, 47] (Table 1.2). Schuler and Eder [6] reported the formation of DNA adducts, namely exocyclic 1, N^2 -propanodeoxyguanosine adducts, formed upon exposure to *trans*-2-hexenal in male F344 rats and detected using ^{32}P -labeling. The DNA adducts were quantifiable in the liver and the tissues that had a direct contact with the compound (e.g. forestomach, glandular stomach, oesophagus) as well as in tissues that the aldehyde could reach only after absorption into the systemic circulation (e.g. kidney) at 200 or 500 mg/kg bw. At 50 mg/kg bw, however, a quantifiable amount of DNA adducts was found only in the oesophagus. In 2008, Stout et al. [7] investigated DNA adduct formation using the same exposure conditions as

Table 1.2 α,β -unsaturated aldehydes genotoxicity or carcinogenicity studies in vivo via oral route

Type of effect	Animal (M/F)	Dose and Duration	Results	Reference
<i>2-propenal (acrolein)</i>				
Carcinogenicity	F344 rats	100, 250 or 625 ppm in water for 2 years	Higher incidence of adenomas of the adrenal cortex at 625 ppm	Ljijnsky and Reuber, 1987 [48]
Carcinogenicity	SD rats (M and F)	0.05, 0.5 or 2.4 mg/kg in water for 2 years	No effect observed	Parent et al., 1992 [49]
Carcinogenicity	CD-1 mice (M and F)	0.05 or 2.0, 4.5 mg/kg in water for 2 years	No effect observed	Parent et al., 1991 [50]
Carcinogenicity	F344 rats (M and F)	0, 0.75, 1.25, 2.5, 5, or 10 mg/kg bw in 0.5% methylcellulose for 14 weeks	Squamous hyperplasia of the forestomach in male rats at 5 and 10 mg/kg bw, in female rats at 2.5 mg/kg or higher	NTP, 2006 [51]
Carcinogenicity	B6C3F ₁ mice (M and F)	0, 1.25, 2.5, 5, 10, or 20 mg/kg bw in 0.5% methylcellulose for 14 weeks	Squamous hyperplasia of the forestomach in male and female mice at 2.5, 5, or 10 mg/kg bw	NTP, 2006 [51]
<i>Crotonaldehyde (2-butenal)</i>				
Genotoxicity	F344 rats (F)	200 or 300 mg/kg bw in corn oil single time	DNA adducts quantifiable in the liver at both doses	Budiawan and Eder, 2000 [47]
Genotoxicity	F344 rats (F)	1 or 10 mg/kg bw in corn oil for 6 weeks	DNA adducts quantifiable in the liver at both doses	Budiawan and Eder, 2000 [47]
<i>trans-2-hexenal</i>				
Genotoxicity	F344 rats (M)	50, 200 or 500 mg/kg bw in corn oil single time	DNA adducts quantifiable in most organs at 200 and 500 mg/kg bw	Schuler and Eder, 1999 [6]
Genotoxicity	F344 rats (M)	50, 200 or 500 mg/kg bw in corn oil single time	DNA adducts quantifiable in the forestomach at 200 mg/kg bw	Stout et al., 2008 [7]
Genotoxicity	F344 rats (M)	10, 30 or 100 mg/kg bw in corn oil for 1 or 4 week(s)	DNA adducts quantifiable in the forestomach at 100 mg/kg bw	Stout et al., 2008 [7]
<i>2,4-hexadienal (mixture of trans-2,4-hexadienal and trans, cis-2,4-hexadienal)</i>				
Carcinogenicity	F344 rats (M and F)	22.5, 45 or 90 mg/kg bw in corn oil for 2 years	Squamous cell neoplasms in the forestomach at 45 and 90 mg/kg bw	NTP, 2003 [52] Chan et al., 2003 [53]
Carcinogenicity	B6C3F ₁ mice (M and F)	30, 60 or 120 mg/kg bw in corn oil for 2 years	Squamous cell neoplasms in the forestomach, and squamous cell carcinoma of the tongue at 120 mg/kg bw	NTP, 2003 [52] Chan et al., 2003 [53]

Type of effect	Animal (M/F)	Dose and Duration	Results	Reference
<i>2,4-hexadienal (mixture of trans, trans-2,4-hexadienal and trans, cis-2,4-hexadienal)</i>				
Genotoxicity	F344 rats (M and F)	7.5, 15, 30, 60 or 120 mg/kg bw in feed, microencapsulated for 2 weeks	No peripheral blood micronucleus observed	NTP, 2003 [52]
Genotoxicity	B6C3F ₁ mice (M and F)	7.5, 15, 30, 60 or 120 mg/kg bw in feed, microencapsulated for 2 weeks	No peripheral blood micronucleus observed	NTP, 2003 [52]
<i>citral (mixture of geranial and neral)</i>				
Carcinogenicity	F344 rats (M and F)	1,000, 2,000 or 4,000 ppm in feed (c.a. 50, 100 or 210 mg/kg bw), microencapsulated / 2 years	No effect observed	NTP, 2003 [54]
Carcinogenicity	B6C3F ₁ mice (M and F)	500, 1,000 or 2,000 ppm in feed (c.a. 60, 120 or 260 mg/kg bw), microencapsulated for 2 years	No effect observed	NTP, 2003 [54]
<i>trans-cinnamaldehyde</i>				
Carcinogenicity	F344 rats (M and F)	1,000, 2,100 or 4,100 ppm in feed (c.a. 50, 100 or 200 mg/kg bw), microencapsulated for 2 years	No effect observed	NTP, 2004 [55] Hooth et al., 2004 [56]
Carcinogenicity	B6C3F ₁ mice (M and F)	1,000, 2,100 or 4,100 ppm in feed (c.a. 125, 270 or 550 mg/kg bw), microencapsulated for 2 years	No effect observed	NTP, 2004 [55] Hooth et al., 2004 [56]
Genotoxicity	F344 rats (M and F)	4,100- 33,000 ppm in water (c.a. 275-4,000 mg/kg bw) for 3 months	No peripheral blood micronucleus observed	NTP, 2004 [55]
Genotoxicity	B6C3F ₁ mice (M and F)	4,100- 33,000 ppm (c.a. 625-5,475 mg/kg bw) for 3 months	No peripheral blood micronucleus observed	NTP, 2004 [55]

Note M : male, F: female

used by Schuler and Eder [6]. Using LC/MS/MS, the DNA adducts were detected at 200 and 500 mg *trans*-2-hexenal/kg bw in the forestomach, glandular stomach and liver but not at 50 mg/kg bw. The adduct levels reported by Stout et al. in the liver were up to 1,000 times lower than the levels reported by Schuler and Eder. Stout et al., discussed that this striking gap may be attributed to the differences in purity of *trans*-2-hexenal (98% vs 99%), in the specificity of quantification methods (LC/MS/MS vs ³²P-labeling), and in the animal fasting status (non-fasted vs not described) between the two studies. Budiawan and Eder [47] reported DNA adduct formation in female F344 rats that were exposed to 200 or 300 mg 2-butenal/kg bw by gavage. The amount of DNA adducts in the liver, lung, kidney and large intestine was quantified using ³²P-labeling. The maximum level of DNA adducts in the liver after single exposure of 200 mg 2-butenal/kg bw was 2.9 adducts/10⁸ nucleotides (nt) at 20 hrs after the exposure.

Negative in vivo genotoxicity has been reported for 2,4-hexadienal and cinnamaldehyde upon oral exposure [52, 55]. Male and female mice were exposed daily to 7.5 to 120 mg/kg bw 2,4-hexadienal for 14 weeks, or 4,100 to 33,000 ppm cinnamaldehyde in the feed (equivalent 650 and 5,475 mg/kg bw/day) for 3 months. Peripheral blood samples were obtained from the mice to determine the frequency of micronuclei in normochromatic erythrocytes. In both studies there was no increase in the frequency of micronucleated normochromatic erythrocytes compared to the control groups.

- **Carcinogenicity**

There are several chronic studies and sub-chronic in vivo studies available where carcinogenicity of α,β -unsaturated aldehydes has been examined [49, 52, 54, 55]. Interestingly, as summarized below and in Table 1.2, these studies reported mixed results depending on the compound.

Cinnamaldehyde

Male and female F344 rats and B6C3F₁ mice were exposed to *trans*-cinnamaldehyde for two years [55]. The compound was encapsulated in starch microcapsules for the stabilisation and placed in the feed. The doses given were between 1,000 and 4,100 ppm, corresponding to 50-200 mg/kg bw/day for rats and 125-550 mg/kg bw/day for mice. Tissues from more than 40 sites were examined for every animal, and there was no development of neoplasms observed due to the exposure to cinnamaldehyde in rats or mice.

Citral

In vivo carcinogenicity of citral was examined in a rodent study [54]. Male and female F344 rats and B6C3F₁ mice were exposed to citral for two years. The compound was encapsulated in starch microcapsules for the stabilization and placed in the feed. The doses given were between 1,000 and 4,000 ppm, corresponding to 50-210 mg/kg bw/day for rats and 60-260 mg/kg bw/day for mice. There were no neoplasms or nonneoplastic lesions observed upon exposure to citral in rats

and male mice. An increase in malignant lymphomas was observed for female mice at the highest exposure group, which was attributed to the consumption of citral.

2-propenal (acrolein)

Two in vivo studies examined the carcinogenicity of 2-propenal. In the study of Parent et al., male and female Sprague-Dawley rats were treated daily with 0-2.5 mg/kg bw/day 2-propenal in water by gavage [49]. After two years, there was no significant increase in the development of neoplasms in the treated animals compared to the control group. In a 14-week study conducted by NTP [51], however, incidences of squamous hyperplasia of the forestomach epithelium showed a dose-dependent increase. In another study [57] F344 rats and B6C3F₁ mice were administered 0–10 mg and 0-20 mg 2-propenal/kg bw/day by gavage, respectively. The frequency of the incidences of neoplasms in the forestomach was significantly increased at 5 and 10 mg/kg bw/day in male rats, at 2.5 mg/kg bw/day or greater in female rats, and at 2.5, 5, or 10 mg/kg bw/day in male and female mice (Table 1.3). 2-Propenal was also shown to significantly increase mortality in both species, and the reduced number of neoplasms in the highest exposure group (i.e. 20 mg/kg bw/day) in mice was attributed to the increased mortality observed at this level of exposure, which amounted to 100% in male and female.

Table 1.3 Number (and percentage) of animals with neoplasm in forestomach per number of animals necropsied upon exposure to 2-propenal (derived from NTP [51])

		F344 rats					
		Control	0.75 mg/kg bw/day	1.25 mg/kg bw/day	2.5 mg/kg bw/day	5 mg/kg bw/day	10 mg/kg bw/day
Male	0/10 (0%)	0/10 (0%)	0/10 (0%)	3/10 (30%)	8/10 (80%)	9/10 (90%)	
Female	0/10 (0%)	0/10 (0%)	3/10 (30%)	5/10 (50%)	8/10 (80%)	10/10 (100%)	
		B6C3F₁ mice					
		Control	1.25 mg/kg bw/day	2.5 mg/kg bw/day	5 mg/kg bw/day	10 mg/kg bw/day	20 mg/kg bw/day
Male	0/10 (0%)	2/10 (20%)	6/10 (60%)	7/10 (70%)	10/10 (100%)	0/10 (0%)	
Female	0/10 (0%)	0/10 (0%)	4/10 (40%)	7/10 (70%)	8/10 (80%)	2/10 (20%)	

2,4-hexadienal

Carcinogenicity of 2,4-hexadienal was examined in a two-year rodent study [52]. Male and female F344 rats and B6C3F₁ mice were exposed daily to 2,4-hexadienal by gavage. The compound was dissolved in corn oil and was deposited directly in the forestomach through a tube. After two years, animals receiving 2,4-hexadienal showed significantly greater occurrences of neoplasms in the forestomach, including papillomas and malignant carcinomas in both species. The occurrence increased dose-dependently (see Table 1.4).

Table 1.4 Number (and percentage) of animals with neoplasm per number of animals necropsied upon exposure to 2,4-hexadienal (derived from NTP [52])

	Control	F344 rats		
		22.5 mg/kg bw/day	45 mg/kg bw/day	90 mg/kg bw/day
Male	0/50 (0%)	3/50 (6%)	10/50 (20%)	29/50 (58%)
Female	0/50 (0%)	1/50(2%)	5/50 (10%)	17/50 (34%)
	Control	B6C3F₁ mice		
		30 mg/kg bw/day	60 mg/kg bw/day	120 mg/kg bw/day
Male	2/50 (4%)	4/50 (8%)	5/50 (10%)	10/50 (20%)
Female	2/50 (4%)	2/49 (4%)	11/50 (22%)	18/50 (36%)

The Joint FAO/WHO Expert Committee on Food Additives (JECFA) mentioned that a development of neoplasia is a common finding in bioassays in which a high concentration of an irritating material is delivered by gavage into the forestomach every day for two years, and the genotoxicity of the compound is not believed to be the basis for its effects in the rodent forestomach but rather, the injury to the forestomach epithelium attributable to exposure is believed to be the primary cause [11]. It was furthermore considered that the conditions of exposure during oral administration are unusual in that physical effects may cause high local concentrations of test substances in the forestomach and prolonged exposure of the epithelium. Also, the forestomach was the only site of increased neoplasia in treated animals. Based on these reasons JECFA concluded that the appearance of forestomach tumours by 2,4-hexadienal in rodents observed in the study by NTP [52] is of no relevance to humans [11].

1.5 Safety evaluation and regulatory status of α,β -unsaturated aldehydes

The Joint FAO/WHO Expert Committee on Food Additives (JECFA) evaluated the safety of 2-alkenals, 2,4-dienals, and cinnamaldehyde and their related carboxylic acids, alcohols and esters as added food flavourings [9-11]. All the substances evaluated were categorized as Cramer Class I in their evaluation scheme, which includes “flavouring agents that have simple chemical structures and efficient modes of metabolism which would suggest a low order of toxicity by the oral route”. For 2-alkenals and 2,4-dienals the human daily exposure levels to these aldehydes were estimated to be below the threshold of toxicological concern (TTC) for Cramer Class I (1,800 $\mu\text{g}/\text{day}$) both in Europe and in the US [9-11]. Therefore JECFA concluded that these substances would not be of safety concern at their currently estimated levels of intake as flavouring agents. The daily intake of cinnamaldehyde was estimated to be 2,500 and 59,000 $\mu\text{g}/\text{day}/\text{capita}$ in Europe and in the US respectively, which exceeds the TTC of 1,800 $\mu\text{g}/\text{day}$ [9]. The Committee proceeded to the next step where the intake levels were compared with the no observed adverse effect level (NOAEL). The NOAEL of cinnamaldehyde was determined to be

620 mg/kg bw/day (i.e. 37,200 mg/day/capita for a person of 60 kg) in a 13-week toxicity study in rat, and the margin of safety of > 600 times compared to the estimated intake level in the US was considered sufficient to conclude that the use of cinnamaldehyde as a flavouring agent is not of concern [9].

In the US, the Expert Panel of the Flavor and Extract Manufacturers Association (FEMA) conducted a safety evaluation on the use of aliphatic, linear α,β -unsaturated aldehydes and related compounds [12], and of cinnamaldehyde and their related compounds [13] as flavouring ingredients. The conclusions were comparable to those of JECFA. The Panel affirmed the GRAS (generally recognized as safe) status of the substances based on their rapid absorption, metabolic detoxification, and excretion in humans and other animals, their low level of flavour use, the wide margins of safety between the conservative estimates of intake and the NOAELs determined from subchronic and chronic studies, and the lack of significant genotoxic and mutagenic potential when tested at non-cytotoxic concentrations. For cinnamaldehyde the Panel additionally mentioned that this evidence of safety is supported by the fact that the intake of cinnamyl derivatives as natural components of traditional foods is much greater than their intake as intentionally added flavoring substances [13]. With this GRAS status, the use of α,β -unsaturated aldehydes as intentionally added food additives is allowed in the US under the Federal Food, Drug, and Cosmetic Act.

EFSA took a different approach for the safety assessment as compared to JECFA or FEMA. The EFSA Panel on Food Contact Materials, Enzymes, Flavourings and Processing Aids evaluated the use of 347 flavouring substances in the EU Register that are α,β -unsaturated aldehydes or related compounds which may give rise to such aldehydes via hydrolysis or oxidation [14]. The flavouring substances were divided into 28 subgroups depending on the structural similarity. For most of the subgroups, the Panel considered that the α,β -unsaturated aldehyde and ketone structures are alerts for genotoxicity and concluded that there is a need for additional information before conclusions can be reached. It was furthermore mentioned that the required data include data on mode of action and metabolism, genotoxicity data especially in vivo or data on carcinogenicity. Based on this opinion of EFSA, the use of most of the aldehydes and related substances has been suspended in the EU under the Regulation (EC) No. 1334/2008 and under the new regulation that came into force in 2013 (Regulation (EU) No. 872/2012).

1.6 Uncertainties in effects of genotoxic agents at low exposure levels

The discrepancy in the conclusions by JECFA and FEMA on one side and the conclusion by the EFSA on the other, clearly illustrates the lack of consensus within authorities and scientists related to safety evaluations of genotoxic agents at low exposure levels. In general it is considered that when DNA is damaged by a xenobiotic genotoxic agent, the damage may result in a mutation during the following DNA synthesis if it is not repaired in time. This mutation may contribute to

tumour development for example by inducing the proliferation of the cell, resulting in the formation of an identifiable focal lesion and accumulation of genetic damage. The so-called one-hit theory assumes that a single DNA damaging event in a cell is able to induce a single point mutation that may lead to increased proliferation of the cell, which may result in a tumour formation. Although current scientific insights rather assume that tumour formation is a multistep process [58], in conventional toxicological risk assessment it is still assumed that tumour formation by genotoxic carcinogens can be a one hit event so that there is no threshold that defines a safe level of exposure.

Because of the absence of a safe level of exposure, genotoxic carcinogenic compounds are not allowed to be intentionally added to foods in the EU. This implies that compounds for which positive in vitro genotoxicity data exist require follow up in vivo studies to exclude the concern over genotoxicity and carcinogenicity. With the implementation of the new EU regulation for food flavouring agents (Regulation (EU) No. 872/2012), this approach now also applies to flavouring agents. Questions can be raised, however, whether the low exposure levels resulting from their use as flavourings, would lead to a significant risk. The effects of the genotoxic agents at low exposure levels may not be significant compared to the effects of endogenous and unavoidable exogenous genotoxic compounds, because of cytoprotective mechanisms including metabolism that swiftly converts DNA damaging agents to non-reactive metabolites to prevent formation of DNA damage, and efficient DNA repair that eliminates DNA damages. Oesche et al. [59] for instance presented that DNA strand breaks caused by styrene oxide caused in V79 Chinese hamster cells were not observed at lower concentrations than 100 μM when the cells were genetically engineered to express human microsomal epoxide hydrolase. The results suggest that the detoxification enzymes may play an important role in the protection against the DNA damaging agent. The importance of DNA repair to prevent genotoxic adverse effects is for example supported by a study by Doak et al. [60]. The alkylating agents methyl methanesulphonate or ethyl methanesulphonate have been known to show non-linear concentration-response curves for gross chromosomal damage and mutagenicity with no-observed effect levels (NOELs) in vitro. Doak et al. investigated gene expression levels involved in DNA repair and found that expression of O⁶-methylguanine DNA methyltransferase is up-regulated at low exposure concentrations within the NOEL, reflecting sub-linear DNA adduct formation and protection against the DNA damage at low exposure concentrations.

It has important implications in the safety evaluation of DNA reactive agents to determine genotoxic effects at low exposure levels relevant to realistic exposure in vivo. However, determination of genotoxic effects at such low exposure levels in vivo is generally problematic. Very sensitive tests are required, and moreover, the experiments may require thousands of animals per dose to quantify an increase in the responses above background levels in a statistically robust manner [61]. In addition, in case of α,β -unsaturated aldehydes, providing in vivo data on all the aldehydes listed as food flavourings would not be realistic considering the large number of

the compounds in the group [14]. Alternative methods to investigate concerns over genotoxicity of α,β -unsaturated aldehyde food flavouring agents at low dose exposure are of high interest. This thesis therefore aims to develop physiologically based in silico models for examination of low dose DNA adduct formation of food-borne α,β -unsaturated aldehydes to facilitate safety evaluation of their use as flavouring agents.

1.7 PBK/D modeling for genotoxic compounds

In order to obtain insights in the kinetic and dynamic behaviour of a chemical at low dose exposure including the possible saturation in metabolism, physiologically based in silico models have proven to be a powerful tool [62-64]. A PBK/D (physiologically based kinetic/dynamic) model is a set of mathematical descriptions simulating a relationship between external exposure levels and chemical concentrations in biological matrices (kinetics) and their effect on the organism (dynamics) over time. In a PBK/D model a body is divided into different compartments. The choice of compartments for the model is a crucial step that has a significant influence on the model outcomes. In general target tissues and tissues that metabolize the substance of interest are represented as individual compartments and non-target tissues are lumped together into “slowly perfused tissues” (e.g. muscle and skin) or “richly perfused tissues” (e.g. brain and spleen) compartments depending on relative perfusion rates [65].

Development of PBK/D models consists of four steps: model representation, parameterization, simulation and evaluation [66]. *Model Representation* involves the development of conceptual and mathematical descriptions of the relevant compartments of the animal as well as the identification of the exposure and metabolic pathways of the chemical. *Model Parameterization* is the step where independent measures of the mechanistic determinants are obtained. The parameters are usually classified as either physiological (e.g. body weight, cardiac output), physico-chemical (e.g. $\log K_{ow}$, tissue: blood partition coefficients) or biochemical (e.g. V_{max} and K_m of metabolism). Physiological parameters can usually be collected from literature, while physico-chemical and biochemical parameters are chemical specific and therefore usually need to be defined for each compound by using in silico modelling or by performing experiments. The step of *Model Simulation* involves the prediction of ADME and further dynamics of a chemical for a defined exposure scenarios, using a numerical integration algorithm. The last step *Model Evaluation* or *Model Validation* involves the comparison of predicted values of the model with experimentally obtained in vivo data. Depending on how well the prediction matches with in vivo data, the model will be refused, refined, or accepted for further use [66]. Once a PBK/D model is developed, it can be used to obtain mechanistic insights in the extrapolation of high exposure doses used in animal studies to the exposure levels relevant for realistic human exposure that are usually orders of magnitude lower. Furthermore, by replacing all parameters in a model specific for rats with the corresponding physiological and kinetic parameters for humans, a

PBK/D models for human can be defined. If parameters in a model are replaced from one individual to another the interindividual (intraspecies) variation can be investigated, which allows examination of the influence of for example polymorphisms in detoxification and/or bioactivation efficiencies [62]. Furthermore, PBK/D models can be used to facilitate read-across from one compound to another structurally related compound that exerts toxicity via a similar mode of action by replacing chemical specific parameters including biochemical and physicochemical parameters [67].

A number of toxicological research papers about physiologically based in silico models have been published for, for instance, drugs, cosmetic products or food constituents. Yet, the majority of the publications aim at simulating ADME of the compounds of interest administered through different exposure routes, and examples of models for genotoxic compounds allowing prediction of DNA damage are limited. In 2007 Young et al. published a PBK/D model simulating DNA adduct formation of glycidamide, a metabolite of acrylamide [68] in rats, mice and humans. In this study, toxicokinetic data as well as DNA binding kinetics in rats and mice were collected by exposing animals to acrylamide in drinking water for 1 week. The PBK/D models developed for rats and mice were subsequently extended to human, by fitting the predictions for acrylamide excretion in urine to observed human data. PBK/D models may be developed based on in vivo data, as shown by Young et al., however, it requires use of animals, and moreover, it may not be feasible for all compounds to obtain kinetic and dynamic data in vivo, especially when a model for DNA adduct formation upon human exposure to an avoidable genotoxic compound needs to be developed. In 2008, Paini et al. developed a model where DNA adduct formation by estragole, one of the alkenylbenzenes present in the diet, is described [64]. The parameters to address metabolism of estragole and DNA adduct formation of 1'-sulfooxyestragole, the ultimate carcinogen of estragole, were obtained by in vitro assays by incubating estragole or its metabolites with relevant tissue fractions or primary cells.

1.8 Objectives and outline of the thesis

The main objective of the present thesis was to develop physiologically based in silico models for examination of DNA adduct formation of food-borne α,β -unsaturated aldehydes at low doses to facilitate safety evaluation of their use as flavouring agents. PBK/D models were developed based on kinetic parameters derived from in vitro incubations using relevant tissue fractions. In order to facilitate the extension of PBK/D models from one α,β -unsaturated aldehyde to other structurally related substances that exert toxicity via a similar mode of action, a QSAR (quantitative structure-activity relationship) approach was applied to accelerate the determination of the kinetic parameters. The PBK/D model outcomes were used to provide mechanistic insights in dose- and species- dependent detoxification and DNA adduct formation by different α,β -unsaturated aldehydes present in the diet.

Chapter 1, the current chapter, introduces occurrence, metabolism, genotoxicity and carcinogenicity, and regulatory status of dietary α,β -unsaturated aldehydes as the basic background information of the compounds. Also, the uncertainty in the evaluation of genotoxicity at low exposure doses, a challenge for the safety evaluation of these flavouring compounds, the use of PBK/D models, and finally the aim and overall objectives of the thesis are introduced.

Chapter 2 presents the development of a PBK/D model for *trans*-2-hexenal in rats. *trans*-2-Hexenal was selected as a model dietary α,β -unsaturated aldehyde for the development of this first PBK/D model enabling prediction of DNA adduct formation at low dose levels. The kinetic parameters are collected by performing in vitro incubations using relevant pooled rat tissue fractions. In order to address the influence of the depletion of GSH, GSH pool kinetics are also described in the model. The model performance is evaluated, and the dose-dependent detoxification and DNA adduct formation are simulated to obtain insights in the significance of the DNA adduct level increase at low doses relevant for human dietary exposure.

Chapter 3 describes the development of a PBK/D model for *trans*-2-hexenal in humans. The structure of the model is based on the rat model developed in Chapter 2. The kinetic parameters are collected by performing in vitro incubations using pooled human tissue fractions. In order to determine the influence of polymorphisms in the detoxification efficiencies on DNA adduct formation, the kinetic parameters are defined also for 11 individuals using individual human tissue fractions. By performing Monte-Carlo simulations, the distribution of formation of DNA adduct levels in the population upon exposure to *trans*-2-hexenal is determined. Based on the outcomes, it is discussed if the increase in DNA adduct levels in the liver due to dietary exposure to *trans*-2-hexenal in the human population is significant compared to reported background levels of DNA adducts.

trans-2-Hexenal is only one of many dietary α,β -unsaturated aldehydes of interest. **Chapter 4** extends the rat PBK/D model developed for *trans*-2-hexenal to 18 other structurally related food-borne α,β -unsaturated aldehydes using a QSAR approach for definition of the PBK/D parameters. The kinetic parameters are first experimentally determined for a training set of 6 acyclic α,β -unsaturated aldehyde to define QSAR models. Based on the QSAR models, kinetic parameters of the other 12 aldehydes are predicted and integrated into PBK/D models. Based on the outcomes, the significance of DNA adduct formation at dietary exposure levels as well as a compound that represents the worst case within the group will be defined.

For most of the aldehydes, in vivo data on genotoxicity and carcinogenicity that can overcome the concerns raised by in vitro genotoxicity data, are lacking. In contrast, cinnamaldehyde has been shown to be not genotoxic or carcinogenic in a rodent study and has been approved as flavouring agent despite its α,β -unsaturated aldehyde moiety. **Chapter 5** therefore investigates DNA adduct formation by cinnamaldehyde at doses where no genotoxicity or carcinogenicity has been observed in vivo, using PBK/D modelling, and compares these DNA adduct levels to those predicted for the 18 aldehydes in Chapter 4. Rat and human PBK/D models

for cinnamaldehyde are built based on biochemical parameters collected by performing in vitro incubations. Based on the PBK/D models outcomes, possibilities to apply read-across from the negative genotoxicity and carcinogenicity results obtained for cinnamaldehyde in vivo to any of the 18 aldehydes will be discussed.

Finally **Chapter 6** presents the overall discussion including the performance of the PBK/D models developed in this thesis and implication of the PBK/D model outcomes for the safety evaluation of food-borne α,β -unsaturated aldehydes used as food flavourings, as well as suggestions for future work.

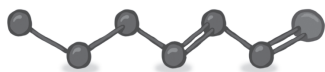
REFERENCES

- [1] Feron, V. J., Til, H. P., de Vrijer, F., Woutersen, R. A., *et al.*, Aldehydes: occurrence, carcinogenic potential, mechanism of action and risk assessment. *Mutat Res* 1991, 259, 363-385.
- [2] Witz, G., Biological interactions of alpha,beta-unsaturated aldehydes. *Free Radic Biol Med* 1989, 7, 333-349.
- [3] Golzer, P., Janzowski, C., Pool-Zobel, B. L., Eisenbrand, G., (E)-2-hexenal-induced DNA damage and formation of cyclic 1,N²-(1,3-propano)-2'-deoxyguanosine adducts in mammalian cells. *Chem Res Toxicol* 1996, 9, 1207-1213.
- [4] Eisenbrand, G., Schuhmacher, J., Golzer, P., The influence of glutathione and detoxifying enzymes on DNA damage induced by 2-alkenals in primary rat hepatocytes and human lymphoblastoid cells. *Chem Res Toxicol* 1995, 8, 40-46.
- [5] Dittberner, U., Eisenbrand, G., Zankl, H., Genotoxic effects of the alpha, beta-unsaturated aldehydes 2-trans-butenal, 2-trans-hexenal and 2-trans, 6-cis-nonadienal. *Mutat Res* 1995, 335, 259-265.
- [6] Schuler, D., Eder, E., Detection of 1,N²-propanodeoxyguanosine adducts of 2-hexenal in organs of Fischer 344 rats by a ³²P-post-labeling technique. *Carcinogenesis* 1999, 20, 1345-1350.
- [7] Stout, M. D., Bodes, E., Schoonhoven, R., Upton, P. B., *et al.*, Toxicity, DNA binding, and cell proliferation in male F344 rats following short-term gavage exposures to *trans*-2-hexenal. *Toxicol Pathol* 2008, 36, 232-246.
- [8] Rezaei, M., Harris, T. M., Rizzo, C. J., Stereoselective synthesis of the 1,N²-deoxyguanosine adducts of cinnamaldehyde. A stereocontrolled route to deoxyguanosine adducts of α,β -unsaturated aldehydes. *Tetrahedron Lett* 2003, 44, 7513-7516.
- [9] JECFA, Evaluation of certain food additives and contaminants : fifty-fifth report of the Joint FAO/WHO expert committee on food additives. http://whqlibdoc.who.int/trs/WHO_TRS_901.pdf. 2001.
- [10] JECFA, Evaluation of Certain Food Additives: sixty-third report of the Joint FAO/WHO Expert Committee on Food Additives. http://whqlibdoc.who.int/trs/WHO_TRs_928.pdf. 2005.
- [11] JECFA, Evaluation of certain food additives and contaminants: Sixty-first report of the Joint FAO/WHO Expert Committee on Food Additives. http://whqlibdoc.who.int/trs/WHO_TRS_922.pdf. 2004.
- [12] Adams, T. B., Gavin, C. L., Taylor, S. V., Waddell, W. J., *et al.*, The FEMA GRAS assessment of alpha,beta-unsaturated aldehydes and related substances used as flavor ingredients. *Food Chem Toxicol* 2008, 46, 2935-2967.
- [13] Adams, T. B., Cohen, S. M., Doull, J., Feron, V. J., *et al.*, The FEMA GRAS assessment of cinnamyl derivatives used as flavor ingredients. *Food Chem Toxicol* 2004, 42, 157-185.
- [14] EFSA, Minutes of the 26th plenary meeting of the scientific panel on food additives, flavourings, processing aids and materials in contact with food. <http://www.efsa.europa.eu/en/events/event/afc071127-m.pdf>. 2007.
- [15] Esterbauer, H., Cheeseman, K. H., Dianzani, M. U., Poli, G., Slater, T. F., Separation and characterization of the aldehydic products of lipid peroxidation stimulated by ADP-Fe²⁺ in rat liver microsomes. *The Biochemical journal* 1982, 208, 129-140.
- [16] Uchida, K., Current status of acrolein as a lipid peroxidation product. *Trends in cardiovascular medicine* 1999, 9, 109-113.
- [17] Mujic, I., Kralj, M. B., Jokic, S., Jarni, K., *et al.*, Changes in aromatic profile of fresh and dried fig - the role of pre-treatments in drying process. *Int J Food Sci Tech* 2012, 47, 2282-2288.
- [18] Zawirska-Wojtasiak, R., Goslinski, M., Szwacka, M., Gajc-Wolska, J., Mildner-Szkudlarz, S., Aroma evaluation of transgenic, thaumatin II-producing cucumber fruits. *Journal of food science* 2009, 74, C204-210.
- [19] Alasalvar, C., Topal, B., Serpen, A., Bahar, B., *et al.*, Flavor characteristics of seven grades of black tea produced in Turkey. *Journal of agricultural and food chemistry* 2012, 60, 6323-6332.
- [20] Du, X., Plotto, A., Song, M., Olmstead, J., Rouseff, R., Volatile composition of four southern highbush blueberry cultivars and effect of growing location and harvest date. *J Agric Food Chem* 2011, 59, 8347-8357.
- [21] Adams, T. B., Doull, J., Goodman, J. I., Munro, I. C., *et al.*, The FEMA GRAS assessment of furfural used as a flavour ingredient. Flavor and Extract Manufacturers' Association. *Food Chem Toxicol* 1997, 35, 739-751.
- [22] Grootveld, M., Atherton, M. D., Sheerin, A. N., Hawkes, J., *et al.*, In vivo absorption, metabolism, and urinary excretion of alpha,beta-unsaturated aldehydes in experimental animals. Relevance to the development of cardiovascular diseases by the dietary ingestion of thermally stressed polyunsaturate-rich culinary oils. *J Clin Invest* 1998, 101, 1210-1218.
- [23] Parent, R. A., Caravello, H. E., Sharp, D. E., Metabolism and distribution of [2,3-¹⁴C]acrolein in Sprague-Dawley rats. *Journal of applied toxicology : JAT* 1996, 16, 449-457.

- [24] Sapienza, P. P., Ikeda, G. J., Warr, P. I., Plummer, S. L., *et al.*, Tissue distribution and excretion of ¹⁴C-labelled cinnamic aldehyde following single and multiple oral administration in male Fischer 344 rats. *Food Chem Toxicol* 1993, *31*, 253-261.
- [25] Diliberto, J. J., Usha, G., Birnbaum, L. S., Disposition of citral in male Fischer rats. *Drug Metab Dispos* 1988, *16*, 721-727.
- [26] Jelski, W., Szmitkowski, M., Alcohol dehydrogenase (ADH) and aldehyde dehydrogenase (ALDH) in the cancer diseases. *Clinica chimica acta; international journal of clinical chemistry* 2008, *395*, 1-5.
- [27] Vasiliou, V., Pappa, A., Petersen, D. R., Role of aldehyde dehydrogenases in endogenous and xenobiotic metabolism. *Chem Biol Interact* 2000, *129*, 1-19.
- [28] Mitchell, D. Y., Petersen, D. R., The oxidation of alpha-beta unsaturated aldehydic products of lipid peroxidation by rat liver aldehyde dehydrogenases. *Toxicol Appl Pharmacol* 1987, *87*, 403-410.
- [29] Klyosov, A. A., Kinetics and specificity of human liver aldehyde dehydrogenases toward aliphatic, aromatic, and fused polycyclic aldehydes. *Biochemistry* 1996, *35*, 4457-4467.
- [30] Solobodowska, S., Giebultowicz, J., Wolinowska, R., Wroczynski, P., Contribution of ALDH1A1 isozyme to detoxification of aldehydes present in food products. *Acta poloniae pharmaceutica* 2012, *69*, 1380-1383.
- [31] Schwobel, J. A. H., Wondrousch, D., Koleva, Y. K., Madden, J. C., *et al.*, Prediction of Michael-Type Acceptor Reactivity toward Glutathione. *Chem Res Toxicol* 2010, *23*, 1576-1585.
- [32] Hayes, J. D., Flanagan, J. U., Jowsey, I. R., Glutathione transferases. *Annual review of pharmacology and toxicology* 2005, *45*, 51-88.
- [33] Balogh, L. M., Roberts, A. G., Shireman, L. M., Greene, R. J., Atkins, W. M., The stereochemical course of 4-hydroxy-2-nonenal metabolism by glutathione S-transferases. *The Journal of biological chemistry* 2008, *283*, 16702-16710.
- [34] Hubatsch, I., Ridderstrom, M., Mannervik, B., Human glutathione transferase A4-4: an alpha class enzyme with high catalytic efficiency in the conjugation of 4-hydroxynonenal and other genotoxic products of lipid peroxidation. *The Biochemical journal* 1998, *330* (Pt 1), 175-179.
- [35] Linhart, I., Frantik, E., Vodickova, L., Vosmanska, M., *et al.*, Biotransformation of acrolein in rat: excretion of mercapturic acids after inhalation and intraperitoneal injection. *Toxicol Appl Pharmacol* 1996, *136*, 155-160.
- [36] Parent, R. A., Paust, D. E., Schrimpf, M. K., Talaat, R. E., *et al.*, Metabolism and distribution of [2,3-¹⁴C]acrolein in Sprague-Dawley rats. II. Identification of urinary and fecal metabolites. *Toxicological sciences : an official journal of the Society of Toxicology* 1998, *43*, 110-120.
- [37] Delbressine, L. P., Klippert, P. J., Reuvers, J. T., Seuttler-Berlage, F., Isolation and identification of mercapturic acids of cinnamic aldehyde and cinnamyl alcohol from urine of female rats. *Arch Toxicol* 1981, *49*, 57-64.
- [38] Srivastava, S., Watowich, S. J., Petrash, J. M., Srivastava, S. K., Bhatnagar, A., Structural and kinetic determinants of aldehyde reduction by aldose reductase. *Biochemistry* 1999, *38*, 42-54.
- [39] Burczynski, M. E., Sridhar, G. R., Palackal, N. T., Penning, T. M., The reactive oxygen species- and Michael acceptor-inducible human aldo-keto reductase AKR1C1 reduces the alpha,beta-unsaturated aldehyde 4-hydroxy-2-nonenal to 1,4-dihydroxy-2-nonenal. *Journal of Biological Chemistry* 2001, *276*, 2890-2897.
- [40] Martin, H. J., Maser, E., Role of human aldo-keto-reductase AKR1B10 in the protection against toxic aldehydes. *Chem Biol Interact* 2009, *178*, 145-150.
- [41] Petrash, J. M., All in the family: aldose reductase and closely related aldo-keto reductases. *Cell Mol Life Sci* 2004, *61*, 737-749.
- [42] Benigni, R., Conti, L., Crebelli, R., Rodomonte, A., Vari, M. R., Simple and alpha,beta-unsaturated aldehydes: correct prediction of genotoxic activity through structure-activity relationship models. *Environmental and molecular mutagenesis* 2005, *46*, 268-280.
- [43] Eder, E., Scheckenbach, S., Deininger, C., Hoffman, C., The possible role of alpha, beta-unsaturated carbonyl compounds in mutagenesis and carcinogenesis. *Toxicol Lett* 1993, *67*, 87-103.
- [44] Eder, E., Deininger, C., Mutagenicity of 2-alkylpropenals in Salmonella typhimurium strain TA 100: structural influences. *Environmental and molecular mutagenesis* 2001, *37*, 324-328.
- [45] Canonero, R., Martelli, A., Marinari, U. M., Brambilla, G., Mutation induction in Chinese hamster lung V79 cells by five alk-2-enals produced by lipid peroxidation. *Mutat Res* 1990, *244*, 153-156.
- [46] Canonero, R., Martelli, A., Marinari, U. M., Brambilla, G., Mutation induction in Chinese hamster lung V79 cells by five alk-2-enals produced by lipid peroxidation. *Mutat Res* 1990, *244*, 153-156.
- [47] Budiawan, Eder, E., Detection of 1,N²-propanodeoxyguanosine adducts in DNA of Fischer 344 rats by an adapted ³²P-post-labeling technique after per os application of crotonaldehyde. *Carcinogenesis* 2000, *21*, 1191-1196.
- [48] Lijinsky, W., Reuber, M. D., Chronic carcinogenesis studies of acrolein and related compounds. *Toxicol Ind Health* 1987, *3*, 337-345.

Chapter 1

- [49] Parent, R. A., Caravello, H. E., Long, J. E., Two-year toxicity and carcinogenicity study of acrolein in rats. *Journal of applied toxicology : JAT* 1992, 12, 131-139.
- [50] Parent, R. A., Caravello, H. E., Long, J. E., Oncogenicity Study of Acrolein in Mice. *J Am Coll Toxicol* 1991, 10, 647-659.
- [51] NTP, NTP Technical Report on the Comparative Toxicity Studies of Allyl Acetate, Allyl Alcohol, and Acrolein Administered by Gavage to F344/N Rats and B6C3F1 Mice. 2006.
- [52] NTP, NTP Technical Report on the Toxicology and Carcinogenesis Studies of 2,4-Hexadienal in F344/N Rats and B6C3F1 Mice (Gavage Studies). http://ntp.niehs.nih.gov/ntp/htdocs/lt_rpts/tr509.pdf. 2003.
- [53] Chan, P. C., Mahler, J., Peddada, S., Lomnitski, L., Nyska, A., Forestomach tumor induction by 2,4-hexadienal in F344N rats and B6C3F1 mice. *Arch Toxicol* 2003, 77, 511-520.
- [54] NTP, NTP Technical Report on the Toxicology and Carcinogenesis Studies of Citral (Microencapsulated) (CAS No.5392-40-5) in F344 Rats and B6C3F1 Mice (Feed Studies). http://ntp.niehs.nih.gov/ntp/htdocs/lt_rpts/tr505.pdf. 2003.
- [55] NTP, NTP Technical Report on the Toxicology and Carcinogenesis Studies of *trans*-Cinnamaldehyde (Microencapsulated) (CAS NO. 14371-10-9) in F344/N Rats and B6C3F1 Mice (Feed Studies). http://ntp.niehs.nih.gov/ntp/htdocs/lt_rpts/tr514.pdf. 2004.
- [56] Hooth, M. J., Sills, R. C., Burka, L. T., Haseman, J. K., *et al.*, Toxicology and carcinogenesis studies of microencapsulated *trans*-cinnamaldehyde in rats and mice. *Food Chem Toxicol* 2004, 42, 1757-1768.
- [57] NTP, Technical report on the comparative toxicity studies of allyl acetate, allyl alcohol, and acrolein. Administered by gavage to F344/N rats and B6C3F1 mice. http://ntp.niehs.nih.gov/ntp/htdocs/st_rpts/tox048.pdf. 2006.
- [58] Hanahan, D., Weinberg, R. A., Hallmarks of cancer: the next generation. *Cell* 2011, 144, 646-674.
- [59] Oesch, F., Herrero, M. E., Hengstler, J. G., Lohmann, M., Arand, M., Metabolic detoxification: Implications for thresholds. *Toxicol Pathol* 2000, 28, 382-387.
- [60] Doak, S. H., Brusehafer, K., Dudley, E., Quick, E., *et al.*, No-observed effect levels are associated with up-regulation of MGMT following MMS exposure. *Mutat Res-Fund Mol M* 2008, 648, 9-14.
- [61] Bailey, G. S., Reddy, A. P., Pereira, C. B., Harttig, U., *et al.*, Nonlinear Cancer Response at Ultralow Dose: A 40800-Animal ED001 Tumor and Biomarker Study. *Chem Res Toxicol* 2009, 22, 1264-1276.
- [62] Rietjens, I. M. C. M., Louisse, J., Punt, A., Tutorial on physiologically based kinetic modeling in molecular nutrition and food research. *Molecular nutrition & food research* 2011, 55, 941-956.
- [63] Punt, A., Freidig, A. P., Delatour, T., Scholz, G., *et al.*, A physiologically based biokinetic (PBBK) model for estragole bioactivation and detoxification in rat. *Toxicol Appl Pharmacol* 2008, 231, 248-259.
- [64] Paini, A., Punt, A., Viton, F., Scholz, G., *et al.*, A physiologically based biodynamic (PBBDD) model for estragole DNA binding in rat liver based on in vitro kinetic data and estragole DNA adduct formation in primary hepatocytes. *Toxicol Appl Pharmacol* 2010, 245, 57-66.
- [65] Krishnan, K., Andersen, M. E., Physiologically based pharmacokinetic modeling in toxicology. *Principles and Methods of Toxicology (Forth Edition) Edition* 2001, 193-239.
- [66] Krishnan, K. a. A. M. E., Chapter 5 Physiologically Based Pharmacokinetic Modeling in Toxicology. *Principles and Methods of Toxicology, Fourth Edition* 2001.
- [67] van den Berg, S. J., Punt, A., Soffers, A. E., Vervoort, J., *et al.*, Physiologically based kinetic models for the alkenylbenzene elemicin in rat and human and possible implications for risk assessment. *Chem Res Toxicol* 2012, 25, 2352-2367.
- [68] Young, J. F., Luecke, R. H., Doerge, D. R., Physiologically based pharmacokinetic/pharmacodynamic model for acrylamide and its metabolites in mice, rats, and humans. *Chem Res Toxicol* 2007, 20, 388-399.



CHAPTER 2

A Physiologically Based In Silico Model for *trans*-2-Hexenal Detoxification and DNA Adduct Formation in Rat

R. Kiwamoto
I. M. C. M. Rietjens
A. Punt

Based on *Chemical Research in Toxicology* (2012) 25 (12): 2630-2641

ABSTRACT

trans-2-Hexenal is an α,β -unsaturated aldehyde that occurs naturally in a wide range of fruits, vegetables, and spices. *trans*-2-Hexenal as well as other α,β -unsaturated aldehydes that are natural food constituents or flavoring agents may raise a concern for genotoxicity due to the ability of the α,β -unsaturated aldehyde moiety to react with DNA. Controversy remains, however, on whether α,β -unsaturated aldehydes result in significant DNA adduct formation in vivo at realistic dietary exposure. In this study, a rat physiologically based in silico model was developed for *trans*-2-hexenal as a model compound to examine the time- and dose-dependent detoxification and DNA adduct formation of this selected α,β -unsaturated aldehyde. The model was developed based on in vitro and literature-derived parameters, and its adequacy was evaluated by comparing predicted DNA adduct formation in the liver of rats exposed to *trans*-2-hexenal with reported in vivo data. The model revealed that at an exposure level of 0.04 mg/kg bw, a value reflecting estimated daily human dietary intake, *trans*-2-hexenal is rapidly detoxified predominantly by conjugation with glutathione (GSH) by glutathione S-transferases. At higher dose levels, depletion of GSH results in a shift to *trans*-2-hexenal oxidation and reduction as the major pathways for detoxification. The level of DNA adduct formation at current levels of human dietary intake was predicted to be more than 3 orders of magnitude lower than endogenous DNA adduct levels. These results support that rapid detoxification of *trans*-2-hexenal reduces the risk arising from *trans*-2-hexenal exposure and that at current dietary exposure levels, DNA adduct formation is negligible.

INTRODUCTION

trans-2-Hexenal is an α,β -unsaturated aldehyde that occurs in a wide range of foods being a natural constituent of fruits, vegetables, and spices [1]. Its maximum level reported in food, amounting to 76 mg/kg, was found in banana [2]. Because of its grassy fresh odor, *trans*-2-hexenal is called a “leaf aldehyde” and has been used as a flavoring agent. The estimated daily intake of *trans*-2-hexenal from food consumption is 2,390 $\mu\text{g}/\text{person}/\text{day}$ as a natural constituent and 57 $\mu\text{g}/\text{person}/\text{day}$ as a food flavoring agent [1], corresponding to 40 and 1 $\mu\text{g}/\text{kg}$ bw/day, respectively, for a 60 kg person.

The α,β -unsaturated aldehyde moiety present in *trans*-2-hexenal has been considered a structural alert for genotoxicity [1, 3]. Because of this α,β -unsaturated aldehyde moiety, *trans*-2-hexenal may react with cellular macromolecules including DNA without the need for bioactivation. Numerous in vitro studies have indicated the genotoxicity of *trans*-2-hexenal in microorganisms or mammalian cells [4-6]. However, few in vivo genotoxicity studies on *trans*-2-hexenal are available. Schuler and Eder [7], using ^{32}P -postlabeling, quantified DNA adduct formation in organs such as forestomach, liver, esophagus, and kidney after a single administration of 200 or 500 mg *trans*-2-hexenal/kg bw to male F344 rats by gavage, but DNA adduct formation was not detectable at 50 mg *trans*-2-hexenal/kg bw. Stout et al. [4] used more specific liquid chromatography tandem mass spectrometry (LC/MS/MS) for analysis of DNA adduct formation in forestomach, glandular stomach, and liver in male F344 rats. DNA adducts, namely, exocyclic 1, N^2 -propanodeoxyguanosine adducts (Hex-PdG), were quantifiable in the forestomach of animals exposed to 100 or 200 mg/kg bw/day for 1 or 4 weeks and in the liver from rats exposed to a single dose of 200 or 500 mg *trans*-2-hexenal/kg bw. It appears that DNA adduct formation occurs only at high irritating doses of *trans*-2-hexenal that are more than 3–4 orders of magnitude higher than the estimated average human dietary intake in vivo. It has been suggested that the DNA adduct formation observed at these high dose levels may not be indicative for DNA adduct formation at lower dose levels because *trans*-2-hexenal might be sufficiently detoxified at lower levels of exposure. This detoxification of *trans*-2-hexenal can proceed by three detoxification pathways in rat liver (Figure 2.1) [5]. The major pathway is conjugation with reduced glutathione (GSH), chemically or catalyzed by glutathione S-transferases (GSTs). Furthermore, aldehyde dehydrogenases (ALDHs) efficiently oxidize *trans*-2-hexenal to 2-hexenoic acid that is no longer DNA reactive. A third route includes reduction to 2-hexan-1-ol mediated by aldose reductases (ARs), which has been suggested to be less efficient than *trans*-2-hexenal oxidation or conjugation with GSH based on results from incubations with primary rat hepatocytes exposed to *trans*-2-hexenal [5].

A question that remains to be answered is whether at realistic dietary exposure levels the various α,β -unsaturated aldehydes will result in significant DNA adduct formation or whether the enzymatic processes are efficient enough to allow rapid detoxification and prevention of DNA

adduct formation. JECFA (Joint FAO/WHO Committee on Food Additives) and the Expert Panel of the FEMA (Flavor and Extract Manufacturers Association) concluded that α,β -unsaturated aldehydes including *trans*-2-hexenal do not present any safety concerns at estimated current intakes resulting from its use as a flavor based on the low level of use [1, 8]. The possible rapid detoxification of α,β -unsaturated aldehydes in vivo was specifically raised by FEMA as an argument in the establishment of GRAS (Generally Recognized as Safe) status. The European Food Safety Authority (EFSA), on the other hand, considered the α,β -unsaturated aldehyde structure to be an alert for genotoxicity, pointing out the need for especially in vivo data before any conclusions to be reached [3].

From these considerations, it becomes clear that understanding dose-dependent DNA adduct formation and detoxification in vivo is an important aspect in the safety evaluation of *trans*-2-hexenal as well as that of many other α,β -unsaturated aldehydes. The overall goal of this study was to characterize dose-dependent effects on detoxification and DNA adduct formation of *trans*-2-hexenal by developing a physiologically based kinetic and dynamic (PBK/D) model in rat, thereby contributing to obtaining insight in these important aspects in the safety evaluation of *trans*-2-hexenal as well as other α,β -unsaturated aldehydes. For the development of the PBK/D model, kinetic parameters for each detoxification pathway and DNA adduct formation were determined in vitro. Performance of the model was evaluated against available literature data on DNA adduct levels in rats exposed to high doses of *trans*-2-hexenal, with the PBK/D model enabling extrapolation to realistic dietary human exposure levels. The results obtained are discussed with respect to implications for the safety evaluation of *trans*-2-hexenal.

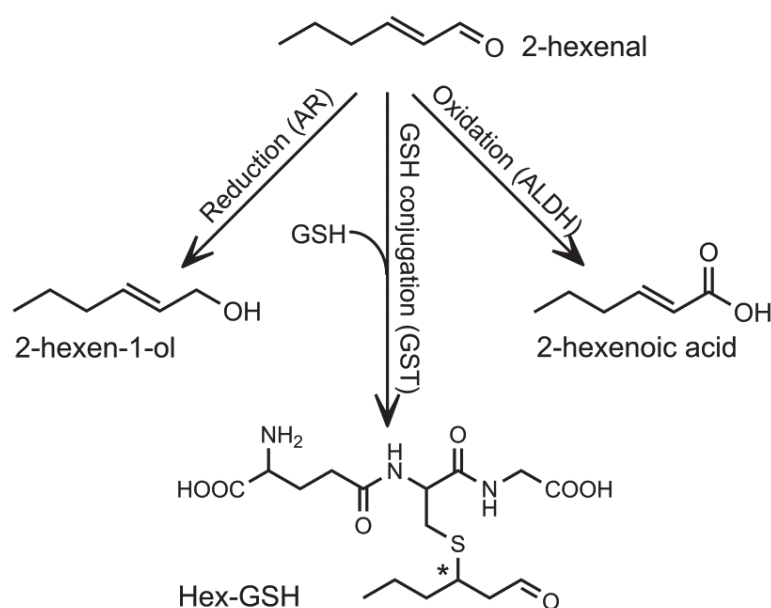


Figure 2.1 Metabolism of *trans*-2-hexenal.

MATERIALS AND METHODS

Chemicals and Biological Materials

trans-2-Hexen-1-al (*trans*-2-hexenal), *trans*-2-hexen-1-ol (2-hexen-1-ol), *trans*-2-hexenoic acid (2-hexenoic acid), 2'-deoxyguanosine monohydrate (2'-dG), diamide, tris (hydroxymethyl) aminomethane, GSH, and GSH assay kit were purchased from Sigma-Aldrich (Zwijndrecht, The Netherlands). Reduced (NADPH) and oxidized (NAD⁺) β -nicotinamide adenine dinucleotide phosphate were obtained from Roche Diagnostics (Mannheim, Germany), and dimethyl sulfoxide (DMSO) was purchased from Acros Organic (NJ). Chromatography grade acetonitrile and methanol were purchased from Biosolve (Valkenswaard, The Netherlands). Chromatography grade trifluoroacetic acid (TFA) was obtained from J. T. Baker (Deventer, The Netherlands). Pooled liver S9 from male F344 rats was obtained from BD Gentest (Worburn, United States). Rat liver mitochondrial fraction and small intestine S9 were prepared in our laboratory from individual outbred male Wistar rats purchased from Harlan (Boxmeer, The Netherlands) as described below.

Isolation of Rat Liver Mitochondrial Fraction and Small Intestine S9

Rat liver mitochondrial fraction was obtained from a male Wistar rat of 365 g to determine the kinetic constants of mitochondrial ALDHs. The rat was sacrificed by inhalation of carbon dioxide. The liver was collected immediately and stored at $-80\text{ }^{\circ}\text{C}$ until further processing. After it was thawed on ice, the liver was homogenized, and the mitochondrial fraction was isolated as described elsewhere [9]. Briefly, the homogenized liver was first centrifuged at 500g for 10 min at $4\text{ }^{\circ}\text{C}$, and the supernatant was removed. The pellet was then resuspended in ice-cold phosphate-buffered saline (PBS) and centrifuged at 10,000g for 10 min. The supernatant was removed, and the pellet was collected as mitochondrial fraction. The collected fraction was washed with PBS to examine contamination with cytosolic ALDHs. Because this additional washing step did not decrease the ALDHs capacity of the mitochondrial fraction, contamination of cytosolic ALDHs in the mitochondrial fraction was considered to be negligible. The obtained mitochondrial fraction was dissolved in PBS at 413 mg mitochondrial fraction/mL and stored at $-80\text{ }^{\circ}\text{C}$.

Rat small intestine S9 was obtained as described elsewhere [10] from a male Wistar rat of 372 g. The rat was sacrificed by inhalation of carbon dioxide. An incision was made lengthwise throughout the collected small intestine, and its mucosa was scraped off carefully. The collected mucosa was stored at $-80\text{ }^{\circ}\text{C}$ until further processing. After it was thawed on ice, the mucosa fraction was mixed with approximately 4 volumes of ice-cold PBS and homogenized using a Potter homogenizer with 15–20 strokes. The homogenized tissue was subsequently centrifuged at 9,000g for 20 min at $4\text{ }^{\circ}\text{C}$. The supernatant was transferred to new Eppendorf tubes and stored at $-80\text{ }^{\circ}\text{C}$. The protein concentration in this S9 preparation was determined by using QuantiPro BCA Assay Kit (Sigma-Aldrich).

Aldehyde Dehydrogenase (ALDH)-Mediated Oxidation of trans-2-Hexenal to 2-Hexenoic Acid

The ALDH activities are known to be present in cytosol and mitochondria [11]. Therefore, incubations were performed with rat liver S9 or rat small intestine S9, which contain tissue cytosol and microsomes [12], or rat liver mitochondrial fraction to determine the kinetic constants for ALDH-mediated oxidation in these different tissue fractions. The incubation mixtures had a final volume of 100 μL , containing (final concentrations) NAD^+ (2 mM) and liver S9 (0.2 mg protein/mL), small intestine S9 (0.34 mg protein/mL), or liver mitochondrial fraction (4.13 mg mitochondrial fraction/mL) in 0.1 M Tris-HCl (pH 7.4). After they were preincubated at 37 $^{\circ}\text{C}$ for 2 min, the reactions were started by the addition of the substrate *trans*-2-hexenal (100–1,000 μM with liver or small intestine S9, 10–500 μM with liver mitochondrial fraction) from a 100 times concentrated stock solution in DMSO. The reactions were carried out for 5 min with liver or small intestine S9 and for 3 min with liver mitochondrial fraction and then terminated by adding 50 μL of ice-cold acetonitrile. The incubation mixtures were subsequently centrifuged for 3 min at 16,000g at 4 $^{\circ}\text{C}$ to precipitate proteins. Blank incubations were performed without the cofactor NAD^+ or tissue fractions. As *trans*-2-hexenal was also oxidized spontaneously to form 2-hexenoic acid during these incubations, the amount of 2-hexenoic acid formed in blank incubations without tissue fractions was subtracted as the background.

The amount of 2-hexenoic acid in the samples was analyzed immediately after the incubation on an ultraperformance liquid chromatography with diode array detection (UPLC-DAD) system consisting of a Waters (Waters, Milford, MA) Acquity solvent manager, sample manager, and photodiode array detector, equipped with a Waters Acquity UPLC BEH C18 column (1.7 μm , 2.1 mm \times 50 mm). The gradient was made with acetonitrile and ultrapure water containing 0.1% (v/v) TFA. The flow rate was 0.6 mL/min, and a gradient was applied from 20 to 30% acetonitrile over 3 min, after which the percentage of acetonitrile was increased to 100% over 0.2 min, kept at 100% for 0.5 min, lowered to 20% over 0.2 min, and kept at these initial conditions for 1.1 min for equilibration. Under these conditions, the retention time of 2-hexenoic acid was 1.3 min. Quantification of 2-hexenoic acid was achieved by comparison of the peak areas in the chromatograms obtained at a wavelength of 210 nm to the calibration curve made using the commercially available standard.

AR-Mediated Reduction of trans-2-Hexenal to 2-Hexen-1-ol

trans-2-Hexenal was incubated with rat liver S9 to determine the kinetic constants for reduction of *trans*-2-hexenal mediated by ARs. The incubation mixtures had a final volume of 100 μL , containing (final concentrations) liver S9 (1 mg protein/mL) in 0.1 M Tris-HCl (pH 7.4). After preincubation at 37 $^{\circ}\text{C}$ for 2 min, the reaction was started by the addition of NADPH (2.5 mM) from a 20 times concentrated stock solution in 0.1 M Tris-HCl (pH 7.4) and *trans*-2-hexenal (50–500 μM) from a 100 times concentrated stock solution in DMSO. After 4 min, the reaction was

terminated by adding 50 μ L of ice-cold acetonitrile. Blank incubations were performed without cofactor NADPH or S9. The incubation mixtures were subsequently centrifuged for 3 min at 16,000g at 4 $^{\circ}$ C to precipitate proteins. The samples were frozen in dry ice immediately after the centrifugation and kept at -20 $^{\circ}$ C to prevent evaporation of 2-hexen-1-ol.

The amount of 2-hexen-1-ol was measured using a UPLC-DAD system equipped as described above. The gradient was made with acetonitrile and ultrapure water containing 0.1% (v/v) formic acid. The flow rate was 0.6 mL/min, and a gradient was applied from 0 to 10% acetonitrile over 10 min, after which the percentage of acetonitrile was increased to 100% over 0.2 min, kept at 100% for 0.5 min, lowered to 0% over 0.3 min, and kept at these initial conditions for 1 min for equilibration. Under these conditions, the retention time of 2-hexen-1-ol was 9.1 min. Quantification of 2-hexen-1-ol was achieved by comparison of the peak areas in the chromatogram obtained at a wavelength of 193 nm to the calibration curve made using the commercially available standard.

GST-Mediated GSH Conjugation of trans-2-Hexenal

Kinetic constants for GST-mediated formation of *trans*-2-hexenal GSH conjugates, namely S-[3-(1-oxohexyl)]-GSH (Hex-GSH), were determined by incubating *trans*-2-hexenal with rat liver or small intestine S9. The incubation mixture had a final volume of 100 μ L, containing (final concentrations) liver S9 (0.2 mg protein/mL) or small intestine S9 (0.64 mg protein/mL) in 0.1 M Tris-HCl (pH 7.4). After preincubation at 37 $^{\circ}$ C for 2 min, the reaction was started by the addition of GSH (5 mM) from a 10 times concentrated stock solution in 0.1 M Tris-HCl (pH 7.4) and *trans*-2-hexenal (500–5000 μ M) from a 100 times concentrated stock solution in DMSO. The reaction was carried out for 3 min with liver S9 and for 4 min with small intestine S9 and terminated by adding 50 μ L of ice-cold acetonitrile. In parallel, incubations without S9 were carried out to quantify the chemical conjugation of *trans*-2-hexenal with GSH. The samples obtained from the incubations were centrifuged for 3 min at 16,000g at 4 $^{\circ}$ C to precipitate proteins, and the resulting supernatant was analyzed by UPLC-DAD immediately after centrifugation.

The amount of Hex-GSH conjugates was measured using a UPLC-DAD system equipped as described above. The gradient was made with acetonitrile and ultrapure water containing 0.1% (v/v) TFA. The flow rate was 0.6 mL/min, and a gradient was applied from 5 to 10% acetonitrile over 2.5 min, after which the percentage of acetonitrile was increased to 100% over 0.2 min, kept at 100% for 0.5 min, lowered to 0% over 0.3 min, kept at 0% over 0.3 min, increased to 5% over 0.2 min, and kept at these initial conditions for 1 min for equilibration. With this condition, two conjugates were found at retention times of 2.2 and 2.4 min, which were absent in incubations without either GSH or *trans*-2-hexenal.

To characterize the products formed, a *trans*-2-hexenal (1 mM) incubation sample with GSH (5 mM) and liver S9 (1 mg protein/mL) and blank samples (without liver S9 or GSH) were

analyzed by LC/MS/MS with postcolumn infusion system. The LC/MS/MS system consisted of a Perkin-Elmer 200 Series HPLC System (Perkin-Elmer, Waltham, MA) coupled to an API 3000 system equipped with electrospray ionisation probe (Applied Biosystem, Foster City, CA). The flow through the analytical column was made with 0.15 mL/min ultrapure water containing 0.1% formic acid and 0.15 mL/min acetonitrile. The mass spectrometric analysis was performed in positive ion mode with the following settings: nebulizer gas, 10 psi; ion spray voltage, 5000 V; ion source temperature, 350 °C; declustering potential, 20 V; focusing potential, 250 V; entrance potential, 14 V; and collision cell exit, 15 V. Nitrogen was used as the sheath gas turbo, ion spray, with a pressure of 7000 L/h. The samples were infused postcolumn with the syringe pump at a flow rate of 1000 μ L/h. The full scan electrospray mass spectra at a collision energy of 15 eV were recorded.

For quantification of Hex-GSH, a calibration curve was prepared by reacting *trans*-2-hexenal with increasing concentrations of GSH. To this end, 10 mM *trans*-2-hexenal was incubated with increasing concentrations of GSH ranging from 50 to 500 μ M in 0.1 M Tris-HCl (pH 8.6). The reactions were performed for 60 min at 37 °C resulting in maximum formation of conjugates. The residual GSH was confirmed to be negligible by using a GSH assay kit (Sigma-Aldrich, Zwijndrecht, The Netherlands). The peak area of two conjugates at wavelength 210 nm in the UPLC chromatograms was summated and related to the quantity of GSH used in the reactions.

Kinetic Analysis

The data for the rate of formation of 2-hexenoic acid and 2-hexen-1-ol with increasing *trans*-2-hexenal concentration were fitted to the standard Michaelis–Menten equation with [S] being the substrate concentration:

$$v = V_{\max} \times [S] / (K_m + [S])$$

The GSH and *trans*-2-hexenal concentration-dependent rate of Hex-GSH formation catalyzed by GSTs was fitted to a two-substrate model Michaelis–Menten equation simulating the ordered sequential ping–pong mechanism [13, 14], with [GSH] and [S] being GSH and *trans*-2-hexenal concentrations, respectively:

$$v = V_{\max} \times [S] \times [\text{GSH}] / (K_{m_H} \times [\text{GSH}] + K_{m_G} \times [S] + [S] \times [\text{GSH}])$$

The apparent maximum velocities (V_{\max}) and the apparent Michaelis–Menten constants (K_m) were determined by fitting the data to the respective equations using GraphPad Prism (version 5.04, GraphPad Software, Inc., La Jolla, CA).

Rate Constant for Nonenzymatic GSH Conjugation to trans-2-Hexenal

The second-order rate constant for the nonenzymatic conjugation of GSH to *trans*-2-hexenal was determined based on a method described by Potter and Tran [15]. Briefly, the time-dependent conjugation between *trans*-2-hexenal and GSH was examined by incubating 0.2 mM *trans*-2-hexenal with 0.5 mM GSH in 0.1 M Tris-HCl (pH 7.4) for 0–30 min at 37 °C. The

reaction was initiated by the addition of *trans*-2-hexenal from a 100 times concentrated stock solution in DMSO and was terminated by adding 4 mM diamide (final concentration) from a 5 times concentrated stock solution in 0.1 M Tris-HCl (pH 7.4). The Hex-GSH formed was quantified immediately after the incubation as described above. The rate constant obtained for the reaction between *trans*-2-hexenal and GSH was also used to describe the second-order rate constant for the reaction between *trans*-2-hexenal and protein reactive sites in the liver and small intestine (see *PBK/D Model Structure*).

Rate Constant for Binding of trans-2-Hexenal to 2'-dG

The second-order rate constant for binding of *trans*-2-hexenal to 2'-dG was determined by examining the time-dependent formation of exocyclic 1,*N*²-propanodeoxyguanosine adducts (Hex-PdG). *trans*-2-Hexenal (25 mM) was reacted with 2'-dG (1.95 mM) in 0.1 M Tris-HCl (pH 7.4) for 0–40 min at 37 °C. After 2 min of preincubation, the reaction was started by adding *trans*-2-hexenal from a 40 times concentrated stock in DMSO. The reaction was terminated by injecting the reaction mixture to the UPLC-DAD system equipped as described above for quantification of the Hex-PdG formed. The gradient was made with acetonitrile and ultrapure water containing 0.1% (v/v) TFA. The flow rate was 0.6 mL/min, and a gradient was applied from 8.5 to 10% acetonitrile over 5 min, after which the percentage of acetonitrile was increased to 100% over 0.2 min, kept at 100% for 0.3 min, lowered to 0% over 0.2 min, kept at 0% over 0.3 min, increased to 8.5% over 0.2 min, and equilibrated at these initial conditions for 0.5 min. Under these conditions, two conjugates were found at retention times of 2.6 and 2.8 min, which were absent in the blank incubations without either *trans*-2-hexenal or 2'-dG. These peaks had the same UV spectra as those of Hex-PdG reported previously [7].

Because the UV absorption pattern of Hex-PdG is comparable to that of 2'-dG [7], they were assumed to have the same molecular extinction coefficient at the respective wavelength of maximum absorption. Quantification of Hex-PdG was achieved by comparison of the peak area of Hex-PdG obtained in UPLC-DAD analysis to the calibration curve of 2'-dG, each at their respective absorption maximum, which amounted to 262 nm for Hex-PdG and 252 nm for 2'-dG.

PBK/D Model Structure

A schematic diagram of the PBK/D model developed is shown in Figure 2.2, and the mass balance equations including a list of abbreviations used in the equations can be found as Supporting Information. The final model includes separate compartments for the liver and small intestine, which were both involved in the metabolism of *trans*-2-hexenal (see *Results*). A separate compartment for fat tissue was included to take into account the relatively higher partition coefficient of *trans*-2-hexenal in fat tissue. All other tissues were lumped into a rapidly perfused tissue group, comprising tissues such as adrenals, brain, and heart, and a slowly perfused tissue group, comprising tissues such as muscle and skin [16]. The uptake of *trans*-2-hexenal from the

intestinal cavity into the small intestine compartment was described by a first-order process. The absorption rate constant (K_a) was set to 5.0 h^{-1} based on the value used for uptake of acrylamide in a PBK model for acrylamide and its metabolite glycidamide [17], resulting in a rapid absorption of *trans*-2-hexenal from the gastrointestinal cavity. On the basis of the in vitro kinetic data conversion of *trans*-2-hexenal to 2-hexenoic acid and GSH conjugates (Hex-GSH) mediated by ALDHs and GSTs, respectively, was described in the liver and small intestine compartments, whereas conversion of *trans*-2-hexenal to 2-hexen-1-ol by ARs was described in the liver compartment only. The kinetic constants for the enzymatic metabolite formations were determined in vitro in the present study. The V_{\max} values for the different pathways in the liver, expressed as $\text{nmol}/\text{min}/(\text{mg S9 protein})$, were scaled to the liver using a S9 protein yield of 143 mg/g liver as scaling factor as derived previously based on the cytosolic and microsomal protein yield [18]. The V_{\max} values for the different metabolic pathways in the small intestine were scaled accordingly using an estimated S9 protein yield of $11.4 \text{ mg/g small intestine}$ as scaling factor [10]. The V_{\max} values for the formation of 2-hexenoic acid in the liver mitochondrial fraction were scaled using a mitochondrial fraction yield of $269 \text{ mg mitochondrial fraction/g liver}$ as scaling factor, which was determined in the present study. The chemical reaction of *trans*-2-hexenal with GSH and protein was included in both the liver and the small intestine compartment. Hex-PdG, the DNA adduct of *trans*-2-hexenal, was described to be formed chemically in the liver. The second-order rate constants of the reactions between *trans*-2-hexenal with GSH or 2'-dG (k_{GSH} and k_{DNA}) were determined in vitro in this study. The reaction of *trans*-2-hexenal with protein in the liver and small intestine was also described by second-order kinetics with a rate that depends on the concentration of *trans*-2-hexenal and of protein reaction sites in the tissue [19]. The second-order rate constant for this reaction, k_{PRO} , was set to the same value as k_{GSH} , based on previous studies [15, 19]. In a study by Potter and Tran [15], second-order rate constants for conjugation of ethyl acrylate, an α,β -unsaturated ether, and protein reactive sites were determined for tissue homogenates from different organs, which each consisted of a mixture of different protein. The second-order rate constants for the reaction of ethyl acrylate with GSH, or with liver or small intestine protein reactive sites were found to be 33, 33, and 32 M/min , respectively, revealing these values to be comparable. On the basis of this observation, in the present study, the second-order rate constant for the reaction between *trans*-2-hexenal and GSH was assumed to also adequately describe the second-order rate constant for the reaction between *trans*-2-hexenal and tissue proteins. For the different metabolites including 2-hexenoic acid, 2-hexen-1-ol, and Hex-GSH, only the formation was taken into account, and no further conversion of these metabolites was modeled. Furthermore, distribution of these metabolites in the body was not taken into account, since this would not affect the ultimate predictions for the detoxification of *trans*-2-hexenal or its binding to DNA.

Equations to describe GSH levels in the liver or small intestine were integrated in the PBK/D model to quantitate the dose-dependent *trans*-2-hexenal-induced depletion of GSH. GSH

was divided into cytosolic and mitochondrial pools since the mitochondrial GSH pool, which usually accounts for 10% of GSH in the liver, is known to be well sequestered and to have a very long half-life as compared to the cytosolic pool that can be depleted more easily [20]. In the model, the mitochondrial GSH pool was therefore not subject to *trans*-2-hexenal-induced GSH depletion, and it only contributed to the total concentration of GSH in the tissue [14]. The reactions reflecting biosynthesis and degradation of GSH due to its regular cellular turnover were described by zero-order production and first-order elimination as described elsewhere [14, 19, 21]. The first-order elimination constant of GSH in a tissue (k_{GLOS_Ti}) and the zero-order GSH synthesis rate constant ($GSYN_{Ti}$) were derived from Potter and Tran [21]. Ninety percent of the synthesized GSH was described to be directed to cytosol, while the rest is used to maintain the GSH levels in mitochondria.

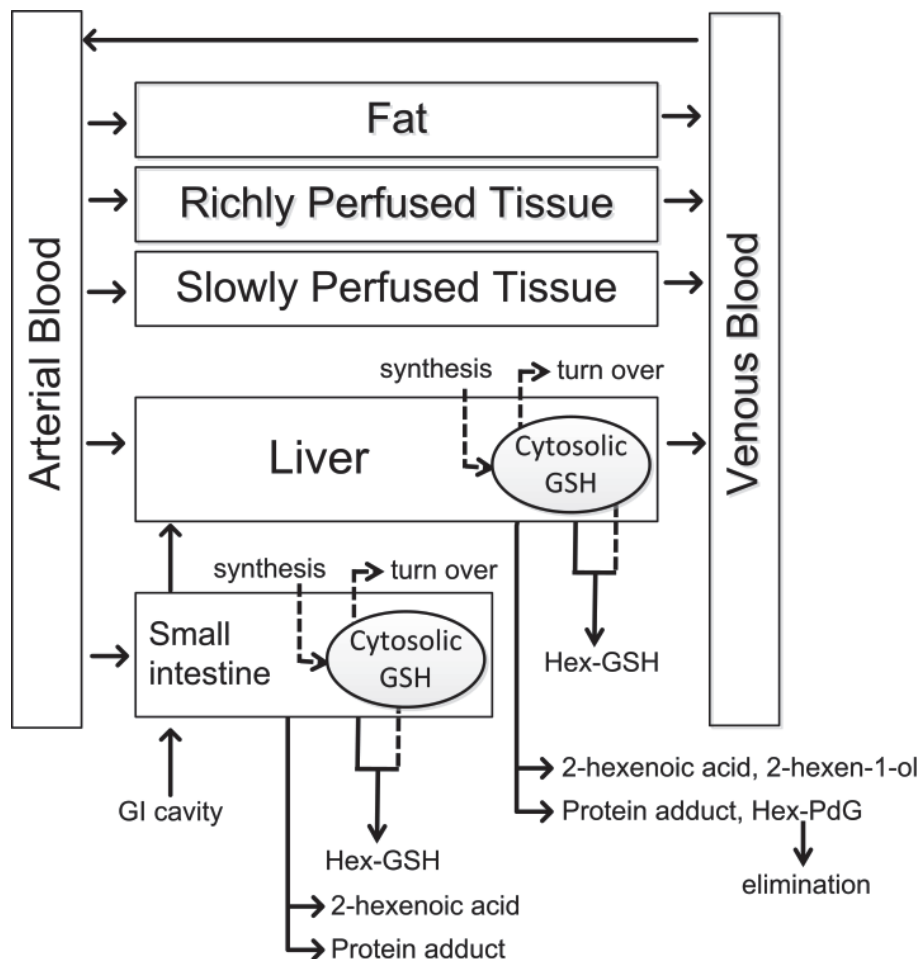


Figure 2.2 Diagram of the proposed PBK/D model for *trans*-2-hexenal in rat. Solid and dashed lines represent the movement of *trans*-2-hexenal and GSH respectively.

The amount of Hex-PdG in the liver was described by second-order formation and first-order elimination due to DNA repair. The half-life of Hex-PdG in the liver ($T_{1/2}$) was derived from data obtained in an in vivo study where a time-dependent decrease of Hex-PdG in the liver of male F344 rats was measured after the animals were exposed to high amount of *trans*-2-hexenal by gavage [7] (see the Results).

The physiological parameters such as organ volumes and blood flows were obtained from the literature [22]. Partition coefficients were estimated from the $\log K_{ow}$ based on a method of DeJongh et al. [23] (Table 2.1). The $\log K_{ow}$ value for *trans*-2-hexenal was estimated with Estimation Program Interface (EPI) Suite version 4.10 provided by the U.S. Environmental Protection Agency and amounted to 1.58. Model equations were coded and numerically integrated in Berkeley Madonna 8.3.18 (Macey and Oster, UC Berkeley, CA), using the Rosenbrock's algorithm for stiff systems.

Sensitivity Analysis

To identify the key parameters that influence the model output the most, a sensitivity analysis was performed. Normalized sensitivity coefficients (SC) were determined according to the following equation: $SC = (C' - C) / (P' - P) \times (P / C)$, where C is the initial value of the model output, C' is the modified value of the model output resulting from an increase in parameter value, P is the initial parameter value, and P' is the modified parameter value [18, 24-26]. On the basis of the literature, a 5% increase in parameter values was chosen, to analyze the effect of a change in parameter on the formation of Hex-PdG in liver [24]. Each parameter was analyzed individually, keeping the other parameters to their initial values.

Table 2.1 Physico-chemical and physiological parameters used in the PBK/D model for *trans*-2-hexenal in rat

Parameters	Symbols	Values	Parameters	Symbols	Values
Physico-chemical Parameters			Blood flow to tissue (% cardiac output) [22]		
fat/blood	PF	9.92	fat	QFc	7.0
liver/blood	PL	1.11	liver (excluding portal vein fraction)	QLc	13.2
small intestine/blood	PSi	1.11	small intestine	QSiC	11.8
richly perfused tissues/blood	PR	1.11	richly perfused	QRc	51.0
slowly perfused tissues/blood	PS	0.55	slowly perfused	QSc	17.0
Physiological Parameters			Initial GSH concentration ($\mu\text{mol/kg}$ tissue) [21]		
Body weight (kg) [22]	BW	0.25	liver	InitGSH _L	6120
Tissue volumes (% body weight) [22]			small intestine	InitGSH _{Si}	1780
fat	VFc	7.0	GSH synthesis ($\mu\text{mol/kg}$ tissue/h) [21]		
liver	VLc	3.4	liver	GSYN _L	869
small intestine	VSiC	1.4	small intestine	GSYN _{Si}	78
arterial blood	VAc	1.85	Apparent first order rate constant for GSH turnover (/h) [21]		
venous blood	VVc	5.55	liver	k_{L_GLOS}	0.142
richly perfused	VRc	4.2	small intestine	k_{Si_GLOS}	0.044
slowly perfused	VSc	67.6	Protein reactive sites ($\mu\text{mol/kg}$ tissue) [15]		
Cardiac output (L/h) [22, 27]	QC	5.4	liver	CPRO _L	5319
			small intestine	CPRO _{Si}	245

RESULTS

Enzymatic Oxidation and Reduction of trans-2-Hexenal

UPLC analysis of incubations of *trans*-2-hexenal in the presence of rat liver or small intestine S9 fractions, which contain both the microsomal and the cytosolic fraction of the cells and NAD^+ as a cofactor, showed that rat liver and small intestine S9 convert *trans*-2-hexenal to 2-hexenoic acid. The peak at retention time 1.3 min was confirmed to be 2-hexenoic acid on the basis of comparison of its UV spectrum and retention time to those of the commercially available standard compound. Conversion of *trans*-2-hexenal to 2-hexenoic acid was also observed in incubations with the mitochondrial fraction derived from male Wistar rat liver. Figure 2.3A shows the rate of formation of 2-hexenoic acid in incubations with the rat liver S9 or mitochondrial fraction or with

small intestine S9 with increasing concentrations of *trans*-2-hexenal. From these curves, assuming first-order Michaelis–Menten kinetics, the apparent kinetic parameters (K_m and V_{max}) of *trans*-2-hexenal oxidation by the different tissue fractions were determined and are presented in Table 2.2.

Conversion of *trans*-2-hexenal to 2-hexen-1-ol occurred in the incubations with rat liver S9 in the presence of NADPH, whereas no formation of 2-hexen-1-ol was observed in incubations with small intestine S9. The peak at retention time 9.1 min was confirmed to be 2-hexen-1-ol on the basis of comparison of its UV spectrum and retention time to those of the commercially available standard compound. Figure 2.3B shows the rate of formation of 2-hexen-1-ol in incubations with rat tissue fractions and increasing concentrations of *trans*-2-hexenal. From these curves, assuming first-order Michaelis–Menten kinetics, the apparent kinetic parameters (K_m and V_{max}) for *trans*-2-hexenal reduction were determined and are presented in Table 2.2.

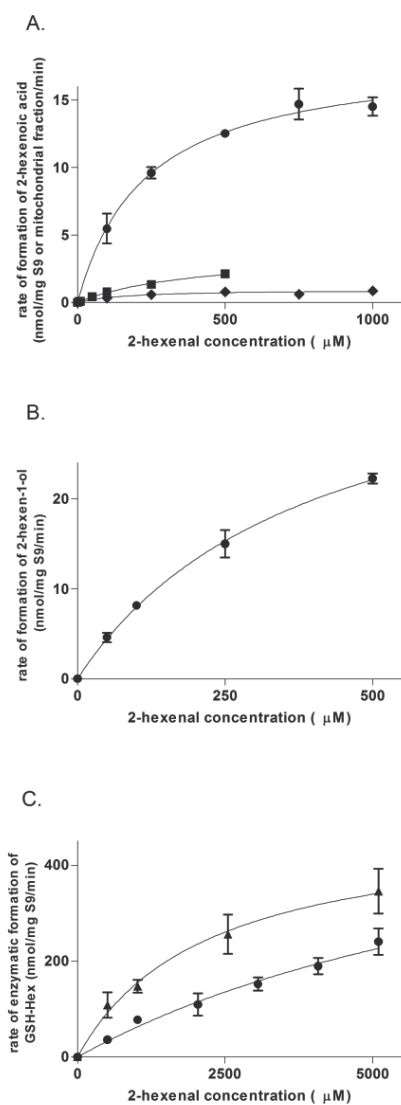


Figure 2.3. *trans*-2-Hexenal concentration dependent rate of formation of metabolites by rat tissue fractions. Formation rate of (A) 2-hexenoic acid by rat liver S9 (●), liver mitochondrial fraction (■), or by rat small intestine S9 (◆), (B) 2-hexen-1-ol by rat liver S9 and (C) Hex-GSH by rat liver (●) and small intestine S9 (▲).

GST-Mediated Conjugation of trans-2-Hexenal with GSH

trans-2-Hexenal is known to react with GSH to form GSH conjugates. UPLC analysis revealed that two conjugates are formed (conjugate 1 and conjugate 2) when *trans*-2-hexenal is incubated with a physiologically relevant concentration of GSH (5 mM) at 37 °C in the absence of tissue fractions. The addition of liver or small intestine S9 to these incubations appeared to increase the formation of conjugate 1 but not of conjugate 2, suggesting GSTs of these organs to be involved only in the formation of conjugate 1. The incubation samples were also analyzed by electrospray mass spectrometry to characterize the conjugates formed. Full-scan electrospray mass spectra showed higher levels of formation of ions at *m/z* 406 in the incubation sample of *trans*-2-hexenal with GSH in the presence of rat liver S9 than in incubations without S9. The *m/z* 406 corresponds to the [M + H]⁺ value expected for protonated Hex-GSH [5]. The ion at *m/z* 406 was absent in the blank incubation without GSH. MS/MS of the protonated molecule [M + H]⁺ established the ions at *m/z* 259 and 331 as arising from *m/z* 406 by loss of 147 and 75, which can be ascribed to the loss of glutamic acid and glycine, respectively, corroborating that the ion at *m/z* 406 contains a GSH moiety. Because chemical conjugation of GSH to an α,β -unsaturated aldehyde will result in a set of stereoisomers [28], conjugate 1 and conjugate 2 were concluded to be a set of stereochemical product at C3 position of Hex-GSH (see Figure 2.1 for the structure).

Table 2.2 Kinetic parameters for metabolism of *trans*-2-hexenal

Metabolite	$K_m^{a,b}$	V_{max}^a	Scaled V_{max}^e	In vivo catalytic efficiency ^f
<i>liver S9 fraction</i>				
Hex-GSH	9247 ± 5237	649 ± 265 ^c	92807	10.0
2-hexenoic acid	230 ± 45	18.5 ± 1.1 ^c	2646	11.5
2-hexen-1-ol	400 ± 70	39.9 ± 3.8 ^c	5706	14.3
<i>liver mitochondria fraction</i>				
2-hexenoic acid	410 ± 88	3.8 ± 0.5 ^d	1022	2.5
<i>small intestine S9 fraction</i>				
Hex-GSH	2172 ± 869	496 ± 87 ^c	5674	2.6
2-hexenoic acid	156 ± 116	0.95 ± 0.18 ^c	10.9	0.07

^aMean ± SD. ^bμM. ^cnmol/min/(mg S9 protein). ^dnmol/min/(mg mitochondria fraction). ^e V_{max} scaled to a tissue expressed as nmol/min/(g tissue). Scaling factors of 143, 35 and 11.4 mg/(g tissue) were used for the liver S9, liver mitochondria and the small intestine S9 fraction respectively. ^fScaled V_{max}/K_m expressed as mL/min/(g tissue)

Further kinetic analysis of GST-mediated *trans*-2-hexenal GSH conjugation focused on the formation of conjugate 1. The reaction was assumed to follow ping-pong kinetics described by a two substrate Michaelis-Menten equation. The required K_m toward GSH (K_{m, Ti_GST_G}) was set at 100 μM in the liver and small intestine being a representative value obtained in kinetic studies on GSTs using different substrates [13, 14]. V_{max} and K_m toward *trans*-2-hexenal (K_{m, Ti_GST_H}) for the GST-mediated formation of Hex-GSH were determined in vitro by using a

physiologically relevant concentration of GSH (5 mM) and increasing concentrations of *trans*-2-hexenal. The amount of Hex-GSH (conjugate 1) formed in the enzymatic incubations was corrected for the amount of Hex-GSH (conjugate 1) formed due to the chemical reaction as determined in incubation without tissue fractions. Figure 2.3C shows the rate of formation of Hex-GSH (conjugate 1) in incubations with rat liver and small intestine S9 and increasing concentrations of *trans*-2-hexenal. From these sets of data, assuming the GST reactions follow ping-pong kinetics, the apparent kinetic parameters [K_m toward *trans*-2-hexenal (K_{m, Ti_GST_H}) and V_{max}] for GST-mediated *trans*-2-hexenal conjugation with GSH were determined and are presented in Table 2.2.

Comparison of the Catalytic Efficiency of Different trans-2-Hexenal Detoxification Pathways

Table 2.2 presents a summary of the kinetic parameters (V_{max} and K_m) for *trans*-2-hexenal detoxification by rat tissue fractions. To make the parameters comparable, the V_{max} values of oxidation, reduction, and GSH conjugation expressed as nmol/min/(mg S9 protein) or nmol/min/(mg mitochondrial pellet) were converted to nmol/min/(g tissue) by using scaling factors. The in vivo catalytic efficiencies derived from the liver S9 incubations expressed per gram liver tissue for oxidation and reduction of *trans*-2-hexenal were 1.2 and 1.4 times the catalytic efficiencies for GST-mediated conversion, respectively, which indicates that for liver S9 formation of 2-hexen-1-ol is the most efficient pathway followed by formation of 2-hexenoic acid and Hex-GSH. The catalytic efficiencies derived from the incubations with small intestine S9 and liver mitochondrial fraction were calculated to be 1–3 orders of magnitude lower than those obtained for liver S9, indicating that in male rat the major enzymatic conversion of *trans*-2-hexenal, when orally ingested, will occur in the liver.

Nonenzymatic Binding of trans-2-Hexenal to 2'-dG, GSH, and Protein

trans-2-Hexenal is known to chemically react with nucleophilic macromolecules including DNA, GSH, and protein, resulting in covalent adducts. To integrate these reactions into the model, the second-order rate constants for the reaction of *trans*-2-hexenal with 2'-dG or GSH were measured based on in vitro incubations at physiological pH. UPLC analysis of incubations of *trans*-2-hexenal with GSH showed two peaks, which were absent in blank incubations performed without either *trans*-2-hexenal or GSH. The areas of these two peaks measured at their absorption maximum (199 nm) were comparable, and both increased with increasing concentrations of *trans*-2-hexenal or GSH. On the basis of these facts, it was concluded that the two peaks represent a set of stereoisomers of *trans*-2-hexenal GSH conjugates, and the summation of the two peaks was used to determine the second-order rate constant for the reaction of *trans*-2-hexenal with GSH, which was found to amount to 5.8×10^{-4} / μ M/h. This value was also used as the second-order rate constant for the reaction of *trans*-2-hexenal with tissue protein in the liver and small intestine in line with the assumptions described elsewhere (see PBK/D Model Structure)

[15, 19]. The *trans*-2-hexenal adducts with 2'-dG are known to consist of a set of two diastereomers (Hex-PdG) (Figure 2.4A) [29]. When *trans*-2-hexenal was chemically reacted with 2'-dG, no clear difference was observed in the amount formed between the diastereomers (Figure 2.4B). The rate constant for the reaction of *trans*-2-hexenal with 2'-dG to form the diastereomers was determined to be 1.6×10^{-7} / $\mu\text{M}/\text{h}$. Comparison of this second-order rate constant for 2'-dG adduct formation to that for GSH adduct formation reveals that chemical reaction of *trans*-2-hexenal with GSH is more than 1,000 times faster than with 2'-dG. This was well expected as electrophile reactivity of *trans*-2-hexenal was reported to be higher with thiol moieties, which are soft nucleophiles than with amine groups that are hard nucleophiles [30].

DNA Adduct Elimination by DNA Repair

DNA adduct formed in the liver was assumed to be reversible due to DNA repair. A half-life of DNA adducts ($T_{1/2}$) was determined based on a study by Schuler and Eder [7] where male F344 rats were exposed to 500 mg *trans*-2-hexenal/kg bw by gavage and Hex-PdG in the liver was quantified at 24, 48, and 96 h after the dosing by using ^{32}P -postlabeling. Assuming first-order elimination of the Hex-PdG after the amount of Hex-PdG reached the highest level at 48 h after the dosing, the half-life of DNA adducts in the liver was estimated by fitting an exponential curve to the reported data and was thus determined to be 38.5 h.

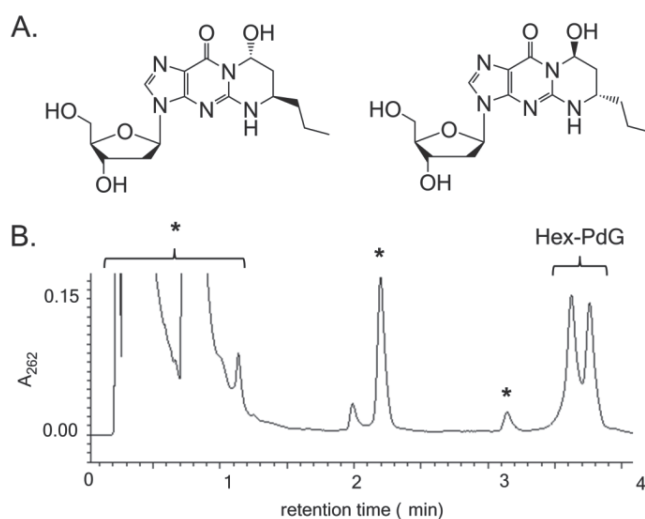


Figure 2.4. Molecular structures of Hex-PdG [7] (A) and a typical UPLC chromatogram of an incubation of *trans*-2-hexenal (86.2 mM) and 2'-dG (10.5 mM) (B). Peaks marked with an asterisk were also present in the blank incubations performed without either 2'-dG or *trans*-2-hexenal.

Performance of the PBK/D Model

With the kinetic constants obtained, the PBK/D model was constructed, which enables prediction of *trans*-2-hexenal detoxification, as well as formation and subsequent elimination of *trans*-2-hexenal DNA adducts (Hex-PdG) in the liver. To evaluate the performance of the PBK/D model, predicted Hex-PdG levels in the liver were compared with in vivo data derived from literature [4, 7]. In the in vivo studies available, DNA adduct levels were quantified in the liver of male F344 rats exposed by gavage to a single dose of 200 or 500 mg *trans*-2-hexenal/kg bw 48 h after the exposure by using ^{32}P -postlabeling [7] or 24 h after dosing by LC/MS/MS [4]. The level

of DNA adducts reported by Stout et al. was 2 orders of magnitude lower than the levels obtained by Schuler and Eder, which may in part be due to the different analytical methods used or the different study design with respect to whether animals were possibly fasted [7] or not [4]. The Hex-PdG level at 200 and 500 mg *trans*-2-hexenal/kg bw was predicted by the PBK/D model to amount to 101 and 580 Hex-PdG/10⁸ nucleotides (nt) after 24 h and 65 and 377 Hex-PdG/10⁸ nt after 48 h, respectively (Table 2.3). At a dose of 200 mg *trans*-2-hexenal/kg bw, the predicted value was 4.1-fold higher than the value reported by Schuler and Eder but 3 orders of magnitude higher than the value reported by Stout et al. Also at 500 mg/kg bw, the discrepancy between the predicted and the observed value of Stout et al. was 3 orders of magnitude, whereas at this dose level the predicted value was only 2.1-fold higher than the value of 179 adducts/10⁸ nt reported by Schuler and Eder.

Table 2.3 Predicted and observed formation of DNA adduct (Hex-PdG) in the liver of a rat after *trans*-2-hexenal exposure

Dose and time point of DNA adduct quantification after dosing	Predicted (adducts/10 ⁸ nt) ^a	In vivo data (adducts/10 ⁸ nt)
200 mg/kg bw, 24h [4]	101	0.2 ^b
500 mg/kg bw, 24h [4]	580	0.099 ^b
200 mg/kg bw, 48h [7]	65	16 ± 12 ^c
500 mg/kg bw, 48h [7]	376	179 ± 52 ^c

^aPredicted amount of Hex-PdG in the liver in μmol was converted to adducts/10⁸ nt by using a DNA content of 1.8 mg/(g liver) [31] and the average molecular weight of four nucleotides (adenine, guanine, cytosine, thymine) of 330. ^bThe value in fmol/(μg DNA) was converted to adducts/10⁸ nt by using the average molecular weight of nucleotides of 330. ^cMean ± SD.

The model was also evaluated by comparison of the predicted extent of GSH adduct formation to in vivo data for excretion of mercapturic acids for male Wistar rats exposed to 2-propenal (acrolein) or 4-hydroxy-2-nonenal, which are comparable α,β -unsaturated aldehydes [32, 33]. To make the predicted values comparable to the in vivo data, the amount of α,β -unsaturated aldehyde conjugates with GSH formed in the liver was assumed to be equal to the mercapturic acids excreted in the urine. In the case of 2-propenal, excretion of mercapturic acid conjugates has been reported to be 10–32% of the dose in male Wistar rats at dose levels ranging from 0.47 to 4.0 mg 2-propenal/kg bw [32]. Because these rats were exposed via intraperitoneal injection, the PBK/D model, which was made to model oral dosing, was modified to model intraperitoneal dosing to allow comparison. To this end, the V_{max} of the detoxification pathways in the small intestine compartment were all set to zero so that *trans*-2-hexenal reaches the liver without being enzymatically converted in the small intestine compartment. The modified model predicted 27% of the α,β -unsaturated aldehyde to be converted to GSH conjugates at a dose level up to 71 $\mu\text{mol}/\text{kg}$ bw (c.a. 7.0 mg *trans*-2-hexenal/kg bw and 4.0 mg 2-propenal/kg bw). In the

case of 4-hydroxy-2-nonenal [33], excretion of mercapturic acid conjugates has been reported to be $27 \pm 5\%$ of the applied intravenous dose of $3.5 \mu\text{g}/\text{kg}$ bw in male Wistar rats after 48 h. At comparable conditions, taking into account intravenous exposure, the model predicted 43% formation of GSH conjugates at this level of exposure. Another study on 4-hydroxy-2-nonenal [34] reported 5.4% excretion as known mercapturic acid conjugates in male Wistar rats exposed to $25 \mu\text{g}/\text{kg}$ bw of 4-hydroxy-2-nonenal via intraperitoneal injection within 12 h. After adjusting the model for intraperitoneal injection the PBK/D model predicted 27% formation of GSH conjugates at this level of exposure.

Sensitivity Analysis

A sensitivity analysis was performed to identify key parameters that mostly determine the amount of Hex-PdG in the liver 24 h after the exposure. Normalized SCs were calculated for all parameters at *trans*-2-hexenal doses of $0.04 \text{ mg}/\text{kg}$ bw, a level that corresponds to the average human dietary exposure, and $200 \text{ mg}/\text{kg}$ bw, a level at which DNA adduct formation in the liver was reported in rats [4, 7]. The parameters for which the $|\text{SC}|$ exceeded 0.1 are shown in Figure 2.5. The results obtained reveal that the levels of Hex-PdG in the liver are influenced significantly by parameters that determine the formation and elimination rate of Hex-PdG, such as the second-order rate constant for the reaction of *trans*-2-hexenal with 2'-dG (k_{DNA}) and the half-life of the DNA adducts ($T_{1/2}$). Parameters determining the *trans*-2-hexenal catalytic detoxification rate in the liver such as V_{max} for oxidation or reduction by liver S9 ($V_{\text{max, LS9_HA}}$ and $V_{\text{max, LS9_HO}}$) and the scaling factor for liver S9 (S9PL) were found to have a considerable higher impact on the level of Hex-PdG at $200 \text{ mg } trans\text{-2-hexenal}/\text{kg}$ bw than at $0.04 \text{ mg}/\text{kg}$ bw, while those determining the detoxification rate in the small intestine such as V_{max} for GST-mediated *trans*-2-hexenal conjugation with GSH ($V_{\text{max, Si_GST}}$) and the scaling factor of small intestine S9 (S9PSi) have a greater influence on the Hex-PdG level at $0.04 \text{ mg } trans\text{-2-hexenal}/\text{kg}$ bw than at $200 \text{ mg}/\text{kg}$ bw.

Model Predictions

Figure 2.6 shows the time-dependent predicted liver concentrations of *trans*-2-hexenal (Figure 2.6A and 2.6B), and the GSH concentrations in the liver and small intestine in male rat (Figure 2.6C and 2.6D) upon exposure to $0.04 \text{ mg}/\text{kg}$ bw, a level that corresponds to the average human dietary exposure (Figure 2.6A and 2.6C), or $200 \text{ mg}/\text{kg}$ bw *trans*-2-hexenal (Figure 2.6B and 2.6D) at which DNA adduct formation in the liver was reported in rats [4, 7]. The predicted time-dependent *trans*-2-hexenal concentration in the liver showed that the *trans*-2-hexenal concentration reached a maximum value around 0.14 and $187 \mu\text{M}$ at a dose of 0.04 and $200 \text{ mg}/\text{kg}$ bw, respectively (Figure 2.6A and 2.6B). At both dose levels, *trans*-2-hexenal is fully converted within 3 h after dosing; therefore, no accumulation of *trans*-2-hexenal in the intestine or liver is expected if a rat would be exposed repeatedly to the same amount of *trans*-2-hexenal at 24

h intervals. The results also indicated that at a dose of 0.04 mg/kg bw, the GSH level of both liver and small intestine is not affected to a significant extent (Figure 2.6C). At a dose of 200 mg *trans*-2-hexenal/kg bw, the GSH concentration in the small intestine dropped rapidly and amounted to only 65% of the initial level after 24 h (Figure 2.6D). In contrast, GSH levels in the liver were predicted to be depleted but restored within 24 h upon dosing at 200 mg/kg bw. Thus, protective levels of GSH are predicted to be unaffected at low doses, whereas the model predicted that at high dose levels significant depletion of GSH occurs, with the incomplete recovery of GSH levels in the small intestine after 24 h pointing at possible exacerbation of the effect if the same amount of 200 mg of *trans*-2-hexenal would be dosed to the animal after a 24 h interval.

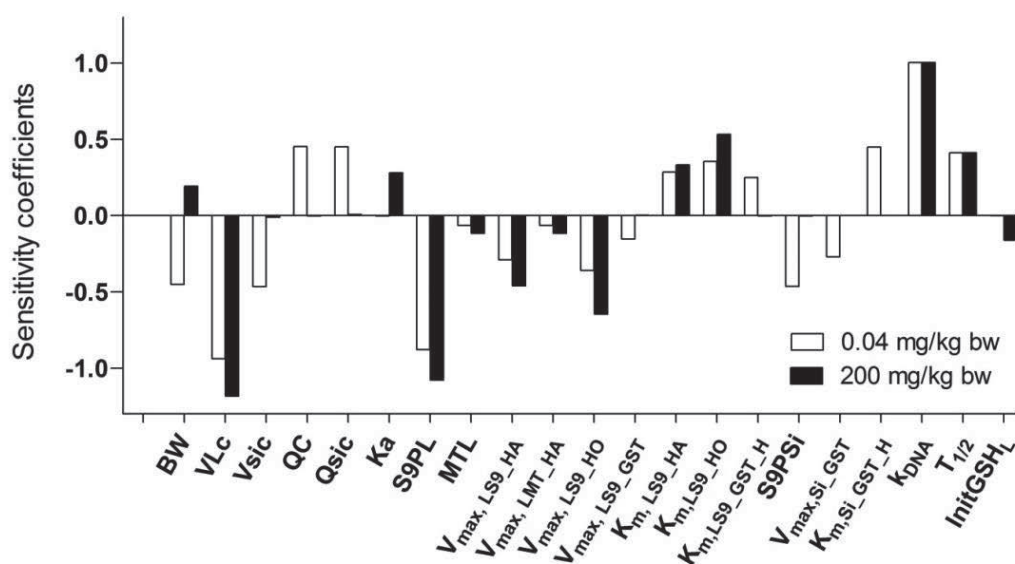


Figure 2.5. Sensitivity of the predicted amount of Hex-PdG in the liver to different model parameters at 24 hours after the exposure. White bars correspond to the normalized sensitivity coefficients at a dose of 0.04 mg/kg bw and black bars at a dose of 200 mg/kg bw. The parameters listed include : body weight (BW); fraction of liver (VLc) and small intestine (VSic); blood flow rates (Qc); fraction of blood flow to small intestine (QSic); linear uptake rate of *trans*-2-hexenal (Ka); scaling factor of liver S9 (S9PL), liver mitochondrial fraction (MTL) and small intestine S9 (S9PSi); V_{max} and K_m measured with liver S9 (LS9), liver mitochondrial fraction (LMT) or small intestine S9 (Si) to form 2-hexenoic acid (HA) or 2-hexen-1-ol (HO); V_{max} to form Hex-GSH measured with liver S9 ($V_{max, LS9_GST}$) or small intestine S9 (V_{max, SI_GST}); K_m toward *trans*-2-hexenal to form Hex-GSH measured with liver S9 ($K_{m, LS9_GST_H}$) or with small intestine S9 (K_{m, SI_GST_H}); second-order rate constant of *trans*-2-hexenal binding to 2'-dG (k_{DNA}); half-life of DNA adduct in the liver ($T_{1/2}$); and initial GSH concentration in the liver (InitGSH_L).

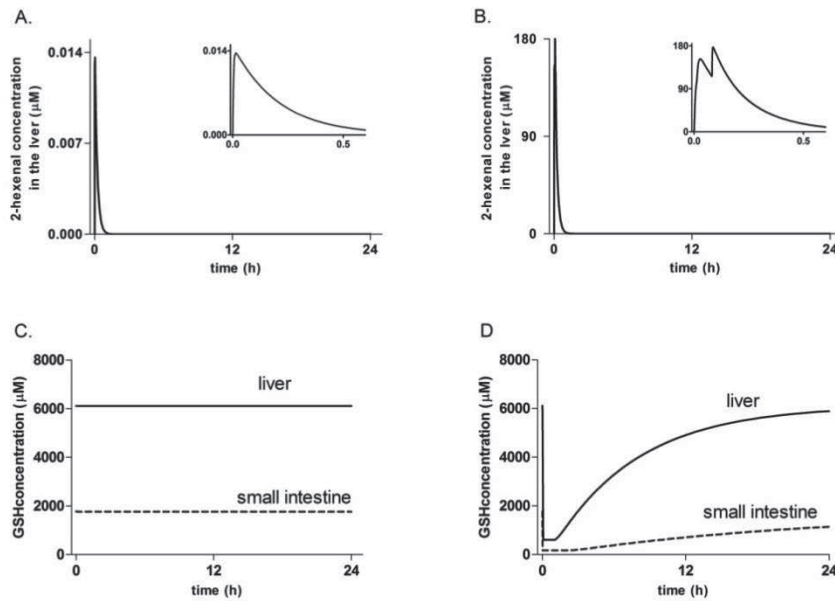


Figure 2.6. Time dependent PBK/D model predicted concentrations of (A and B) *trans*-2-hexenal in the liver, and (C and D) GSH in the liver (solid line) and small intestine (dashed line) following exposure to 0.04 mg/kg bw (A and C) or 200 mg/kg bw (B and D) of *trans*-2-hexenal.

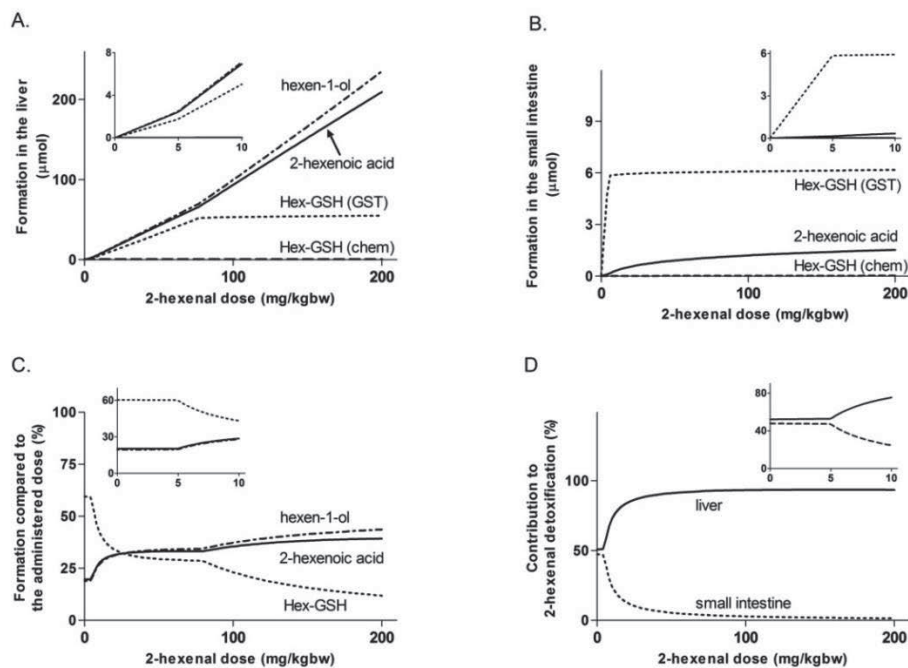
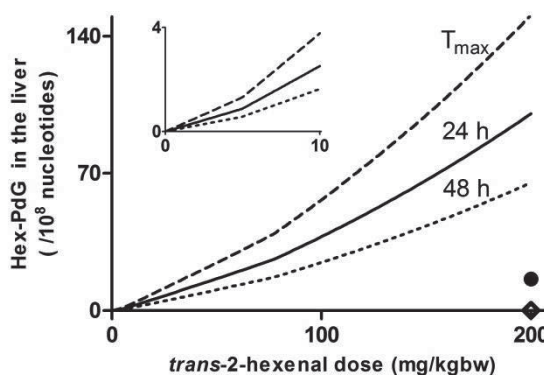


Figure 2.7. The PBK/D model predicted dose-dependent amount of 2-hexenoic acid, 2-hexen-1-ol and Hex-GSH (chemically or catalyzed by GSTs) in (A) the liver and in (B) the small intestine, and (C) the amount of 2-hexenoic acid, 2-hexen-1-ol and Hex-GSH compared to the administered *trans*-2-hexenal dose at 24 hours after the exposure in a rat, and (D) the predicted percentage of contribution to *trans*-2-hexenal detoxification by the liver and the small intestine compartment. The inserted windows show the same dose-dependent values up to 10 mg *trans*-2-hexenal/kg bw.

The developed model was also used to predict the *trans*-2-hexenal dose-dependent metabolites formation (Figure 2.7A–C). The predictions indicated that at dose levels below 80 mg/kg bw, all three pathways for *trans*-2-hexenal, including reduction to 2-hexen-1-ol, oxidation to 2-hexenoic acid, and conjugation to GSH, contribute to *trans*-2-hexenal detoxification in the liver (Figure 2.7A). The model predicted that the relative percentage of *trans*-2-hexenal detoxified by GSTs in the liver decreases at *trans*-2-hexenal dose levels above 80 mg/kg bw due to the complete depletion of liver cytosolic GSH. In the small intestine, on the other hand, the conjugation to GSH catalyzed by GSTs was the most important detoxification pathway, followed by oxidation to 2-hexenoic acid (Figure 2.7B). At *trans*-2-hexenal dose levels higher than 5 mg *trans*-2-hexenal/kg bw, the GSH in the small intestine was completely depleted, and the amount of Hex-GSH formed by GSTs plateaued at around 6 μmol . Hex-GSH formation by chemical conjugation accounted for less than 1.2% of the total Hex-GSH formation in both compartments (Figure 2.7A and 2.7B). Altogether, it was predicted that the major *trans*-2-hexenal metabolite formed in both the liver and the small intestine of a male rat is GSH-Hex at dose levels below 30 mg *trans*-2-hexenal/kg bw and that 2-hexen-1-ol and 2-hexenoic acid become the major metabolites at higher dose levels up to 200 mg/kg bw (Figure 2.7C). The relative contribution of the liver and the small intestine to *trans*-2-hexenal detoxification was also examined (Figure 2.7D). At a dose of 0.04 mg/kg bw a considerable part (48% of the dose) of *trans*-2-hexenal is detoxified in the small intestine before reaching the liver, but the contribution of the small intestine decreases rapidly and the role is taken over by the liver at dose levels above 5 mg/kg bw. The percentage of detoxification by the small intestine then rapidly decreases to less than 9% at dose levels around 30 mg/kg bw and is further reduced to 1.5% at 200 mg/kg bw.

The *trans*-2-hexenal dose-dependent DNA adduct formation in the liver 24 and 48 h after the oral exposure as well as the maximum amount of DNA adducts predicted to be formed after exposure to *trans*-2-hexenal was examined (Figure 2.8). The model predicted formation of DNA adducts in the liver at a maximum level of 0.01 adducts per 10^8 nt upon exposure to 0.04 mg *trans*-2-hexenal/kg bw, corresponding to $0.47 \times 10^{-5}\%$ of the applied dose. At a dose of 200 mg/kg bw, this value amounted to a maximum of 151 adducts per 10^8 nt, corresponding to $1.4 \times 10^{-5}\%$ of the applied dose. This relative increase in DNA adduct formation with the dose is mainly due to cytosolic GSH depletion occurring in the small intestine at dose levels above 5 mg/kg bw and in the liver at dose levels above 80 mg/kg bw.

Figure 2.8. The PBK/D model predicted dose-dependent Hex-PdG level in the liver observed at different time points including T_{\max} (---), 24 hours (—) or 48 hours (.....) after dosing. The insert shows the same values up to 10 mg/kg bw. In vivo DNA adduct formations at dose 200 mg/kg bw observed 24 hours (\diamond) [4] and 48 hours (\bullet) [7] after administration are also indicated.



DISCUSSION

trans-2-Hexenal is an α,β -unsaturated aldehyde present in our diet as natural constituent and a flavoring agent. Because of the presence of an α,β -unsaturated aldehyde moiety, *trans*-2-hexenal may react with cellular macromolecules including GSH, protein and DNA [3]. Adverse effects may occur as a result of protein adduct formation because protein adducts may disrupt the structure and/or function of the protein. Yet, formation of DNA adducts raises concerns for genotoxicity and is therefore key to the risk assessment of various α,β -unsaturated aldehydes used for flavoring including *trans*-2-hexenal [3]. It remains controversial, however, whether the genotoxicity that has been observed in numerous in vitro studies will actually occur in vivo upon exposure to the low amounts of *trans*-2-hexenal found in the diet. It especially has been suggested that swift detoxification in vivo during first-pass metabolism prevents the reactivity of *trans*-2-hexenal to be displayed in vivo [1]. Still, there is no experimental evidence showing that such a swift detoxification of *trans*-2-hexenal indeed occurs in vivo. In the present study, a PBK/D model describing dose-dependent detoxification and DNA adduct formation of *trans*-2-hexenal in male rat liver was developed to obtain insights in the kinetics of *trans*-2-hexenal including its time- and dose-dependent detoxification.

To evaluate the performance of the developed PBK/D model, the predicted DNA adduct (Hex-PdG) levels in the liver were compared to results from two in vivo studies, in which male F344 rats were orally exposed to high single doses of *trans*-2-hexenal (200 or 500 mg/kg bw). The amount of Hex-PdG predicted by the model to be formed in the liver was 4.1-fold higher at 200 mg *trans*-2-hexenal/kg bw and was only 2.1-fold higher at 500 mg/kg bw in comparison with the data reported by Schuler and Eder [7], indicating that the constructed model captures the critical kinetic and dynamic reactions of *trans*-2-hexenal. On the other hand, the prediction was 2–3 orders of magnitude higher than the data obtained by Stout et al. [4] at both doses. Stout et al. attributed the striking gap between their own data and those reported by Schuler and Eder [7] to

differences in study methodology such as in the technique used to quantify DNA adducts; LC/MS/MS in the study of Stout et al. [4] and ^{32}P -postlabeling in the study reported by Schuler and Eder. [29] In addition, while animals were not fasted before dosing in the study by Stout et al., fasting before dosing may have been applied in the study of Schuler and Eder since there is no indication on whether or not animals were fasted before dosing [4]. A difference in animal fasting might explain the discrepancy between predicted DNA adduct levels by the developed model and the data of Schuler and Eder [29] on the one hand and the data reported by Stout et al. [4] on the other hand because *trans*-2-hexenal is well capable of reacting with protein thiol groups of other contents in the gastrointestinal tract, and such a matrix effect could reduce the actual level of exposure and resulting DNA adduct formation. If, for instance, 99% of *trans*-2-hexenal would react with the food contents in the gastrointestinal tract and thus only 1% of the administered dose would be taken up by the small intestine compartment, the predicted Hex-PdG adduct formation at a dose of 200 and 500 mg/kg bw would be only 1.7- and 8.9-fold higher than the observed DNA adduct levels reported by Stout et al. [4] at the same dose levels, respectively. It should furthermore be noted that in both the study of Stout et al. [4] and of Schuler and Eder [29] part of the *trans*-2-hexenal was probably not taken up completely in the in vivo studies due to severe damage to the mucosal tissue of the gastrointestinal tract at 200 and 500 mg/kg bw [4], whereas swift and complete absorption of *trans*-2-hexenal was assumed in our model.

The constructed model was further evaluated by comparison of the predicted percentage of the *trans*-2-hexenal dose administered converted to GSH conjugates and comparing this percentage to the percentage of mercapturic acid excreted in the urine of rats exposed to the related α,β -unsaturated aldehydes 2-propenal [32] or 4-hydroxy-2-nonenal [33, 34]. The fact that the predicted proportion of GSH conjugates to the total administered dose was within 4-fold of the levels reported further supports the adequate performance of the PBK/D model constructed in this study.

The current study is the first attempt to show the quantitative integration and comparison of different metabolic routes of *trans*-2-hexenal in an in vivo model for different exposure levels. So far, *trans*-2-hexenal has been considered to be metabolized predominantly to 2-hexenoic acid, followed by conversion to Hex-GSH and to 2-hexen-1-ol to a minor extent [1, 4, 5] based on in vivo data using other aliphatic α,β -unsaturated aldehydes than *trans*-2-hexenal or related compounds [35, 36] and an in vitro study where a fixed concentration of *trans*-2-hexenal was used [5]. The model developed in this study revealed that the formation of different metabolites changes depending on the administered *trans*-2-hexenal dose. Hex-GSH was observed to be the most abundant at exposure levels below 30 mg/kg bw. Formation of this metabolite amounted to 60% of the dose at a dose level of 0.04 mg/kg bw, which corresponds to the average dietary human intake of *trans*-2-hexenal, but decreased to 32% of the dose at a dose level of 30 mg/kg bw.

The effect of the observed dose-dependent changes in detoxification reactions on DNA adduct formation could be evaluated with the developed PBK/D model, allowing us to obtain insight in the shape of the dose–response behavior at dose levels that cannot be obtained experimentally. The complete depletion of GSH in the small intestine at 5 mg/kg bw and the liver at 80 mg/kg bw resulted in relative increased DNA adduct formation with further increasing doses, which is in line with what has been proposed previously in vivo [37] (Figure 2.8). Yet, the dose-dependent effects in DNA adduct formation can be considered small and may not provide an argument against linear extrapolation of DNA adduct formation observed in animal experiments at high doses to dose levels that are relevant for the human situation. The relevance of such low levels of DNA adducts in terms of risk might be evaluated by comparing these levels to background levels of DNA adduct formation. The model predicted formation of a maximum level of DNA adducts in the liver of 0.01 adducts per 10^8 nt after exposure to 0.04 mg *trans*-2-hexenal/kg bw, a dose level that corresponds to the average daily intake of *trans*-2-hexenal [1]. This level is 3 orders of magnitude lower than the general background levels of endogenous DNA adducts for small molecular weight alkylating electrophiles reported to amount to 10–100 adducts/ 10^8 nt [38–41]. For high consumers (95th percentile) of fruits, the daily intake of *trans*-2-hexenal has been estimated to correspond to 0.178 mg/kg bw/day for a person of 60 kg [37]. At this dose level, the maximum Hex-PdG formation was predicted to be around 4.6 times higher than the maximum adduct level observed with 0.04 mg *trans*-2-hexenal/kg bw but still 3 orders of magnitude lower than background DNA adduct level. This suggests that the risks from *trans*-2-hexenal DNA adduct formation in the liver at dose levels relevant for dietary human intake might be negligible. It also should be noted that the model developed in the present study represents a worst case scenario in terms of exposure to *trans*-2-hexenal, assuming complete uptake of *trans*-2-hexenal as a bolus dose without taking matrix effects into account, whereas in real life, exposure to *trans*-2-hexenal from the diet may be spread over a day and occurs in a complex food matrix with a variety of scavenging thiol moieties.

When comparing the predicted DNA adduct formation to background levels, it is important to take any uncertainty in the model predictions into account. The present study aimed at integrating in vitro-derived kinetic and dynamic parameters to predict in vivo dose-dependent DNA adduct formation. Uncertainty can occur in the usage and scaling of in vitro-derived parameters. In vitro incubations were, for instance, performed at saturating cofactor concentrations and might overestimate reaction rates to some extent when cofactor levels are not saturating in vivo [42]. Additional in vitro experiments examining the rate of metabolism at different cofactor concentrations revealed that especially reduction of *trans*-2-hexenal by ARs may be lower when cofactor levels are not saturating in vivo. Lower levels of reduction of *trans*-2-hexenal observed at physiologically relevant concentration of NADPH (0.25 mM) [42] would result in a 4-fold increase in the predicted amount of DNA adduct formation in the liver, which is still 3 orders of magnitude lower than background levels of DNA adducts. Alternatively,

uncertainty in other parameters may have an opposite effect on DNA adduct formation. Uncertainty can, for instance, occur in the estimation of the rate of DNA repair, for which the half-life was estimated to be 38.5 h based on an in vivo study. A shorter half-life for DNA repair of less than 3 h has been observed for an α,β -unsaturated aldehyde 4-hydroxy-2-nonenal in vitro [43]. Such differences DNA repair kinetics have been reported to occur when DNA repair kinetics are biphasic, resulting in a fast removal at first with half-lives ranging from 15 min to 2 h, which then slows down to a half-life of 48 h [44, 45]. No indication can be given at present whether DNA repair kinetics of *trans*-2-hexenal adducts are biphasic. A more efficient DNA repair would result in lower DNA adduct levels.

The rat PBK/D model developed in this study can form a basis for the development of a PBK/D model for *trans*-2-hexenal detoxification and DNA adduct formation in humans to obtain insight in possible species differences in kinetics and dynamics of this compound. Furthermore, the model developed in the current study might form a basis for PBK/D models for other dietary α,β -unsaturated aldehydes. This is especially relevant considering that a number of compounds were categorized to possess structural alerts for genotoxicity by EFSA, and in vivo testing on these compounds is required before conclusions on their safety can be reached in case of positive in vitro genotoxicity data [3]. Overall, the current study supports rapid in vivo detoxification of *trans*-2-hexenal and reveals that at dose levels representative for estimated human dietary intake DNA adduct formation in male rat liver is negligible.

REFERENCES

- [1] Adams, T. B., Gavin, C. L., Taylor, S. V., Waddell, W. J., *et al.*, The FEMA GRAS assessment of alpha,beta-unsaturated aldehydes and related substances used as flavor ingredients. *Food Chem Toxicol* 2008, *46*, 2935-2967.
- [2] Feron, V. J., Til, H. P., de Vrijer, F., Woutersen, R. A., *et al.*, Aldehydes: occurrence, carcinogenic potential, mechanism of action and risk assessment. *Mutat Res* 1991, *259*, 363-385.
- [3] EFSA, Minutes of the 26th plenary meeting of the scientific panel on food additives, flavourings, processing aids and materials in contact with food. <http://www.efsa.europa.eu/en/events/event/afc071127-m.pdf>. 2007.
- [4] Stout, M. D., Bodes, E., Schoonhoven, R., Upton, P. B., *et al.*, Toxicity, DNA binding, and cell proliferation in male F344 rats following short-term gavage exposures to *trans*-2-hexenal. *Toxicol Pathol* 2008, *36*, 232-246.
- [5] Eisenbrand, G., Schuhmacher, J., Golzer, P., The influence of glutathione and detoxifying enzymes on DNA damage induced by 2-alkenals in primary rat hepatocytes and human lymphoblastoid cells. *Chem Res Toxicol* 1995, *8*, 40-46.
- [6] Golzer, P., Janzowski, C., Pool-Zobel, B. L., Eisenbrand, G., (E)-2-hexenal-induced DNA damage and formation of cyclic 1,N²-(1,3-propano)-2'-deoxyguanosine adducts in mammalian cells. *Chem Res Toxicol* 1996, *9*, 1207-1213.
- [7] Schuler, D., Eder, E., Detection of 1,N²-propanodeoxyguanosine adducts of 2-hexenal in organs of Fischer 344 rats by a ³²P-post-labeling technique. *Carcinogenesis* 1999, *20*, 1345-1350.
- [8] JECFA, Evaluation of Certain Food Additives: sixty-third report of the Joint FAO/WHO Expert Committee on Food Additives. http://whqlibdoc.who.int/trs/WHO_TRs_928.pdf. 2005.
- [9] Bhattacharjee, S., de Haan, L. H., Evers, N. M., Jiang, X., *et al.*, Role of surface charge and oxidative stress in cytotoxicity of organic monolayer-coated silicon nanoparticles towards macrophage NR8383 cells. *Part Fibre Toxicol* 2010, *7*, 25.
- [10] van de Kerkhof, E. G., de Graaf, I. A., Groothuis, G. M., In vitro methods to study intestinal drug metabolism. *Current drug metabolism* 2007, *8*, 658-675.
- [11] Klyosov, A. A., Rashkovetsky, L. G., Tahir, M. K., Keung, W. M., Possible role of liver cytosolic and mitochondrial aldehyde dehydrogenases in acetaldehyde metabolism. *Biochemistry* 1996, *35*, 4445-4456.
- [12] Jia, L., Liu, X., The conduct of drug metabolism studies considered good practice (II): in vitro experiments. *Current drug metabolism* 2007, *8*, 822-829.
- [13] Csanady, G. A., Filser, J. G., A physiological toxicokinetic model for inhaled propylene oxide in rat and human with special emphasis on the nose. *Toxicological sciences : an official journal of the Society of Toxicology* 2007, *95*, 37-62.
- [14] Johanson, G., Filser, J. G., A physiologically based pharmacokinetic model for butadiene and its metabolite butadiene monoxide in rat and mouse and its significance for risk extrapolation. *Arch Toxicol* 1993, *67*, 151-163.
- [15] Potter, D. W., Tran, T. B., Rates of ethyl acrylate binding to glutathione and protein. *Toxicol Lett* 1992, *62*, 275-285.
- [16] Ramsey, J. C., Andersen, M. E., A physiologically based description of the inhalation pharmacokinetics of styrene in rats and humans. *Toxicol Appl Pharmacol* 1984, *73*, 159-175.
- [17] Kirman, C. R., Gargas, M. L., Deskin, R., Tonner-Navarro, L., Andersen, M. E., A physiologically based pharmacokinetic model for acrylamide and its metabolite, glycidamide, in the rat. *Journal of toxicology and environmental health. Part A* 2003, *66*, 253-274.
- [18] Punt, A., Freidig, A. P., Delatour, T., Scholz, G., *et al.*, A physiologically based biokinetic (PBBK) model for estragole bioactivation and detoxification in rat. *Toxicol Appl Pharmacol* 2008, *231*, 248-259.
- [19] Frederick, C. B., Potter, D. W., Chang-Mateu, M. I., Andersen, M. E., A physiologically based pharmacokinetic and pharmacodynamic model to describe the oral dosing of rats with ethyl acrylate and its implications for risk assessment. *Toxicol Appl Pharmacol* 1992, *114*, 246-260.
- [20] Griffith, O. W., Meister, A., Origin and turnover of mitochondrial glutathione. *Proceedings of the National Academy of Sciences of the United States of America* 1985, *82*, 4668-4672.
- [21] Potter, D. W., Tran, T. B., Apparent rates of glutathione turnover in rat tissues. *Toxicol Appl Pharmacol* 1993, *120*, 186-192.
- [22] Brown, R. P., Delp, M. D., Lindstedt, S. L., Rhomberg, L. R., Beliles, R. P., Physiological parameter values for physiologically based pharmacokinetic models. *Toxicol Ind Health* 1997, *13*, 407-484.
- [23] DeJongh, J., Verhaar, H. J., Hermens, J. L., A quantitative property-property relationship (QPPR) approach to estimate in vitro tissue-blood partition coefficients of organic chemicals in rats and humans. *Arch Toxicol* 1997, *72*, 17-25.

- [24] Evans, M. V., Andersen, M. E., Sensitivity analysis of a physiological model for 2,3,7,8-tetrachlorodibenzo-p-dioxin (TCDD): assessing the impact of specific model parameters on sequestration in liver and fat in the rat. *Toxicological sciences : an official journal of the Society of Toxicology* 2000, *54*, 71-80.
- [25] Paini, A., Punt, A., Viton, F., Scholz, G., *et al.*, A physiologically based biodynamic (PBBD) model for estragole DNA binding in rat liver based on in vitro kinetic data and estragole DNA adduct formation in primary hepatocytes. *Toxicol Appl Pharmacol* 2010, *245*, 57-66.
- [26] Rietjens, I. M. C. M., Louisse, J., Punt, A., Tutorial on physiologically based kinetic modeling in molecular nutrition and food research. *Molecular nutrition & food research* 2011, *55*, 941-956.
- [27] Krishnan, K., Andersen, M. E., Physiologically based pharmacokinetic modeling in toxicology. *Principles and Methods of Toxicology (Forth Edition Edition)* 2001, 193-239.
- [28] Balogh, L. M., Roberts, A. G., Shireman, L. M., Greene, R. J., Atkins, W. M., The stereochemical course of 4-hydroxy-2-nonenal metabolism by glutathione S-transferases. *The Journal of biological chemistry* 2008, *283*, 16702-16710.
- [29] Schuler, D., Budiawan, B., Eder, E., Development of a ^{32}P -postlabeling method for the detection of 1, N^2 -propanodeoxyguanosine adducts of 2-hexenal in vivo. *Chem Res Toxicol* 1999, *12*, 335-340.
- [30] Chan, K., Poon, R., O'Brien, P. J., Application of structure-activity relationships to investigate the molecular mechanisms of hepatocyte toxicity and electrophilic reactivity of alpha,beta-unsaturated aldehydes. *Journal of applied toxicology : JAT* 2008, *28*, 1027-1039.
- [31] Paini, A., Punt, A., Scholz, G., Gremaud, E., *et al.*, In vivo validation of DNA adduct formation by estragole in rats predicted by physiologically based biodynamic modelling. *Mutagenesis* 2012.
- [32] Linhart, I., Frantik, E., Vodickova, L., Vosmanska, M., *et al.*, Biotransformation of acrolein in rat: excretion of mercapturic acids after inhalation and intraperitoneal injection. *Toxicol Appl Pharmacol* 1996, *136*, 155-160.
- [33] Alary, J., Bravais, F., Cravedi, J. P., Debrauwer, L., *et al.*, Mercapturic acid conjugates as urinary end metabolites of the lipid peroxidation product 4-hydroxy-2-nonenal in the rat. *Chem Res Toxicol* 1995, *8*, 34-39.
- [34] de Zwart, L. L., Hermanns, R. C., Meerman, J. H., Commandeur, J. N., Vermeulen, N. P., Disposition in rat of [2- ^3H]-trans-4-hydroxy-2,3-nonenal, a product of lipid peroxidation. *Xenobiotica; the fate of foreign compounds in biological systems* 1996, *26*, 1087-1100.
- [35] deBethizy, J. D., Udinsky, J. R., Scribner, H. E., Frederick, C. B., The disposition and metabolism of acrylic acid and ethyl acrylate in male Sprague-Dawley rats. *Fundamental and applied toxicology : official journal of the Society of Toxicology* 1987, *8*, 549-561.
- [36] Grootveld, M., Atherton, M. D., Sheerin, A. N., Hawkes, J., *et al.*, In vivo absorption, metabolism, and urinary excretion of alpha,beta-unsaturated aldehydes in experimental animals. Relevance to the development of cardiovascular diseases by the dietary ingestion of thermally stressed polyunsaturate-rich culinary oils. *J Clin Invest* 1998, *101*, 1210-1218.
- [37] Eder, E., Schuler, D., An approach to cancer risk assessment for the food constituent 2-hexenal on the basis of 1, N^2 -propanodeoxyguanosine adducts of 2-hexenal in vivo. *Arch Toxicol* 2000, *74*, 642-648.
- [38] Paini, A., Scholz, G., Marin-Kuan, M., Schilter, B., *et al.*, Quantitative comparison between in vivo DNA adduct formation from exposure to selected DNA-reactive carcinogens, natural background levels of DNA adduct formation and tumour incidence in rodent bioassays. *Mutagenesis* 2011, *26*, 605-618.
- [39] La, D. K., Swenberg, J. A., DNA adducts: biological markers of exposure and potential applications to risk assessment. *Mutat Res* 1996, *365*, 129-146.
- [40] Swenberg, J. A., Fryar-Tita, E., Jeong, Y. C., Boysen, G., *et al.*, Biomarkers in toxicology and risk assessment: informing critical dose-response relationships. *Chem Res Toxicol* 2008, *21*, 253-265.
- [41] Gupta, R. C., Lutz, W. K., Background DNA damage for endogenous and unavoidable exogenous carcinogens: a basis for spontaneous cancer incidence? *Mutat Res* 1999, *424*, 1-8.
- [42] Glock, G. E., McLean, P., Levels of oxidized and reduced diphosphopyridine nucleotide and triphosphopyridine nucleotide in animal tissues. *The Biochemical journal* 1955, *61*, 388-390.
- [43] Choudhury, S., Pan, J., Amin, S., Chung, F. L., Roy, R., Repair kinetics of trans-4-hydroxynonenal-induced cyclic 1, N^2 -propanodeoxyguanine DNA adducts by human cell nuclear extracts. *Biochemistry* 2004, *43*, 7514-7521.
- [44] Spencer, W. A., Singh, J., Orren, D. K., Formation and differential repair of covalent DNA adducts generated by treatment of human cells with (+/-)-anti-dibenzo[a,1]pyrene-11,12-diol-13,14-epoxide. *Chem Res Toxicol* 2009, *22*, 81-89.
- [45] Episkopou, H., Kyrtpoulos, S. A., Sfrikakis, P. P., Fousteri, M., *et al.*, Association between transcriptional activity, local chromatin structure, and the efficiencies of both subpathways of nucleotide

excision repair of melphalan adducts. *Cancer Res* 2009, 69, 4424-4433.

SUPPORTING INFORMATION

PBK/D model equations

(1) Uptake from GI cavity

The uptake of *trans*-2-hexenal from the intestinal cavity into the small intestine compartment was described by a first-order process as follows:

$$\begin{aligned} dAGI/dt &= -K_a * AGI \\ \text{InitAGI} &= \text{DOSE} \end{aligned}$$

where

AGI Amount of *trans*-2-hexenal remaining in GI cavity (μmol)
 K_a Linear uptake rate (/h)
 DOSE Amount of *trans*-2-hexenal administered in a rat (μmol).

(2) Slowly perfused tissue, richly perfused tissue and fat

Amount *trans*-2-hexenal in slowly perfused tissue, richly perfused tissue or fat compartment was described as follows:

$$\begin{aligned} dAT_i/dt &= QT_i * (CA - CVT_i) \\ CT_i &= AT_i / VT_i \\ CVT_i &= CT_i / PT_i \end{aligned}$$

where

AT_i Amount of *trans*-2-hexenal in a tissue (μmol)
 QT_i Blood flow into a tissue (L/h)
 CA Concentration of *trans*-2-hexenal in arterial blood perfusing a tissue ($\mu\text{mol/L}$)
 CVT_i Concentration of *trans*-2-hexenal in venous blood leaving a tissue ($\mu\text{mol/L}$)
 CT_i Concentration of *trans*-2-hexenal in a tissue ($\mu\text{mol/kg}$)
 VT_i Volume of a tissue (kg)
 PT_i Tissue/blood partition coefficient of *trans*-2-hexenal

(3) Liver

Amount *trans*-2-hexenal in the liver (AL , μmol) is described as follows:

$$\begin{aligned} dAL/dt &= QL * CA + QSi * CVS_i - (QL + QSi) * CVL - (\text{eq.1} + \text{eq.2} + \text{eq.3} + \text{eq.4} + \text{eq.5} + \text{eq.6}) \\ CL &= AL / VL \\ CVL &= CL / PL \end{aligned}$$

where

QL Blood flow into the liver (L/h)
 QSi Blood flow into the small intestine (L/h)
 CVS_i Concentration of *trans*-2-hexenal in venous blood leaving the small intestine ($\mu\text{mol/L}$)
 CVL Concentration of *trans*-2-hexenal in venous blood leaving the liver ($\mu\text{mol/L}$)
 CL Concentration of *trans*-2-hexenal in the liver ($\mu\text{mol/L}$)
 PL Liver/blood partition coefficient of *trans*-2-hexenal

Amount *trans*-2-hexenal oxidized to 2-hexenoic acid enzymatically in the liver ($AMLHA$, μmol) is described to follow Michaelis-Menten equation:

$$\begin{aligned} dAMLHA/dt &= V_{S_{\max, LS9_HA}} * CVL / (K_{m, LS9_HA} + CVL) + V_{S_{\max, LMT_HA}} * CVL / (K_{m, LMT_HA} + CVL) \end{aligned} \quad \text{----- eq. 1}$$

where

$V_{S_{\max, LS9_HA}}$ Scaled V_{\max} for enzymatic oxidation of *trans*-2-hexenal in the liver cytosol of microsomes ($\mu\text{mol/h}$)
 $K_{m, LS9_HA}$ K_m for enzymatic oxidation of *trans*-2-hexenal in cytosol or microsomes in the liver cytosol of microsomes (μM)
 $V_{S_{\max, LMT_HA}}$ Scaled V_{\max} for enzymatic oxidation of *trans*-2-hexenal in the liver mitochondria ($\mu\text{mol/h}$)
 K_{m, LMT_HA} K_m for enzymatic oxidation of *trans*-2-hexenal in the liver mitochondria (μM)

Amount *trans*-2-hexenal reduced to 2-hexen-1-ol in the liver (AMLHO, μmol) is described to follow Michaelis-Menten-equation:

$$d\text{AMLHO}/dt = V_{S_{\max, L_HO}} * \text{CVL} / (K_{m, L_HO} + \text{CVL}) \quad \text{----- eq. 2}$$

where

$V_{S_{\max, L_HO}}$ Scaled V_{\max} for enzymatic reduction of *trans*-2-hexenal in the liver ($\mu\text{mol/h}$)
 K_{m, L_HO} K_m for enzymatic reduction of *trans*-2-hexenal in the liver (μM)

Amount *trans*-2-hexenal metabolized in liver to GSH conjugation by GSTs (AMLHG_{GST}, μmol) is described by a two substrate ping-pong model:

$$d\text{AMLHG}_{\text{GST}}/dt = \frac{V_{S_{\max, L_Hex-GSH}} * \text{CVL} * \text{CLcGSH}}{(K_{m, L_Hex-GSH_G} * \text{CVL} + K_{m, L_Hex-GSH_H} * \text{CLcGSH} + \text{CLcGSH} * \text{CVL})} \quad \text{----- eq.3}$$

where

$V_{S_{\max, L_GST}}$ Scaled V_{\max} for enzymatic conjugation of *trans*-2-hexenal in the liver ($\mu\text{mol/h}$)
 CLcGSH Concentration of GSH in the liver cytosol ($\mu\text{mol/kg}$)
 K_{m, L_GST_H} K_m toward *trans*-2-hexenal for enzymatic conjugation of *trans*-2-hexenal in the liver (μM)
 K_{m, L_GST_G} K_m toward GSH for enzymatic conjugation of *trans*-2-hexenal in the liver (μM)

Amount *trans*-2-hexenal chemically bound in liver to GSH (AMLHG_{chem}, μmol) is described as following:

$$d\text{AMLHG}_{\text{chem}}/dt = k_{\text{GSH}} * \text{CVL} * \text{CLcGSH} * \text{VL} \quad \text{----- eq.4}$$

where

k_{GSH} First order rate constant of *trans*-2-hexenal binding to GSH ($1/\mu\text{mol/h}$)
 VL Volume of the liver (kg)

Amount *trans*-2-hexenal protein adducts in the liver (AMLHP, μmol) is described as following:

$$d\text{AMLHP}/dt = k_{\text{PRO}} * \text{CVL} * \text{CPRO}_L * \text{VL} \quad \text{----- eq.5}$$

where

k_{PRO} First order rate constant of *trans*-2-hexenal binding to protein reaction sites in a tissue ($1/\mu\text{mol/h}$)
 CPRO_L Concentration of protein reaction sites in the liver ($\mu\text{mol/kg liver}$)

Amount of DNA adduct (Hex-PdG) in liver (AMLHPdG, μmol) is described by subtracting elimination of DNA adduct from the formation:

$$d\text{AMLHPdG}/dt = k_{\text{DNA}} * \text{CVL} * \text{CLdG} * \text{VL} - \text{AMLHPdG} * (\ln 2 / T_{1/2}) \quad \text{----- eq.6}$$

where

k_{DNA} First order rate constant of *trans*-2-hexenal binding to 2'-dG ($1/\mu\text{mol/h}$)
 CLdG Concentration of 2'-dG in the liver ($\mu\text{mol/kg liver}$)
 $T_{1/2}$ Half-life of Hex-PdG in the liver (h)

CLdG was calculated to be 1,36 $\mu\text{mol/kg liver}$ by using the average molecular weight of nucleotides (330 g/mol) and reported concentration of DNA in a rat liver (ALDNA, 1.8 g/kg liver).

Amount of GSH present in liver cytosol (AMLcGSH, μmol) is described by zero-order synthesis and reduction by first-order elimination due to turnover and depletion by *trans*-2-hexenal:

$$d\text{AMLcGSH} = \text{GSYN}_L * \text{VL} * 0.9 - (\text{eq.3} + \text{eq.4} + k_{\text{GLOS}_L} * \text{AMLcGSH}) \quad \text{----- eq.7}$$

$$\text{Init AMLcGSH} = \text{InitGSH}_L * \text{VL} * 0.9$$

$$\text{CLcGSH} = \text{AMLcGSH} / \text{VL}$$

where

GSYN_L Rate of GSH synthesis in the liver ($\mu\text{mol/h}$)
 k_{GLOS_L} First-order rate of GSH turnover in the liver ($1/h$)
 InitGSH_L Initial concentration of GSH in the liver ($\mu\text{mol/kg liver}$)

When eq.7 gave negative values, the value zero was used as the amount of GSH in the liver cytosol.

(4) Small intestine

The amount *trans*-2-hexenal in small intestine tissue, (ASi, μmol) is described as follows:

Chapter 2

$$\begin{aligned} dASi/dt &= QSI*(CA - CVS_i) - Ka*AGI - (eq.8 + eq.9 + eq.10 + eq.11) \\ CS_i &= AS_i/VS_i \\ CVS_i &= CS_i/PS_i \end{aligned}$$

where

CS_i Concentration of *trans*-2-hexenal in the small intestine (μmol/L)
 VS_i Volume of the small intestine (kg)
 PS_i Small intestine/blood partition coefficient of *trans*-2-hexenal

Amount *trans*-2-hexenal enzymatically oxidized 2-hexenoic acid (AMSiHA, μmol) in the small intestine is described by Michaelis-Menten equation:

$$dAMSiHA/dt = V_{S_{max,Si_HA}} * CVS_i / (K_{m,Si_HA} + CVS_i) \quad \text{----- eq.8}$$

where

V_{S_{max,Si_{_}HA}} Scaled V_{max} for enzymatic oxidation of *trans*-2-hexenal in the small intestine (μmol/h)
 K_{m,Si_{_}HA} K_m for enzymatic oxidation of *trans*-2-hexenal in small intestine (μM).

Amount 2-hexenal metabolized in the small intestine to GSH conjugation by GSTs (AMSiHG_{GST}, μmol) is described in the same way as in the liver (see eq. 6):

$$\begin{aligned} dAMSiHG_{GST}/dt &= \\ & V_{S_{max,Si_GST}} * CVS_i * CSicGSH / \\ & (K_{m,Si_GST_G} * CVS_i + K_{m,Si_GST_H} * CSicGSH + CSicGSH * CVS_i) \quad \text{----- eq.9} \end{aligned}$$

where

V_{S_{max,Si_{_}GST}} Scaled V_{max} for enzymatic conjugation of *trans*-2-hexenal in the small intestine (μmol/h)
 CSicGSH Concentration of GSH in the small intestine cytosol (μmol/kg)
 K_{m,Si_{_}GST_{_}H} K_m toward *trans*-2-hexenal for enzymatic conjugation of *trans*-2-hexenal in the small intestine (μM)
 K_{m,Si_{_}GST_{_}G} K_m toward GSH for enzymatic conjugation of *trans*-2-hexenal in the small intestine (μM)

Amount *trans*-2-hexenal chemically bound in the small intestine to GSH (AMSiHG_{chem}, μmol) is described as following:

$$dAMSiHG_{chem}/dt = k_{GSH} * CVS_i * CSicGSH * VS_i \quad \text{----- eq.10}$$

where

k_{GSH} First order rate constant of *trans*-2-hexenal binding to GSH (/μmol/h)
 VS_i Volume of the small intestine (kg)

Amount *trans*-2-hexenal chemically bound to protein reaction sites in the small intestine (AMSiHP, μmol) is described as following:

$$dAMSiHP/dt = k_{PRO} * CVS_i * CPRO_{Si} * VS_i \quad \text{----- eq.11}$$

where

k_{PRO} First order rate constant of *trans*-2-hexenal binding to protein reaction sites in a tissue (/μmol/h)
 CPRO_{Si} Concentration of protein reaction sites in the liver (μmol/kg liver)

Amount of GSH present in the small intestine cytosol (AMSiGSH, μmol) is described in the same way as in the liver (eq 10):

$$\begin{aligned} dAMSiGSH &= GSYN_{Si} * VS_i * 0.9 - (eq.9 + eq.10 + k_{GLOS_Si} * AMSiGSH) \quad \text{----- eq.12} \\ Init\ AMSiGSH &= InitGSH_{Si} * VS_i * 0.9 \\ CSicGSH &= AMSiGSH / VS_i \end{aligned}$$

where

GSYN_{Si} Rate of GSH synthesis in the small intestine (μmol/h)
 k_{GLOS_{_}Si} First-order rate of GSH turnover in the small intestine (/h)
 InitGSH_{Si} Initial concentration of GSH in the small intestine (μmol/kg liver)

As was the case in the liver, the value zero was used as the amount of GSH in the small intestine cytosol when eq.12 gave negative values.

(5) Venous blood and arterial blood

Concentration of *trans*-2-hexenal in venous blood (CV) and in arterial blood (CA, both in $\mu\text{mol/L}$) was described as follows:

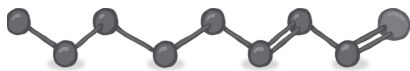
$$dAV/dt = (QF*CVF + (QL+QSi)*CVL + QR*CVR + QS*CVS - QC*CV)$$

$$CV = AV/VV$$

$$CV = CA$$

where

AV	Amount of <i>trans</i> -2-hexenal in venous blood (μmol)
QF	Blood flow into fat (L/h)
CVF	Concentration of <i>trans</i> -2-hexenal in venous blood leaving fat ($\mu\text{mol/L}$)
QR	Blood flow into richly perfused tissue (L/h)
CVR	Concentration of <i>trans</i> -2-hexenal in venous blood leaving richly perfused tissue ($\mu\text{mol/L}$)
QS	Blood flow into slowly perfused tissue (L/h)
CVS	Concentration of <i>trans</i> -2-hexenal in venous blood leaving slowly perfused tissue ($\mu\text{mol/L}$)



CHAPTER 3

A Physiologically Based In Silico Model for *trans*-2-Hexenal Detoxification and DNA Adduct Formation in Human Including Interindividual Variation Indicates Efficient Detoxification and a Negligible Genotoxicity Risk

R. Kiwamoto
A. Spenkelink
I. M. C. M. Rietjens
A. Punt

Based on *Archives of Toxicology* (2013) 87(9): 1725-1737

ABSTRACT

A number of α,β -unsaturated aldehydes are present in food both as natural constituents and as flavouring agents. Their reaction with DNA due to their electrophilic α,β -unsaturated aldehyde moiety may result in genotoxicity as observed in some in vitro models, thereby raising a safety concern. A question that remains is whether in vivo detoxification would be efficient enough to prevent DNA adduct formation and genotoxicity. In this study, a human physiologically based kinetic/dynamic (PBK/D) model of *trans*-2-hexenal, a selected model α,β -unsaturated aldehyde, was developed to examine dose-dependent detoxification and DNA adduct formation in humans upon dietary exposure. The kinetic model parameters for detoxification were quantified using relevant pooled human tissue fractions as well as tissue fractions from 11 different individual subjects. In addition, Monte Carlo simulations were performed so that the impact of interindividual variation in *trans*-2-hexenal detoxification on the DNA adduct formation in the population as a whole could be examined. The PBK/D model revealed that DNA adduct formation due to *trans*-2-hexenal exposure was 0.039 adducts/ 10^8 nucleotides (nt) at the estimated average *trans*-2-hexenal dietary intake (0.04 mg/kg bw) and 0.18 adducts/ 10^8 nt at the 95th percentile of the dietary intake (0.178 mg/kg bw) in the most sensitive people. These levels are three orders of magnitude lower than natural background DNA adduct levels that have been reported in disease-free humans (6.8–110 adducts/ 10^8 nt), suggesting that the genotoxicity risk for the human population at realistic dietary daily intakes of *trans*-2-hexenal may be negligible.

INTRODUCTION

A number of α,β -unsaturated aldehydes such as *trans*-2-hexenal, *trans*-2-nonenal, and *trans*, *trans*-2,4-hexadienal are present in our diet as natural constituents and may also be intentionally added as pure compounds to food as flavouring ingredients [1]. Due to their α,β -unsaturated aldehyde moiety, α,β -unsaturated aldehydes can react with cellular macromolecules including DNA without the need for bioactivation [2]. Their reaction with DNA may result in genotoxicity as shown in some in vitro models, thereby raising a safety concern. The European Food Safety Authority (EFSA) regarded the α,β -unsaturated aldehyde moiety as a structural alert for genotoxicity and concluded that data on genotoxicity of several α,β -unsaturated aldehydes were required to overrule the concerns over genotoxicity when considering the use of these compounds as food flavouring agents [3]. A question that remains is whether in vivo detoxification of the α,β -unsaturated aldehyde would be efficient enough to prevent DNA adduct formation. Such an argument would be in line with that of the Joint FAO/WHO Committee on Food Additives (JECFA) and the Expert Panel of the Flavor and Extract Manufacturers Association (FEMA), who concluded that various α,β -unsaturated aldehydes that are of interest as flavouring ingredients do not present any safety concerns at estimated current intakes due to the low level of use in food and possible rapid detoxification at low dietary exposure [1, 4]. Based on these considerations, the aim of the present study was to provide an insight into dose-dependent detoxification and DNA adduct formation upon dietary exposure to *trans*-2-hexenal, a selected model α,β -unsaturated aldehyde, by developing a human physiologically based kinetic/dynamic (PBK/D) model. *trans*-2-Hexenal is one of the most prominent α,β -unsaturated aldehydes in our diet [1]. *trans*-2-Hexenal is present in a wide range of plant-based foods including vegetables, fruits, and beverages as a natural constituent [5, 6]. *trans*-2-Hexenal has also been used as a food flavouring agent due to its grassy fresh odour [1]. The estimated daily intake of *trans*-2-hexenal from food consumption is 2,390 $\mu\text{g}/\text{person}/\text{day}$ as a natural constituent and 57 $\mu\text{g}/\text{person}/\text{day}$ as a food flavouring agent [1], corresponding to 40 and 1 $\mu\text{g}/\text{kg bw}/\text{day}$ for a 60-kg person. Genotoxicity of *trans*-2-hexenal has been observed in in vitro studies using bacterial or mammalian cells [7-9]. *trans*-2-Hexenal is detoxified via three pathways: oxidation to 2-hexenoic acid by aldehyde dehydrogenases (ALDHs), reduction to 2-hexen-1-ol by aldose reductases (ARs), and conjugation with reduced glutathione (GSH) either chemically or catalysed by glutathione S-transferases (GSTs) (Figure. 3.1) [8]. In vivo studies using male F344 rats revealed that exocyclic 1,*N*²-propanodeoxyguanosine (Hex-PdG) adducts, *trans*-2-hexenal DNA adducts, are formed in the liver upon the administration of high irritating doses of *trans*-2-hexenal (200 or 500 mg/kg bw), but not at doses of 50 mg/kg bw and lower [10, 11]. This observation suggests that *trans*-2-hexenal may be swiftly detoxified in vivo at the levels representative for the estimated human dietary intake, and DNA adduct formation upon oral exposure to *trans*-2-hexenal at these levels may be insignificant or at least below the detection limit of the method applied for the measurement of the DNA adducts.

To quantitatively integrate the dose-dependent metabolic conversion of *trans*-2-hexenal via different detoxification routes and to determine the impact of these reactions on DNA adduct formation *in vivo*, we have previously developed a physiologically based kinetic/dynamic (PBK/D) model for *trans*-2-hexenal in rat [12]. In the present study, a human PBK/D model for *trans*-2-hexenal detoxification and DNA binding was defined, taking interindividual differences in detoxification into account. The results obtained provided an insight into the genotoxicity in humans arising from exposure to low realistic dietary levels of *trans*-2-hexenal present in our diet, which cannot be examined experimentally *in vivo*.

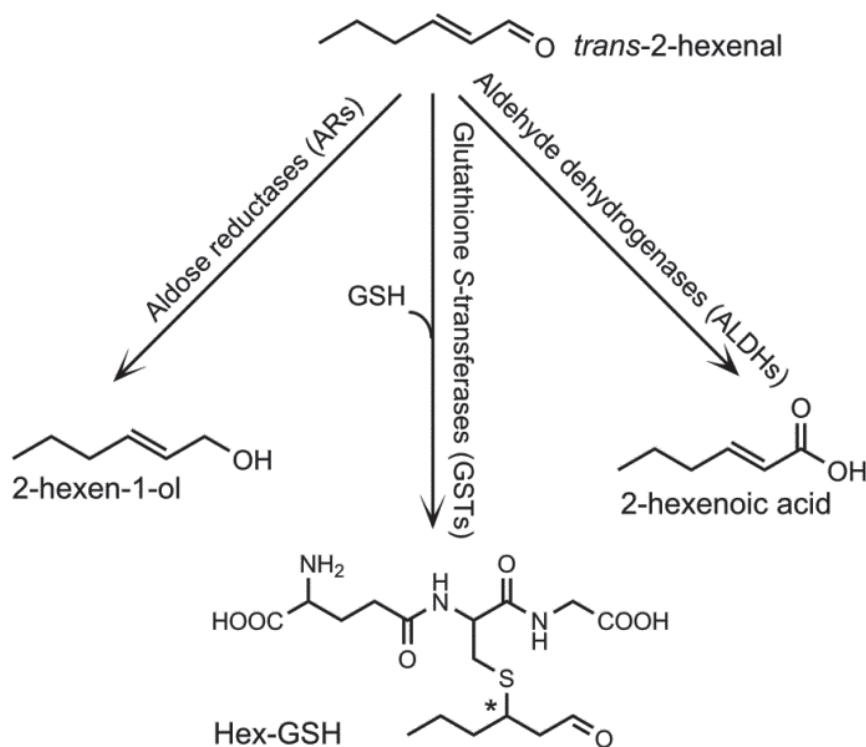


Figure 3.1. Metabolism of *trans*-2-hexenal. The asterisk represents a chiral centre.

MATERIALS AND METHODS

Materials and chemicals

trans-2-Hexen-1-al (*trans*-2-hexenal), *trans*-2-hexen-1-ol (2-hexen-1-ol), *trans*-2-hexenoic acid (2-hexenoic acid), 2'-deoxyguanosine (2'-dG), tris (hydroxymethyl) aminomethane, and GSH were purchased from Sigma-Aldrich (Zwijndrecht, the Netherlands). Reduced (NADPH) and oxidized (NAD⁺) β -nicotinamide adenine dinucleotide phosphates were obtained from Roche Diagnostics (Mannheim, Germany), and dimethyl sulphoxide (DMSO) was purchased from Acros Organic (NJ, USA). Acetonitrile (ULC/MS) and methanol (HPLC Supra-gradient) were purchased from Biosolve (Valkenswaard, the Netherlands). Trifluoroacetic acid (TFA) was obtained from

VWR International (Darmstadt, Germany). Pooled human liver S9 was obtained from Celsis (Baltimore, USA). Pooled human small intestine S9 of mixed gender and eleven individual human liver S9 samples were purchased from Xenotech (Lenexa, USA).

Aldehyde dehydrogenase (ALDH)-catalysed oxidation of trans-2-hexenal to 2-hexenoic acid

trans-2-Hexenal was incubated with human liver or small intestine S9 to determine the kinetic constants for ALDH-mediated oxidation of *trans*-2-hexenal. The final volume of the incubation mixtures was 100 μ l. Each incubation mixture contained (final concentrations) pooled human liver S9 (0.42 mg protein/ml), individual human liver S9 (0.4 mg protein/ml), or pooled human small intestine S9 (0.4 mg protein/ml) and NAD⁺ (2 mM) in 0.1 M Tris-HCl (pH 7.4). After pre-incubation at 37 °C for 2 min, the reactions were initiated by the addition of the substrate *trans*-2-hexenal (50–750 μ M) from 100 times concentrated stock solutions in DMSO. The mixtures were incubated at 37 °C for 5 min with pooled or individual liver S9 and 6 min with pooled small intestine S9. The reactions were terminated by adding 50 μ l ice-cold acetonitrile. The incubation mixtures were subsequently centrifuged for 3 min at 13,000 \times g at 4 °C to precipitate the proteins. Blank incubations were performed without the cofactor NAD⁺ or without S9. Because *trans*-2-hexenal also oxidizes spontaneously to form 2-hexenoic acid during these incubations, the amount of 2-hexenoic acid present in blank incubations without S9 was subtracted as background. The amount of 2-hexenoic acid in the samples was analysed immediately after the incubation using an ultra-performance liquid chromatography diode array detection (UPLC-DAD) system consisting of a Waters Acquity solvent manager, sample manager, and photodiode array detector (Waters, Milford, MA, USA), equipped with a Waters Acquity UPLC BEH C18 column (1.7 μ m, 2.1 \times 50 mm) as described previously [12].

Aldose reductase (AR)-catalysed reduction of trans-2-hexenal to 2-hexen-1-ol

trans-2-Hexenal was incubated with human liver or small intestine S9 to determine the kinetic constants for AR-mediated reduction of *trans*-2-hexenal. The final volume of the incubation mixtures was 100 μ l. Each incubation mixture contained (final concentrations) pooled human liver S9 (0.42 mg protein/ml), individual human liver S9 (0.4 mg protein/ml), or pooled human small intestine S9 (0.4 mg protein/ml) in 0.1 M Tris-HCl (pH 7.4). After pre-incubation at 37 °C for 3 min, the reactions were initiated by the addition of NADPH (2.5 mM) from a 20 times concentrated stock solution in 0.1 M Tris-HCl (pH 7.4) and *trans*-2-hexenal (50–750 μ M) from 100 times concentrated stock solutions in DMSO. After 6 min, the reactions were terminated by adding 50 μ l ice-cold acetonitrile. Blank incubations were performed without the cofactor NADPH or without S9. The incubation mixtures were subsequently centrifuged for 3 min at 13,000 \times g at 4 °C to precipitate the proteins. The resulting supernatants were immediately frozen in dry ice and stored at –80 °C until analysis to prevent evaporation of 2-hexen-1-ol. The amount of 2-hexen-1-ol was measured using a UPLC-DAD system as described previously [12].

Glutathione S-transferase (GST)-catalysed conjugation of GSH with trans-2-hexenal

Kinetic constants for GST-mediated formation of *trans*-2-hexenal–GSH conjugates (S-[3-(1-oxohexyl)]-GSH (Hex–GSH)) were determined by incubating *trans*-2-hexenal in the presence of human liver or small intestine S9. The final volume of the incubation mixtures was 100 μ l. The incubation mixtures contained (final concentrations) pooled human liver S9 (0.84 mg protein/ml), individual human liver S9 (0.8 mg protein/ml), or pooled human small intestine S9 (0.4 mg protein/ml) in 0.1 M Tris–HCl. For the incubations with liver S9, a lower pH (7.0) was used than for the incubations with small intestine (7.4) to reduce the background chemical formation of Hex–GSH and to accurately determine the formation catalysed by liver GSTs, which activity (nmol/min/mg S9 protein) was observed to be lower than that by small intestine GSTs (supporting information 3.1C). After pre-incubation at 37 °C for 3 min, the reaction was initiated by the addition of GSH (2.5 mM) from a 10 times concentrated stock solution in 0.1 M Tris–HCl (pH 7.0 with liver S9 and pH 7.4 with small intestine S9) and *trans*-2-hexenal (1,000–3,000 μ M with liver S9 and 500–3,000 μ M with small intestine S9) from 100 times concentrated stock solutions in DMSO. Incubations were carried out for 4 min with liver S9 or 3 min with small intestine S9. The reactions were terminated by adding 50 μ l ice-cold acetonitrile. In parallel, mixtures without S9 were incubated to quantify background levels of Hex–GSH that were chemically formed during the incubation. The samples obtained from the incubations were centrifuged for 3 min at 13,000 \times g at 4 °C to precipitate the S9 proteins, and the resulting supernatant was analysed by UPLC-DAD as described previously [12] immediately after centrifugation.

Kinetic analysis

The K_m and V_{max} values for the formation of 2-hexenoic acid and 2-hexen-1-ol were determined by fitting the data of the rate of the reaction with increasing *trans*-2-hexenal concentration to the standard Michaelis–Menten equation with [Hex] being the *trans*-2-hexenal concentration:

$$v = V_{max} \times [S] / (K_m + [S])$$

The *trans*-2-hexenal-concentration-dependent rate of liver GST-mediated Hex–GSH formation showed no saturation and a linear increase with *trans*-2-hexenal concentrations up to 3,000 μ M *trans*-2-hexenal in the presence of saturating concentration of GSH (2.5 mM) (see supporting information 3.1C). The first-order rate constant (K) of *trans*-2-hexenal conjugation with GSH mediated by human liver GSTs was obtained from this plot. The formation of GST-mediated Hex–GSH in the small intestine depending on the concentrations of GSH and *trans*-2-hexenal was described by ping-pong kinetics [13, 14] with the following equation, where [Hex] and [GSH] represent the concentration of *trans*-2-hexenal and GSH, respectively, and K_{m_G} and K_{m_H} the K_m values towards GSH and *trans*-2-hexenal, respectively:

$$v = V_{max} \times [Hex] \times [GSH] / (K_{m_G} \times [Hex] + K_{m_H} \times [GSH] + [Hex] \times [GSH])$$

The apparent maximum velocities (V_{\max}), the apparent Michaelis–Menten constants (K_m), and the apparent first order rate constant (K) were determined by fitting the data to the respective equations using GraphPad Prism (version 5.04, GraphPad Software, Inc., La Jolla, USA).

PBK/D model structure

A human PBK/D model describing the *trans*-2-hexenal detoxification and DNA adduct formation in the liver was developed based on the previously defined PBK/D model for *trans*-2-hexenal in male rats [12]. The schematic diagram of the human model is shown in Figure 3.2. The mass balance equations including a list of abbreviations used in the equations are presented as supporting information 3.2. The human model includes separate compartments for liver and small intestine as tissues that were involved in enzymatic detoxification of *trans*-2-hexenal. A separate compartment for fat tissue was included to account for the relatively high partition coefficient of *trans*-2-hexenal in fat tissue. Other tissues were lumped into a rapidly perfused tissue group (e.g. adrenals, brain, heart) and a slowly perfused tissue group (e.g. muscle, skin) [15]. The physiological parameters such as organ volumes and blood flows were obtained from the literature [16]. Partition coefficients were estimated from the $\log K_{ow}$ based on a method of DeJongh et al. [17] (Table 3.1). The $\log K_{ow}$ value for *trans*-2-hexenal was estimated with estimation program interface (EPI) Suite version 4.10 provided by the US Environmental Protection Agency and amounted to 0.25. Model equations were coded and numerically integrated in Berkeley Madonna 8.3.18 (Macey and Oster, UC Berkeley, CA, USA) using the Rosenbrock's algorithm for stiff systems.

The uptake of *trans*-2-hexenal from the intestinal lumen into the small intestine compartment was described by a first order process with the absorption rate constant 5.0 /h. This value was used previously for the uptake of acrylamide in the PBK model for acrylamide and its metabolite glycidamide, resulting in a rapid absorption of the ingested compound [18]. Conversion of *trans*-2-hexenal to 2-hexenoic acid or to 2-hexen-1-ol, and GST-mediated *trans*-2-hexenal conjugation with GSH were described in the liver and small intestine compartments based on the results of *trans*-2-hexenal incubations with tissue fractions. Neither further conversion nor distribution of *trans*-2-hexenal metabolites in the body was modeled because none of these would affect the predictions of the *trans*-2-hexenal detoxification and DNA adduct formation. The kinetic constants for the enzymatic metabolite formations were determined in vitro in the present study. The V_{\max} and K values expressed as nmol/min/(mg S9 protein) or ml/min/(mg S9 protein) were scaled to (g tissue) using S9 protein yields of 143 mg/(g liver) or 11.4 mg/(g small intestine) as scaling factors as described previously [19, 20]. The non-enzymatic reaction of *trans*-2-hexenal with GSH and protein was included in the liver and small intestine [21]. The second-order rate constants for *trans*-2-hexenal reaction with GSH (k_{GSH}) was obtained previously for the rat PBK/D model for *trans*-2-hexenal [12]. The second-order rate constant for *trans*-2-hexenal binding to protein reactive sites (k_{PRO}) was set to the same value as k_{GSH} based on

a study where the second-order rate constants for the reaction of ethyl acrylate with GSH, liver, or small intestine protein reactive sites were found to be comparable to each other (33, 33, and 32/M/min, respectively) [22].

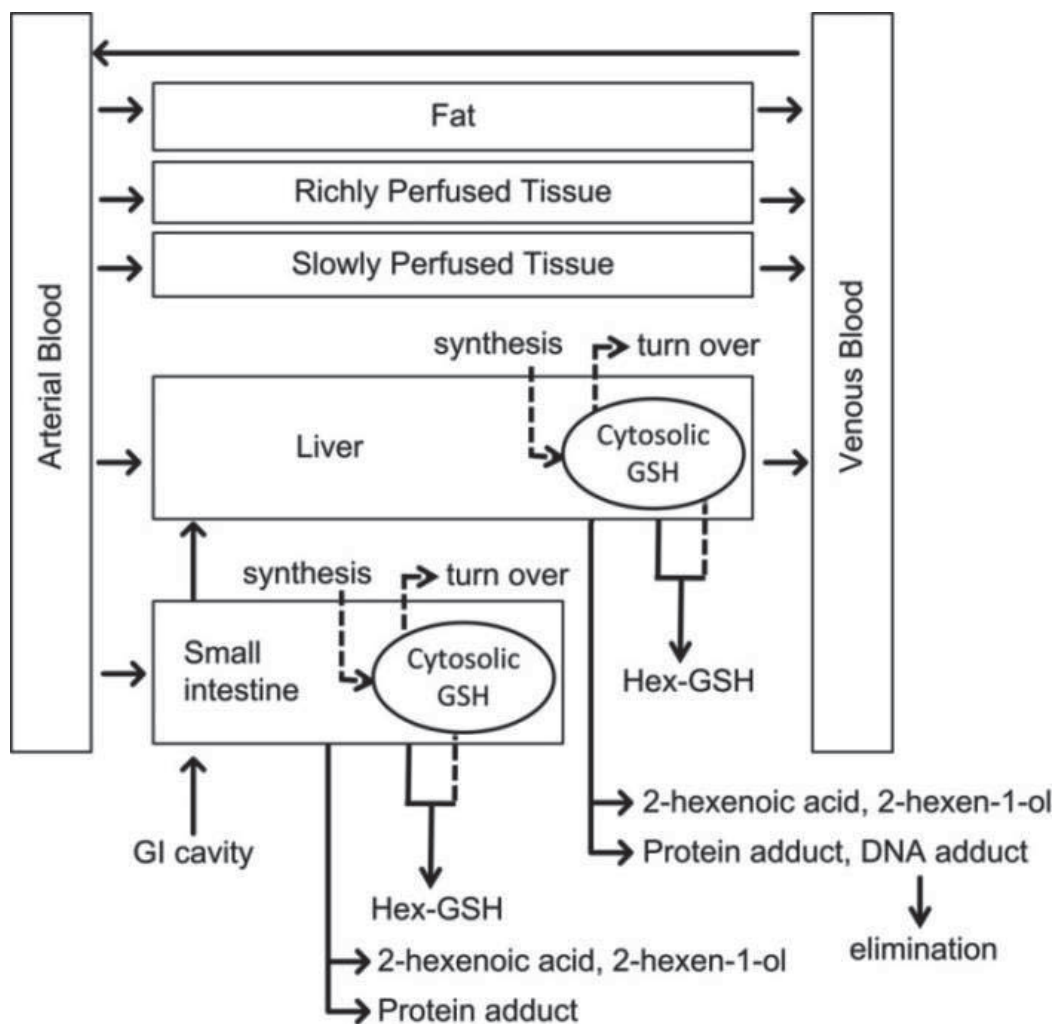


Figure 3.2. Diagram of the proposed PBK/D model for *trans*-2-hexenal in human. The solid and dashed lines represent the movement of *trans*-2-hexenal and GSH, respectively.

Table 3.1 Parameters used in the PBK/D model for *trans*-2-hexenal in human

Parameters	Symbols	Values	Parameters	Symbols	Values
Physico-chemical Parameters^a			small intestine	QSic	8.6
fat/blood	PF	26.1	richly perfused	QRc	47.3
liver/blood	PL	1.6	slowly perfused	QSc	24.8
small intestine/blood	PSI	1.6	Initial GSH concentration ($\mu\text{mol/kg}$ tissue)		
richly perfused tissues/blood	PR	1.6	liver ^c	InitGSH _L	5639
slowly perfused tissues/blood	PS	1.3	small intestine ^d	InitGSH _{Si}	1250
Physiological Parameters			GSH synthesis ($\mu\text{mol/kg}$ tissue/h) ^e		
Body weight (kg) ^a	BW	60	liver	GSYN _L	1122
Tissue volumes (% body weight) ^a			small intestine	GSYN _{Si}	27
fat	VFc	21.4	Apparent first order rate constant for GSH turnover (rat) (/h) ^e		
liver	VLc	2.6	liver	k_{L_GLOS}	0.142
small intestine	VSic	0.9	small intestine	k_{Si_GLOS}	0.044
arterial blood	VAc	2.0	Protein reactive sites (rat) ($\mu\text{mol/kg}$ tissue) ^f		
venous blood	VVc	5.9	liver	CPRO _L	3000
richly perfused	VRc	4.1	small intestine	CPRO _{Si}	774
slowly perfused	VSc	51.7	Biochemical Parameters		
Cardiac output (L/h) ^{a,b}	QC	310	Second order rate constant for chemical reaction with <i>trans</i> -2-hexenal ($\mu\text{M/h}$) ^g		
Blood flow to tissue (% cardiac output) ^a			GSH	k_{GSH}	5.8×10^{-4}
fat	QFc	5.2	2'-dG	k_{DNA}	1.6×10^{-7}
liver (excluding portal vein fraction)	QLc	14.1	Protein reaction sites in different tissues		
				k_{PRO}	5.8×10^{-4}

^aBrown et al. [16], ^bKrishnan and Andersen [23], ^cSweeney et al. [24], ^dAssimakopoulos et al. [25], ^ePotter and Tran [26], ^fPotter and Tran [22], ^gKiwamoto et al. [12]

Equations to describe GSH levels in the liver or small intestine were integrated in the PBK/D model to examine the influence of *trans*-2-hexenal-induced depletion of GSH on the model outcomes. The GSH pools were divided into cytosolic and mitochondrial pools. Only the cytosolic GSH was used to scavenge *trans*-2-hexenal and was therefore subject to depletion upon exposure to *trans*-2-hexenal [13]. The reactions reflecting biosynthesis and degradation of GSH due to its regular cellular turnover were described by zero-order synthesis and first-order elimination as described elsewhere [13, 21, 26]. Ninety per cent of the synthesized GSH was directed to cytosol, while the rest (10 %) was directed to mitochondria as an input for the regular GSH turnover in the mitochondrial pool. The amount of Hex-PdG in the liver was described by second order formation and first-order elimination due to DNA repair. The half-life ($T_{1/2}$) 38.5 h was used for DNA adducts elimination as described previously for the PBK/D model for *trans*-2-hexenal in rat [12].

Sensitivity analysis

To identify the key parameters that influence the model output, a sensitivity analysis was performed. Normalized sensitivity coefficients (SC) were determined according to the following equation: $SC = (C' - C)/(P' - P) \times (P/C)$, where C is the initial value of the model output, C' is the modified value of the model output resulting from an increase in parameter value, P is the initial parameter value, and P' is the modified parameter value [27-30]. Based on the literature [27], a 5 % increase in parameter values was chosen to analyse the effect of a change in parameter on maximum levels of *trans*-2-hexenal DNA adducts (Hex-PdG) in liver at a dose relevant to the estimated average *trans*-2-hexenal dietary intake (0.04 mg/kg bw). Each parameter was analysed individually, keeping the other parameters to their initial values.

Monte Carlo simulation

To predict the impact of interindividual variability in the kinetic parameters for the various *trans*-2-hexenal detoxification reactions on DNA adduct formation in the liver in the human population, a total number of 10,000 simulations were performed, assuming that the variation observed in the 11 individuals is representative of the whole population [31, 32]. For each simulation, the V_{max} , K_m , and K values were randomly selected from a log-normal distribution that was defined by the kinetic parameters obtained from the 11 individuals. The V_{max} , K_m , and K values were observed to vary independently from each other. The mean μ_w and standard deviation σ_w describing the log-normal distribution of each parameter in the liver were derived from the mean μ_x and coefficient of variation of the non-ln-transformed data using the following equation [32, 33]:

$$\mu_w = \ln[\mu_x / \sqrt{1 + CV_x^2}] \quad \text{and} \quad \sigma_w^2 = \ln(1 + CV_x^2)$$

where CV_x is the coefficient of variation of the non-ln-transformed V_{max} , K_m , and K values as observed with the 11 individual human subjects of the present study. For K_m and V_{max} values in the small intestine, mean μ_x was set to the values obtained from the pooled human small intestine S9. Due to the limited availability of small intestine S9 from different individuals, the kinetic parameters in the small intestine were not determined for the different individual subjects. To calculate the standard deviation σ_w and the mean μ_w , the reactions in the small intestine were assumed to have the same coefficient of variation (CV_x) as those of the same reaction in the liver, which ranged between 0.24 and 0.78 (Table 3.3). These values are comparable or higher than 0.3, which is a value generally applied when no information on the coefficient of variation is available [34]. The equations of the model are presented as supporting information 3.3.

RESULTS

Enzymatic oxidation and reduction of trans-2-hexenal

UPLC analysis revealed that in incubations with pooled human liver or small intestine S9, *trans*-2-hexenal was oxidized to 2-hexenoic acid in the presence of NAD⁺ as a cofactor. In the presence of NADPH as a cofactor, pooled human liver and small intestine S9 reduced *trans*-2-hexenal into 2-hexen-1-ol. The rate of formation of 2-hexenoic acid and 2-hexen-1-ol with increasing concentrations of *trans*-2-hexenal as observed in the different incubations is presented as supporting information 3.1A and 3.1B. From these plots, the apparent kinetic parameters (K_m and V_{max}) of *trans*-2-hexenal oxidation and reduction were obtained, and these are presented in Table 3.2.

GST-catalysed conjugation of trans-2-hexenal with GSH

trans-2-Hexenal reacts with GSH at its C3 position, resulting in the formation of a set of diastereomers of Hex–GSH (conjugate 1 and conjugate 2) with the chirality centre at the C3 position (Fig. 3.1) [35]. In incubations with pooled human liver or small intestine S9, an increase in the formation of both Hex–GSH stereoisomers was observed (data not shown). Further kinetic analysis of human GST-mediated formation of Hex–GSH therefore focused on the formation of both stereoisomers together. The *trans*-2-hexenal-concentration-dependent formation rate of Hex–GSH mediated by liver GSTs showed no saturation and a linear increase with *trans*-2-hexenal concentrations up to 3,000 μ M (supporting information 3.1C). The apparent first-order rate constant K for the formation rate of Hex–GSH depending on *trans*-2-hexenal concentrations was 0.0071 ± 0.0006 ml/min/(mg S9 protein). In case of small intestine, the formation of Hex–GSH mediated by GST present in the human pooled small intestine S9 was fitted to the ping-pong model, which is a two-substrate Michaelis–Menten equation. The apparent V_{max} and K_m towards *trans*-2-hexenal were determined and are presented in Table 3.2. The apparent K_m towards GSH was set at 100 μ M based on literature, being a representative value obtained using various substrates [13, 14].

Table 3.2 Kinetic parameters for metabolism of *trans*-2-hexenal in human. For comparison data from rat previously reported [12] are also presented.

Metabolites	Organ	Species	K_m (μM) ^a	V_{\max} (nmol/min/mg S9 protein) ^a	Scaled V_{\max} (nmol/min/g tissue) ^{a,b}	CE ^c (ml/min/g tissue)	K (ml/min/mg S9 protein) ^a	Scaled K (ml/min/g tissue) ^{a,b}
2-Hexenoic acid	Liver	Human	75.2±18.6	9.7±0.6	1387±87	18.4	n.a. ^d	n.a.
		Rat	230±45	18.5±1.1	2646±157	11.5	n.a.	n.a.
2-Hexen-1-ol	Liver	Human	145 ± 65	35.4±5.1	5062±715	34.9	n.a.	n.a.
		Rat	400±70	39.9±3.8	5706±543	14.3	n.a.	n.a.
Hex-GSH	Liver	Human	n.a.	n.a.	n.a.	n.a.	0.0071±0.0006	1.0±0.1
2-Hexenoic acid	Small intestine	Rat	9247±5237	649±265	92807±37895	10	n.a.	n.a.
		Human	458±187	5.2±1.1	60±13	0.13	n.a.	n.a.
2-Hexen-1-ol	Small intestine	Rat	156±116	0.95±0.18	10.9±2.1	0.07	n.a.	n.a.
		Human	372 ± 121	15.0±2.2	172±25	0.46	n.a.	n.a.
Hex-GSH	Small intestine	Rat	n.d. ^e	n.d.	n.d.	n.d.	n.d.	n.d.
		Human	752±388	35.3±6.8	403±78	0.54	n.a.	n.a.
		Rat	2172±869	496±87	5674±992	2.6	n.a.	n.a.

^aMean ± standard error of the fit, ^b V_{\max} or K was scaled to nmol/min/(g tissue) or ml/min/(g tissue) using scaling factors of 143 mg S9 protein/(g liver) and 11.4 mg S9 protein/(g small intestine). ^cIn vivo catalytic efficiencies (Scaled V_{\max}/K_m), ^dn.a. = not applicable, ^en.d. = not detected

Comparison of the catalytic efficiency of trans-2-hexenal detoxification pathways by humans and male rats

Table 3.2 provides a comparison of the kinetic parameters for *trans*-2-hexenal detoxification by pooled human S9 fractions with those obtained with pooled male rat S9 fractions as reported previously [12]. To make the parameters comparable, the V_{\max} and K values expressed as nmol/min/(mg S9 protein) or ml/min/(mg S9 protein) were converted to nmol/min/(g tissue) or ml/min/(g tissue) using scaling factors as defined in the “Materials and methods” section. In the liver, interspecies differences were especially observed in *trans*-2-hexenal reduction and GST-mediated formation of Hex–GSH. The K_m for reduction of *trans*-2-hexenal was 2.8-fold lower for human compared with rat, resulting in a 2.4-fold higher catalytic efficiency in reduction of *trans*-2-hexenal by human liver compared with rat liver. The GST-mediated formation of Hex–GSH was linear with increasing concentrations of *trans*-2-hexenal up to 3,000 μ M in human liver, but not in rat liver. Comparing the in vivo GST catalytic efficiency (V_{\max}/K_m) for rat liver and the scaled K for human liver, the rat liver appeared to be ten-fold more efficient than human liver in catalyzing conjugation of *trans*-2-hexenal with GSH. In the small intestine, interspecies differences were mainly observed in GST mediated *trans*-2-hexenal conjugation with GSH and in reduction to 2-hexen-1-ol. The in vivo catalytic efficiency for Hex–GSH formation by human small intestine was 4.8-fold lower compared with rat intestine, mainly due to a 14 times lower V_{\max} for GSH conjugation by human small intestine. In case of reduction to 2-hexen-1-ol, the comparison of in vivo catalytic efficiencies revealed that whereas reduction of *trans*-2-hexenal was not observed in rat small intestine, this reaction was the most efficient detoxification pathway in human small intestine.

Performance of the human PBK/D model

To evaluate the performance of the human PBK/D model, the model outcomes need to be compared with relevant observed human data. Because there are no human in vivo data available on *trans*-2-hexenal kinetics or DNA adduct formation in the liver, human data for acrolein, a structurally related α,β -unsaturated aldehyde, were used for the evaluation [36]. In the in vivo study by Watzek et al., a male person was dosed with 7.5 μ g/kg bw acrolein in drinking water. 2-Propenal (acrolein) excretion in urine as mercapturic acids [N-acetyl-S-(3-hydroxypropyl)cysteine and N-acetyl-S-(carboxyethyl)cysteine] was quantified using liquid chromatography–tandem mass spectrometry (LC/MS/MS). The study reported 26 % of the administered acrolein to be excreted as mercapturic acids within 24 h. To allow comparison between the observed human in vivo data and the PBK/D model outcome, the amount of α,β -unsaturated aldehyde excreted in urine as mercapturic acids was considered to be equal to the amount of the α,β -unsaturated aldehyde conjugates with GSH in the liver or small intestine. The human PBK/D model predicted 30 % of the α,β -unsaturated aldehyde to conjugate with GSH at a dose level 0.13 μ mol/kg bw (c.a. 7.5 μ g 2-propenal/kg bw and 13 μ g *trans*-2-hexenal/kg bw), which was only 1.1-fold higher than the observed level.

Sensitivity analysis

A sensitivity analysis was performed to identify key parameters that determine the amount of *trans*-2-hexenal DNA adducts (Hex–PdG) in the liver at T_{\max} , the time when the maximum DNA adduct level is predicted to be reached after administration of *trans*-2-hexenal. Normalized SC were calculated for all parameters at a *trans*-2-hexenal dose of 0.04 mg/kg bw, which is a level corresponding to the estimated average human dietary intake. The parameters for which the sensitivity coefficient exceeded 0.1 in absolute value are presented as supporting information 3.4. The sensitivity analysis of the human model showed that the predicted level of Hex–PdG in the human liver was influenced significantly by the second-order rate constant for the reaction of *trans*-2-hexenal with 2'-dG. The parameters that determine the detoxification rate in the liver, namely V_{\max} and K_m for oxidation and reduction, and the scaling factor of liver S9 also showed a significant impact on the predicted Hex–PdG level. In addition, the kinetic parameters of reduction and conjugation of *trans*-2-hexenal with GSH in the human small intestine as well as the scaling factor of small intestine S9 were also found to be important determinants.

The human PBK/D model predictions

The human-PBK/D model-based predictions for metabolite formation in the liver and small intestine as percentage of the administered dose are presented in Figure 3.3A. The human model revealed that at 0.04 mg/kg bw, the estimated average human dietary intake, 50 % of the *trans*-2-hexenal is reduced to 2-hexen-1-ol. Twenty-nine per cent of the administered *trans*-2-hexenal was predicted to be conjugated with GSH, and 21 % to be oxidized to 2-hexenoic acid. Cytosolic GSH in the small intestine was predicted to be completely depleted at a dose of 4 mg/kg bw and above. As a result, detoxification of *trans*-2-hexenal via GSH conjugation rapidly decreased compared to the other pathways at doses higher than 4 mg/kg bw. Of the administered dose of 0.04 mg/kg bw *trans*-2-hexenal, 58 % was detoxified in the small intestine before reaching the liver compartment (Figure 3.3B). The liver was shown to detoxify more than half of the administered *trans*-2-hexenal at doses higher than 5 mg/kg bw. Although there were some differences in the detoxification kinetics between human and rat, the predicted interspecies differences in the dose-dependent DNA adduct formation in the liver were limited (Figure 3.3C). Up to 163 mg/kg bw, the maximum DNA adduct formation in the human liver did not exceed 110 adducts/ 10^8 nt, which is considered as natural background level of DNA adducts in the liver (see “Discussion” section).

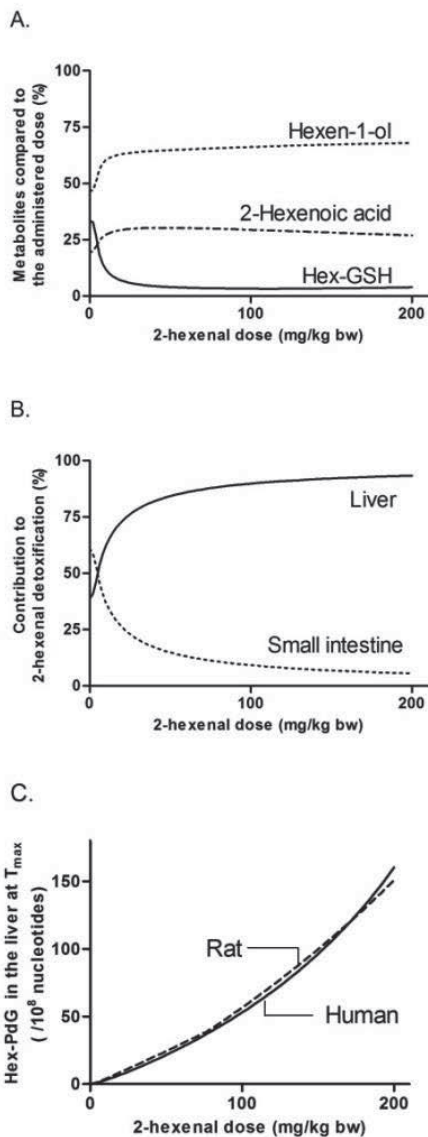


Figure 3.3. The human PBK/D model predictions. The PBK/D model-based predicted dose-dependent (A) formation of *trans*-2-hexenal metabolites in human presented as percentage of the administered dose 24 h after exposure, (B) contribution to *trans*-2-hexenal detoxification in human by the liver and small intestine, and (C) maximum formation of *trans*-2-hexenal DNA adducts (Hex-PdG) in the liver at T_{max} in human (solid line) and in rat (dashed line), the latter taken from our previous work [12].

Interindividual variation in *trans*-2-hexenal detoxification and its influence on DNA adduct formation

Table 3.3 shows the kinetic constants for detoxification of *trans*-2-hexenal via different metabolic routes as determined with incubations with liver S9 fractions of 11 individual human subjects. The in vivo catalytic efficiencies for *trans*-2-hexenal oxidation to 2-hexenoic acid and reduction to 2-hexen-1-ol varied from 5.5 to 28.7 ml/min/(g liver) and from 2.4 to 36.1 ml/min/(g liver), respectively. The scaled apparent first order rate constant K for GST-mediated GSH conjugation in the liver varied between 1.01 and 2.68 ml/min/(g liver) for eight individuals, but the K of the remaining three individuals (H0291, H0297, and H0393) was remarkably lower.

DNA adduct formation in the liver of the 11 individual human subjects upon oral exposure to *trans*-2-hexenal was estimated by replacing the V_{max} , K_m , and K values in the liver compartment of the PBK/D model with the parameters obtained using liver S9 of each individual

subject. Because kinetic parameters in small intestine were not determined for different individual subjects, the V_{\max} and K_m values in the small intestine were kept to the values obtained using pooled human small intestine S9. At a *trans*-2-hexenal dose of 0.04 mg/kg bw, the estimated average human dietary intake, the maximum DNA adduct formation after oral exposure ranged from 0.007 to 0.033 adducts/ 10^8 nt within the 11 individuals (Table 3.3). These values are four orders of magnitude lower than natural background DNA adduct level found in disease-free human liver (6.8–110 adducts/ 10^8 nt) (see “Discussion” section). The maximum DNA adduct formation in the liver was also examined at a dose of 0.178 mg/kg bw, which represents the 95th percentile of the estimated daily intake of *trans*-2-hexenal for a human of 60 kg (Eder and Schuler 2000) (Table 3.3). At this exposure level, the predicted maximum DNA adduct formation in the liver amounted to 0.032–0.147 adducts/ 10^8 nt among the 11 individuals and was thus shown to be still three orders of magnitude lower than natural background DNA adduct levels. Subsequently, Monte Carlo simulations were performed to investigate possible interindividual variation in *trans*-2-hexenal DNA adduct formation in the liver for the human population caused by interindividual variation in *trans*-2-hexenal detoxification efficiencies. The probability distributions used for these Monte Carlo simulations were derived from V_{\max} , K_m , or K values of three detoxification pathways in the liver determined in this study. Figure 3.4 shows the results obtained from the Monte Carlo simulation at a dose of 0.04 and 0.178 mg *trans*-2-hexenal/kg bw. The 50th and 99th percentiles were 0.015 and 0.039 adducts/ 10^8 nt, respectively, at 0.04 mg/kg bw, and 0.065 and 0.18 adducts/ 10^8 nt, respectively, at 0.178 mg/kg bw.

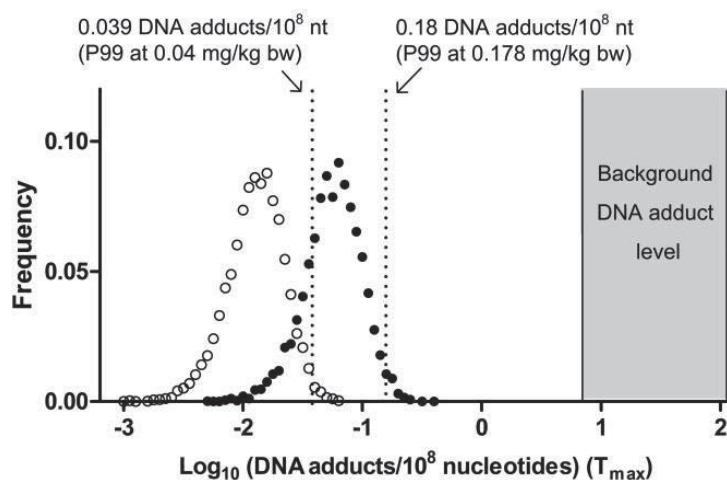


Figure 3.4. Results from Monte Carlo simulations predicting the frequency distribution of maximum Hex-PdG levels for the general population at *trans*-2-hexenal doses of 0.04 mg/kg bw (open circles) and 0.178 mg/kg bw (closed circles). The grey range indicates the natural background levels of exocyclic guanine adducts reported in disease-free human livers (6.8 to 110 DNA adducts/ 10^8 nt).

Table 3.3 Kinetic values of formation of 2-hexenoic acid, 2-hexen-1-ol and Hex-GSH in human individual in the liver

Code	Age	Gender	2-hexenoic acid			2-hexen-1-ol			Hex-GSH			Predicted DNA adduct level at T_{max}	
			K_m (μ M)	V_{max} (nmol/min/mg S9 protein)	CE (ml/min/g tissue) ^{a,b}	K_m (μ M)	V_{max} (nmol/min/mg S9 protein)	CE (ml/min/g tissue) ^{a,b}	K (ml/min/mg S9 protein)	Scaled K (ml/min/g liver) ^b	0.04 mg/kg bw (10^8 nt) ^c	0.178 mg/kg bw (10^8 nt) ^c	
H0428 ^d	57	F	106	14.4	19.3	231	58.3	36.1	0.015	2.17	0.007	0.032	
H0422	69	M	79	8.8	15.9	274	27.4	14.3	0.012	1.70	0.009	0.038	
H0297	4	F	69	13.8	28.7	232	13.3	8.2	<0.006	<0.86	0.011	0.050	
H0280 ^d	36	F	78	10.8	19.8	348	31.8	13.1	0.019	2.68	0.012	0.051	
H0432	60	M	145	8.1	8.0	147	25.5	24.8	0.009	1.34	0.012	0.054	
H0393	30	F	99	11.8	17.2	320	30.0	13.4	<0.006	<0.86	0.013	0.060	
H0311 ^d	21	M	101	11.2	15.8	418	28.4	9.7	0.015	2.13	0.015	0.066	
H0236	17	M	120	9.1	10.9	223	20.5	13.1	0.008	1.13	0.016	0.072	
H0291 ^d	18	F	101	7.0	9.9	161	10.2	9.1	<0.006	<0.86	0.021	0.095	
H0322	1	M	241	9.3	5.5	137	10.6	11.1	0.007	1.01	0.023	0.103	
H0420 ^d	42	M	122	7.5	8.8	564	9.4	2.4	0.007	1.02	0.033	0.147	
Mean±SD	n.a. ^f	n.a.	115±47	10.2±2.5	14.5±6.7	278±129	24.1±14.2	14.1±9.1	0.008±0.007 ^c	1.2±0.9 ^e	n.a.	n.a.	
CV ^g (%)	n.a.	n.a.	41.2	24.2	46.4	46.4	58.9	64.4	77.7	77.7	n.a.	n.a.	

^aIn vivo catalytic efficiencies (scaled V_{max}/K_m). ^b V_{max} or K obtained was scaled to nmol/min/g liver or ml/min/g liver using scaling factor of 143 mg, S9 protein/g liver. ^cCalculated assuming the K of H0297, H0393 and H0291 were 0, ^dRecent smokers, ^ecoefficient of variation, ^fn.a. = not applicable

DISCUSSION

In the present study, detoxification and subsequent DNA adduct formation in the liver upon oral exposure to *trans*-2-hexenal, a prominent α,β -unsaturated aldehyde in food, at realistic dietary exposure levels were examined by developing a human PBK/D model. The structure of the human model was based on the rat *trans*-2-hexenal PBK/D model, which was previously developed [12]. The parameters for the human PBK/D model were derived from literature or in vitro experiments using human tissue fractions. The model predicted that 30 % of the administered *trans*-2-hexenal conjugates to GSH at a dose of 0.13 $\mu\text{mol/kg bw}$, which was only 1.1-fold higher than the in vivo data obtained from a human exposed to acrolein, a related α,β -unsaturated aldehyde. This result indicates that the human model captured the critical kinetics of *trans*-2-hexenal adequately at the examined level of exposure.

To investigate the relative importance of DNA adduct formation due to *trans*-2-hexenal exposure, a comparison can be made to natural background DNA adduct levels that is continuously present in the human body as a consequence of endogenous processes and oxidative stress [37, 38]. Lower DNA adduct levels than relevant endogenous levels may suggest a limited genotoxicity risk of a xenobiotic, *trans*-2-hexenal in this case. Caution should, however, be taken when performing such a comparison because the ultimate cancer risk depends on the mutagenic potential of the DNA adduct, which may not necessarily be the same for xenobiotics of interest and endogenous compounds [39]. In case of *trans*-2-hexenal, a set of two diastereomers of exocyclic guanine adducts (Hex-PdG) in rat [10, 11] are formed that are structurally similar to the exocyclic guanine adducts formed by crotonaldehyde and malondialdehyde, which are endogenous metabolites formed upon lipid peroxidation [37, 38]. The background level of crotonaldehyde adducts has previously been reported to amount to 0.27–1.37 $\mu\text{mol/mol}$ guanine (i.e. 6.8–34.3 adducts/ 10^8 nt) [38], and that of malondialdehyde adducts to 50–110 adducts/ 10^8 nt in disease-free human liver [37]. Based on these studies, the natural background levels of exocyclic guanine adducts can be estimated to range from 6.8 to 110 adducts/ 10^8 nt. The human PBK/D model predicted a maximum DNA adduct formation in the liver of 0.008 and 0.034 adducts/ 10^8 nt at doses of 0.04 and 0.178 mg/kg bw, respectively. These two doses correspond to the 50th and the 95th percentile daily intakes of *trans*-2-hexenal from our diet for a 60-kg person [40]. Furthermore, the impact of interindividual variation in *trans*-2-hexenal detoxification kinetic parameters on DNA adduct formation was examined by measuring liver kinetic parameters in 11 individual human subjects. To generate a general population distribution in DNA adduct formation, the Monte Carlo simulation approach was used, assuming that the variation observed with these 11 individuals represents the variation in the human population. Among the most sensitive people (the 99th percentile of the population), DNA adduct formation was simulated to be up to 0.18 adducts/ 10^8 nt at 0.178 mg/kg bw. These results indicate that even in a person whose *trans*-2-hexenal detoxification efficiency is at the lowest percentile of the population, dietary

exposure to *trans*-2-hexenal at the current levels of intake does not increase DNA adduct levels in human liver by more than 3 % (6.98 compared to 6.80 adducts/ 10^8 nt) from the natural background levels.

The Monte Carlo simulations showed that these most sensitive persons displayed low catalytic efficiencies especially in the reduction of *trans*-2-hexenal in the liver, GST-catalysed conjugation with GSH in the small intestine, and oxidation in the liver compared to the average population (32, 44, and 49 % of the average population, respectively). The catalytic efficiencies of the other reactions remained between 62 and 94 % of those of the average population. This observation suggests that interindividual variation in *trans*-2-hexenal reduction in the liver may play the most important role in *trans*-2-hexenal detoxification, especially when low efficiency in the reduction is not compensated by high GST-mediated GSH conjugation or by oxidation.

Overall, when DNA adduct levels are predicted, it is important to take any uncertainties in the model into consideration. For example, the kinetic parameters were derived in vitro using saturated concentrations of cofactors, and this might result in underestimation in the formation of DNA adducts. On the other hand, the choices of other parameters such as a long half-life of *trans*-2-hexenal DNA adducts might have led to overestimation of DNA adduct levels in the liver [12]. Also, *trans*-2-hexenal reacts with protein thiol groups in the food component present in human gastrointestinal mucosa and thus may only partly be absorbed in vivo, while the human model assumed complete and swift absorption of administered *trans*-2-hexenal. If an uncertainty factor of 10 would be applied to account for such uncertainties in the extrapolation of in silico to the in vivo situation, the formation of DNA adducts due to *trans*-2-hexenal exposure would be 1.8 instead of 0.18 at 0.178 mg/kg bw in the most sensitive people, which is still lower than the natural background DNA adduct levels.

Altogether, the present study elucidates a possible negligible risk upon oral exposure to *trans*-2-hexenal at realistic dietary exposure levels for the human general population including individuals whose *trans*-2-hexenal detoxification efficiencies are low. Furthermore, the present study provides a proof of principle for the use of a PBK/D model to predict DNA adduct formation in an individual or the population as a whole.

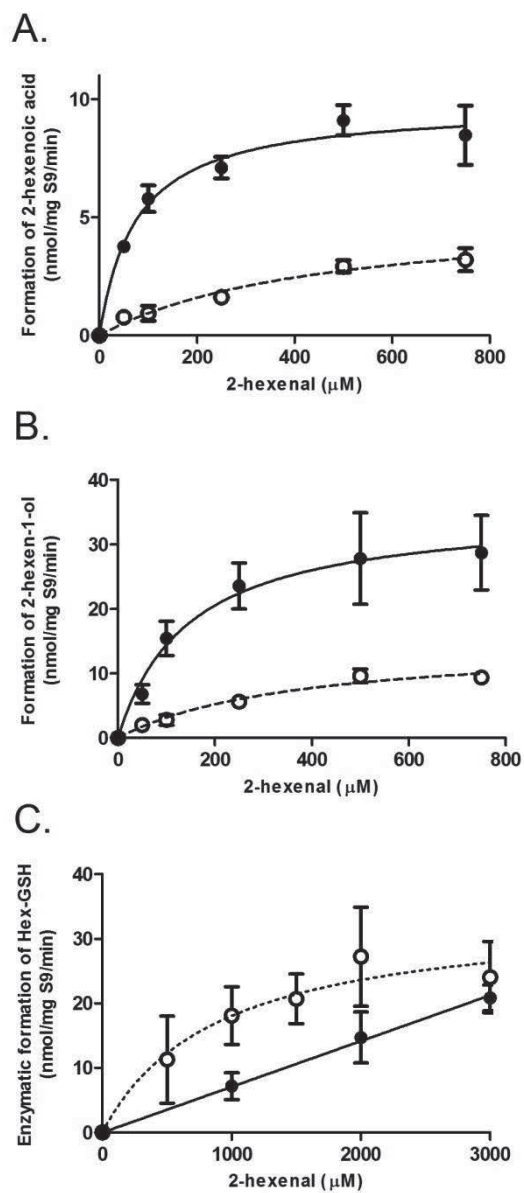
REFERENCES

- [1] Adams, T. B., Gavin, C. L., Taylor, S. V., Waddell, W. J., *et al.*, The FEMA GRAS assessment of alpha,beta-unsaturated aldehydes and related substances used as flavor ingredients. *Food Chem Toxicol* 2008, *46*, 2935-2967.
- [2] Witz, G., Biological interactions of alpha,beta-unsaturated aldehydes. *Free Radic Biol Med* 1989, *7*, 333-349.
- [3] EFSA, Minutes of the 26th plenary meeting of the the scientific panel on food additives, flavourings, processing aids and materials in contact with food. <http://www.efsa.europa.eu/en/events/event/afc071127-m.pdf>. 2007.
- [4] JECFA, Evaluation of Certain Food Additives: sixty-third report of the Joint FAO/WHO Expert Committee on Food Additives. http://whqlibdoc.who.int/trs/WHO_TRS_928.pdf. 2005.
- [5] Feron, V. J., Til, H. P., de Vrijer, F., Woutersen, R. R. A., *et al.*, Aldehydes: occurrence, carcinogenic potential, mechanism of action and risk assessment. *Mutat Res* 1991, *259*, 363-385.
- [6] Eder, E., Deininger, C., Mutagenicity of 2-alkylpropanals in Salmonella typhimurium strain TA 100: structural influences. *Environmental and molecular mutagenesis* 2001, *37*, 324-328.
- [7] Eder, E., Scheckenbach, S., Deininger, C., Hoffman, C., The possible role of alpha, beta-unsaturated carbonyl compounds in mutagenesis and carcinogenesis. *Toxicol Lett* 1993, *67*, 87-103.
- [8] Eisenbrand, G., Schuhmacher, J., Golzer, P., The influence of glutathione and detoxifying enzymes on DNA damage induced by 2-alkenals in primary rat hepatocytes and human lymphoblastoid cells. *Chem Res Toxicol* 1995, *8*, 40-46.
- [9] Golzer, P., Janzowski, C., Pool-Zobel, B. L., Eisenbrand, G., (E)-2-hexenal-induced DNA damage and formation of cyclic 1,N²-(1,3-propano)-2'-deoxyguanosine adducts in mammalian cells. *Chem Res Toxicol* 1996, *9*, 1207-1213.
- [10] Schuler, D., Eder, E., Detection of 1,N²-propanodeoxyguanosine adducts of 2-hexenal in organs of Fischer 344 rats by a ³²P-post-labeling technique. *Carcinogenesis* 1999, *20*, 1345-1350.
- [11] Stout, M. D., Bodes, E., Schoonhoven, R., Upton, P. B., *et al.*, Toxicity, DNA binding, and cell proliferation in male F344 rats following short-term gavage exposures to *trans*-2-hexenal. *Toxicol Pathol* 2008, *36*, 232-246.
- [12] Kiwamoto, R., Rietjens, I. M. C. M., Punt, A., A physiologically based in silico model for *trans*-2-hexenal detoxification and DNA adduct formation in rat. *Chem Res Toxicol* 2012, *25*, 2630-2641.
- [13] Johanson, G., Filser, J. G., A physiologically based pharmacokinetic model for butadiene and its metabolite butadiene monoxide in rat and mouse and its significance for risk extrapolation. *Arch Toxicol* 1993, *67*, 151-163.
- [14] Csanady, G. A., Filser, J. G., A physiological toxicokinetic model for inhaled propylene oxide in rat and human with special emphasis on the nose. *Toxicological sciences : an official journal of the Society of Toxicology* 2007, *95*, 37-62.
- [15] Ramsey, J. C., Andersen, M. E., A physiologically based description of the inhalation pharmacokinetics of styrene in rats and humans. *Toxicol Appl Pharmacol* 1984, *73*, 159-175.
- [16] Brown, R. P., Delp, M. D., Lindstedt, S. L., Rhomberg, L. R., Beliles, R. P., Physiological parameter values for physiologically based pharmacokinetic models. *Toxicol Ind Health* 1997, *13*, 407-484.
- [17] DeJongh, J., Verhaar, H. J., Hermens, J. L., A quantitative property-property relationship (QPPR) approach to estimate in vitro tissue-blood partition coefficients of organic chemicals in rats and humans. *Arch Toxicol* 1997, *72*, 17-25.
- [18] Kirman, C. R., Gargas, M. L., Deskin, R., Tonner-Navarro, L., Andersen, M. E., A physiologically based pharmacokinetic model for acrylamide and its metabolite, glycidamide, in the rat. *Journal of toxicology and environmental health. Part A* 2003, *66*, 253-274.
- [19] Medinsky, M. A., Leavens, T. L., Csanady, G. A., A., Gargas, M. L., Bond, J. A., In vivo metabolism of butadiene by mice and rats: a comparison of physiological model predictions and experimental data. *Carcinogenesis* 1994, *15*, 1329-1340.
- [20] van de Kerkhof, E. G., de Graaf, I. A., Groothuis, G. M., In vitro methods to study intestinal drug metabolism. *Current drug metabolism* 2007, *8*, 658-675.
- [21] Frederick, C. B., Potter, D. W., Chang-Mateu, M. M. I., Andersen, M. E., A physiologically based pharmacokinetic and pharmacodynamic model to describe the oral dosing of rats with ethyl acrylate and its implications for risk assessment. *Toxicol Appl Pharmacol* 1992, *114*, 246-260.
- [22] Potter, D. W., Tran, T. B., Rates of ethyl acrylate binding to glutathione and protein. *Toxicol Lett* 1992, *62*, 275-285.
- [23] Krishnan, K., Andersen, M. E., Physiologically based pharmacokinetic modeling in toxicology. *Principles and Methods of Toxicology (Forth Edition)* 2001, 193-239.
- [24] Sweeney, L. M., Gargas, M. L., Strother, D. E., Kedderis, G. L., Physiologically based pharmacokinetic model parameter estimation and

- sensitivity and variability analyses for acrylonitrile disposition in humans. *Toxicological sciences : an official journal of the Society of Toxicology* 2003, *71*, 27-40.
- [25] Assimakopoulos, S. F., Thomopoulos, K. C., Patsoukis, N., Georgiou, C. D., *et al.*, Evidence for intestinal oxidative stress in patients with obstructive jaundice. *European journal of clinical investigation* 2006, *36*, 181-187.
- [26] Potter, D. W., Tran, T. B., Apparent rates of glutathione turnover in rat tissues. *Toxicol Appl Pharmacol* 1993, *120*, 186-192.
- [27] Evans, M. V., Andersen, M. E., Sensitivity analysis of a physiological model for 2,3,7,8-tetrachlorodibenzo-p-dioxin (TCDD): assessing the impact of specific model parameters on sequestration in liver and fat in the rat. *Toxicological sciences : an official journal of the Society of Toxicology* 2000, *54*, 71-80.
- [28] Punt, A., Freidig, A. P., Delatour, T., Scholz, G., *et al.*, A physiologically based biokinetic (PBBK) model for estragole bioactivation and detoxification in rat. *Toxicol Appl Pharmacol* 2008, *231*, 248-259.
- [29] Paini, A., Punt, A., Viton, F., Scholz, G., *et al.*, A physiologically based biodynamic (PBBD) model for estragole DNA binding in rat liver based on in vitro kinetic data and estragole DNA adduct formation in primary hepatocytes. *Toxicol Appl Pharmacol* 2010, *245*, 57-66.
- [30] Rietjens, I. M. C. M., Louisse, J., Punt, A., Tutorial on physiologically based kinetic modeling in molecular nutrition and food research. *Molecular nutrition & food research* 2011, *55*, 941-956.
- [31] Punt, A., Jeurissen, S. M., Boersma, M. G., Delatour, T., *et al.*, Evaluation of human interindividual variation in bioactivation of estragole using physiologically based biokinetic modeling. *Toxicological sciences : an official journal of the Society of Toxicology* 2010, *113*, 337-348.
- [32] Martati, E., Boersma, M. G., Spengelink, A., Khadka, D. B., *et al.*, Physiologically based biokinetic (PBBK) modeling of safrole bioactivation and detoxification in humans as compared with rats. *Toxicological sciences : an official journal of the Society of Toxicology* 2012, *128*, 301-316.
- [33] Zhang, X., Tsang, A. M., Okino, M. S., Power, F. F. W., *et al.*, A physiologically based pharmacokinetic/pharmacodynamic model for carbofuran in Sprague-Dawley rats using the exposure-related dose estimating model. *Toxicological sciences : an official journal of the Society of Toxicology* 2007, *100*, 345-359.
- [34] Covington, T. R., Robinan Gentry, P., Van Landingham, C. B., Andersen, M. E., *et al.*, The use of Markov chain Monte Carlo uncertainty analysis to support a Public Health Goal for perchloroethylene. *Regulatory toxicology and pharmacology : RTP* 2007, *47*, 1-18.
- [35] Balogh, L. M., Roberts, A. G., Shireman, L. M., Greene, R. J., Atkins, W. M., The stereochemical course of 4-hydroxy-2-nonenal metabolism by glutathione S-transferases. *The Journal of biological chemistry* 2008, *283*, 16702-16710.
- [36] Watzek, N., Scherbl, D., Feld, J., Berger, F., *et al.*, Profiling of mercapturic acids of acrolein and acrylamide in human urine after consumption of potato crisps*. *Molecular nutrition & food research* 2012.
- [37] Chaudhary, A. K., Nokubo, M., Reddy, G. R., Yeola, S. N., *et al.*, Detection of endogenous malondialdehyde-deoxyguanosine adducts in human liver. *Science* 1994, *265*, 1580-1582.
- [38] Nath, R. G., Chung, F. L., Detection of exocyclic exocyclic 1,N²-propanodeoxyguanosine adducts as common DNA lesions in rodents and humans. *Proceedings of the National Academy of Sciences of the United States of America* 1994, *91*, 7491-7495.
- [39] Paini, A., Scholz, G., Marin-Kuan, M., Schilter, B., *et al.*, Quantitative comparison between in vivo DNA adduct formation from exposure to selected DNA-reactive carcinogens, natural background levels of DNA adduct formation and tumour incidence in rodent bioassays. *Mutagenesis* 2011, *26*, 605-618.
- [40] Eder, E., Schuler, D., An approach to cancer risk assessment for the food constituent 2-hexenal on the basis of 1,N²-propanodeoxyguanosine adducts of 2-hexenal in vivo. *Arch Toxicol* 2000, *74*, 642-648.

SUPPORTING INFORMATION

Supporting Information 3.1. *trans*-2-Hexenal concentration-dependent formation rate of metabolites by human tissue fractions. The formation rate of 2-hexenoic acid (A), 2-hexen-1-ol (B), and GST mediated formation rate of Hex-GSH (C) in human liver (closed circles, solid lines) and small intestine (open circles, dashed lines).



Supporting Information 3.2. Human PBK/D model equations.

(1) Uptake from GI cavity

The uptake of *trans*-2-hexenal from the intestinal cavity into the small intestine compartment was described by a first-order process as follows:

$$\begin{aligned} dAGI/dt &= -K_a * AGI \\ \text{InitAGI} &= \text{DOSE} \end{aligned}$$

where

AGI Amount of *trans*-2-hexenal remaining in GI cavity (μmol)
 K_a Linear uptake rate (/h)
 DOSE Amount of *trans*-2-hexenal administered in a rat (μmol).

(2) Slowly perfused tissue, richly perfused tissue and fat

Amount *trans*-2-hexenal in slowly perfused tissue, richly perfused tissue or fat compartment was described as follows:

$$\begin{aligned} dAT_i/dt &= QT_i * (CA - CVT_i) \\ CT_i &= AT_i / VT_i \\ CVT_i &= CT_i / PT_i \end{aligned}$$

where

AT_i Amount of *trans*-2-hexenal in a tissue (μmol)
 QT_i Blood flow into a tissue (L/h)
 CA Concentration of *trans*-2-hexenal in arterial blood perfusing a tissue ($\mu\text{mol/L}$)
 CVT_i Concentration of *trans*-2-hexenal in venous blood leaving a tissue ($\mu\text{mol/L}$)
 CT_i Concentration of *trans*-2-hexenal in a tissue ($\mu\text{mol/kg}$)
 VT_i Volume of a tissue (kg)
 PT_i Tissue/blood partition coefficient of *trans*-2-hexenal

(3) Liver

Amount *trans*-2-hexenal in the liver (AL, μmol) is described as follows:

$$\begin{aligned} dAL/dt &= QL * CA + QS_i * CVS_i - (QL + QS_i) * CVL - (\text{eq.1} + \text{eq.2} + \text{eq.3} + \text{eq.4} + \text{eq.5} + \text{eq.6}) \\ CL &= AL / VL \\ CVL &= CL / PL \end{aligned}$$

where

QL Blood flow into the liver (L/h)
 QS_i Blood flow into the small intestine (L/h)
 CVS_i Concentration of *trans*-2-hexenal in venous blood leaving the small intestine ($\mu\text{mol/L}$)
 CVL Concentration of *trans*-2-hexenal in venous blood leaving the liver ($\mu\text{mol/L}$)
 CL Concentration of *trans*-2-hexenal in the liver ($\mu\text{mol/L}$)
 PL Liver/blood partition coefficient of *trans*-2-hexenal

Amount *trans*-2-hexenal oxidized to 2-hexenoic acid enzymatically in the liver (AMLHA, μmol) is described to follow Michaelis-Menten equation:

$$dAMLHA/dt = V_{S_{\max, L_HA}} * CVL / (K_{m, L_HA} + CVL) \quad \text{----- eq. 1}$$

where

V<sub>S_{max, L_{HA}} Scaled V_{max} for enzymatic oxidation of *trans*-2-hexenal in the liver ($\mu\text{mol/h}$)
 K_{m, L_{HA}} K_m for enzymatic oxidation of *trans*-2-hexenal in the liver (μM)</sub>

Amount *trans*-2-hexenal reduced to 2-hexen-1-ol in the liver (AMLHO, μmol) is described to follow Michaelis-Menten-equation:

$$dAMLHO/dt = V_{S_{\max, L_HO}} * CVL / (K_{m, L_HO} + CVL) \quad \text{----- eq. 2}$$

where

V<sub>S_{max, L_{HO}} Scaled V_{max} for enzymatic reduction of *trans*-2-hexenal in the liver ($\mu\text{mol/h}$)
 K_{m, L_{HO}} K_m for enzymatic reduction of *trans*-2-hexenal in the liver (μM)</sub>

Amount *trans*-2-hexenal metabolized in liver to GSH conjugation by GSTs (AMLHG_{GST}, μmol) is

Chapter 3

described as following :

$$d\text{AMLHG}_{\text{GST}}/dt = K_s * \text{CVL} \quad \text{----- eq.3}$$

where

K_s Scaled first order rate constant derived in this study for enzymatic conjugation of 2-hexanal with GSH in the liver (μM)

Amount *trans*-2-hexenal chemically bound in liver to GSH ($\text{AMLHG}_{\text{chem}}$, μmol) is described as following:

$$d\text{AMLHG}_{\text{chem}}/dt = k_{\text{GSH}} * \text{CVL} * \text{CGSH}_{\text{LC}} * \text{VL} \quad \text{----- eq.4}$$

where

k_{GSH} Second order rate constant of *trans*-2-hexenal binding to GSH ($/\mu\text{mol/h}$)

VL Volume of the liver (kg)

CGSH_{LC} Concentration of GSH in the liver cytosol ($\mu\text{mol/kg}$ liver)

Amount *trans*-2-hexenal protein adducts in the liver (AMLHP , μmol) is described as following:

$$d\text{AMLHP}/dt = k_{\text{PRO}} * \text{CVL} * \text{CPRO}_{\text{L}} * \text{VL} \quad \text{----- eq.5}$$

where

k_{PRO} Second order rate constant of *trans*-2-hexenal binding to protein reaction sites in a tissue ($/\mu\text{mol/h}$)

CPRO_{L} Concentration of protein reaction sites in the liver ($\mu\text{mol/kg}$ liver)

The formation of DNA adduct (Hex-PdG) in the liver ($\text{AMLHP}_{\text{form}}$) was described as following:

$$d\text{AMLHP}_{\text{form}}/dt = k_{\text{DNA}} * \text{CVL} * \text{CdG}_{\text{L}} * \text{VL} \quad \text{----- eq.6}$$

where

k_{DNA} Second order rate constant of *trans*-2-hexenal binding to 2'-dG ($/\mu\text{mol/h}$)

CdG_{L} Concentration of 2'-dG in the liver ($\mu\text{mol/kg}$ liver)

CdG_{L} was calculated to be 1.36 $\mu\text{mol/kg}$ liver using the average molecular weight of nucleotides (330 g/mol) and reported concentration of DNA in a rat liver (1.8 g/kg liver).

Amount of DNA adduct (Hex-PdG) in liver (AMLHP , μmol) is described by subtracting elimination of DNA adduct from the formation:

$$d\text{AMLHP}/dt = \text{eq.6} - \text{AMLHP} * (\ln 2 / T_{1/2})$$

where

$T_{1/2}$ Half-life of Hex-PdG in the liver (h)

Amount of GSH present in the liver cytosol (AMGSH_{LC} , μmol) is described by zero-order synthesis and reduction by first-order elimination due to turnover and depletion by *trans*-2-hexenal:

$$d\text{AMGSH}_{\text{LC}} = \text{GSYN}_{\text{L}} * \text{VL} * 0.9 - (\text{eq.3} + \text{eq.4} + k_{\text{L_GLOS}} * \text{AMGSH}_{\text{LC}}) \quad \text{----- eq.7}$$

$$\text{Init AMGSH}_{\text{LC}} = \text{InitGSH}_{\text{L}} * \text{VL} * 0.9$$

$$\text{CGSH}_{\text{LC}} = \text{AMLcGSH} / \text{VL}$$

where

GSYN_{L} Rate of GSH synthesis in the liver ($\mu\text{mol/h}$)

$k_{\text{L_GLOS}}$ First-order rate of GSH turnover in the liver ($/\text{h}$)

$\text{InitGSH}_{\text{L}}$ Initial concentration of GSH in the liver ($\mu\text{mol/kg}$ liver)

When eq.7 gave negative values, the value zero was used as the amount of GSH in the liver cytosol.

(4) Small intestine

The amount *trans*-2-hexenal in small intestine tissue, (ASi , μmol) is described as follows:

$$d\text{ASi}/dt = \text{QSi} * (\text{CA} - \text{CVSi}) + \text{Ka} * \text{AGI} - (\text{eq.8} + \text{eq.9} + \text{eq.10} + \text{eq.11} + \text{eq.12})$$

$$\text{CSi} = \text{ASi} / \text{VSi}$$

$$\text{CVSi} = \text{CSi} / \text{PSi}$$

where

CSi Concentration of *trans*-2-hexenal in the small intestine ($\mu\text{mol/L}$)

VSi Volume of the small intestine (kg)

PSi Small intestine/blood partition coefficient of *trans*-2-hexenal

Amount *trans*-2-hexenal enzymatically oxidized 2-hexenoic acid (AMSiHA, μmol) in the small intestine is described by Michaelis-Menten equation:

$$d\text{AMSiHA}/dt = V_{S_{\text{max,Si_HA}}} * \text{CVSi} / (K_{m, \text{Si_HA}} + \text{CVSi}) \quad \text{----- eq.8}$$

where

$V_{S_{\text{max,Si_HA}}}$ Scaled V_{max} for enzymatic oxidation of *trans*-2-hexenal in the small intestine ($\mu\text{mol/h}$)
 $K_{m, \text{Si_HA}}$ K_m for enzymatic oxidation of *trans*-2-hexenal in small intestine (μM).

Amount *trans*-2-hexenal reduced to 2-hexen-1-ol in the small intestine (AMSiHO, μmol) is described to follow Michaelis-Menten-equation:

$$d\text{AMSiHO}/dt = V_{S_{\text{max, Si_HO}}} * \text{CVSi} / (K_{m, \text{Si_HO}} + \text{CVSi}) \quad \text{----- eq. 9}$$

where

$V_{S_{\text{max,Si_HO}}}$ Scaled V_{max} for enzymatic reduction of *trans*-2-hexenal in the small intestine ($\mu\text{mol/h}$)
 $K_{m, \text{Si_HO}}$ K_m for enzymatic reduction of *trans*-2-hexenal in the small intestine (μM)

Amount *trans*-2-hexenal metabolized in the small intestine to GSH conjugation by GST (AMSiHG_{GST}, μmol) is described by a two substrate ping-pong model:

$$d\text{AMSiHG}_{\text{GST}}/dt = \frac{V_{S_{\text{max, Si_GST}}} * \text{CVSi} * \text{CGSH}_{\text{SiC}}}{(K_{m, \text{Si_GST_G}} * \text{CVSi} + K_{m, \text{Si_GST_H}} * \text{CGSH}_{\text{SiC}} + \text{CGSH}_{\text{SiC}} * \text{CVSi})} \quad \text{----- eq.10}$$

where

$V_{S_{\text{max, Si_GST}}}$ Scaled V_{max} for enzymatic conjugation of *trans*-2-hexenal in the small intestine ($\mu\text{mol/h}$)
 CGSH_{SiC} Concentration of GSH in the small intestine cytosol ($\mu\text{mol/kg}$)
 $K_{m, \text{Si_GST_H}}$ K_m toward *trans*-2-hexenal for enzymatic conjugation of *trans*-2-hexenal in the small intestine (μM)
 $K_{m, \text{Si_GST_G}}$ K_m toward GSH for enzymatic conjugation of *trans*-2-hexenal in the small intestine (μM)

Amount *trans*-2-hexenal chemically bound in the small intestine to GSH (AMSiHG_{chem}, μmol) is described as following:

$$d\text{AMSiHG}_{\text{chem}}/dt = k_{\text{GSH}} * \text{CVSi} * \text{CGSH}_{\text{SiC}} * \text{VSi} \quad \text{----- eq.11}$$

where

k_{GSH} First order rate constant of *trans*-2-hexenal binding to GSH ($1/\mu\text{mol/h}$)
 VSi Volume of the small intestine (kg)

Amount *trans*-2-hexenal chemically bound to protein reaction sites in the small intestine (AMSiHP, μmol) is described as following:

$$d\text{AMSiHP}/dt = k_{\text{PRO}} * \text{CVSi} * \text{CPRO}_{\text{Si}} * \text{VSi} \quad \text{----- eq.12}$$

where

k_{PRO} First order rate constant of *trans*-2-hexenal binding to protein reaction sites in a tissue ($1/\mu\text{mol/h}$)
 CPRO_{Si} Concentration of protein reaction sites in the liver ($\mu\text{mol/kg liver}$)

Amount of GSH present in the small intestine cytosol (AMGSH_{SiC}, μmol) is described in the same way as in the liver (eq 10):

$$d\text{AMGSH}_{\text{SiC}} = \text{GSYN}_{\text{Si}} * \text{VSi} * 0.9 - (\text{eq.10} + \text{eq.11} + k_{\text{GLOS_Si}} * \text{AMGSH}_{\text{SiC}}) \quad \text{----- eq.13}$$

$$\text{Init AMGSH}_{\text{SiC}} = \text{InitGSH}_{\text{Si}} * \text{VSi} * 0.9$$

$$\text{CGSH}_{\text{SiC}} = \text{AMSiHG}_{\text{SiC}} / \text{VSi}$$

where

GSYN_{Si} Rate of GSH synthesis in the small intestine ($\mu\text{mol/h}$)
 $k_{\text{GLOS_Si}}$ First-order rate of GSH turnover in the small intestine ($1/h$)
 $\text{InitGSH}_{\text{Si}}$ Initial concentration of GSH in the small intestine ($\mu\text{mol/kg liver}$)

As was the case in the liver, the value zero was used as the amount of GSH in the small intestine cytosol when eq.13 gave negative values.

(5) Venous blood and arterial blood

Concentration of *trans*-2-hexenal in venous blood (CV) and in arterial blood (CA, both in $\mu\text{mol/L}$) was described as follows:

Chapter 3

$$dAV/dt = QF*CVF + (QL+QSi)*CVL + QR*CVR + QS*CVS - QC*CV$$
$$CV = AV/(AV+VV)$$
$$CV = CA$$

where

AV	Amount of <i>trans</i> -2-hexenal in venous blood (μmol)
QF	Blood flow into fat (L/h)
CVF	Concentration of <i>trans</i> -2-hexenal in venous blood leaving fat ($\mu\text{mol/L}$)
QR	Blood flow into richly perfused tissue (L/h)
CVR	Concentration of <i>trans</i> -2-hexenal in venous blood leaving richly perfused tissue ($\mu\text{mol/L}$)
QS	Blood flow into slowly perfused tissue (L/h)
CVS	Concentration of <i>trans</i> -2-hexenal in venous blood leaving slowly perfused tissue ($\mu\text{mol/L}$)

Supporting Information 3.3. Equations added to the human PBK/D model to perform Monte Carlo simulations.

The following equations were added to the equation 1 of supporting information 3.1 to perform Monte Carlo simulations:

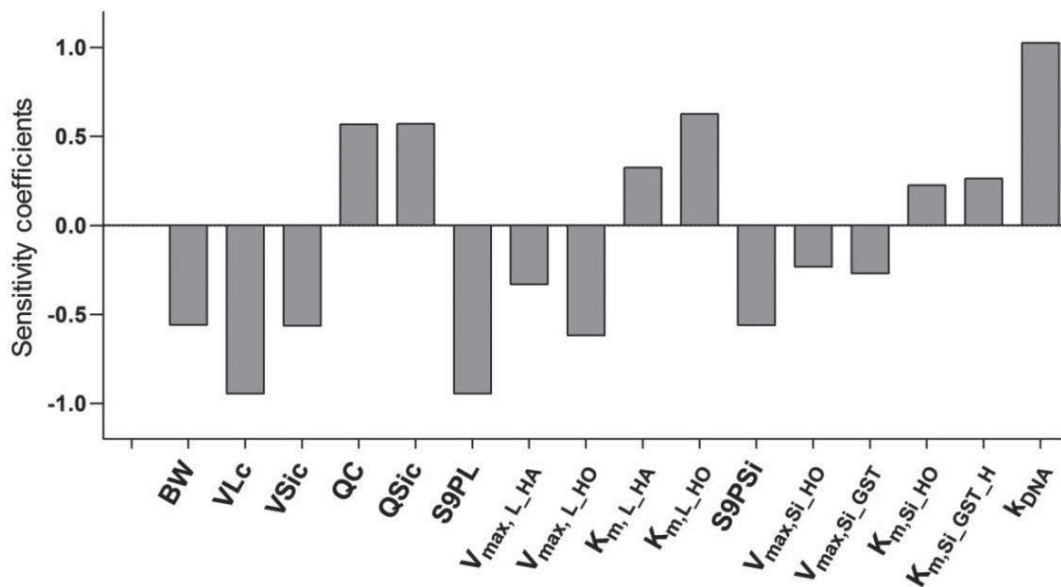
$$V_{S_{\max,L_HA}} = \text{init}(\exp(\text{normal}(\mu_w(V_{\max,L_HA}), \sigma_w(V_{\max,L_HA})))$$

$$K_{m,L_HA} = \text{init}(\exp(\text{normal}(\mu_w(K_{m,L_HA}), \sigma_w(K_{m,L_HA})))$$

where $V_{S_{\max,L_HA}}$ and K_{m,L_HA} are scaled V_{\max} and K_m for *trans*-2-hexenal oxidation in the liver, respectively. The same equations were added to the equation 2, 3, 8, 9 and 10 of the human PBK/D model in order to perform Monte Carlo simulations for $V_{S_{\max}}$, K_m and K_s values of *trans*-2-hexenal oxidation in the small intestine, and *trans*-2-hexenal reduction and GST mediated conjugation to GSH in the liver and the small intestine.

Supporting Information 3.4. Sensitivity analysis of the predicted amount of Hex-PdG in the liver to different model parameters at T_{\max} to 0.04 mg *trans*-2-hexenal/kg bw.

The parameters listed in the figures are the following: body weight (BW); fraction of the liver (VLC) and the small intestine (VSic); blood flow rate (QC); fraction of the blood flow to the small intestine (QSic); scaling factor of liver S9 (S9PL); V_{\max} and K_m in the liver to form 2-hexenoic acid (HA) or 2-hexen-1-ol (HO); scaling factor of small intestine S9 (S9PSi); V_{\max} and K_m in the small intestine to form 2-hexen-1-ol (HO) or Hex-GSH; K_m toward *trans*-2-hexenal in the small intestine to form Hex-GSH (K_{m, si_GST_H}); and second-order rate constant of *trans*-2-hexenal binding to 2'-dG (k_{DNA})





CHAPTER 4

An integrated QSAR-PBK/D modelling approach for predicting detoxification and DNA adduct formation of 18 acyclic food-borne α,β -unsaturated aldehydes

R. Kiwamoto
A. Spenkelink
I. M. C. M. Rietjens
A. Punt

Based on *Toxicology and Applied Pharmacology* (2014) 282(1): 108-117

ABSTRACT

Acyclic α,β -unsaturated aldehydes present in food raise a concern because the α,β -unsaturated aldehyde moiety is considered a structural alert for genotoxicity. However, controversy remains on whether in vivo at realistic dietary exposure DNA adduct formation is significant. The aim of the present study was to develop physiologically based kinetic/dynamic (PBK/D) models to examine dose-dependent detoxification and DNA adduct formation of a group of 18 food-borne acyclic α,β -unsaturated aldehydes without 2- or 3-alkylation, and with no more than one conjugated double bond. Parameters for the PBK/D models were obtained using quantitative structure–activity relationships (QSARs) defined with a training set of six selected aldehydes. Using the QSARs, PBK/D models for the other 12 aldehydes were defined. Results revealed that DNA adduct formation in the liver increases with decreasing bulkiness of the molecule especially due to less efficient detoxification. 2-Propenal (acrolein) was identified to induce the highest DNA adduct levels. At realistic dietary intake, the predicted DNA adduct levels for all aldehydes were two orders of magnitude lower than endogenous background levels observed in disease free human liver, suggesting that for all 18 aldehydes DNA adduct formation is negligible at the relevant levels of dietary intake. The present study provides a proof of principle for the use of QSAR-based PBK/D modelling to facilitate group evaluations and read-across in risk assessment.

INTRODUCTION

A number of acyclic α,β -unsaturated aldehydes are present in different foods and beverages of plant origin as natural constituents. For instance, *trans*-2-hexenal can be found in banana, *trans*-2-*cis*-6-nonadienal in cucumber [1], and *trans*-2-octenal in orange oil [2]. Due to their unique odour, many of such aldehydes are used as food flavouring agents. However, their α,β -unsaturated aldehyde moiety is considered a structural alert for genotoxicity raising a food safety concern [3]. In 2007, the European Food Safety Authority (EFSA) launched a risk assessment of 347 flavouring substances being α,β -unsaturated aldehydes or ketones and precursors which give rise to such carbonyl substances [3]. EFSA considered that there is a need for additional information on most of the substances, including especially *in vivo* genotoxicity data, before conclusions can be reached [3]. As a result, in EU the use of many acyclic α,β -unsaturated aldehydes as food flavouring agents has been suspended under Regulation (EC) No. 1334/2008.

Numerous *in vitro* studies have shown the genotoxic and mutagenic potency of acyclic α,β -unsaturated aldehydes [4-6], but these *in vitro* models do not account for possible detoxification occurring *in vivo*. The aldehyde group ($-\text{CHO}$) present in the α,β -unsaturated aldehyde moiety can be oxidised to a carboxylic acid group ($-\text{COOH}$) by aldehyde dehydrogenases (ALDHs) [7, 8], or reduced to a hydroxyl group ($-\text{OH}$) by aldose reductases (ARs) [9]. In addition, α,β -unsaturated aldehydes react spontaneously with glutathione (GSH) forming GSH conjugates, which are no longer electrophilic, and this conjugation is enhanced by glutathione S-transferases (GSTs) [10, 11]. In 2008, the Expert Panel of the Flavor and Extract Manufacturers Association (FEMA) concluded the use of α,β -unsaturated aldehydes as food flavouring agents to be safe based on the low level of use as well as the possible rapid detoxification of the substances *in vivo* [12]. The question that remains to be answered is whether detoxification is indeed sufficient to prevent significant DNA adduct formation of acyclic α,β -unsaturated aldehydes *in vivo*. Using *trans*-2-hexenal as model compound, we have previously shown that physiologically based kinetic/dynamic (PBK/D) modelling gives insights in detoxification and DNA adduct formation of α,β -unsaturated aldehydes *in vivo* [13, 14]. The PBK/D models for *trans*-2-hexenal for rat and human revealed that DNA adduct formation in the liver due to intake of *trans*-2-hexenal at human dietary exposure levels would be three to six orders of magnitude lower than the natural background levels of structurally similar 1,*N*²-exocyclic propanodeoxyguanosine adducts in disease free human liver. Based on this observation we concluded that at realistic dietary exposure levels the DNA adduct formation may be negligible [13, 14]. *trans*-2-Hexenal is, however, only one of the many α,β -unsaturated aldehydes present in diet and it remains unknown whether the results would be similar for the other acyclic α,β -unsaturated aldehydes. Detoxification and DNA binding efficiencies may be different depending on the molecular structure [4, 8, 10, 15]. The aim of the present study is to

develop PBK/D models to examine dose-dependent detoxification and DNA adduct formation of a group of 18 acyclic α,β -unsaturated aldehydes, increasing the efficiency of the model development by obtaining the kinetic parameters for the PBK/D models using quantitative structure–activity relationships (QSARs). QSAR models were defined based on a training set of six selected aldehydes and PBK/D model parameters for the other 12 aldehydes were subsequently estimated using these QSARs. The α,β -unsaturated aldehydes investigated included 18 food-borne acyclic α,β -unsaturated aldehydes without 2- or 3-alkylation, and with no more than one conjugated double bond [3] (Figure 4.1). The PBK/D models thus defined were used to characterize dose-dependent DNA adduct formation and to evaluate the possible risks arising from exposure to the aldehydes at realistic dietary exposure levels.

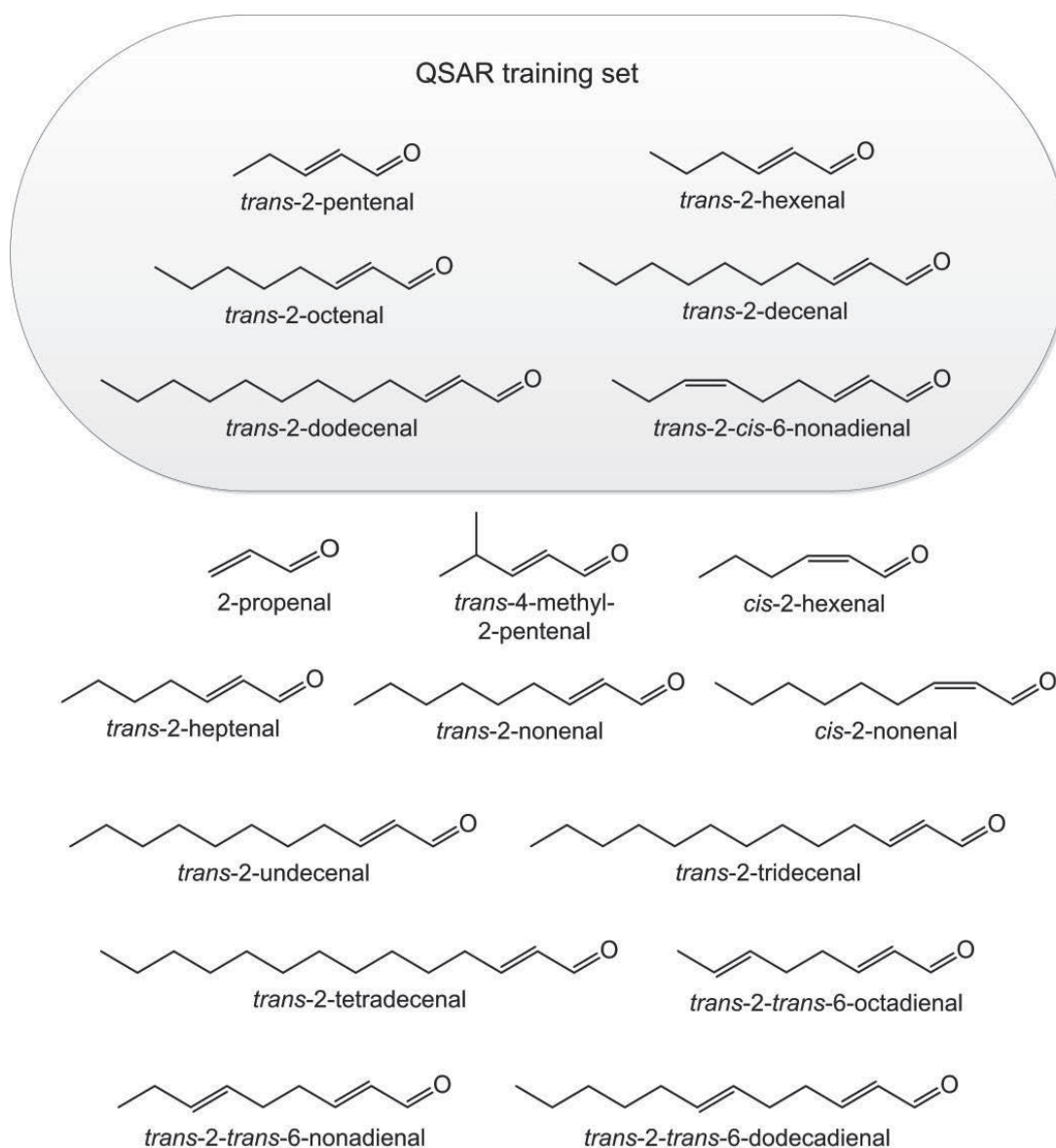


Figure 4.1. The structure of the 18 food-borne acyclic α,β -unsaturated aldehydes included in the present study.

MATERIALS AND METHODS

Chemicals and biological materials

α,β -Unsaturated aldehydes, α,β -unsaturated carboxylic acids, α,β -unsaturated alcohols, 2'-deoxyguanosine (2'-dG), tris (hydroxymethyl) aminomethane, and reduced glutathione (GSH) were purchased from Sigma-Aldrich (Zwijndrecht, The Netherlands). Reduced (NADPH) and oxidised (NAD⁺) β -nicotinamide adenine dinucleotide phosphate were obtained from Roche Diagnostics (Mannheim, Germany). DMSO was purchased from Acros Organic (New Jersey, USA). Chromatography grade acetonitrile was purchased from Biosolve (Valkenswaard, The Netherlands). Chromatography grade trifluoroacetic acid (TFA) and formic acid were purchased from VWR International (Darmstadt, Germany). Pooled liver S9 from male F344 rats and pooled intestine S9 from male Sprague Dawley rats were obtained from BD Gentest (Worburn, USA) and Xenotech (Lenexa, USA), respectively.

The selection of six training set compounds

Among the 18 food-borne acyclic α,β -unsaturated aldehydes, six aldehydes were selected as training set from the aldehydes listed in FGE 1.1.1 by EFSA [3] (Figure 4.1). The number of compounds in the training set ($n = 6$) was such that it fulfils the requirement that the number of data points or compounds should preferably be at least five times the number of descriptors in order to prevent over-fitting of the data or generation of chance correlations [16, 17]. 2-Propenal was not included in the training set because it was expected to evaporate during the incubations at 37 °C to obtain kinetic parameters due to its high volatility (269 Torr). Among the remaining compounds, six commercially available aldehydes (*trans*-2-pentenal, *trans*-2-hexenal, *trans*-2-octenal, *trans*-2-decenal, *trans*-2-dodecenal, and *trans*-2-*cis*-6-nonadienal) were selected to cover the widest range of the chain length within the training set to develop QSARs for the PBK/D model parameters.

Aldehyde dehydrogenase (ALDH) mediated oxidation

To determine the required PBK/D parameters the six aldehydes in the training set were individually incubated with rat liver or small intestine S9. The final volume of the incubation mixtures was 100 μ l. The incubation mixtures contained (final concentrations) NAD⁺ (2 mM) and liver S9 (0.01–0.4 mg protein/ml) or small intestine S9 (0.12–0.6 mg protein/ml) in 0.1 M Tris–HCl (pH 7.4). After pre-incubation for 2 min, the reactions were initiated by the addition of a substrate aldehyde from a 100 times concentrated stock solution in DMSO. The final concentrations of each aldehyde ranged from 1 to 10,000 μ M, depending on the K_m . The mixtures were incubated at 37 °C for 2 to 5 min. The formation of the corresponding carboxylic acids was linear with time and S9 protein concentration under the experimental conditions used (data not shown). The incubations were terminated by adding 50 μ l ice-cold acetonitrile. The incubation

mixtures were subsequently centrifuged for 3 min at 13,000 g at 4 °C to precipitate the proteins. The amount of carboxylic acids in each sample was determined immediately using a Waters Acquity ultra-performance liquid chromatography with diode array detection (UPLC-DAD) (Waters, Milford, MA), equipped with a Waters Acquity UPLC BEH C18 column (1.7 μm , 2.1 \times 50 mm). The UPLC methods applied are presented in supplementary information 1. The carboxylic acids were quantified at a wavelength of 210 nm using the calibration curve of commercially available *trans*-2-hexenoic acid. Because carboxylic acids were also found to some extent in blank incubations without NAD⁺ or tissue fractions, the amount in incubations without tissue fractions was subtracted as background.

Aldose reductase (AR) mediated reduction

The six aldehydes of the QSAR training set were individually incubated with rat liver S9. The final volume of the incubation mixtures was 100 μl . The incubation mixtures contained (final concentration) pooled rat liver S9 (1–2 mg protein/ml) in 0.1 M Tris–HCl (pH 7.4). After pre-incubation for 2 min, the reactions were initiated by the addition of NADPH (2.5 mM) from a 20 times concentrated stock solution in 0.1 M Tris–HCl (pH 7.4), and a substrate aldehyde from a 100 times concentrated stock solution in DMSO. The final concentrations of the aldehydes ranged between 50–1,000 μM . After incubation for 4 or 6 min, the reactions were terminated by adding 50 μl ice-cold acetonitrile. The formation of alcohols was linear with incubation time and S9 protein concentrations under these incubation conditions (data not shown). The incubation mixtures were centrifuged for 3 min at 13,000 g at 4 °C, and the resulting supernatants were kept on dry ice until further analysis by UPLC. The UPLC methods applied are presented in supplementary information 1. Quantification of the alcohols was achieved at a wavelength of 193 nm using calibration curves of commercially available standard compounds for *trans*-2-penten-1-ol, *trans*-2-hexen-1-ol and *trans*-2, *cis*-6-nonadien-1-ol. A calibration curve of 2-undecen-1-ol was used to quantify *trans*-2-decen-1-ol and *trans*-2-dodecen-1-ol.

Glutathione S-transferase (GST) mediated GSH conjugation

The apparent first-order constant (k) for GST mediated conjugation was determined by incubating different concentrations of the five out of six acyclic α,β -unsaturated aldehydes of the QSAR training set (Figure 4.1) individually in the presence of GSH and rat tissue fractions. The final volume of the incubation mixtures was 100 μl . The incubation mixtures contained rat liver S9 (0.05–0.15 mg protein/ml) or small intestine S9 (0.12–0.2 mg protein/ml) in 0.1 M Tris–HCl (pH 7.4). After pre-incubation for 2 min, the reaction was initiated by adding GSH (3 mM) from a 17 times concentrated stock solution in 0.1 M Tris–HCl (pH 7.4) and a substrate aldehyde from a 100 times concentrated stock solution in DMSO. The final concentrations of the aldehyde ranged from 50 to 1,000 μM . After 3 min, the incubations were terminated by adding 50 μl ice-cold acetonitrile. The formation of GSH conjugates catalysed by GSTs was linear with time and S9

protein concentrations under the experimental conditions applied (data not shown). The samples were centrifuged for 3 min at 13,000 g at 4 °C and the resulting supernatant was analysed by UPLC-DAD immediately. The UPLC methods applied are presented in supplementary information 4.1. A calibration curve to quantify the GSH conjugates was obtained for each aldehyde by reacting an aldehyde (10 mM) with different lower concentrations of GSH (100–500 μ M) in 0.1 M Tris–HCl (pH 8.6) [13]. The conjugates were quantified based on the peak areas determined at a wavelength of 200 nm. Because the aldehydes also react chemically with GSH, chemical formation of GSH conjugates in the blank incubations without tissue fractions was subtracted as background from the amount measured in the enzymatic incubations. The second-order rate constants for chemical binding of the aldehydes to GSH were determined in separate experiments performed as described below.

Chemical conjugation with 2'-dG

The second-order rate constant for binding of acyclic α,β -unsaturated aldehydes to 2'-dG (k_{DNA}) was determined by examining the time-dependent formation of 2'-dG adducts for four out of the six aldehydes of the QSAR training set. The k_{DNA} for *trans*-2-hexenal was taken from the previous study [13]. A fixed concentration of *trans*-2-pentenal, *trans*-2-octenal, *trans*-2-decenal or *trans*-2-*cis*-6-nonadienal (1, 0.87, 0.85, and 0.86 mM, respectively) was incubated with 2'-dG (1.95 mM) in 0.1 M Tris–HCl (pH 7.4) at 37 °C for up to 50, 60, 105, or 135 min, respectively. The formation of 2'-dG adducts was linear with time and substrate concentrations under these experimental conditions (data not shown). After 2 min of pre-incubation, the reactions were started by adding the aldehyde from a 100 times concentrated stock in DMSO. The reactions were terminated by injection to the UPLC-DAD system. The 2'-dG adducts were quantified as described previously to quantify 2'-dG adducts of *trans*-2-hexenal (Hex-PdG) [13]. The UPLC methods used are described in supplementary information 4.1.

Chemical conjugation with GSH

The second-order rate constant for binding of the aldehydes to GSH (k_{GSH}) was determined by examining the time-dependent formation of GSH conjugates for *trans*-2-octenal, *trans*-2-decenal, *trans*-2-dodecenal and *trans*-2-*cis*-6-nonadienal. Each aldehyde (0.4 mM) was incubated with 1 mM GSH in 0.1 M Tris–HCl (pH 7.4) at 37 °C for up to 30 min. After 5 min of pre-incubation, the reactions were started by adding the aldehyde from a 100 times concentrated stock in DMSO. The final volume of the incubation samples was 1,000 μ l. Every 3 or 5 min, 100 μ l of the sample was taken and mixed with 25 μ l of 20 mM diamide dissolved in 0.1 M Tris–HCl (pH 7.4) to terminate the reaction. GSH conjugates in the samples were quantified immediately as described above using a UPLC-DAD system. The k_{GSH} for *trans*-2-hexenal was taken from the previous study [13].

Kinetic analysis

The data for the rate of oxidation and reduction with increasing α,β -unsaturated aldehydes concentration were fitted to the standard Michaelis–Menten equation with [S] being the concentration of the acyclic α,β -unsaturated aldehyde substrate:

$$v = V_{\max} \times [S] / (K_m + [S])$$

The formation of GST mediated GSH conjugates was described to depend on the concentrations of GSH and of the α,β -unsaturated aldehydes by the following equation, where [GSH] and K_{m_G} represent the concentration of cytosolic GSH, and the K_m for GSH, respectively:

$$v = k \cdot [S] \cdot [GSH] / (K_{m_G} + [GSH])$$

The apparent V_{\max} , K_m and k values were determined by fitting the data to the respective equations using GraphPad Prism (version 5.04, GraphPad Software, Inc. (La Jolla, USA)) except for K_{m_G} , which was set to 100 μ M based on literature data obtained with various substrates [18, 19].

QSAR model development and statistical analysis

QSAR models for the K_m for oxidation and the k for GSH conjugation were described using linear regression in Microsoft® Excel 2010 (Microsoft, Redmond, USA), relating the experimentally derived K_m or k to molecular descriptors. The equations were in the form

$$\text{Ln } K_m \text{ or } \text{Ln } k = a \times (\text{molecular descriptor}) + b$$

where a and b were fitting parameters. With six model aldehydes in the training set to define the QSARs, no more than one descriptor could be included in an equation, because the number of data points/compounds (n) should be at least five times the number of molecular descriptors (d) included ($n/d \geq 5$) [17]. Both $\log K_{ow}$ and the molecular refractivity (MR) were tested as possible molecular descriptors. $\log K_{ow}$ values were estimated with Estimation Program Interface (EPI) Suite version 4.10 provided by the US Environmental Protection Agency, and MR values were obtained with ChemBioDraw Ultra version 12.0 (Perkin Elmer, Massachusetts, USA).

The quality of the QSAR models was characterised by r^2 , s , and the internally cross-validated coefficient of determination (r^2_{int}). Cross validation of the models was performed using a leave-one-out (LOO) method, and calculated according to the formula:

$$r^2_{int} = 1 - (\text{PRESS}/\text{SSD})$$

where predictive sum of squares (PRESS) is the sum of the squared differences between actual and predicted kinetic parameters when a compound is omitted from the regression and SSD is the sum-of-squares deviation for each actual kinetic parameter from the mean parameter value of all the compounds in the training set [17, 20]. A QSAR model is considered acceptable when $r^2_{int} \geq 0.5$ [17, 21].

PBK/D model structure

The same structure as the rat PBK/D model for *trans*-2-hexenal developed in our previous study [13] was applied with modifications (Figure 4.2). The physiological parameters such as organ

volumes and blood flows were obtained from the literature [22] and are presented in Table 4.1. Tissue:blood partition coefficients were estimated based on a method of DeJongh et al. [23] from the $\log K_{ow}$ (supplementary information 4.2). Model equations (supplementary information 4.3) were coded and numerically integrated in Berkeley Madonna 8.3.18 (Macey and Oster, UC Berkeley, CA, USA), using the Rosenbrock's algorithm for stiff systems. The uptake of aldehydes into the small intestine compartment was described by a first-order process with the absorption rate constant 5.0 h^{-1} , resulting in a rapid absorption [24]. Detoxification was described in the liver and small intestine compartments. The V_{max} values expressed as $\text{nmol}/\text{min}/(\text{mg S9 protein})$ and k values expressed as $\text{ml}/\text{min}/(\text{mg S9 protein})$ were scaled to be expressed as $\text{nmol}/\text{min}/(\text{g tissue})$ and $\text{ml}/\text{min}/(\text{g tissue})$ respectively, using S9 protein yields of $143 \text{ mg}/(\text{g liver})$ or $11.4 \text{ mg}/(\text{g small intestine})$ as scaling factors [13, 25, 26]. Chemical conjugation of the aldehydes with GSH or protein reactive sites in the liver or small intestine was described as previously reported [13, 14]. Equations to describe GSH levels in the liver and small intestine were included as previously described [13] to examine possible depletion of GSH induced by the dietary aldehydes. The amount of DNA adducts formed in the liver was described by second-order formation and first-order elimination due to DNA repair. The half-life of the DNA adducts was set for all aldehydes to be 38.5 h based on the results obtained in an in vivo study using *trans*-2-hexenal [27].

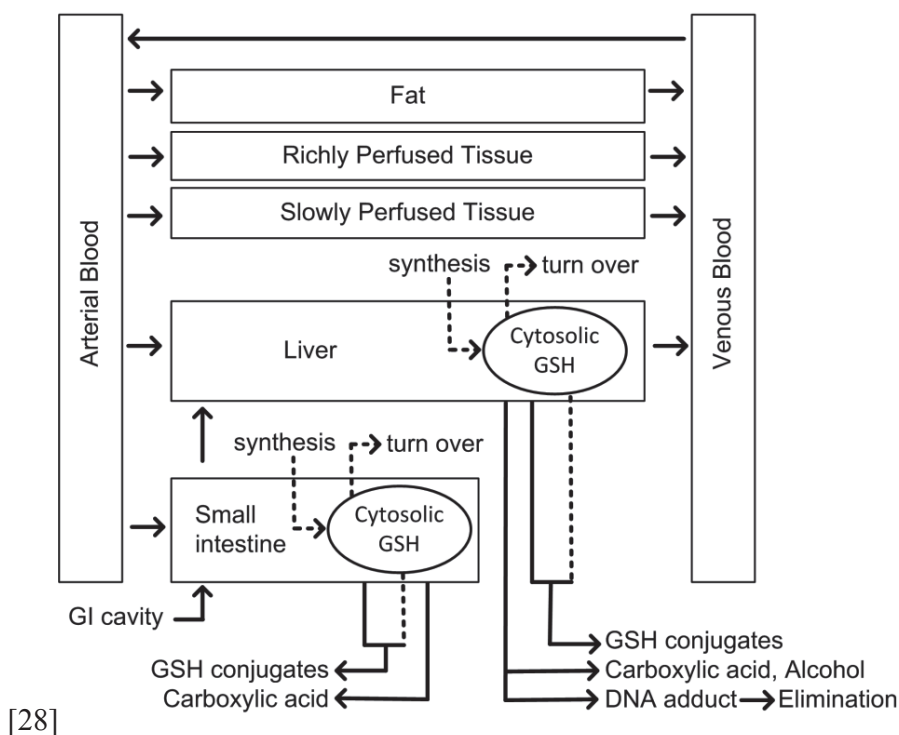


Figure 4.2. The schematic diagram of the PBK/D models for α,β -unsaturated aldehydes in rat. The solid and dashed lines represent the flow of α,β -unsaturated aldehyde and GSH, respectively.

Table 4.1 Parameters used in the PBK/D models

Parameters	Symbols	Values
Body weight (kg) ^a	BW	0.25
Tissue volumes (% body weight) ^a		
fat	VFc	7.0
liver	VLc	3.4
small intestine	VSIc	1.4
arterial blood	VAc	1.85
venous blood	VVc	5.55
richly perfused	VRc	4.2
slowly perfused	VSc	67.6
Cardiac output (L/h) ^{a,b}	QC	5.4
Blood flow to tissue (% cardiac output) ^a		
fat	QFc	7.0
liver (excluding portal vein fraction)	QLc	13.2
small intestine	QSIc	11.8
richly perfused	QRc	51.0
slowly perfused	QSc	17.0
Initial GSH concentration (μmol/kg tissue)		
liver ^c	InitGSH _L	6120
small intestine ^c	InitGSH _{Si}	1780
GSH synthesis (μmol/kg tissue/h)		
liver	GSYN _L	869
small intestine	GSYN _{Si}	78
Apparent first order rate constant for GSH turnover (h) ^c		
liver	k_{L_GLOS}	0.142
small intestine	k_{Si_GLOS}	0.044
Protein reactive sites (μmol/kg tissue) ^d		
liver	CPRO _L	5319
small intestine	CPRO _{Si}	245

^aBrown et al. [22], ^bKrishnan and Andersen [29], ^cPotter and Tran [30], ^dPotter and Tran

For the PBK/D models that are developed for the training set of six aldehydes, the values for V_{max} , K_m and k for aldehyde oxidation, aldehyde reduction or GST mediated GSH conjugation, and values for k_{GSH} and k_{DNA} were obtained based on results from in vitro incubations. For the PBK/D models for the other 12 aldehydes the K_m for aldehyde oxidation and the k for GST mediated GSH conjugation were set to the values calculated with the QSARs developed in this study. The V_{max} for aldehyde reduction and oxidation, the K_m for aldehyde reduction, k_{GSH} and the k_{DNA} were set at the average values obtained with the aldehydes in the training set, since the values for the training set aldehydes were comparable and were not significantly influenced by the aldehyde structure (see Results section). The models thus obtained for the 12 structurally related aldehydes are referred to as the “QSAR-based PBK/D models” throughout the article.

Sensitivity analysis

Normalised sensitivity coefficients (SC) were determined according to the equation: $SC = (C' - C)/(P' - P) \times (P/C)$, where P and P' are the initial and modified parameter values respectively, and C and C' are the initial and modified values of the model output resulting from an increase in parameter value respectively [31, 32]. A 5% increase in parameter values was chosen to analyze the effect of a change in parameter on maximum DNA adduct levels in the liver caused by each aldehyde. The estimated dietary intake as listed in Table 4.5 was used for the analysis. When the intake level for a compound is not known, the estimated dietary intake for 2-propenal (0.017 mg/kg bw) was used as the highest intake value from the series of aldehydes examined in the present study. Each parameter was analyzed individually, keeping the other parameters to their initial values.

RESULTS

Detoxification parameters

Chemical specific detoxification parameters were derived by in vitro incubations for the six acyclic α,β -unsaturated aldehydes (Figure 4.1) in the training set. The rat liver and small intestine S9 converted the six aldehydes into the related carboxylic acids. The reduction to alcohols was observed with pooled liver S9 but not with small intestine S9. The formation of metabolites was plotted against substrate concentrations (supplementary information 4.4A–C), and from these data the apparent kinetic parameters (K_m and V_{max}) were derived (Table 4.2). α,β -Unsaturated aldehydes chemically bind to GSH to form GSH conjugates. The second-order rate constants (k_{GSH}) for the chemical binding were determined and are presented in Table 4.2. The binding of α,β -unsaturated aldehydes with GSH is accelerated by GST [10, 33]. In vitro incubations with rat liver or small intestine S9 revealed that the formation rate of GSH conjugates mediated by GST increased linearly with increasing concentrations of aldehydes (supplementary information 4.4D and E). The apparent first-order rate constants obtained from the plots (k) are presented in Table 4.2. The V_{max} and K_m for reduction of *trans*-2-octenal to *trans*-2-octen-1-ol and the second-order rate constant for the chemical reaction between *trans*-2-pentenal and GSH (k_{GSH}) were not determined because the peaks of the products could not be separated with the UPLC analysis from the peaks of other compounds present in the incubation samples.

Table 4.2 Biochemical parameters determined by in vitro incubations.

Metabolites /products		<i>trans</i> -2-pentenal	<i>trans</i> -2-hexenal	<i>trans</i> -2-octenal	<i>trans</i> -2-decenal	<i>trans</i> -2-dodecenal	<i>trans</i> -2- <i>cis</i> -6-nonadienal	Average
Carboxylic acid (liver)	$K_m^{a,b}$	5101	230	7.4	2.0	1.6	9.4	892
	$V_{max}^{a,c}$	36.6	18.5	34.2	26.5	21.1	20.2	27.6
Carboxylic acid (small intestine)	$K_m^{a,b}$	5430	737	22.8	4.4	2.9	43.7	1040
	$V_{max}^{a,c}$	4.8	7.0	3.4	2.3	2.7	5.6	4.3
Alcohol (liver)	$K_m^{a,b}$	361	169	N.D. ^f	66.3	75.6	88.3	152
	$V_{max}^{a,c}$	13.7	28.0	N.D. ^f	21.5	16.5	12.4	18.4
GSH conjugates (liver)	$k^{a,d}$	0.07	0.35	2.1	3.9	5.4	2.2	2.4
	$k^{a,d}$	0.03	0.12	0.74	1.5	3.6	0.74	1.2
2'-dG adducts	$k_{DNA}^{a,e}$	4.8×10^{-7}	1.6×10^{-7}	3.8×10^{-7}	1.3×10^{-7}	N.D. ^f	5.4×10^{-7}	3.4×10^{-7}
GSH chemical conjugation	$k_{GSH}^{a,e}$	N.D. ^f	5.8×10^{-4}	9.3×10^{-4}	8.5×10^{-4}	3.7×10^{-4}	10.5×10^{-4}	7.6×10^{-4}

^aMean of duplicate or triplicate measurements, ^bμM, ^cnmol/min/(mg S9 protein), ^dml/min/(mg S9 protein), ^e/μM/h, ^fN.D.= not determined

Chemical binding to 2'-dG

Acyclic α,β-unsaturated aldehydes bind covalently to DNA, resulting in formation of exocyclic 1,*N*²-propanodeoxyguanosine adducts [27, 34-36]. UPLC analysis revealed that one or two peaks appear when an aldehyde was incubated with 2'-dG, and that the peaks were absent in blank incubations without either the aldehyde or 2'-dG (supplementary information 4.5). The second-order rate constants for binding of the aldehydes with 2'-dG (k_{DNA}) were determined and are presented in Table 4.2. The value of k_{DNA} for *trans*-2-dodecenal was not determined, because the 2'-dG adduct formation was insufficient to be quantified using UPLC.

QSAR models for detoxification parameters

The K_m for oxidation and the k for GST mediated GSH conjugation varied more than ten times when comparing the values for the six aldehydes in the training set (Table 4.2). QSAR models were therefore developed for these two chemical specific biochemical parameters (Figure 4.3), and were assessed statistically for their goodness-of-fit (r^2 and standard deviation) and robustness (r^2_{int}) (Table 4.3) [17, 20]. The natural logarithm of the K_m values for oxidation correlated quantitatively with $\log K_{ow}$ or MR, and decreased with increasing hydrophobicity ($\log K_{ow}$) or bulkiness (MR) of the molecule. The natural logarithm of the k for GST mediated GSH conjugation also correlated with $\log K_{ow}$ or MR, increasing with increasing hydrophobicity or bulkiness. The statistical analysis (Table 4.3) showed that the fit of the QSAR models (r^2) and the robustness (r^2_{int}) were both good for the four models with MR as a descriptor ($r^2 - r^2_{int} < 0.3$, $r^2_{int} > 0.5$) [17], and therefore these QSARs were considered adequate for further predictions. No QSAR model was developed for the other chemical specific biochemical parameters including V_{max} and K_m for reduction, and the second-order rate constant of aldehyde binding to GSH (k_{GSH}) or to DNA (k_{DNA}), because the differences in these values for the training set aldehydes were less than

ten-fold, and no significant influence of the aldehyde structures was observed. These parameters were therefore considered to be best described by the average values observed for the aldehydes in the training set.

Table 4.3 Statistical analysis of the QSAR models

Metabolite	Kinetic parameter	Descriptor	r^{2a}	s^b	r_{int}^{2c}
Carboxylic acid (liver)	K_m	$\text{Log}K_{ow}$	0.84	1.4	0.4
		MR	0.90	1.1	0.7
Carboxylic acid (small intestine)	K_m	$\text{Log}K_{ow}$	0.91	1.0	0.7
		MR	0.92	0.9	0.8
GSH conjugates (liver)	k	$\text{Log}K_{ow}$	0.86	0.7	0.6
		MR	0.92	0.5	0.9
GSH conjugates (small intestine)	k	$\text{Log}K_{ow}$	0.94	0.5	0.8
		MR	0.97	0.3	0.9

^aCoefficient of determination, ^bStandard error of estimate, ^cCross validated correlation coefficient

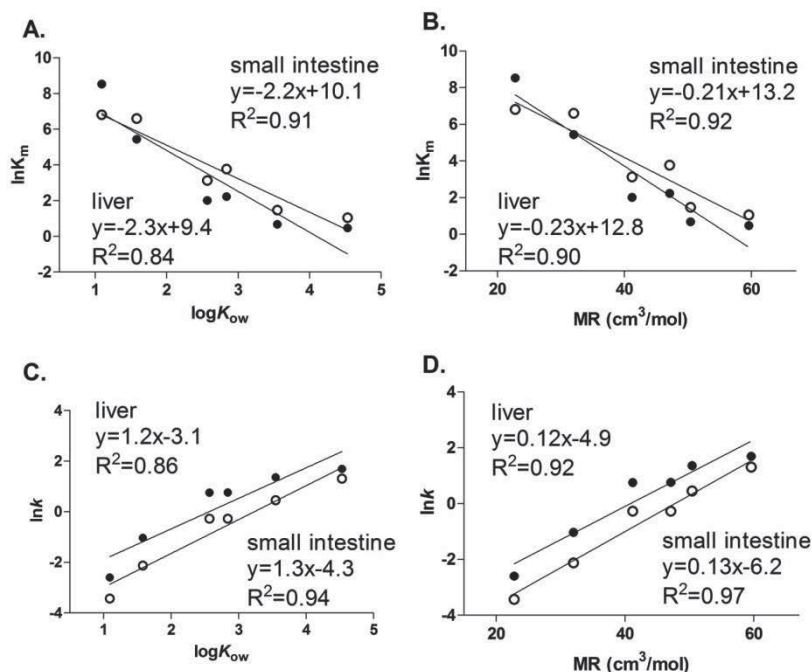


Figure 4.3 QSAR models correlating the K_m of ALDH mediated oxidation with $\text{log}K_{ow}$ (A) or molecular refraction (MR) (B), and the k of GST mediated GSH conjugation with $\text{log}K_{ow}$ (C) or MR (D). The closed and open circles represent the in vitro derived data obtained using rat liver S9 and small intestine S9, respectively.

Evaluation of the PBK/D models

The performance of the QSAR-based PBK/D models was evaluated by comparing the predicted values with in vivo data reported by Linhart et al. [37] for 2-propenal. In this study, 2-propenal

(acrolein) was administered to rats by intraperitoneal (i.p.) injection. To account for the difference in the administration route, the V_{\max} and k values in the small intestine of the PBK/D model were set to zero so that 2-propenal administered via i.p. injection would reach the liver without being detoxified in the small intestine. In addition, it was assumed that all GSH conjugates would be further converted to mercapturic acids. The comparison revealed that the PBK/D model predicted level of 2-propenal GSH conjugates was only up to 3.3-fold higher than the in vivo reported level excreted as mercapturic acids [37] (Table 4.4). To further evaluate the PBK/D models, the formation of DNA adducts was compared with in vivo data for DNA adduct formation upon exposure of rats to 2-butenal (crotonaldehyde) [36] or *trans*-2-hexenal [27, 38](Table 4.4). The PBK/D models overestimated the DNA adduct levels by 947-fold and 9717-fold compared to the data reported by Budiawan et al. on 2-butenal [36] and by Stout et al. on *trans*-2-hexenal [38], respectively. However, the overestimation was only 3.5-fold when the predicted values were compared with the data reported by Schuler and Eder on *trans*-2-hexenal DNA adduct formation [27].

Table 4.4 Comparison of the PBK/D model outcomes and data obtained from rat studies

Reference	Compounds	Rats/ Routes	Dose (mg/kgbw)	Outcome/ Time point	Observed levels	PBK/D model outcome
Linhart et al. [37]	2-propenal (acrolein)	Wistar (M)/ i.p. injection	0.47-4.0	Mercapturic acids/ 24h	10-32% of dose	32.3-32.6% of dose
Budiawan and Eder, [36]	2-butenal (crotonaldehyde)	F344 (F)/ gavage	200, 300	DNA adducts in the liver/ 20h	2.9 and 3.4 adducts/ 10^8 nt	1240 and 3220 adducts/ 10^8 nt
Stout et al. [38]	<i>trans</i> -2-hexenal	F344 (M)/ gavage	200, 500	DNA adducts in the liver/ 24h	0.2 and 0.099 adducts/ 10^8 nt	94 and 962 adducts/ 10^8 nt
Schuler and Eder [27]	<i>trans</i> -2-hexenal	F344 (M)/ gavage	200, 500	DNA adducts in the liver/ 48h	16 and 179 adducts/ 10^8 nt	61 and 625 adducts/ 10^8 nt

PBK/D model based predictions on DNA adduct formation

Figure 4.4A shows the dose-dependent maximum DNA adduct formation in the liver predicted by the PBK/D models for the six compounds in the QSAR training set. DNA adduct formation decreased with increasing bulkiness. Overall, the PBK/D models predicted that *trans*-2-pentenal is most potent in forming DNA adducts among the six aldehydes in the training set. At 0.04 mg/kg bw, the level corresponding to the average human dietary intake of *trans*-2-hexenal [12], the

maximum predicted DNA adduct formation in the liver was 0.15, 0.006, 0.0007, 0.0004, 0.00002 and 0.00002 adducts/ 10^8 nt for *trans*-2-pentenal, *trans*-2-hexenal, *trans*-2-*cis*-6-nonadienal, *trans*-2-octenal, *trans*-2-decenal, and *trans*-2-dodecenal, respectively. These levels are at least an order of magnitude lower than natural background levels of structurally similar 1, N^2 -exocyclic propanodeoxyguanosine adducts observed in disease free human liver (6.8–110 adducts/ 10^8 nt) [39, 40].

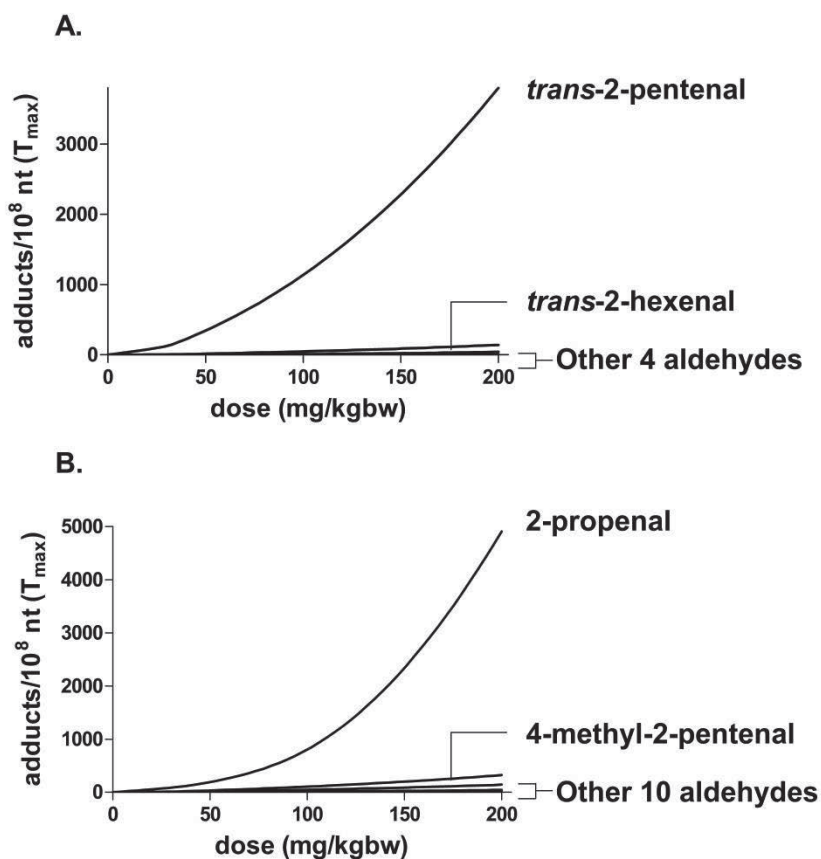


Figure 4.4. Dose-dependent maximum levels of DNA adducts in the liver as predicted by PBK/D models using in vitro derived parameters for the six aldehydes of the training set (A) and by QSAR-based PBK/D models for the remaining 12 aldehydes included in the study (B).

Dose-dependent DNA adduct formation was also examined using the QSAR-based PBK/D models for a range of food flavouring acyclic α,β -unsaturated aldehydes. For this examination, α,β -unsaturated aldehydes listed in subgroup 1.1.1 of EFSA Flavouring Group Evaluation (FGE) 19 were selected except for 4,5-epoxydec-2(*trans*)-enal [3], which was not considered to be in the applicability domain of the QSAR models because of its epoxide group. The QSAR-based PBK/D models predicted that 2-propenal induces the highest DNA adduct levels among the 18 aldehydes (Figure 4.4B), primarily due to its low detoxification efficiency via oxidation or GST mediated GSH conjugation. Furthermore, the DNA adduct formation at the intake levels that are relevant for human dietary exposure for each acyclic α,β -unsaturated

aldehyde was examined (Table 4.5). The estimated daily intake levels used for these predictions were derived from data reported by the Joint FAO/WHO Expert Committee on Food Additives (JECFA) based on the annual production volumes of each aldehyde [41, 42]. The intake was estimated for populations in Europe and the US, and the highest value of either of the two regions is listed in Table 4.5. For 2-propenal, no exposure levels based on the production volumes were found but an estimated exposure of 0.017 mg/kg bw/day from food consumption has been reported [43]. The PBK/D models predicted 0.036 adducts/10⁸ nt for 2-propenal and values between 10⁻¹⁰ and 10⁻³ adducts/10⁸ nt for the other 17 aldehydes (Table 4.5), which were well below the natural background levels of structurally similar 1,N²-exocyclic propanodeoxyguanosine adducts in disease free human liver [39, 40].

Table 4.5 Dietary exposure levels of acyclic α,β -unsaturated aldehydes listed as food flavouring agents by EFSA [3].

Compounds	Levels ($\mu\text{g}/\text{kgbw}/\text{d}$)	Predicted maximum DNA adduct levels (adduct/10 ⁸ nt)
2-propenal	17 ^a	0.036
2-pentenal	0.002 ^b	7.4×10 ⁻⁶
4-methyl-2-pentenal	N.A. ^c	-
<i>trans</i> -2-hexenal	13.20 ^b	2.0×10 ⁻³
<i>cis</i> -2-hexenal		
<i>trans</i> -2-heptenal	0.10 ^b	1.2×10 ⁻⁵
<i>trans</i> -2-octenal	0.50 ^b	4.4×10 ⁻⁶
<i>trans</i> -2-nonenal	0.07 ^b	7.2×10 ⁻⁷
<i>cis</i> -2-nonenal		
<i>trans</i> -2-decenal	0.10 ^b	4.9×10 ⁻⁸
2-undecenal	0.007 ^b	3.2×10 ⁻⁹
<i>trans</i> -2-dodecenal	0.27 ^b	1.3×10 ⁻⁷
2-tridecenal	0.01 ^b	1.3×10 ⁻¹⁰
2-tetradecenal	N.A.	-
<i>trans</i> -2- <i>cis</i> -6-octadienal	N.A.	-
<i>trans</i> -2- <i>cis</i> -6-nonadienal	0.40 ^d	7.1×10 ⁻⁶
<i>trans</i> -2- <i>trans</i> -6-nonadienal	0.0001 ^d	1.8×10 ⁻⁹
2,6-dodecadial	0.01 ^d	5.0×10 ⁻¹⁰

^aEstimated amount present in food [43], ^bEstimated amount consumed as food flavouring agent [42], ^cN.A.= not available in literature, ^dEstimated amount consumed as food flavouring agent [41]

Sensitivity analysis

A sensitivity analysis was performed to identify key parameters that determine the DNA adduct levels in the liver at T_{max}, the time point at which the DNA adduct level was predicted to reach its maximum after administration of the aldehydes (Figure 4.5). The results showed that DNA adduct

formation is significantly influenced by the second-order rate constant for binding to 2'-dG (k_{DNA}), the volume of the liver (VLC), and the scaling factor for liver S9 (S9PL) for all 18 compounds. The degree of influence of the other parameters, including four parameters for which QSARs were developed, varied depending on the compound. Among the four parameters estimated by QSARs, the median of the |SC| was the largest with the k for GSH conjugation in the small intestine (k_{Si}). This parameter appeared to have a significant influence on the predicted liver DNA adduct levels for 2-dodecenal (|SC|= 0.71) but its influence was limited for the PBK/D model outcome for 2-propenal (|SC| < 0.1). The |SC| of the K_m for oxidation in the liver and small intestine (K_{m,L_CA} and K_{m,SI_CA}) were large especially for the molecules with large MR such as 2-tetradecenal, and the smallest |SC|s were observed for 2-propenal. The influence of k for GSH conjugation in the liver (k_L) was the largest for 2-methylpentenal (|SC| = 0.58) and it was shown to be insignificant for the model outcome of 2-tetradecenal (|SC| < 0.1).

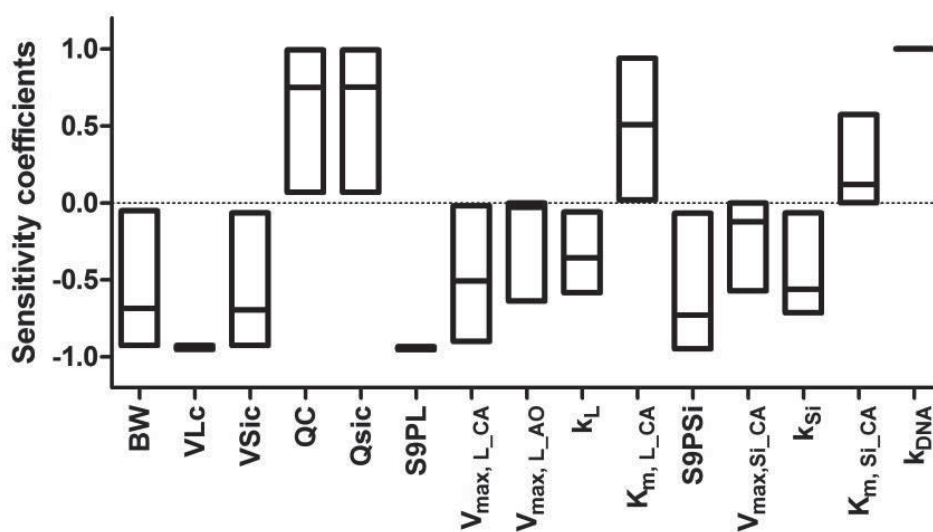


Figure 4.5. Sensitivity analysis for the PBK/D model based predictions of the maximum amount of DNA adduct formation in the liver for the 18 α,β -unsaturated aldehyde. The normalized sensitivity coefficients (SC) were obtained at the estimated dietary exposure level to each compound as listed in Table 4.5, or at 0.017 mg/kg bw when the exposure level of a compound is unknown. The parameters which |SC| is larger than 0.1 are listed in the figure. The bottom and the top of the boxes represent the maximum and minimum normalized sensitivity coefficients (SCs) obtained among the 18 compounds, and the lines in the boxes represent the medians. The parameters listed in the figure are the following: body weight (BW), fraction of the liver (VLC) and the small intestine (VSic); blood flow rate (QC); fraction of the blood flow to the small intestine (Qsic); scaling factor of liver S9 (S9PL) or of small intestine S9 (S9PSi); V_{max} and K_m to form carboxylic acid in the liver (V_{max,L_CA} , K_{m,L_CA}) or in the small intestine (V_{max,SI_CA} , K_{m,SI_CA}), or to form alcohol in the liver (V_{max,L_AO} , K_{m,L_AO}); k for GST catalysed GSH conjugations in the liver (k_L) and small intestine (k_{Si}); and second-order rate constant of the aldehydes binding with 2'-dG (k_{DNA}).

DISCUSSION

The aim of the present study was to build rat PBK/D models for a series of food-borne acyclic α,β -unsaturated aldehydes and to examine detoxification and DNA adduct formation especially at dose levels relevant for human dietary exposure. Considering the large number of α,β -unsaturated aldehydes, QSAR models were developed to estimate chemical specific parameters namely K_m or k values for the detoxification pathways. The QSAR models revealed that the K_m for ALDH mediated oxidation decreased and the k for GST mediated GSH conjugation increased with increasing hydrophobicity or bulkiness of the aldehyde substrate. These findings are in line with results reported in the literature [8, 10, 15]. For example, Klysov [8] showed that the longer the chain length of 2-alkanals the lower the K_m of human cytosolic ALDH. Furthermore Danielson et al. [15] attributed the increased specificity constants (k_{cat}/K_m) of mammalian cytosolic GST with increasing hydrophobicity of 4-hydroxy-2-alkenals to the hydrophobic nature of the electrophilic substrate-binding site in GSTs. The presence of a hydrophobic binding site in GSTs corroborates the significant correlation observed between the k of GST and hydrophobicity of 2-alkenals in the present study. Other kinetic constants did not depend on the aldehyde structural characteristics within the six compounds in the training set.

For evaluation of the PBK/D models the outcomes of the different PBK/D models were compared with reported in vivo data. The predicted proportion of 2-propenal excreted as mercapturic acids as well as the predicted DNA adduct levels in the liver upon exposure of rats to *trans*-2-hexenal matched well with the in vivo data reported by Linhart et al. [37] or by Schuler and Eder [27], respectively. However, predicted DNA adduct levels induced by 2-butenal and *trans*-2-hexenal were respectively three and four orders of magnitude higher compared with data reported by Budiawan and Eder [36] or Stout et al. [38]. These striking gaps may be explained by the animal feeding status in the in vivo studies. While the PBK/D models assumed the complete absorption of administered aldehyde, a part of the aldehyde in the in vivo studies might have been depleted by food matrix present in the stomach and small intestine lumen because the rats were not fasted in the study by Stout et al. [38], and might not have been fasted in the study by Budiawan and Eder [36] before the dosing. The PBK/D model based predictions can therefore be considered to provide worse case estimates of the DNA adduct formation assuming complete absorption of the administered aldehydes.

The present study illustrated that the integration of QSARs with PBK/D modelling facilitates group evaluations and read-across among compounds with similar structures. However, it should be noted that the QSAR-based PBK/D models developed did not include possible differences in DNA repair efficiencies among different aldehydes, which could be subject for further studies. The PBK/D models developed for 18 acyclic α,β -unsaturated aldehydes revealed that with decreasing bulkiness increasing amounts of DNA adducts are formed in the liver, which appears to be primarily due to lower levels of aldehyde detoxification via oxidation or GST

mediated GSH conjugation. While EFSA has selected *trans*-2-hexenal, 2-octenal, and *trans*-2-*cis*-6-nonadienal as representative compounds to evaluate the genotoxicity of the 18 aldehydes based on the length, lipophilicity, and results from an unpublished (Q)SAR study [44], our results suggest 2-propenal would be most potent in forming DNA adducts. For all 18 aldehydes, the predicted DNA adduct levels were well below the natural background levels of structurally similar 1,*N*²-exocyclic deoxyguanosine adducts in disease free human liver (6.8–110 adducts/10⁸ nt) [39, 40]. Based on these results it is concluded that DNA adduct formation caused by the 18 food-borne acyclic α,β -unsaturated aldehydes may be negligible. This conclusion is in line with what was previously concluded for *trans*-2-hexenal [13, 14] and may be corroborated by findings of chronic studies with rats or mice orally exposed to 2-propenal [45-47] that did not reveal increased tumour development up to exposures of 10 mg 2-propenal/kg bw/day, whereas higher dose levels induced mortality within a week [47]. The PBK/D model predicted a formation of 27 adduct/10⁸ nt in the liver at an exposure of 10 mg 2-propenal/kg bw, which is still within the natural background DNA adduct levels observed in disease free human liver.

A fundamental assumption for the approach based on QSARs is that the series of compounds in the applicability domain show similar properties [21]. In the present study we limited the applicability domain to acyclic α,β -unsaturated aldehydes without 2- or 3-alkylation, with no more than one conjugated double bond, and without any extra functional group. The 18 compounds used in the present study, either in the test set or in the training set, fall within this specific applicability domain. The molecular descriptor MR range in the test set (16.9–60.9) is mostly covered by that in the training set (22.8–59.6). The statistical analysis indicated that the goodness-of-fit and the robustness of the four QSAR models with MR as the molecular descriptor developed in the present study were all sufficient. We acknowledge that in QSAR development internal validation using the training/test set splitting technique or the leave-out-many cross validation method, with a significant % of the calibration compounds left out at each step and repeating this for different selections is often recommended and applied [16, 20]. However, such an approach would be in contrast to the aim of our study, which was not the development of the QSARs per se, but the description of correlations with sufficient quality to enable the prediction of PBK/D model parameters for other congeners in the series, eliminating the need to experimentally determine the parameters for all compounds in the series. Furthermore, one should keep in mind that the PBK/D model outcomes are only partially dependent on QSAR estimated parameters. The degree of the sensitivity of the PBK/D model outcomes to the QSAR estimated parameters varies for each compound. In case of the PBK/D model for 2-propenal, which was predicted to induce the highest DNA adduct levels among the 18 aldehydes, the sensitivity analysis revealed that among the four parameters estimated by QSARs the predicted DNA adduct level is the most sensitive to the *k* for GSH conjugation in the liver. The normalised |SC| was 0.31, indicating that the overestimation of 10-fold in this parameter would have resulted in the underestimation of 3.1-fold in the DNA adduct level in the liver. This level of difference in the

DNA adduct level prediction does not affect the general conclusions of the present study about the significance of the DNA adducts formed by the 18 food-borne acyclic α,β -unsaturated aldehydes.

Altogether, the present study elucidates a possible negligible DNA adduct formation in the liver upon oral exposure to a range of acyclic food-borne α,β -unsaturated aldehydes at relevant levels of dietary intake. Furthermore, the present study provides a proof of principle for the use of a combined QSAR-PBK/D modelling approach to facilitate group evaluations and read-across among compounds with similar structures.

REFERENCES

- [1] Zawirska-Wojtasiak, R., Goslinski, M., Szwacka, M., Gajc-Wolska, J., Mildner-Szkudlarz, S., Aroma evaluation of transgenic, thaumatin II-producing cucumber fruits. *Journal of food science* 2009, *74*, C204-210.
- [2] Feron, V. J., Til, H. P., de Vrijer, F., Woutersen, R. A., *et al.*, Aldehydes: occurrence, carcinogenic potential, mechanism of action and risk assessment. *Mutat Res* 1991, *259*, 363-385.
- [3] EFSA, Minutes of the 26th plenary meeting of the scientific panel on food additives, flavourings, processing aids and materials in contact with food. <http://www.efsa.europa.eu/en/events/event/afc071127-m.pdf>. 2007.
- [4] Eder, E., Scheckenbach, S., Deininger, C., Hoffman, C., The possible role of alpha, beta-unsaturated carbonyl compounds in mutagenesis and carcinogenesis. *Toxicol Lett* 1993, *67*, 87-103.
- [5] Eder, E., Deininger, C., Mutagenicity of 2-alkylpropenals in Salmonella typhimurium strain TA 100: structural influences. *Environmental and molecular mutagenesis* 2001, *37*, 324-328.
- [6] Janzowski, C., Glaab, V., Mueller, C., Straesser, U., *et al.*, Alpha,beta-unsaturated carbonyl compounds: induction of oxidative DNA damage in mammalian cells. *Mutagenesis* 2003, *18*, 465-470.
- [7] Lindahl, R., Petersen, D. R., Lipid aldehyde oxidation as a physiological role for class 3 aldehyde dehydrogenases. *Biochem Pharmacol* 1991, *41*, 1583-1587.
- [8] Klyosov, A. A., Kinetics and specificity of human liver aldehyde dehydrogenases toward aliphatic, aromatic, and fused polycyclic aldehydes. *Biochemistry* 1996, *35*, 4457-4467.
- [9] Endo, S., Matsunaga, T., Fujita, A., Tajima, K., *et al.*, Rat aldose reductase-like protein (AKR1B14) efficiently reduces the lipid peroxidation product 4-oxo-2-nonenal. *Biological & pharmaceutical bulletin* 2010, *33*, 1886-1890.
- [10] Eisenbrand, G., Schuhmacher, J., Golzer, P., The influence of glutathione and detoxifying enzymes on DNA damage induced by 2-alkenals in primary rat hepatocytes and human lymphoblastoid cells. *Chem Res Toxicol* 1995, *8*, 40-46.
- [11] Hayes, J. D., Flanagan, J. U., Jowsey, I. R., Glutathione transferases. *Annual review of pharmacology and toxicology* 2005, *45*, 51-88.
- [12] Adams, T. B., Gavin, C. L., Taylor, S. V., Waddell, W. J., *et al.*, The FEMA GRAS assessment of alpha,beta-unsaturated aldehydes and related substances used as flavor ingredients. *Food Chem Toxicol* 2008, *46*, 2935-2967.
- [13] Kiwamoto, R., Rietjens, I. M. C. M., Punt, A., A physiologically based in silico model for *trans*-2-hexenal detoxification and DNA adduct formation in rat. *Chem Res Toxicol* 2012, *25*, 2630-2641.
- [14] Kiwamoto, R., Spenkelink, A., Rietjens, I. M. C. M., Punt, A., A physiologically based in silico model for *trans*-2-hexenal detoxification and DNA adduct formation in human including interindividual variation indicates efficient detoxification and a negligible genotoxicity risk. *Arch Toxicol* 2013.
- [15] Danielson, U. H., Esterbauer, H., Mannervik, B., Structure-Activity-Relationships of 4-Hydroxyalkenals in the Conjugation Catalyzed by Mammalian Glutathione Transferases. *Biochemical Journal* 1987, *247*, 707-713.
- [16] Tropsha, A., Gramatica, P., Gombar, V. K., The importance of being earnest: Validation is the absolute essential for successful application and interpretation of QSPR models. *Qsar Comb Sci* 2003, *22*, 69-77.
- [17] Zvinavashe, E., Murk, A. J., Rietjens, I. M. C. M., Promises and Pitfalls of Quantitative Structure-Activity Relationship Approaches for Predicting Metabolism and Toxicity. *Chem Res Toxicol* 2008, *21*, 2229-2236.
- [18] Johanson, G., Filser, J. G., A physiologically based pharmacokinetic model for butadiene and its metabolite butadiene monoxide in rat and mouse and its significance for risk extrapolation. *Arch Toxicol* 1993, *67*, 151-163.
- [19] Csanady, G. A., Filser, J. G., A physiological toxicokinetic model for inhaled propylene oxide in rat and human with special emphasis on the nose. *Toxicological sciences : an official journal of the Society of Toxicology* 2007, *95*, 37-62.
- [20] OECD, Guidance Document on the Validation of (Quantitative) Structure-Activity Relationships [(Q)SAR] Models. 2007.
- [21] Eriksson, L., Jaworska, J., Worth, A. P., Cronin, M. T., *et al.*, Methods for reliability and uncertainty assessment and for applicability evaluations of classification- and regression-based QSARs. *Environ Health Perspect* 2003, *111*, 1361-1375.
- [22] Brown, R. P., Delp, M. D., Lindstedt, S. L., Rhomberg, L. R., Beliles, R. P., Physiological parameter values for physiologically based pharmacokinetic models. *Toxicol Ind Health* 1997, *13*, 407-484.
- [23] DeJongh, J., Verhaar, H. J., Hermens, J. L., A quantitative property-property relationship (QPPR) approach to estimate in vitro tissue-blood partition coefficients of organic chemicals in rats and humans. *Arch Toxicol* 1997, *72*, 17-25.
- [24] Kirman, C. R., Gargas, M. L., Deskin, R., Tonner-Navarro, L., Andersen, M. E., A

- physiologically based pharmacokinetic model for acrylamide and its metabolite, glycidamide, in the rat. *Journal of toxicology and environmental health. Part A* 2003, *66*, 253-274.
- [25] van de Kerkhof, E. G., de Graaf, I. A., Groothuis, G. M., In vitro methods to study intestinal drug metabolism. *Current drug metabolism* 2007, *8*, 658-675.
- [26] Punt, A., Paini, A., Boersma, M. G., Freidig, A. P., *et al.*, Use of physiologically based biokinetic (PBBK) modeling to study estragole bioactivation and detoxification in humans as compared with male rats. *Toxicological sciences : an official journal of the Society of Toxicology* 2009, *110*, 255-269.
- [27] Schuler, D., Eder, E., Detection of 1,N²-propanodeoxyguanosine adducts of 2-hexenal in organs of Fischer 344 rats by a ³²P-post-labeling technique. *Carcinogenesis* 1999, *20*, 1345-1350.
- [28] Potter, D. W., Tran, T. B., Rates of ethyl acrylate binding to glutathione and protein. *Toxicol Lett* 1992, *62*, 275-285.
- [29] Krishnan, K., Andersen, M. E., Physiologically based pharmacokinetic modeling in toxicology. *Principles and Methods of Toxicology (Forth Edition)* 2001, 193-239.
- [30] Potter, D. W., Tran, T. B., Apparent rates of glutathione turnover in rat tissues. *Toxicol Appl Pharmacol* 1993, *120*, 186-192.
- [31] Evans, M. V., Andersen, M. E., Sensitivity analysis of a physiological model for 2,3,7,8-tetrachlorodibenzo-p-dioxin (TCDD): assessing the impact of specific model parameters on sequestration in liver and fat in the rat. *Toxicological sciences : an official journal of the Society of Toxicology* 2000, *54*, 71-80.
- [32] Punt, A., Freidig, A. P., Delatour, T., Scholz, G., *et al.*, A physiologically based biokinetic (PBBK) model for estragole bioactivation and detoxification in rat. *Toxicol Appl Pharmacol* 2008, *231*, 248-259.
- [33] Balogh, L. M., Roberts, A. G., Shireman, L. M., Greene, R. J., Atkins, W. M., The stereochemical course of 4-hydroxy-2-nonenal metabolism by glutathione S-transferases. *The Journal of biological chemistry* 2008, *283*, 16702-16710.
- [34] Chung, F. L., Young, R., Hecht, S. S., Formation of cyclic 1,N²-propanodeoxyguanosine adducts in DNA upon reaction with acrolein or crotonaldehyde. *Cancer Res* 1984, *44*, 990-995.
- [35] Douki, T., Ames, B. N., An HPLC-EC assay for 1,N²-propano adducts of 2'-deoxyguanosine with 4-hydroxynonenal and other alpha,beta-unsaturated aldehydes. *Chem Res Toxicol* 1994, *7*, 511-518.
- [36] Budiawan, Eder, E., Detection of 1,N²-propanodeoxyguanosine adducts in DNA of Fischer 344 rats by an adapted ³²P-post-labeling technique after per os application of crotonaldehyde. *Carcinogenesis* 2000, *21*, 1191-1196.
- [37] Linhart, I., Frantik, E., Vodickova, L., Vosmanska, M., *et al.*, Biotransformation of acrolein in rat: excretion of mercapturic acids after inhalation and intraperitoneal injection. *Toxicol Appl Pharmacol* 1996, *136*, 155-160.
- [38] Stout, M. D., Bodes, E., Schoonhoven, R., Upton, P. B., *et al.*, Toxicity, DNA binding, and cell proliferation in male F344 rats following short-term gavage exposures to *trans*-2-hexenal. *Toxicol Pathol* 2008, *36*, 232-246.
- [39] Chaudhary, A. K., Nokubo, M., Reddy, G. R., Yeola, S. N., *et al.*, Detection of endogenous malondialdehyde-deoxyguanosine adducts in human liver. *Science* 1994, *265*, 1580-1582.
- [40] Nath, R. G., Chung, F. L., Detection of exocyclic 1,N²-propanodeoxyguanosine adducts as common DNA lesions in rodents and humans. *Proceedings of the National Academy of Sciences of the United States of America* 1994, *91*, 7491-7495.
- [41] JECFA, Evaluation of certain food additives and contaminants: Sixty-first report of the Joint FAO/WHO Expert Committee on Food Additives. http://whqlibdoc.who.int/trs/WHO_TRS_922.pdf. 2004.
- [42] JECFA, Evaluation of Certain Food Additives: sixty-third report of the Joint FAO/WHO Expert Committee on Food Additives. http://whqlibdoc.who.int/trs/WHO_TRs_928.pdf. 2005.
- [43] Guth, S., Habermeyer, M., Baum, M., Steinberg, P., *et al.*, Thermally induced process-related contaminants: The example of acrolein and the comparison with acrylamide: Opinion of the Senate Commission on Food Safety (SKLM) of the German Research Foundation (DFG). *Molecular nutrition & food research* 2013.
- [44] EFSA, List of alpha, beta-Unsaturated Aldehydes and Ketones representative of FGE.19 substances for Genotoxicity Testing. Statement of the Panel on Food Contact Materials, Enzymes, Flavourings and Processing Aids(CEF). 2008.
- [45] Parent, R. A., Caravello, H. E., Long, J. E., Oncogenicity Study of Acrolein in Mice. *J Am Coll Toxicol* 1991, *10*, 647-659.
- [46] Parent, R. A., Caravello, H. E., Long, J. E., Two-year toxicity and carcinogenicity study of acrolein in rats. *Journal of applied toxicology : JAT* 1992, *12*, 131-139.
- [47] NTP, Technical report on the comparative toxicity studies of allyl acetate, allyl alcohol, and acrolein. Administered by gavage to F344/N rats and B6C3F1 mice. http://ntp.niehs.nih.gov/ntp/htdocs/st_rpts/tox048.pdf. 2006.

SUPPORTING INFORMATION

Supporting Information 4.1. UPLC methods to quantify *trans*-2-pentenal, *trans*-2-hexenal, *trans*-2-octenal, *trans*-2-decenal, *trans*-2-dodecenal, and *trans*-2-*cis*-6-nonadienal metabolites (A-C) and 2'-dG adducts (D) in incubation samples .

(A) Carboxylic acids

The gradient was made with acetonitrile and ultrapure water containing 0.1% (v/v) TFA. The flow rate was 0.6 mL/min. Each analysis was followed by the default cleaning and equilibration step (i.e. the percentage of acetonitrile was increased to 100% over 0.2 min, maintained for 0.2 min, lowered to 0% over 0.2 min, kept for 0.2 min, increased to the initial condition over 0.2 min and maintained for 1.0 min for equilibration).

Aldehyde	UPLC method	Retention time
<i>trans</i> -2-pentenal	From 10 to 10.5% acetonitrile over 2 min, or from 6 to 9% acetonitrile over 3 min.	1.6 min 2.3 min
<i>trans</i> -2-hexenal	From 20 to 30% acetonitrile over 2 min.	1.3 min
<i>trans</i> -2-octenal	From 32 to 47% acetonitrile over 2.5 min.	1.7 min
<i>trans</i> -2-decenal	From 46 to 62% acetonitrile over 2.5 min.	1.5 min
<i>trans</i> -2-dodecenal	From 56 to 68% acetonitrile over 2 min.	1.6 min
<i>trans</i> -2- <i>cis</i> -6-nonadienal	From 35 to 43% acetonitrile over 2 min.	1.4 min

(B) Alcohols

The gradient was made with acetonitrile and ultrapure water containing 0.1% (v/v) formic acid. The flow rate was 0.6 mL/min. Each analysis was followed by the default cleaning and equilibration step as described in (A).

Aldehyde	UPLC method	Retention time
<i>trans</i> -2-pentenal	From 0 to 5% acetonitrile over 6 min.	5.3 min
<i>trans</i> -2-hexenal	From 0 to 10% acetonitrile over 10 min.	9.3 min
<i>trans</i> -2-decenal	From 30 to 39% acetonitrile over 9 min.	7.7 min
<i>trans</i> -2-dodecenal	From 37 to 50% acetonitrile over 13 min.	1.5 min
<i>trans</i> -2- <i>cis</i> -6-nonadienal	From 25 to 32% acetonitrile over 7 min.	3.9 min

(C) GSH conjugates

The gradient was made with acetonitrile and ultrapure water containing 0.1% (v/v) TFA. The flow rate was 0.6 mL/min. Each analysis was followed by the default cleaning and equilibration step as described in (A).

Aldehyde	UPLC method	Retention time
<i>trans</i> -2-pentenal	From 6 to 8% acetonitrile over 2 min.	0.82 and 0.91 min
<i>trans</i> -2-hexenal	From 5 to 10% acetonitrile over 2.5 min.	2.2 and 2.4 min
<i>trans</i> -2-octenal	From 21 to 25% acetonitrile over 2 min.	0.9 and 1.0 min
<i>trans</i> -2-decenal	From 21 to 25% acetonitrile over 2 min.	1.4 and 1.5 min
<i>trans</i> -2-dodecenal	From 28 to 32% acetonitrile over 2 min.	1.5 and 1.6 min
<i>trans</i> -2- <i>cis</i> -6-nonadienal	From 16 to 17% acetonitrile over 2 min.	1.1 and 1.2 min

(D) 2'-dG adducts

The gradient was made with acetonitrile and ultrapure water containing 0.1% (v/v) TFA. The flow rate was 0.6 mL/min. Each analysis was followed by the default cleaning and equilibration step as described in (A).

Aldehyde	UPLC method	Retention time
<i>trans</i> -2-pentenal	From 92 to 91 % acetonitrile over 5 min.	1.2 and 1.3 min
<i>trans</i> -2-hexenal	From 8.5 to 10% acetonitrile over 5 min.	3.0 min
<i>trans</i> -2-octenal	From 15 to 20% acetonitrile over 5 min.	3.9 min
<i>trans</i> -2-decenal	From 27 to 32% acetonitrile over 5 min.	2.8 min
<i>trans</i> -2- <i>cis</i> -6-nonadienal	From 15 to 20% acetonitrile over 5 min.	4.2 min

Supporting Information 4.2. Tissue/blood partition coefficients

Compounds	Fat/blood	Liver/blood Small intestine/blood Richly perfused tissues/blood	Slowly perfused tissues/blood
2-propenal	1.3	0.83	0.46
2-pentenal	4.7	0.96	0.51
4-methyl-2-pentenal	8.9	1.1	0.54
2-hexenal <i>trans</i> -2-hexenal <i>cis</i> -2-hexenal	9.9	1.1	0.55
2-heptenal <i>trans</i> -2-heptenal	20.5	1.3	0.60
2-octenal <i>trans</i> -2-octenal	40.5	1.7	0.68
2-nonenal <i>trans</i> -2-nonenal <i>cis</i> -2-nonenal	71.7	2.3	0.79
2-decenal <i>trans</i> -2-decenal	110	3.2	0.94
2-undecenal	146	4.5	1.1
<i>trans</i> -2-dodecenal 2-dodecenal	171	6.4	1.4
2-tridecenal	186	8.3	1.7
2-tetradecenal	193	10.7	2.2
<i>trans</i> -2- <i>cis</i> -6-octadienal	30.3	1.5	0.64
2,6-nonadienal <i>trans</i> -2- <i>cis</i> -6-nonadienal <i>trans</i> -2- <i>trans</i> -6-nonadienal	56.3	2.0	0.74
2,6-dodecadienal	92.6	2.8	0.86

Supporting Information 4.3. PBK/D model equations

(1) Uptake from GI cavity

The uptake of aldehyde from the intestinal cavity into the small intestine compartment was described by a first-order process as follows:

$$\begin{aligned} dAGI/dt &= -K_a * AGI \\ \text{InitAGI} &= \text{DOSE} \end{aligned}$$

where

AGI	Amount of aldehyde remaining in GI cavity (μmol)
K_a	Linear uptake rate (/h)
DOSE	Amount of aldehyde administered in a rat (μmol)

(2) Slowly perfused tissue, richly perfused tissue and fat

Amount aldehyde in slowly perfused tissue, richly perfused tissue or fat compartment was described as follows:

$$\begin{aligned} dATi/dt &= QT_i * (CA - CVT_i) \\ CT_i &= AT_i / VT_i \\ CVT_i &= CT_i / PT_i \end{aligned}$$

where

ATi	Amount of aldehyde in a tissue (μmol)
QTi	Blood flow into a tissue (L/h)
CA	Concentration of aldehyde in arterial blood perfusing a tissue ($\mu\text{mol/L}$)
CVTi	Concentration of aldehyde in venous blood leaving a tissue ($\mu\text{mol/L}$)
CTi	Concentration of aldehyde in a tissue ($\mu\text{mol/kg}$)
VTi	Volume of a tissue (kg)
PTi	Tissue/blood partition coefficient of aldehyde

(3) Liver

Amount aldehyde in the liver (AL , μmol) is described as follows:

$$\begin{aligned} dAL/dt &= QL * CA + QSi * CVS_i - (QL + QSi) * CVL - (\text{eq.1} + \text{eq.2} + \text{eq.3} + \text{eq.4} + \text{eq.5} + \text{eq.6}) \\ CL &= AL / VL \\ CVL &= CL / PL \end{aligned}$$

where

QL	Blood flow into the liver (L/h)
QSi	Blood flow into the small intestine (L/h)
CVSi	Concentration of aldehyde in venous blood leaving the small intestine ($\mu\text{mol/L}$)
CVL	Concentration of aldehyde in venous blood leaving the liver ($\mu\text{mol/L}$)
CL	Concentration of aldehyde in the liver ($\mu\text{mol/L}$)
PL	Liver/blood partition coefficient of aldehyde

Amount aldehyde oxidized to carboxylic acid enzymatically in the liver (AMLCA, μmol) is described to follow Michaelis-Menten equation:

$$d\text{AMLCA}/dt = V_{s_{\text{max}, L_CA}} * CVL / (K_{m, L_CA} + CVL) \quad \text{----- eq. 1}$$

where

$V_{s_{\text{max}, L_CA}}$	Scaled V_{max} for enzymatic oxidation of aldehyde in the liver ($\mu\text{mol/h}$)
K_{m, L_CA}	K_m for enzymatic oxidation of aldehyde in the liver (μM)

Amount aldehyde reduced to alcohol in the liver (AMLAO, μmol) is described to follow Michaelis-Menten equation:

$$d\text{AMLAO}/dt = V_{s_{\text{max}, L_AO}} * CVL / (K_{m, L_AO} + CVL) \quad \text{----- eq. 2}$$

where

$V_{s_{\text{max}, L_AO}}$	Scaled V_{max} for enzymatic reduction of aldehyde in the liver ($\mu\text{mol/h}$)
K_{m, L_AO}	K_m for enzymatic reduction of aldehyde in the liver (μM)

Amount aldehyde metabolized in liver to GSH conjugation by GSTs (AMLG_{GST}, μmol) is described as

Chapter 4

following :

$$d\text{AMLAG}_{\text{GST}}/dt = k_{\text{S,L}} * \text{CVL} * \text{CGSH}_{\text{LC}} / (\text{K}_{\text{m,G}} + \text{CGSH}_{\text{LC}}) \quad \text{----- eq.3}$$

where

$k_{\text{S,L}}$ Scaled first order rate constant derived in this study for enzymatic conjugation of aldehyde with GSH in the liver (ml/h)

CGSH_{LC} Concentration of GSH in liver cytosol ($\mu\text{mol/kg}$ liver), calculated from eq.7

$\text{K}_{\text{m,G}}$ K_{m} toward GSH for enzymatic GSH conjugation of aldehyde (μM)

Amount aldehyde chemically bound in liver to GSH ($\text{AMLAG}_{\text{chem}}$, μmol) is described as following:

$$d\text{AMLAG}_{\text{chem}}/dt = k_{\text{GSH}} * \text{CVL} * \text{CGSH}_{\text{LC}} * \text{VL} \quad \text{----- eq.4}$$

where

k_{GSH} Second order rate constant of aldehyde binding to GSH ($/\mu\text{mol/h}$)

VL Volume of the liver (kg)

Amount aldehyde protein adducts in liver (AMLAP , μmol) is described as following:

$$d\text{AMLAP}/dt = k_{\text{GSH}} * \text{CVL} * \text{CPRO}_{\text{L}} * \text{VL} \quad \text{----- eq.5}$$

where

CPRO_{L} Concentration of protein reaction sites in the liver ($\mu\text{mol/kg}$ liver)

The formation of DNA adduct in the liver ($\text{AMLDA}_{\text{form}}$) was described as following:

$$d\text{AMLDA}_{\text{form}}/dt = k_{\text{DNA}} * \text{CVL} * \text{CdG}_{\text{L}} * \text{VL} \quad \text{----- eq.6}$$

where

k_{DNA} Second order rate constant of aldehyde binding to 2'-dG ($/\mu\text{mol/h}$)

CdG_{L} Concentration of 2'-dG in the liver ($\mu\text{mol/kg}$ liver)

CdG_{L} was calculated to be 1.36 $\mu\text{mol/kg}$ liver using the average molecular weight of nucleotides (330 g/mol) and reported concentration of DNA in a rat liver (1.8 g/kg liver).

Amount of DNA adduct in liver (AMLDA , μmol) is described by subtracting elimination of DNA adduct from the formation:

$$d\text{AMLDA}/dt = \text{eq.6} - \text{AMLDA} * (\ln 2 / T_{1/2})$$

where

$T_{1/2}$ Half-life of DNA adduct in the liver (h)

Amount of GSH present in the liver cytosol (AMGSH_{LC} , μmol) is described by zero-order synthesis and reduction by first-order elimination due to turnover and depletion by aldehyde:

$$d\text{AMGSH}_{\text{LC}} = \text{GSYN}_{\text{L}} * \text{VL} * 0.9 - (\text{eq.3} + \text{eq.4} + k_{\text{L,GLOS}} * \text{AMGSH}_{\text{LC}}) \quad \text{----- eq.7}$$

$$\text{Init AMGSH}_{\text{LC}} = \text{InitGSH}_{\text{L}} * \text{VL} * 0.9$$

$$\text{CGSH}_{\text{LC}} = \text{AMLcGSH} / \text{VL}$$

where

GSYN_{L} Rate of GSH synthesis in the liver ($\mu\text{mol/h}$)

$k_{\text{L,GLOS}}$ First-order rate of GSH turnover in the liver ($/\text{h}$)

$\text{InitGSH}_{\text{L}}$ Initial concentration of GSH in the liver ($\mu\text{mol/kg}$ liver)

When eq.7 gave negative values, the value zero was used as the amount of GSH in the liver cytosol.

(4) Small intestine

The amount aldehyde in small intestine tissue, (ASi , μmol) is described as follows:

$$d\text{ASi}/dt = \text{QSi} * (\text{CA} - \text{CVSi}) + \text{Ka} * \text{AGI} - (\text{eq.8} + \text{eq.9} + \text{eq.10} + \text{eq.11})$$

$$\text{CSi} = \text{ASi} / \text{VSi}$$

$$\text{CVSi} = \text{CSi} / \text{PSi}$$

where

CSi Concentration of aldehyde in the small intestine ($\mu\text{mol/L}$)

VSi Volume of the small intestine (kg)

PSi Small intestine/blood partition coefficient of aldehyde

Amount aldehyde enzymatically oxidized carboxylic acid (AMSiCA , μmol) in the small intestine is

described by Michaelis-Menten equation:

$$d\text{AMSiCA}/dt = V_{s_{\text{max,Si_CA}}} * \text{CVSi} / (K_{m_{\text{Si_CA}}} + \text{CVSi}) \quad \text{----- eq.8}$$

where

$V_{s_{\text{max,Si_CA}}}$ Scaled V_{max} for enzymatic oxidation of aldehyde in the small intestine ($\mu\text{mol/h}$)
 $K_{m_{\text{Si_CA}}}$ K_m for enzymatic oxidation of aldehyde in small intestine (μM)

Amount aldehyde metabolized in small intestine to GSH conjugation by GSTs ($\text{AMSiAG}_{\text{GST}}$, μmol) is described as following :

$$d\text{AMSiAG}_{\text{GST}}/dt = k_{s_{\text{Si}}} * \text{CVSi} * \text{CGSH}_{\text{SiC}} / (K_{m_{\text{G}}} + \text{CGSH}_{\text{SiC}}) \quad \text{----- eq.9}$$

where

$k_{s_{\text{Si}}}$ Scaled first order rate constant derived in this study for enzymatic conjugation of aldehyde with GSH in small intestine (ml/h)
 CGSH_{SiC} Concentration of GSH in small intestine cytosol ($\mu\text{mol/kg}$ small intestine), calculated from eq.8
 $K_{m_{\text{G}}}$ K_m toward GSH for enzymatic GSH conjugation of aldehyde (μM)

Amount aldehyde chemically bound in small intestine to GSH ($\text{AMSiAG}_{\text{chem}}$, μmol) is described as following:

$$d\text{AMLAG}_{\text{chem}}/dt = k_{\text{GSH}} * \text{CVSi} * \text{CGSH}_{\text{SiC}} * \text{VSi} \quad \text{----- eq.10}$$

where

k_{GSH} Second order rate constant of aldehyde binding to GSH ($1/\mu\text{mol/h}$)
 VSi Volume of the small intestine (kg)

Amount aldehyde protein adducts in small intestine (AMSiAP , μmol) is described as following:

$$d\text{AMSiAP}/dt = k_{\text{GSH}} * \text{CSiL} * \text{CPRO}_{\text{Si}} * \text{VSi} \quad \text{----- eq.11}$$

where

CPRO_{Si} Concentration of protein reaction sites in the small intestine ($\mu\text{mol/kg}$ liver)

Amount of GSH present in small intestine cytosol ($\text{AMGSH}_{\text{SiC}}$, μmol) is described in the same way as in the liver:

$$\begin{aligned} d\text{AMGSH}_{\text{SiC}} &= \text{GSYN}_{\text{Si}} * \text{VSi} * 0.9 - (\text{eq.9} + \text{eq. 10} + k_{\text{GLOS}_{\text{Si}}} * \text{AMGSH}_{\text{SiC}}) \quad \text{----- eq. 12} \\ \text{Init AMGSH}_{\text{SiC}} &= \text{InitGSH}_{\text{Si}} * \text{VSi} * 0.9 \\ \text{CGSH}_{\text{SiC}} &= \text{AMSicGSH} / \text{VSi} \end{aligned}$$

where

GSYN_{Si} Rate of GSH synthesis in small intestine ($\mu\text{mol/h}$)
 $k_{\text{GLOS}_{\text{Si}}}$ First-order rate of GSH turnover in small intestine (1/h)
 $\text{InitGSH}_{\text{Si}}$ Initial concentration of GSH in small intestine ($\mu\text{mol/kg}$ small intestine)

As was the case in the liver, the value zero was used as the amount of GSH in the small intestine cytosol when eq.12 gave negative values.

(5) Venous blood and arterial blood

Concentration of aldehyde in venous blood (CV) and in arterial blood (CA, both in $\mu\text{mol/L}$) was described as follows:

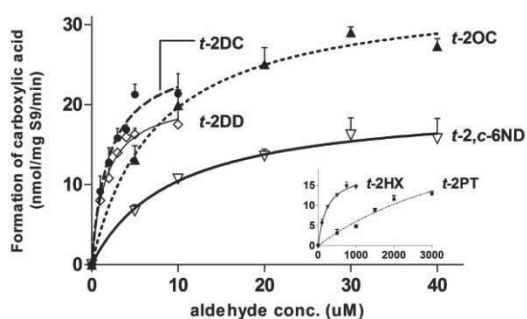
$$\begin{aligned} d\text{AV}/dt &= \text{QF} * \text{CVF} + (\text{QL} + \text{QSi}) * \text{CVL} + \text{QR} * \text{CVR} + \text{QS} * \text{CVS} - \text{QC} * \text{CV} \\ \text{CV} &= \text{AV} / (\text{VA} + \text{VV}) \\ \text{CV} &= \text{CA} \end{aligned}$$

where

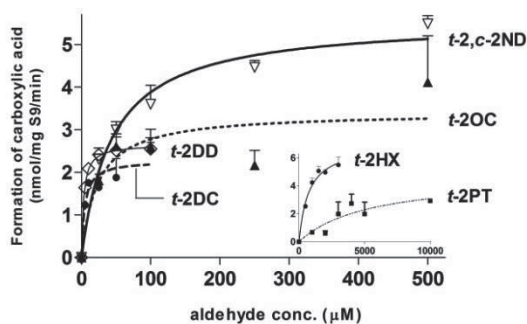
AV Amount of aldehyde in venous blood (μmol)
 QF Blood flow into fat (L/h)
 CVF Concentration of aldehyde in venous blood leaving fat ($\mu\text{mol/L}$)
 QR Blood flow into richly perfused tissue (L/h)
 CVR Concentration of aldehyde in venous blood leaving richly perfused tissue ($\mu\text{mol/L}$)
 QS Blood flow into slowly perfused tissue (L/h)
 CVS Concentration of aldehyde in venous blood leaving slowly perfused tissue ($\mu\text{mol/L}$)

Supporting information 4.4. α,β -Unsaturated aldehyde concentration-dependent rate of metabolite formation by rat tissue fractions. The figures show the enzymatic conversion rate of α,β -unsaturated aldehyde to carboxylic acids in the liver (A) and small intestine (B), to alcohols in the liver (C), and to GSH conjugates in the liver (D) and small intestine (E). The abbreviations stands for *trans*-2-pentenal (t-2PT), *trans*-2-hexenal (t-2HX), *trans*-2-octenal (t-2OC), *trans*-2-decenal (t-2DC), *trans*-2-dodecenal (t-2DD), and *trans*-2-*cis*-6-nonadienal (t-2,c-6ND).

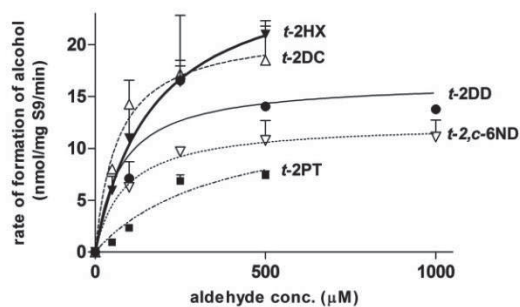
A.



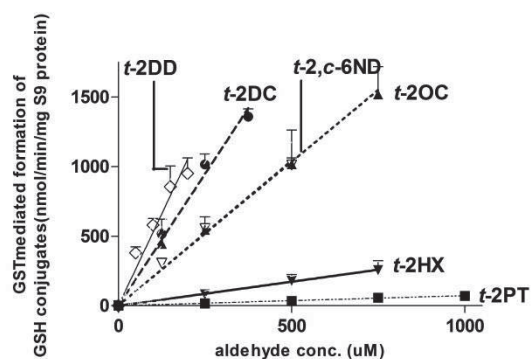
B.



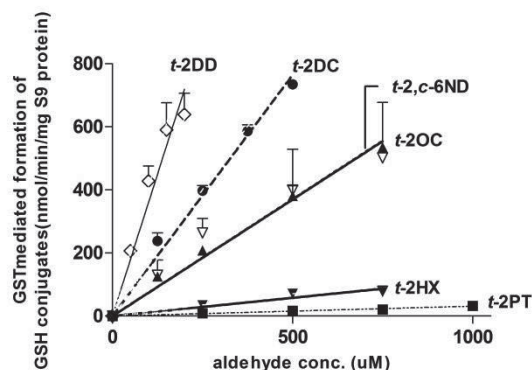
C.



D.



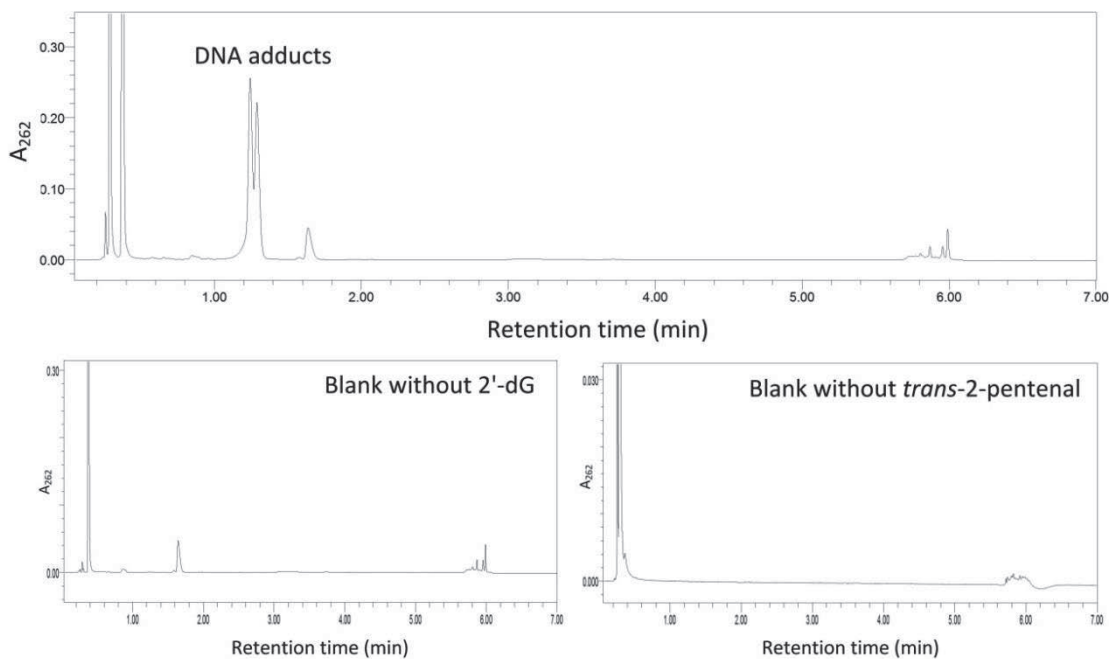
E.



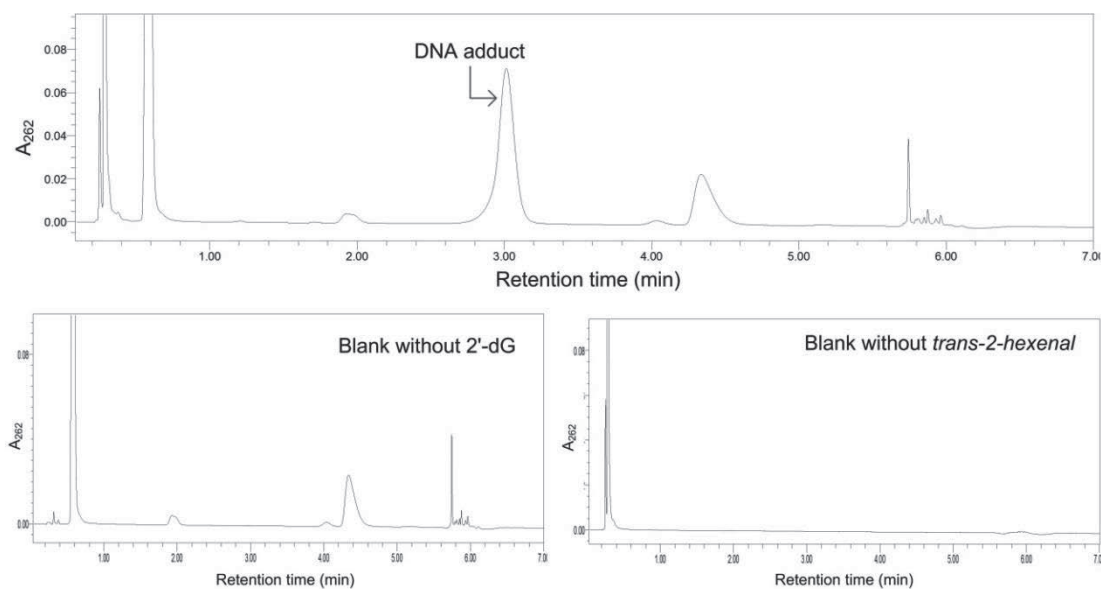
Supporting Information 4.5. UPLC chromatograms of 2'-dG adducts

Each aldehyde (10 mM) was incubated with 1.95 mM 2'-dG for 48 hrs at room temperature. The chromatograms were obtained at wavelength 262 nm.

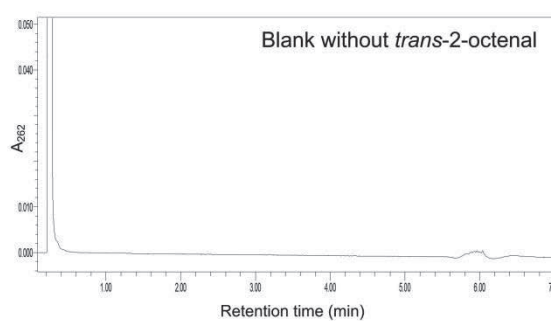
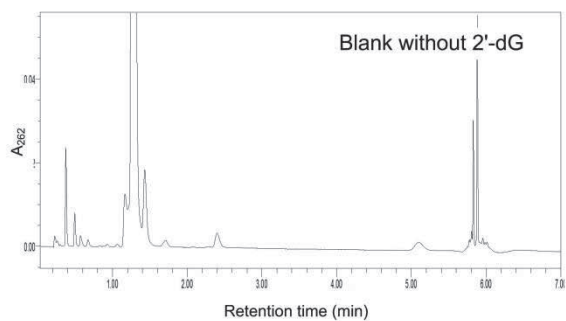
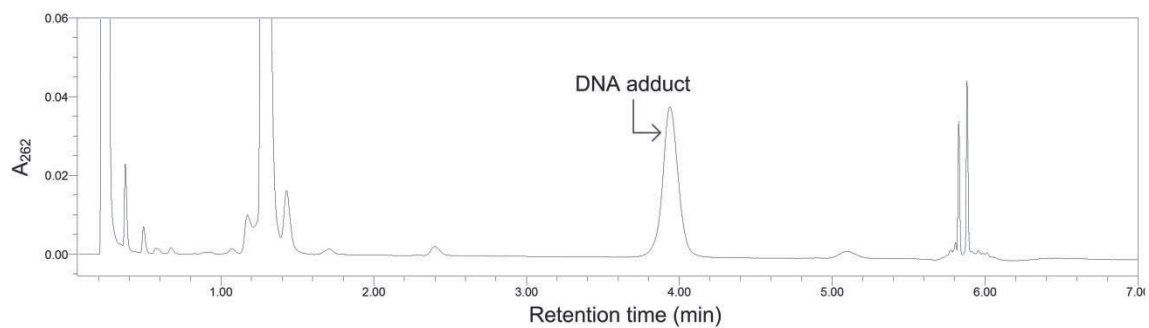
trans-2-pentenal



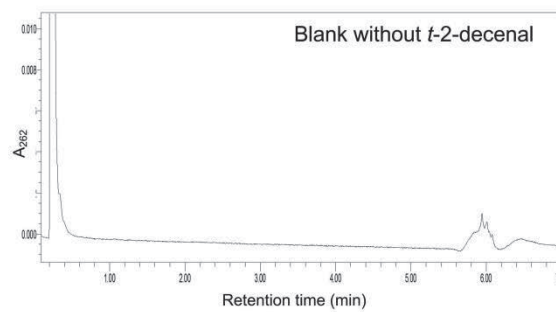
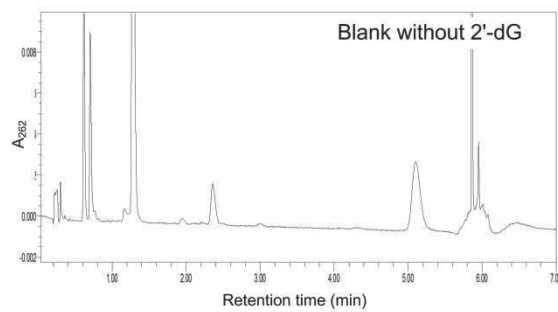
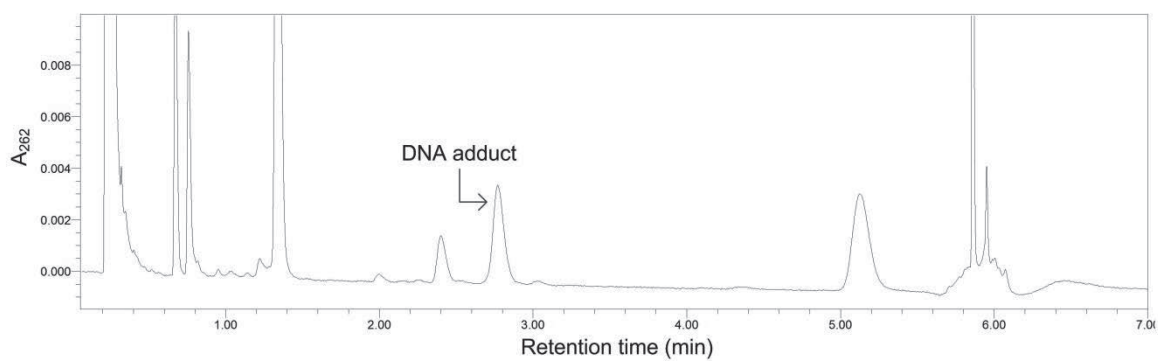
trans-2-hexenal



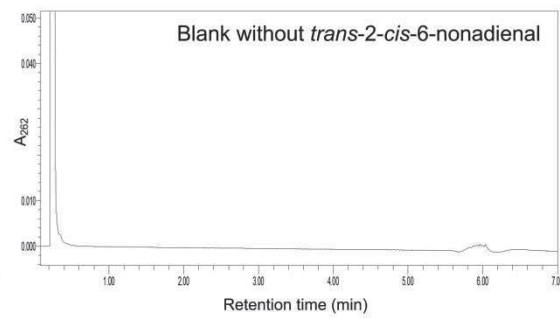
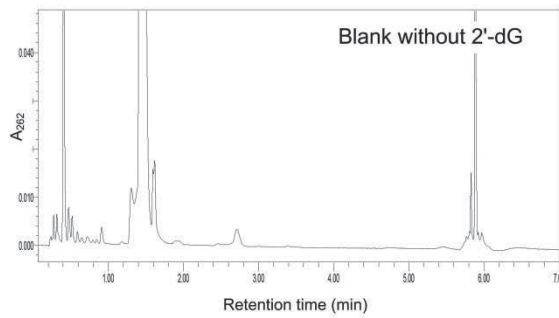
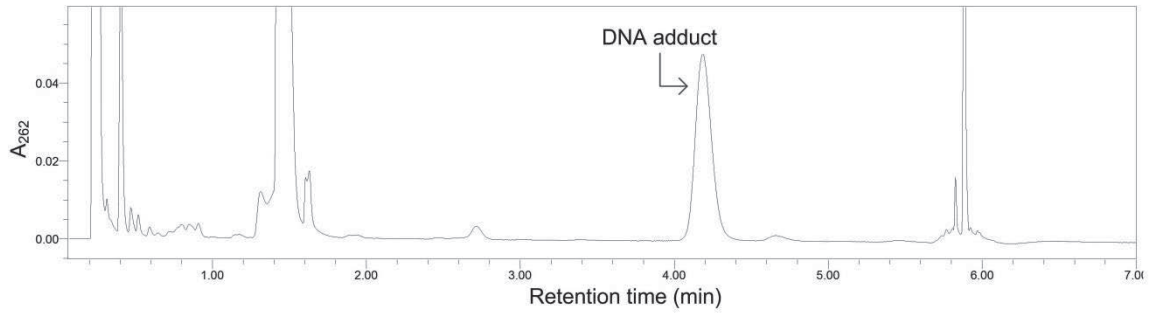
trans-2-octenal

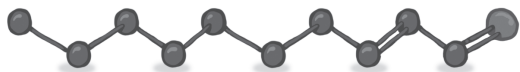


trans-2-decenal



trans-2-*cis*-6-nonadienal





CHAPTER 5

Dose-dependent DNA adduct formation by cinnamaldehyde and other food-borne α,β -unsaturated aldehydes predicted by physiologically based in silico modeling

R. Kiwamoto
D. Ploeg
I.M.C.M. Rietjens
A. Punt

Submitted

ABSTRACT

There are various α,β -unsaturated aldehydes present in our diet as natural constituents and food flavouring agents. Genotoxicity of α,β -unsaturated aldehydes shown in vitro may raise a concern for the use of the aldehydes as food flavourings, while in vivo at low dose exposures the formation of DNA adducts may be prevented by adequate detoxification. Unlike many α,β -unsaturated aldehydes for which in vivo data on genotoxicity and carcinogenicity are absent, cinnamaldehyde was shown not to be genotoxic or carcinogenic in vivo. The aim of the present study was to examine DNA adduct formation by cinnamaldehyde using physiologically based kinetic/dynamic (PBK/D) modelling, and to compare these cinnamaldehyde DNA adduct levels to those predicted previously for 18 other food-borne α,β -unsaturated aldehydes. The cinnamaldehyde PBK/D models were developed based on kinetic parameters obtained by performing in vitro incubations. In rats, cinnamaldehyde was shown to induce higher DNA adducts per exposure dose than 6 out of the 18 food borne acyclic α,β -unsaturated aldehydes, indicating these 6 aldehydes may also test negative for genotoxicity and carcinogenicity at high dose levels. At the highest cinnamaldehyde dose that was tested for carcinogenicity in vivo and tested negative, the DNA adduct formation by cinnamaldehyde was predicted to be at least three orders of magnitude higher than the predictions of DNA adduct formation by the 18 other food-borne aldehydes at their respective estimated daily intake. These result corroborate the conclusion that for all the 18 α,β -unsaturated aldehydes DNA adduct formation at doses relevant for human dietary exposure does not raise a safety concern. The present study furthermore illustrates that physiologically based in silico modelling approach facilitates a science-based comparison and read-across on the possible risks posed by food-borne DNA reactive agents.

INTRODUCTION

There are various α,β -unsaturated aldehydes present in our diet as natural constituents and as intentionally added food flavouring agents. α,β -Unsaturated aldehydes are electrophilic due to their α,β -unsaturated aldehyde moiety and can react with electron rich macromolecules including DNA, leading to the formation of DNA adducts [1]. Various aldehydes have been found positive in a number of in vitro genotoxicity tests [2-4], which may raise a concern with respect to genotoxicity upon the use of α,β -unsaturated aldehydes as food flavouring agents. The European Food Safety Authority (EFSA) considers the α,β -unsaturated aldehyde moiety an alert for genotoxicity and requires in vivo genotoxicity data to overrule any positive in vitro genotoxicity results [5]. Consequently, the use of more than 70 α,β -unsaturated aldehydes and their related compounds, which may give rise to such aldehydes by metabolism in vivo as food flavouring agents, has been suspended in the EU since 2013 (Commission Implementing Regulation (EU) No. 872/2012 of 1 October 2012). The EFSA has requested more data, especially in vivo data on genotoxicity for further discussion [6]. In contrast, the Expert Panel of the Flavoring Extract Manufacturers' Association (FEMA) and the Joint FAO/WHO Expert Committee on Food Additives (JECFA) have concluded that there is no significant risk associated with the use of α,β -unsaturated aldehydes and related compounds based on their low levels of use, and possible rapid detoxification [7-9].

The highest exposure to α,β -unsaturated aldehydes via diet is attributed to cinnamaldehyde [10]. Cinnamaldehyde occurs naturally in cassia and cinnamon oils isolated from cinnamon trees as the primary ingredient [11]. It has a strong odour of cinnamon and a sweet taste, and therefore has been extensively used as flavouring agent in foods and beverages [11, 12]. The estimated daily intake (EDI) of cinnamaldehyde from addition as flavouring substance is up to 59,000 $\mu\text{g}/\text{person}/\text{day}$ in the US [13]. Unlike most α,β -unsaturated aldehydes, cinnamaldehyde was judged by EFSA not to be genotoxic or carcinogenic [14]. This conclusion was based on a negative animal genotoxicity and carcinogenicity study [11]. In this study, rats and mice were fed daily up to 4,100 ppm of *trans*-cinnamaldehyde in modified corn starch and sucrose microcapsules mixed in their feed [11], which corresponds approximately to 200 and 550 mg cinnamaldehyde/kg bw/day for rat and mice, respectively. After two years, there was no evidence of a statistically significant increase in the incidence of neoplasms in any group treated with cinnamaldehyde.

An important question is whether the safety of dietary exposure to other α,β -unsaturated aldehydes, which have been shown to be genotoxic in vitro while in vivo genotoxicity and carcinogenicity data are limited, could be established based on read-across from these data on cinnamaldehyde. To this end, the level of DNA adducts formed in vivo by the different structurally similar compounds could be compared, taking chemical dependent differences in reactivity and detoxification efficiencies into account. Upon ingestion, α,β -unsaturated aldehydes

are converted to less electrophilic molecules via three pathways: oxidation, conjugation with glutathione (GSH) and reduction (Figure 5.1). α,β -Unsaturated aldehydes are oxidized to relevant carboxylic acids in a reaction catalysed by NAD^+ -dependent aldehyde dehydrogenases (ALDHs) [11, 13, 15-17]. Conjugation of the aldehydes with glutathione (GSH) occurs spontaneously and the reaction is significantly accelerated in the presence of glutathione S-transferases (GSTs) [18, 19]. Reduction of the aldehydes is catalysed by aldose reductases (ARs), and the α,β -unsaturated alcohol metabolites formed upon this reduction may be oxidized back to α,β -unsaturated aldehydes by alcohol dehydrogenases (ADHs) [20, 21]. If the α,β -unsaturated aldehydes come into contact with DNA, they react primarily with 2'-deoxyguanosine by Michael addition to form exocyclic 1, N^2 -propanodeoxyguanosine adducts [22-24]. While sharing a common mode of action within the group, detoxification efficiencies and the reaction efficiencies with DNA vary depending on the structure of the aldehyde [25]. This variation may result in different levels of DNA adducts and genotoxic potential of the compounds both in vitro as well as in vivo.

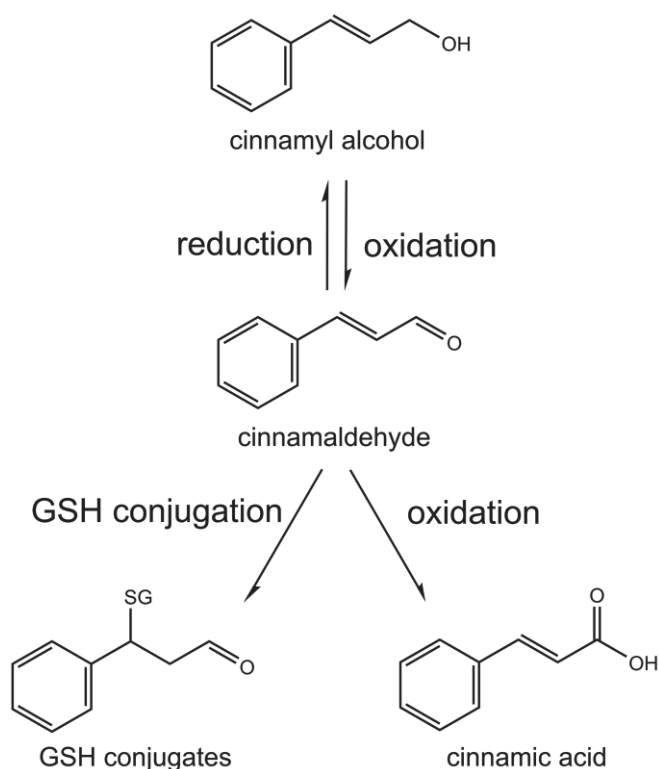


Figure 5.1. Metabolism of cinnamaldehyde

This study aims at examining dose-dependent detoxification and DNA adduct formation of cinnamaldehyde using physiologically based kinetic/dynamic (PBK/D) models to facilitate a read-across of the data on cinnamaldehyde to other food-borne α,β -unsaturated aldehydes for which PBK/D models have already been defined in our previous work [25]. PBK/D modelling was shown to be a powerful tool to quantitatively integrate kinetic parameters for all biochemical

reactions and predict in vivo DNA adduct formation at different dose levels [16, 25, 26]. In the present study PBK/D models that predict DNA adduct formation by cinnamaldehyde in rat and human liver were developed based on kinetic parameters collected in experiments with in vitro incubations with relevant tissue fractions. The PBK/D-model based predictions for the level of DNA adducts formed in the liver upon exposure to cinnamaldehyde were then compared with the PBK/D-model based predictions for DNA adduct formation by the 18 other food-borne acyclic α,β -unsaturated aldehydes for which we defined PBK/D models previously [16, 25, 26]. The results obtained are discussed with respect to the application of read-across of the in vivo genotoxicity data for cinnamaldehyde to the other food-borne α,β -unsaturated aldehydes, for which in vivo data are limited.

MATERIALS AND METHODS

Chemicals and biological materials

trans-Cinnamaldehyde (cinnamaldehyde), *trans*-cinnamic acid (cinnamic acid), *trans*-cinnamyl alcohol (cinnamyl alcohol), 2'-deoxyguanosine monohydrate (2'-dG), tris (hydroxymethyl) aminomethane, and reduced glutathione (GSH) were purchased from Sigma-Aldrich (Zwijndrecht, The Netherlands). Dimethyl sulfoxide (DMSO) was purchased from Acros Organic (New Jersey, USA). Chromatography grade acetonitrile was purchased from Biosolve (Valkenswaard, The Netherlands). Chromatography grade trifluoroacetic acid (TFA) was obtained from J.T.Baker (Deventer, The Netherlands). Pooled liver S9 from male F344 rats was obtained from BD Gentest (Worburn, USA), and pooled human liver S9 was obtained from Celsis (Baltimore, USA). Pooled intestine S9 from male Sprague Dawley rats and from human of mixed gender were purchased from Xenotech (Lenexa, USA).

Aldehyde dehydrogenase (ALDH) mediated oxidation of cinnamaldehyde to cinnamic acid

To determine the kinetic parameters for oxidation of cinnamaldehyde, incubations were performed with rat or human tissue S9. The final volume of the incubation mixtures was 100 μ l. The incubation mixtures contained (final concentrations) NAD^+ (2 mM) and liver S9 (1 mg protein/ml) or small intestine S9 (0.12 mg protein/ml) in 0.1 M Tris-HCl (pH 7.4). After pre-incubation for 2 min, the reactions were initiated by the addition of cinnamaldehyde from 100 times concentrated stock solutions in DMSO. The final concentrations of the aldehyde ranged from 10 to 3000 μ M. The mixtures were incubated at 37 °C for 5 min. The incubations were terminated by addition of 50 μ l ice-cold acetonitrile. The incubation mixtures were subsequently centrifuged for 3 min at 13,000g at 4 °C to precipitate the proteins. The formation of cinnamic acid in each sample was analysed immediately using a Waters Acquity ultra-performance liquid chromatography with diode array detection (UPLC-DAD) (Waters, Milford, MA), equipped with a Waters Acquity UPLC BEH C18 column (1.7 μ m, 2.1 \times 50 mm). The gradient was made with

acetonitrile and ultrapure water containing 0.1% (v/v) TFA. The flow rate was 0.6 mL/min, and a gradient was applied from 25 to 29% acetonitrile over 2 min, after which the percentage of acetonitrile was increased to 100% over 0.2 min, kept at 100% for 0.2 min, lowered to 0% over 0.2 min, kept at 0% for 0.2 min, increased to 25% in 0.2 min and kept at these initial conditions for 1 min for equilibration. The retention time of cinnamic acid was 1.3 min. Cinnamic acid was quantified based on peak areas obtained at a wavelength of 277 nm using a calibration curve made using commercially available cinnamic acid. Because cinnamic acid was also detected in blank incubations without NAD⁺ or tissue fractions, the amount in incubations without tissue fractions was subtracted as background.

Aldose reductase (AR) mediated reduction of cinnamaldehyde to cinnamyl alcohol

To determine the kinetic parameters for reduction, cinnamaldehyde was incubated with rat or human tissue S9. The final volume of the incubation mixtures was 100 μ l. The incubation mixtures contained NADPH (2.5 mM) and liver S9 (0.6 mg protein/ml) or small intestine S9 (0.2 mg protein/ml) in 0.1 M Tris-HCl (pH 7.4). After pre-incubation for 3 min, the reactions were initiated by the addition of cinnamaldehyde from 100 times concentrated stock solutions in DMSO. The final concentrations of cinnamaldehyde ranged from 100 to 1000 μ M. The mixtures were incubated at 37 °C for 4 min. The incubations were terminated by addition of 50 μ l ice-cold acetonitrile. The incubation mixtures were subsequently centrifuged for 3 min at 13,000g at 4 °C, and the supernatant was immediately frozen in dry ice to prevent the evaporation of the metabolite until further UPLC analysis. For the UPLC analysis, the same equipment and method as used to quantify cinnamic acid was applied (see above). The retention time of cinnamyl alcohol was 1.1 min. Cinnamyl alcohol was quantified at a wavelength of 250 nm using a calibration curve made using commercially available cinnamyl alcohol.

Glutathione S-transferase (GST) mediated GSH conjugation of cinnamaldehyde

The kinetic parameters for the GST mediated conjugation of cinnamaldehyde were determined by incubating different concentrations of cinnamaldehyde in the presence of GSH and tissue fractions. The final volume of the incubation mixtures was 100 μ L. The incubation mixtures contained liver S9 (0.4 mg protein/ml) or small intestine S9 (0.16 mg protein/ml) in 0.1 M Tris-HCl (pH 7.4). After pre-incubation for 3 min, the reaction was initiated by the addition of GSH (3 mM) from a 17 times concentrated stock solution in 0.1 M Tris-HCl (pH 7.4) and cinnamaldehyde from 100 times concentrated stock solutions in DMSO. The final concentrations of cinnamaldehyde ranged from 250 to 3,000 μ M. After 4 min, the incubations were terminated by the addition of 50 μ l ice-cold acetonitrile. The samples were centrifuged for 3 min at 13,000 g at 4°C and the resulting supernatant was analysed by UPLC-DAD immediately. The gradient was made with acetonitrile and ultrapure water containing 0.1% (v/v) TFA. The flow rate was 0.6 mL/min, and a gradient was applied from 12 to 14% acetonitrile over 1 min, after which the

percentage of acetonitrile was increased to 100% over 0.2 min, kept at 100% for 0.2 min, lowered to 0% over 0.2 min and kept at this condition for 0.2 min, increased to 12% over 0.2 min, and kept at these initial conditions for 1 min for equilibration. With this method, the retention times of two GSH conjugates formed were 0.46 and 0.53 min. A calibration curve to quantify the GSH conjugates was obtained by reacting cinnamaldehyde (10 mM) with different low concentrations of GSH (100-500 μ M) in 0.1 M Tris-HCl (pH 8.6) as described previously [16]. The conjugates were quantified based on the peak areas determined at a wavelength of 200 nm. Because cinnamaldehyde spontaneously reacts with GSH, chemical formation of the GSH conjugates in the blank incubations without tissue fractions was subtracted as background from the amount measured in the enzymatic incubations.

Alcohol dehydrogenase (ADH) mediated oxidation of cinnamyl alcohol to cinnamaldehyde

The kinetic parameters for oxidation of cinnamyl alcohol back to cinnamaldehyde were determined by incubating cinnamyl alcohol with tissue fractions. The final volume of the incubation mixtures was 100 μ l. The incubation mixtures contained NAD^+ (2 mM) and liver S9 (0.4 mg protein/ml for human and 1 mg protein/ml for rat) or small intestine S9 (0.2 mg protein/ml) in 0.1 M Tris-HCl (pH 7.4). After pre-incubation for 3 min, the reactions were initiated by the addition of cinnamyl alcohol from 100 times concentrated stock solutions in DMSO. The final concentrations of cinnamyl alcohol ranged from 100 to 1,000 μ M. The mixtures were incubated at 37 $^{\circ}$ C for 1.5 min or 3 min. The incubations were terminated by addition of 50 μ l ice-cold acetonitrile. The incubation mixtures were subsequently centrifuged for 3 min at 13,000 g at 4 $^{\circ}$ C to precipitate the proteins. The supernatants were frozen immediately on dry ice to prevent evaporation of the metabolites. The UPLC method that was used to quantify cinnamic acid was applied to quantify cinnamaldehyde, and cinnamic acid formed from cinnamaldehyde by NAD^+ -dependent ALDHs during the incubation (see above). The retention times of cinnamaldehyde and cinnamic acid were 1.6 min and 1.3 min, respectively. The amounts of cinnamaldehyde and cinnamic acid were quantified based on peak areas obtained at wavelengths of 290 nm and 277 nm respectively, using the calibration curves made using commercially available compounds. Blank incubations without tissue fractions were performed in parallel and the amount of the cinnamic acid and cinnamaldehyde measured in the blank incubations was subtracted as background.

Chemical reaction of cinnamaldehyde with GSH

The second-order rate constant for the nonenzymatic conjugation of cinnamaldehyde with GSH (k_{GSH}) was determined based on a method described by Potter and Tran [27]. Briefly, the time-dependent conjugation between cinnamaldehyde and GSH was examined by incubating 0.2 mM cinnamaldehyde with 0.5 mM GSH in 0.1 M Tris-HCl (pH 7.4) for 15–60 min at 37 $^{\circ}$ C. The reaction was initiated by the addition of cinnamaldehyde from a 100 times concentrated stock

solution in DMSO and was terminated by adding 4 mM diamide (final concentration) from a 5 times concentrated stock solution in 0.1 M Tris-HCl (pH 7.4). The GSH conjugates were quantified immediately using UPLC as already described (see above).

Chemical reaction of cinnamaldehyde with 2'-dG

The second-order rate constant for binding of cinnamaldehyde with 2'-dG (k_{DNA}) was determined by examining the time-dependent formation of 1, N^2 -propanodeoxyguanosine adducts. Cinnamaldehyde (5 mM) was incubated with 2'-dG (1.95 mM) in 0.1 M Tris-HCl (pH 7.4) for 1-5 hours at 37 °C. After 2 min of preincubation, the reaction was started by addition of cinnamaldehyde from a 100 times concentrated stock in DMSO. The reaction was terminated by injecting the reaction mixture to the UPLC-DAD system. The gradient was made with acetonitrile and ultrapure water containing 0.1% (v/v) TFA. The flow rate was 0.6 mL/min, and a gradient was applied from 8 to 15% acetonitrile over 10 min, after which the percentage of acetonitrile was increased to 100% over 0.2 min, kept at 100% for 0.2 min, lowered to 0% over 0.2 min, kept at 0% for 0.2 min, increased to 8% over 0.2 min, and equilibrated at these initial conditions for 1 min. Peaks for two adducts were found at retention times of 4.6 and 5.0 min respectively. Both peaks were absent in the blank incubations without either cinnamaldehyde or 2'-dG. Because the UV absorption patterns of the 2'-dG adducts were comparable to that of 2'-dG, it was assumed that 2'-dG adducts and 2'-dG have the same molecular extinction coefficient at the respective wavelength of maximum absorption. Quantification of 2'-dG adducts could thus be achieved by comparison of the peak area of 2'-dG adducts obtained at a wavelength 262 nm to the calibration curve of 2'-dG obtained at a wavelength 252 nm.

Kinetic analysis

The data for the rate of ALDH-mediated oxidation and AR-mediated reduction with increasing cinnamaldehyde concentrations, and ADH-mediated oxidation with increasing concentrations of cinnamyl alcohol were fitted to the standard Michaelis-Menten equation with [S] being the concentration of the substrate aldehyde or alcohol:

$$v = V_{\text{max}} \cdot [S] / (K_m + [S])$$

The GSH and cinnamaldehyde concentration-dependent rate of GSH conjugate formation catalysed by GSTs was fitted to a two-substrate model Michaelis–Menten equation simulating the ordered sequential ping–pong mechanism, with [GSH] and [S] being GSH and cinnamaldehyde concentrations, respectively:

$$v = V_{\text{max}} \cdot [S] \cdot [\text{GSH}] / (K_{m_G} \cdot [S] + K_m \cdot [S] + [\text{GSH}] \cdot [S])$$

The apparent V_{max} and K_m values were determined by fitting the data to the respective equations using GraphPad Prism (version 5.04, GraphPad Software, Inc. (La Jolla, USA)) except for K_{m_G} , which was set to 100 μM based on literature data obtained with various substrates [28, 29].

PBK/D model development

The PBK/D models for cinnamaldehyde in rat and human were developed based on the previously defined models for *trans*-2-hexenal [16, 26]. For both species, a submodel describing the formation, oxidation and distribution of cinnamyl alcohol was built and connected to the cinnamaldehyde model. The structure of the newly developed cinnamaldehyde models is displayed in Figure 5.2. The physiological parameters such as organ volumes were obtained from the literature [30] as presented in Table 5.1. Tissue:blood partition coefficients were estimated based on a method of DeJongh et al. [31] from the $\log K_{ow}$. $\log K_{ow}$ values were estimated with Estimation Program Interface (EPI) Suite version 4.10 provided by the US Environmental Protection Agency. Model equations (supporting information) were coded and numerically integrated in Berkeley Madonna 8.3.18 (Macey and Oster, UC Berkeley, CA, USA), using the Rosenbrock's algorithm for stiff systems. The uptake of cinnamaldehyde into the small intestine compartment was described by a first-order process with an absorption rate constant of 5.0 h^{-1} , the same rate as used previously for *trans*-2-hexenal that represents a rapid uptake of the compounds [16, 26, 32]. Metabolism of cinnamaldehyde was described to occur in the liver and small intestine. The V_{max} values expressed as $\text{nmol}/\text{min}/(\text{mg S9 protein})$ were scaled to be expressed as $\text{nmol}/\text{min}/(\text{g tissue})$ using S9 protein yields of 143 mg/g liver or 11.4 mg/g small intestine as scaling factors [16, 33, 34]. For cinnamic acid and GSH conjugates, no further reaction than the formation was modelled because these metabolites are not converted back to the parent compound and the further reaction of these metabolites does not influence the model outcome of interest. Chemical conjugation of cinnamaldehyde with GSH or protein reactive sites in the liver or small intestine was described as previously reported [16, 26]. Equations to describe GSH levels in the liver and small intestine were integrated in the model as previously described [16] to examine possible depletion of GSH induced by the aldehyde. The amount of DNA adducts formed in the liver was described by second-order formation and first-order elimination due to DNA repair. The half-life of the DNA adducts was set to be 38.5 hrs based on the results obtained in an in vivo study using *trans*-2-hexenal [35].

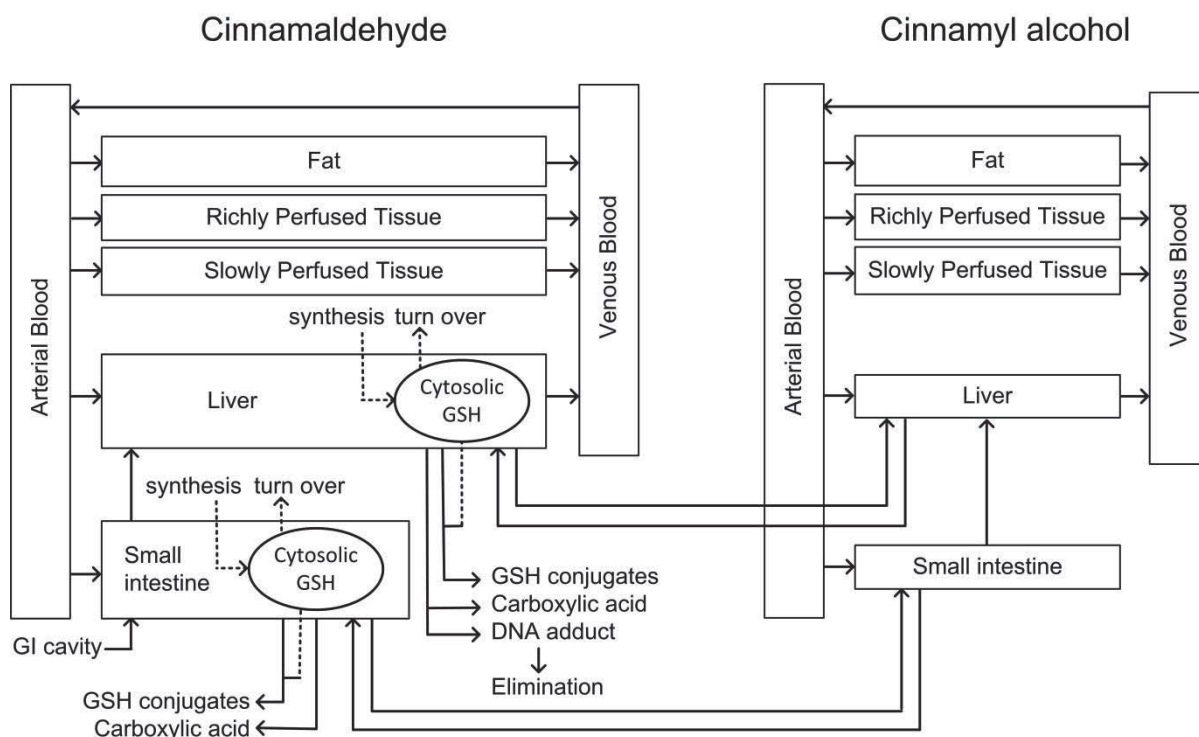


Figure 5.2. Structural diagram of the cinnamaldehyde PBK/D models. The solid line represent the movement of cinnamaldehyde or cinnamyl alcohol, and the dashed lines represent the movement of GSH.

Sensitivity analysis

To identify the key parameters that influence the model output of the newly developed cinnamaldehyde models the most, a sensitivity analysis was performed. Normalized sensitivity coefficients (SC) were determined according to the following equation: $SC = (C' - C)/(P' - P) \times (P/C)$, where C is the initial value of the model output, C' is the modified value of the model output resulting from an increase in parameter value, P is the initial parameter value, and P' is the modified parameter value. On the basis of the literature, a 5% increase in parameter values was chosen to analyse the effect of a change in parameter on the formation of 2'-dG adducts in the liver. Each parameter was analysed individually, keeping the other parameters to their initial values.

Table 5.1 Physicochemical and physiological parameters of the cinnamaldehyde PBK/D models

Parameters	Symbols	Rat	Human
Physico-chemical Parameters Cinnamaldehyde ^a			
fat/blood	PF	14.2	39.3
liver/blood	PL	1.21	2.04
small intestine/blood	PSI	1.21	2.04
richly perfused tissues/blood	PR	1.21	2.04
slowly perfused tissues/blood	PS	0.57	1.57
Physico-chemical Parameters Cinnamyl Alcohol ^a			
fat/blood	PohF	14.6	40.5
liver/blood	PohL	1.22	2.09
small intestine/blood	PohSI	1.22	2.09
richly perfused tissues/blood	PohR	1.22	2.09
slowly perfused tissues/blood	PohS	0.57	1.60
Physiological Parameters			
Body weight (kg) ^a	BW	0.25	70
Tissue volumes (% body weight) ^a			
fat	VFc	7	21.4
liver	VLc	3.4	2.6
small intestine	VSic	1.4	0.9
arterial blood	VAc	1.9	2.0
venous blood	VVc	5.6	5.9
richly perfused	VRc	4.2	4.1
slowly perfused	VSc	67.6	51.7
Cardiac output (L/h)	QC	5.4	310
Blood flow to tissue (% cardiac output) ^a			
fat	QFc	0.07	5.2
liver (excluding portal vein)	QLc	0.13	14.1
small intestine	QSic	0.12	8.6
richly perfused	QRc	0.64	47.3
slowly perfused	QSc	0.17	24.8
Initial GSH concentration ($\mu\text{mol/kg}$ tissue)			
Liver ^c	InitGSH _L	6120	5639
small intestine ^d	InitGSH _{Si}	1780	1250
GSH synthesis ($\mu\text{mol/kg}$ tissue/h) ^d			
liver	GSYN _L	6.6	1122
small intestine	GSYN _{Si}	0.25	27
Apparent first order rate constant for GSH turnover (rat) (/h) ^e			
liver	k_{L_GLOS}	0.142	0.142
small intestine	k_{Si_GLOS}	0.044	0.044
Protein reactive sites ($\mu\text{mol/kg}$ tissue) ^f			
liver	CPRO _L	3000	3000
small intestine	CPRO _{Si}	774	774

^a Brown et al. [30], ^b Jeffrey et al. [36], ^d Sweeney et al. [37], ^d Assimakopoulos et al. [38], ^e Potter and Tran [39], ^f Potter and Tran [27]

RESULTS

Enzyme mediated oxidation, GSH conjugation and reduction of cinnamaldehyde

UPLC analysis of the incubations indicated that cinnamaldehyde is converted to cinnamic acid, GSH conjugates or cinnamyl alcohol in the presence of human or rat tissue fractions and relevant cofactors. The kinetic parameters obtained from these incubations for different detoxification reactions are presented in Table 5.2. The most remarkable species difference was observed in oxidation. The estimated in vivo catalytic efficiencies (CEs) in human were two orders of magnitude higher compared to rat both in the liver and small intestine, due to lower K_m values in human. GST mediated conjugation of cinnamaldehyde with GSH was more efficient in rat than in human. The estimated in vivo CEs for reduction of cinnamaldehyde were comparable between the two species.

Table 5.2 Kinetic parameters for oxidation, reduction and GSH conjugations of cinnamaldehyde in human and rat.

Organ	Metabolites	Species	$K_m^{a,b}$	$V_{max}^{a,c}$	Scaled $V_{max}^{a,d}$	In vivo CE ^e
Liver	Cinnamic acid	Human	8.5	9.7	1387	163
		Rat	6332	64	9211	1.5
	GSH conjugates	Human	1681	37	5343	3.2
		Rat	4927	457	65313	13
	Cinnamyl alcohol	Human	333	73	10460	31
		Rat	124	29	4161	34
Small intestine	Cinnamic acid	Human	70	21	236	3.4
		Rat	4094	25	291	0.07
	GSH conjugates	Human	ND ^f	ND	ND	ND
		Rat	596	63	717	1.2
	Cinnamyl alcohol	Human	90	30	347	3.9
		Rat	75	5.8	67	0.9

^aBest fit values. ^b μ M. ^cnmol/min/(mg S9 protein). ^d V_{max} scaled to a tissue expressed as nmol/min/(g tissue). Scaling factors of 143 and 11.4 mg S9 protein/(g tissue) were used for the liver and small intestine S9 fraction. ^eEstimated in vivo catalytic efficiency expressed as mL/min/(g tissue). Calculated from scaled V_{max}/K_m . ^fNot detected.

Enzyme mediated oxidation of cinnamyl alcohol

The UPLC analysis of the incubations indicated that cinnamyl alcohol is oxidized back to cinnamaldehyde and further to cinnamic acid when it is incubated in the presence of tissue fractions and NAD^+ . The kinetic parameters for this oxidation reaction are presented in Table 5.3. The estimated in vivo CEs for oxidation of cinnamyl alcohol to cinnamaldehyde were smaller than those for reduction of cinnamaldehyde to cinnamyl alcohol in both species. The relatively slow oxidation of cinnamyl alcohol compared to its formation, indicates that cinnamaldehyde is swiftly reduced to the alcohol and may circulate in the body in the form of the alcohol before its conversion back to the aldehyde.

Table 5.3 Kinetic parameters for oxidation of the alcohols in human and rat

Organ	Species	$K_m^{a,b}$	$V_{max}^{a,c}$	Scaled $V_{max}^{a,d}$	In vivo CE ^e
Liver	Human	4167	221	31603	7.6
	Rat	1254	15	2114	1.6
Small intestine	Human	290	5.0	57	0.2
	Rat	ND ^f	ND	ND	ND

^aBest fit values. ^b μM . ^c $\text{nmol}/\text{min}/(\text{mg S9 protein})$. ^d V_{max} scaled to a tissue expressed as $\text{nmol}/\text{min}/(\text{g tissue})$. Scaling factors of 143 and 11.4 mg S9 protein/(g tissue) were used for the liver and small intestine S9 fraction. ^eIn vivo catalytic efficiency expressed as $\text{mL}/\text{min}/(\text{g tissue})$. Calculated from scaled V_{max}/K_m . ^fNot detected.

Chemical reaction with GSH and 2'-dG

The second-order rate constant of the chemical reaction of cinnamaldehyde with GSH (k_{GSH}) was $6.6 \times 10^{-4} / \mu\text{M}/\text{h}$. This value is within the same range as the k_{GSH} values of the 6 acyclic α,β -unsaturated aldehydes (i.e. *trans*-2-pentenal, *trans*-2-hexenal, *trans*-2-octenal, *trans*-2-decenal, *trans*-2-dodecenal, *trans*-2-*cis*-6-nonadienal) obtained in our previous study [16], which were between 3.7×10^{-4} and $10.5 \times 10^{-4} / \mu\text{M}/\text{h}$. The second-order rate constant of the reaction between cinnamaldehyde and 2'-dG (k_{DNA}), $1.6 \times 10^{-8} / \mu\text{M}/\text{h}$, was smaller than the k_{DNA} values of the 6 acyclic aldehydes, which ranged between 1.3×10^{-7} and $5.4 \times 10^{-7} / \mu\text{M}/\text{h}$ [16].

Performance of the PBK/D models

In order to evaluate the performance of the newly developed PBK/D models for cinnamaldehyde, the results obtained with the rat model were compared with in vivo data reported in literature. As a first step, the proportion of cinnamaldehyde metabolized to cinnamic acid or GSH conjugates was examined (Table 5.4). There are three in vivo studies [15, 20, 40], where proportions of different metabolites excreted in urine were reported for rats exposed to single doses of 2 to 500 mg cinnamaldehyde/kg bw via gavage or intraperitoneal (ip) injection. In case a prediction was compared with in vivo data obtained upon ip injection, the cinnamaldehyde was modelled to enter directly into the liver in the rat PBK/D models.

Peters et al. [15] and Sapienza et al. [40] reported the amounts of five urinary metabolites (i.e. hippuric acid, benzoyl glucuronide, 3-hydroxy-3-phenylpropionic acid (HPPA), cinnamoylglycine, and benzoic acid), which are all produced following oxidation of cinnamaldehyde to cinnamic acid, excreted by rats exposed to cinnamaldehyde by gavage or ip injection. At exposure levels higher than 250 mg/kg bw, the prediction for cinnamaldehyde excretion via cinnamic acid matched best with the in vivo data on the sum of the excretion of the five aldehyde metabolites and the difference was less than 1.6-fold. At lower doses of 2 and 50 mg/kg bw the differences between the prediction and observed data were higher, amounting to 5.4 to 8.9-fold. A comparison was also made between the predicted formation of GSH conjugates and literature data on excretion of these metabolites as mercapturic acids, which are the ultimate

metabolites of GSH conjugates excreted in the urine. Delbressine et al. reported that excreted mercapturic acids amounted to 14.8% of the applied dose of 250 mg cinnamaldehyde/kg bw in female Wistar rats [20]. The PBK/D model predicted that 41% of the administered cinnamaldehyde dose would be metabolized via conjugation to GSH, which is 2.8-fold higher than the in vivo data (Table 5.4).

Table 5.4 Comparison of the rat cinnamaldehyde PBK/D model outcomes and in vivo observed data

Reference for in vivo data	Type of rats, gender	Dose (mg/kg bw)	Exposure route	Metabolites (Ultimate metabolites found in rat urine)	Proportion of the metabolites to the administered dose (%)		Predicted/ Observed
					Observed	Predicted	
Peters [15]	F344, male	2	ip injection	Cinnamic acid (Hippuric acid,	89.0	10	8.9
	F344, female	2	ip injection	benzoyl glucuronide,	89.3	10	8.9
	F344, male	250	ip injection	HPPA,	83.8	59	1.4
	F344, female	250	ip injection	cinnamoyl glycine, benzoic acid)	88.1	59	1.5
	F344, male	250	oral		88.0	56	1.6
Sapienza et al., [40]	F344, male	50	oral	idem	86.8	16	5.4
	F344, male	500	oral		91.5	71	1.3
Delbressine et al. [20]	Wistar, female	250	ip injection	GSH conjugates (mercapturic acids)	14.8±1.9	41	2.8

In the next step, the time-dependent prediction of cinnamaldehyde concentrations in blood in rat was compared with the values reported by Yuan et al., [41] or Zhao et al.[42] (Figure 5.3). In these in vivo studies, the time-dependent changes in cinnamaldehyde blood concentration in rats were monitored following the exposure to 250 or 500 mg/kg bw cinnamaldehyde by gavage or to 5 to 25 mg/kg bw cinnamaldehyde via intravenous (iv) injection. Upon iv injection (Figure 5.3A-D), the cinnamaldehyde blood concentrations predicted for different doses adequately matched with the data reported except for the maximum concentration (C_{max}). The predictions on C_{max} following iv exposure were 10-17-fold higher than the data reported by Yuan et al., and 450-fold higher than the data reported by Zhao et al. Results obtained for oral exposure revealed that the cinnamaldehyde concentrations in blood increase rapidly and reach C_{max} within 0.1 hour after dosing (Figure 5.3E and F). After the C_{max} is reached, the predicted concentrations declined rapidly at first, followed by a relatively slow decline phase. The rapid decline is due to the efficient conversion of the aldehyde via oxidation, reduction or conjugation with GSH, and then the blood level stabilizes because the metabolism of cinnamaldehyde and the oxidation of

cinnamyl alcohol to cinnamaldehyde tend to equilibrate, resulting in the relatively slow decline phase. The predicted C_{\max} values following oral administration were 204 and 896 μM at 250 and 500 mg/kg bw, respectively. These values overestimated the in vivo observed values up to 48-fold when compared with C_{\max} values reported by Yuan et al. [41], and up to 545-fold when compared the C_{\max} reported by Zhao et al. [42]. During the slow decline phase, which was observed approximately 2 hours after the dosing, the PBK/D model based predicted cinnamaldehyde levels were up to 58-times higher than the values reported by Zhao et al. [42] but were within 6.4-fold compared to the values reported by Yuan et al. [41].

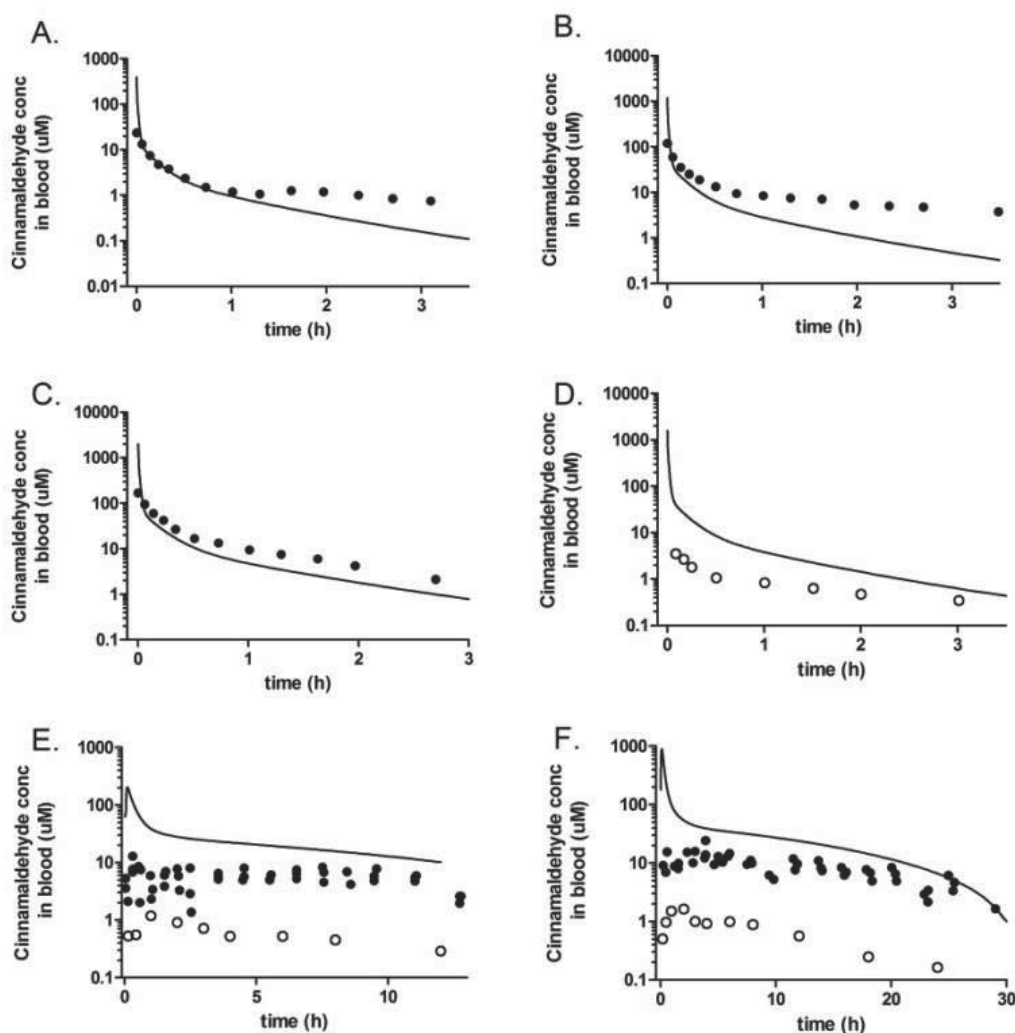


Figure 5.3. Comparison of the rat PBK/D model predicted cinnamaldehyde levels in blood and in vivo observed values. The closed and open circles represent the in vivo cinnamaldehyde levels in blood in rat reported by Yuan et al. [41] and Zhao et al. [42], respectively, upon cinnamaldehyde administration of (A) 5 mg/kg bw by iv injection, (B) 15 mg/kg bw by iv injection, (C) 25 mg/kg bw by iv injection, (D) 20 mg/kg bw by iv injection, (E) 250 mg/kg bw by gavage, and (F) 500 mg/kg bw by gavage. The solid lines in all graphs represent the rat PBK/D model prediction.

Little has been reported about kinetics of cinnamaldehyde in human. Cocciara et al. [43] reviewed an unpublished study where two healthy male volunteers were orally exposed to 0.7 mg/kg bw cinnamaldehyde capsulated in gelatine. It was reported that 96.2-96.5% of the recovered compounds were excreted in urine as either hippuric acid, benzoyl glucuronide, HPPA or benzoyl acid, the ultimate metabolites of cinnamic acid. The human PBK/D model predicted 98 % of cinnamaldehyde to be oxidized to cinnamic acid at 0.7 mg/kg bw, which matched very well with the in vivo data.

Sensitivity analysis

A sensitivity analysis was performed to reveal which parameters influence the PBK/D model predicted DNA adduct formation in the liver at T_{\max} , the time when the maximum DNA adduct level is reached. This analysis was performed at the EDI of cinnamaldehyde of 0.99 mg/kg bw. Only the parameters which showed an absolute sensitivity coefficient higher than 0.1 ($|SC| > 0.1$) either in the rat or human model are presented in Figure 5.4. The results indicated that DNA adduct levels are significantly influenced by the second-order rate constant for the binding to 2'-dG (k_{DNA}), the volume of the liver (V_{Lc}), and the scaling factor for liver S9 (S9PL) as it was previously reported for *trans*-2-hexenal PBK/D models [16, 26] and for the rat models for the 18 acyclic α,β -unsaturated aldehydes [25]. Apart from these three parameters, the analysis revealed that the model outcome is also influenced by the V_{\max} and K_m of GST mediated conjugation with GSH in the liver (V_{\max,L_GST} and K_{m,L_GST}) in rat, but this influence was insignificant in the human model. In contrast to the rat model, the human model outcome is significantly influenced by the V_{\max} and K_m of oxidation in the liver (V_{\max,L_CA} and K_{m,L_CA}).

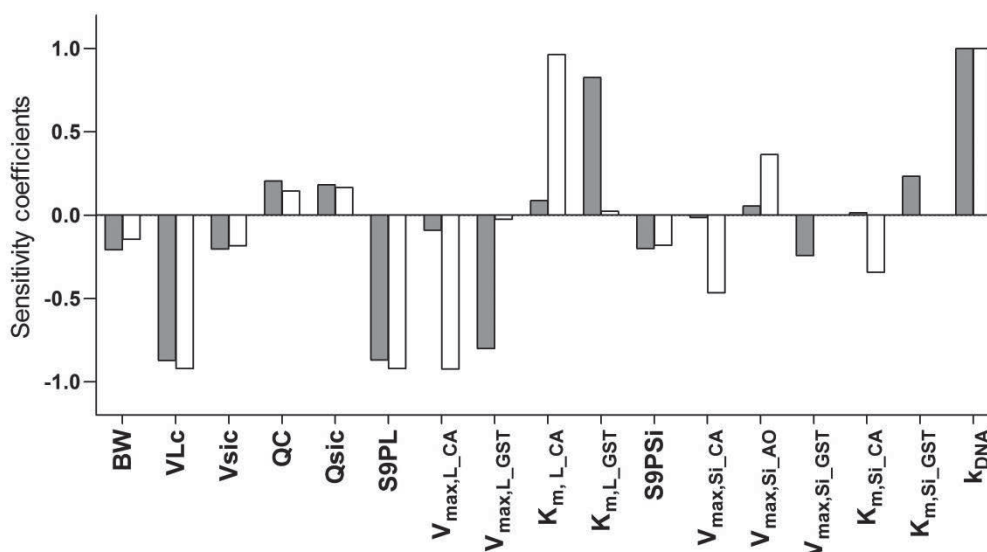


Figure 5.4. Sensitivity analysis of the predicted amount of maximum DNA adducts in the liver at 0.99 mg cinnamaldehyde/kg bw for rat (grey bars) and for human (white bars). The parameters listed in the figures are the following: body weight (BW); fraction of the liver (VLC) and the small intestine (VSic); blood flow rate (QC); fraction of the blood flow to the small intestine (QSic); scaling factor of liver S9 (S9PL); V_{max} and K_m in the liver to form cinnamic acid (V_{max,L_CA} and K_{m,L_CA}) or GSH conjugations mediated by GSTs (V_{max,L_GST} and K_{m,L_GST}); scaling factor of small intestine S9 (S9PSi); V_{max} and K_m in the small intestine to form cinnamic acid (V_{max,Si_CA} and K_{m,Si_CA}), cinnamyl alcohol (V_{max,Si_AO}) or GSH conjugations mediated by GSTs (V_{max,Si_GST} and K_{m,Si_GST}); and second-order rate constant of cinnamaldehyde binding to 2'-dG (k_{DNA})

PBK/D model outcomes for cinnamaldehyde

Using the PBK/D models, interspecies differences in detoxification and DNA adduct formation of cinnamaldehyde were examined (Figure 5.5). In rat, the majority of cinnamaldehyde forms GSH conjugates and oxidation was revealed to be a minor metabolic route at exposure levels lower than 200 mg/kg bw (Figure 5.5A). However, the oxidation of cinnamaldehyde was predicted to be the major pathway in human at all doses due to the high CEs of ALDHs (Figure 5.5B). Subsequently, the DNA adduct formation in the liver was plotted at different doses ranging between 0.99 mg/kg bw, a dose representing the EDI for a person of 70 kg [13], and 200 mg/kg bw, the highest dose at which level there was no development of neoplasm observed due to cinnamaldehyde in rats [11] (Figure 5.5C). DNA adduct formation in human was predicted to be lower than in rat, primarily due to the lower K_m for detoxification via oxidation of the aldehyde in human liver and small intestine. At 0.99 mg/kg bw, 0.065 and 0.008 adduct formation per 10^8 nt were predicted to occur in rat and human, respectively. At 200 mg/kg bw, the maximum DNA adduct level was predicted to be comparable for rat and human, amounting to 79 adducts/ 10^8 nt in rat and 68 adducts/ 10^8 nt in human.

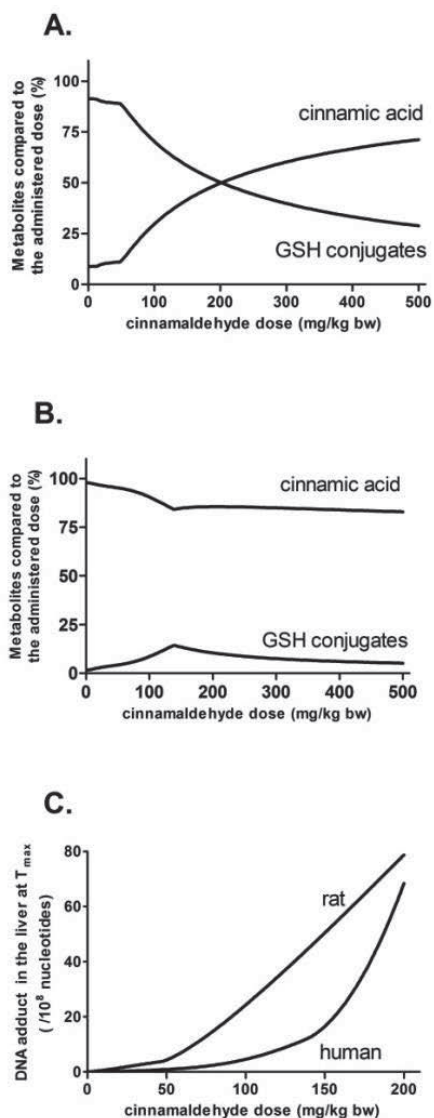


Figure 5.5. Cinnamaldehyde PBK/D model outcomes on dose-dependent change in proportion of the metabolites to the administered cinnamaldehyde dose in rat (A) and in human (B), and on dose-dependent maximum DNA adduct formation in both species (C).

DNA adduct levels for 18 acyclic α,β -unsaturated aldehydes compared to cinnamaldehyde in rats

The dose-dependent DNA adduct formation in rat liver as predicted for cinnamaldehyde was compared with the results previously obtained for 18 acyclic α,β -unsaturated aldehydes [25]. Dose-dependent DNA adduct formation in rat liver by cinnamaldehyde as well as the 18 aldehydes is presented in Figure 5.6. The values for the 18 aldehydes were predicted by the PBK/D models developed in our previous study [25]. These PBK/D models developed in the previous study contained no submodel for the respective alcohols. In order to harmonize the model structures between the 18 aldehydes and cinnamaldehyde, cinnamaldehyde PBK/D model outcomes without the cinnamyl alcohol submodel is also presented for the comparison in Figure 5.6. The difference in DNA adduct levels predicted by the two models for cinnamaldehyde was less than 9-fold being lower for the model without the cinnamyl alcohol submodel. The results

revealed that, either with or without the cinnamyl alcohol submodel, DNA adduct formation by 6 aldehydes (*trans*-2-dodecenal, undecenal, *trans*-2-decenal, 2,6-dodecadienal, 2-tridecenal, and 2-tetradecenal) would be lower than that caused by cinnamaldehyde, and for 6 other aldehydes (2-propenal, 2-pentenal, 4-methyl-2-pentenal, *trans*-2-heptenal, and *trans*- and *cis*-2-hexenal) DNA adduct formation was predicted to be higher than that for cinnamaldehyde at doses up to 200 mg/kg bw. For the remaining 6 aldehydes (*trans*-2-*cis*-6-octadienal, *trans*-2-*cis*-6-nonadienal, *trans*-2-*trans*-6-nonadienal, *trans*-2-nonenal, *cis*-2-nonenal, *trans*-2-octenal) DNA adduct levels were within the range of the cinnamaldehyde models with or without the cinnamyl alcohol submodel.

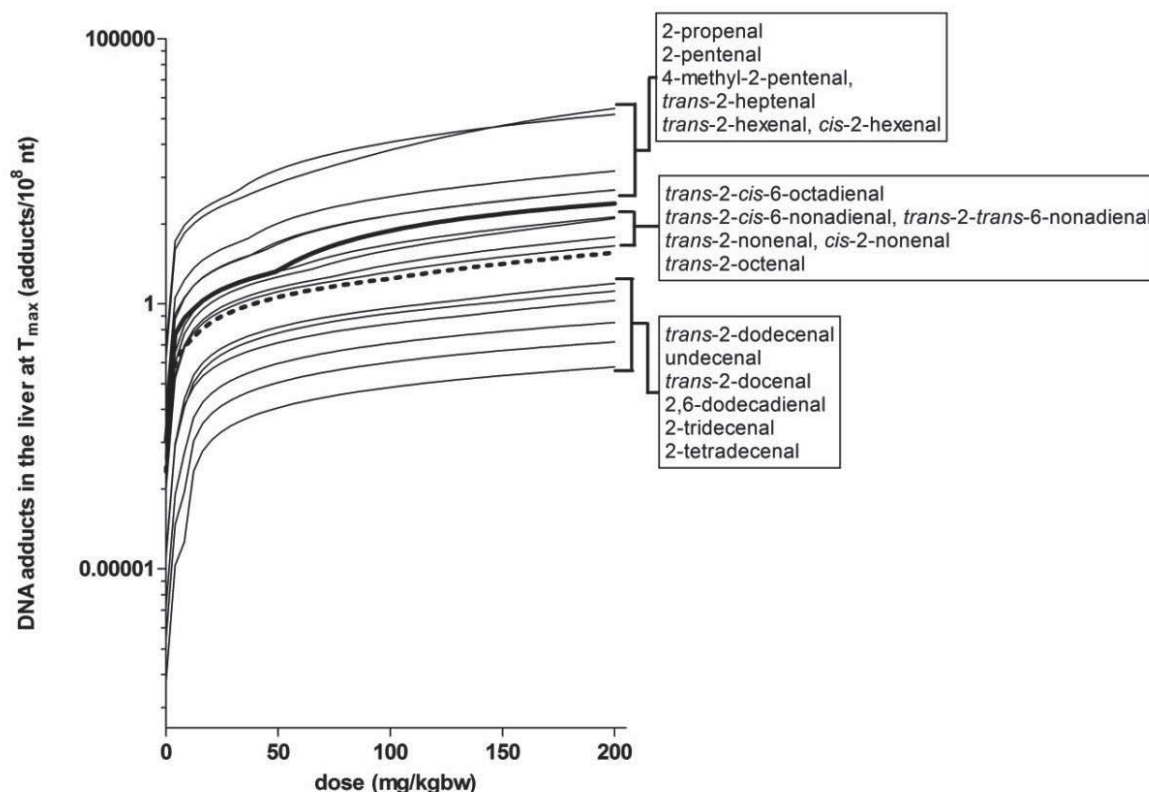


Figure 5.6. Dose-dependent DNA adduct formation by cinnamaldehyde and 18 food-borne acyclic α,β -unsaturated aldehydes in rat liver. The DNA adduct formation by the 18 aldehydes were derived from our previous study [25] and are presented with thin solid lines. In the cases where curves overlap, names of the respective aldehydes are presented on the same line in the boxes. The values for cinnamaldehyde predicted by the PBK/D models developed in the present study are presented with a thick solid line (model with the cinnamyl alcohol submodel) or with a thick dashed line (model without the cinnamyl alcohol submodel).

The levels of DNA adducts predicted to be formed in rat liver upon exposure to the 18 acyclic α,β -unsaturated aldehydes at their respective EDIs have previously been predicted by the PBK/D models [25] as summarized in Table 5.5. The DNA adduct levels for the acyclic α,β -unsaturated aldehydes varied between 1.3×10^{-10} and 0.036 adducts/ 10^8 nt at their EDI values [25]. These levels are 3 to 12 orders of magnitude lower than the DNA adduct levels of

cinnamaldehyde at a dose of 200 mg/kg bw, the highest dose level tested that did not result in carcinogenicity in rats, amounting to 79 adducts/10⁸ nt. Upon exposure to cinnamaldehyde at its EDI, formation of 0.065 and 0.017 DNA adducts per 10⁸ nt was predicted in rats by the PBK/D model with and without the cinnamyl alcohol submodel, respectively. These levels were 10¹ to 10⁸-fold higher than the values obtained for the other aldehydes except for 2-propenal, indicating that at realistic exposure levels cinnamaldehyde is expected to result in higher levels of DNA adduct formation than these 17 acyclic α,β -unsaturated aldehydes.

Table 5.5 Predicted maximum DNA adduct formation in rat liver by 18 food-borne acyclic α,β -unsaturated aldehydes at their respective EDIs. The values for DNA adducts were derived from Kiwamoto et al. [25].

Compounds	Levels ($\mu\text{g}/\text{kgbw}/\text{d}$)	Predicted maximum DNA adduct levels (adduct/10 ⁸ nt)
2-propenal	17 ^a	0.036
2-pentenal	0.002 ^b	7.4×10 ⁻⁶
4-methyl-2-pentenal	N.A. ^c	-
<i>trans</i> -2-hexenal	13.20 ^b	2.0×10 ⁻³
<i>cis</i> -2-hexenal		
<i>trans</i> -2-heptenal	0.10 ^b	1.2×10 ⁻⁵
<i>trans</i> -2-octenal	0.50 ^b	4.4×10 ⁻⁶
<i>trans</i> -2-nonenal	0.07 ^b	7.2×10 ⁻⁷
<i>cis</i> -2-nonenal,		
<i>trans</i> -2-decenal	0.10 ^b	4.9×10 ⁻⁸
2-undecenal	0.007 ^b	3.2×10 ⁻⁹
<i>trans</i> -2-dodecenal	0.27 ^b	1.3×10 ⁻⁷
2-tridecenal	0.01 ^b	1.3×10 ⁻¹⁰
2-tetradecenal	N.A.	-
<i>trans</i> -2- <i>cis</i> -6-octadienal	N.A.	-
<i>trans</i> -2- <i>cis</i> -6-nonadienal	0.40 ^d	7.1×10 ⁻⁶
<i>trans</i> -2- <i>trans</i> -6-nonadienal	0.0001 ^d	1.8×10 ⁻⁹
2,6-dodecadienal	0.01 ^d	5.0×10 ⁻¹⁰

^aEstimated amount present in food [44]. ^bEstimated amount consumed as food flavouring agent [9]. ^cN.A.= not available in literature, ^dEstimated amount consumed as food flavouring agent [8]

DISCUSSION

Humans are ubiquitously exposed to numerous α,β -unsaturated aldehydes, with one of the major sources being food. Due to the electrophilic and therefore reactive nature of these compounds with DNA, the use of α,β -unsaturated aldehydes as food flavouring agents may present a food safety concern. While some α,β -unsaturated aldehydes such as cinnamaldehyde have been

observed not to be genotoxic or carcinogenic in vivo [11], the safety of many other α,β -unsaturated aldehydes is a matter for ongoing debate because no in vivo genotoxicity or carcinogenicity studies have been conducted on these compounds. To overrule the positive results obtained in in vitro genotoxicity tests with the α,β -unsaturated aldehydes, especially in vivo data have been requested by EFSA [6]. Cinnamaldehyde is one of the few α,β -unsaturated aldehydes for which genotoxicity and carcinogenicity have been tested in vivo [11]. In a chronic feeding study in rats, no carcinogenicity was observed after daily exposure of rats to cinnamaldehyde up to 200 mg/kg bw/day after two years.

To facilitate a science-based comparison and read-across from the data on cinnamaldehyde, in the present study rat and human PBK/D models for cinnamaldehyde were developed based on in vitro derived kinetic parameters. These models could predict the level of DNA adduct formation expected at dose levels at which cinnamaldehyde was tested negative for genotoxicity and carcinogenicity in vivo. In these PBK/D models cinnamaldehyde was described to be metabolized via three enzyme-mediated pathways in the liver and small intestine. A submodel for the reduced metabolite cinnamyl alcohol was included because the alcohol metabolite enters the systemic circulation [42] and can be enzymatically converted back to the parent aldehyde, which will influence the predicted levels of DNA adducts formed in the liver. The rat cinnamaldehyde PBK/D model predictions matched well with in vivo observed data especially at doses higher than 250 mg/kg bw, when the predicted proportions of metabolites formed were compared with data found in literature. Comparison of the predictions on time-dependent cinnamaldehyde blood levels with in vivo data revealed that the difference was within 10-fold except for the peak concentrations (C_{\max}) that were reached immediately after the dosing. The difference up to 450-fold in C_{\max} between the predictions and the in vivo data upon iv injection may partly be explained by the 10-20 sec required for the sample injection and the subsequent time needed to flush the cannula inserted in the jugular vein in the in vivo studies [41, 42]. The PBK/D model administration of all cinnamaldehyde via iv injection occurs at once. If the injection time of 20 sec is included in the PBK/D model, overestimations in the predicted C_{\max} are lowered from 10-17-fold to 4.4-7.4-fold compared to the data reported by Yuan et al. [41], and from 450 to 201-fold compared to the data reported by Zhao et al. [42]. Upon oral administration, the predicted C_{\max} were higher up to 545-fold than the observed values. While the cinnamaldehyde uptake was described only in small intestine in the model, in practice the aldehyde may partly be absorbed already in forestomach and glandular stomach upon gavage [45]. A PBK/D model that describes this prolonged uptake would improve the prediction for the time-dependent kinetics and C_{\max} . In general, the predicted cinnamaldehyde levels in blood matched better with the data reported by Yuan et al [41] but were higher up to two orders of magnitudes than the data reported by Zhao et al. [42]. In these two in vivo studies, the blood samples were processed differently after sampling: the samples were mixed with formaldehyde immediately after the sampling by Yuan et al. [41] to stabilize cinnamaldehyde, whereas this

process was not included in the study by Zhao et al. [42]. Yuan et al. [41, 46] reported that the cinnamaldehyde concentrations decreased with a half-life of 9 min at 23 °C after sampling without the addition of formaldehyde because cinnamaldehyde continued to bind with blood protein. This rapid cinnamaldehyde elimination after sampling may have caused the underestimation of the cinnamaldehyde blood levels in the study by Zhao et al. [42] and this may in part also explain the deviation of these data from the PBK/D predictions.

Using the newly developed rat and human PBK/D models for cinnamaldehyde, interspecies differences in detoxification and DNA adduct formation of cinnamaldehyde were examined. The models revealed that the primary detoxification route shifts from conjugation with GSH to oxidation at exposure levels higher than 200 mg/kg bw in rat, while the major route remains to be oxidation throughout the examined dose range in human. The estimated in vivo CEs for cinnamaldehyde oxidation by human small intestine and liver were two orders of magnitude higher than those for rat. Considering that the estimated CEs for in vivo oxidation of *trans*-2-hexenal, a six carbon acyclic α,β -unsaturated aldehyde, in the liver were comparable between human and rat [26] the results suggest that different ALDH isoenzymes may play a role in the oxidation of cinnamaldehyde and *trans*-2-hexenal. The higher oxidation efficiencies of cinnamaldehyde in human resulted in lower levels of DNA adducts formed in human than in rat. The predicted levels were 8.6-fold and 1.2-fold higher in rat than in human at 0.99 mg/kg bw and 200 mg/kg bw, respectively.

The rat PBK/D model for cinnamaldehyde predicted the maximum DNA adduct formation at 200 mg/kg bw to be 79 adducts/ 10^8 nt in the liver, which is within the natural background levels of structurally similar 1, N^2 -exocyclic propanodeoxyguanosine adducts observed in diseased free human liver (6.8-110 adducts/ 10^8 nt) [47, 48]. This is in line with the findings in the long-term rodent study where cinnamaldehyde doses up to 200 mg/kg bw/day did not increase the occurrence of neoplasms despite the high levels of exposure [11]. At its EDI, 0.99 mg cinnamaldehyde/kg bw, formation of 0.008 DNA adducts per 10^8 nt was predicted in human. This level of DNA adduct is 4 orders of magnitude lower than the predicted value of 79 adducts/ 10^8 nt in rat liver at 200 mg cinnamaldehyde/kg bw, the exposure level where no carcinogenicity was observed in vivo, and 3 orders of magnitude lower than the natural background levels of structurally similar DNA adducts observed in diseased free human liver. These results support the conclusion that human dietary exposure to cinnamaldehyde is not of concern with respect to genotoxicity as was also concluded by FEMA, JECFA and EFSA [10, 13, 49]. Although it may be argued that even higher exposures to α,β -unsaturated aldehydes may still lead to significant DNA adduct formations, higher levels of exposure are not likely to occur due to the self-limiting use of flavouring agents, with higher exposure leading to off-flavours.

The DNA adduct levels predicted for cinnamaldehyde were furthermore compared with DNA adduct formation predicted for 18 other food-borne acyclic α,β -unsaturated aldehydes in our previous study [25]. This comparison is of interest given that for these 18 α,β -unsaturated

aldehydes in vivo genotoxicity and carcinogenicity data are limited or even absent. The comparison may thus facilitate read-across from cinnamaldehyde for which negative in vivo data on genotoxicity and carcinogenicity are available. The PBK/D model based comparison in dose-dependent formation of DNA adducts, namely 1,*N*²-exocyclic propanodeoxyguanosine adducts in rat revealed that DNA adduct formation by 6 out of the 18 aldehydes (i.e. *trans*-2-dodecenal, undecenal, *trans*-2-decenal, 2,6-dodecadienal, 2-tridecenal, 2-tetradecenal) would be lower than by cinnamaldehyde at doses up to 200 mg/kg bw. Although the reactivity of the 6 aldehydes with DNA (k_{DNA}) is higher than that of cinnamaldehyde, detoxification via oxidation and conjugation with GSH were estimated to be higher with these 6 aldehydes [25], leading to lower DNA adduct formation of these 6 aldehydes. These results highlight the importance to account for the overall kinetics of compounds in addition to their reactivity with DNA when studying genotoxicity of DNA reactive agents. Lower DNA adduct formation by the 6 aldehydes than cinnamaldehyde suggests that these 6 aldehydes would also test negative for genotoxicity and carcinogenicity at high dose levels. To investigate in vivo genotoxicity or carcinogenicity of the other 12 aldehydes, an in vivo genotoxicity study using 2-propenal may be of use because 2-propenal represents the worst-case analogue given that it was predicted to induce the highest levels of DNA adduct formation within the series [25].

At their respective EDI, the formation of DNA adducts by the acyclic α,β -unsaturated aldehydes appears to be 1 to 8 orders of magnitude lower than DNA adduct formed by cinnamaldehyde at its EDI, except for 2-propenal. DNA adduct formation by 2-propenal at its EDI (0.036 adducts/ 10^8 nt) was predicted to be about 2-fold higher than that by cinnamaldehyde (0.017 adducts/ 10^8 nt) predicted using the rat PBK/D model without the cinnamyl alcohol submodel. Compared to the DNA adduct level of cinnamaldehyde at 200 mg/kg bw (79 adducts/ 10^8 nt), the dose that tested negative in the in vivo study, DNA adducts by all 18 acyclic α,β -unsaturated aldehydes at their EDI were 3 to 12 orders of magnitude lower. Considering that cinnamaldehyde at this exposure level of 200 mg/kg bw per day did not show carcinogenicity in vivo, these differences in the DNA adduct levels indicate that for all these 18 α,β -unsaturated aldehydes DNA adduct formation at doses relevant for human dietary exposure does not raise a safety concern. This further supports the conclusions obtained in our previous studies [16, 25, 26], where DNA adduct formation by the 18 aldehydes was compared with the natural background levels of structurally similar 1,*N*²-exocyclic propanodeoxyguanosine adducts, that DNA adduct formation is negligible for the 18 aldehydes at the relevant levels of dietary intake. It should be noted that the PBK/D models for the 18 other aldehydes did not contain the submodel for their reduced alcohol metabolites [25]. Comparison of such a model for cinnamaldehyde to the model containing a submodel for cinnamyl alcohol revealed that this may lead to an underestimation of at most 9-fold. This leads to the conclusion that the formation of DNA adducts by the 18 acyclic α,β -unsaturated aldehydes at their respective EDI would still be 2 to 11 orders of magnitude lower than the DNA adduct level of cinnamaldehyde at 200 mg/kg bw.

In conclusion, the results obtained in this study enabled read-across from cinnamaldehyde to 18 food borne acyclic α,β -unsaturated aldehydes and supported the conclusion that for all these 18 α,β -unsaturated aldehydes DNA adduct formation at doses relevant for human dietary exposure does not raise a safety concern. The present study overall illustrated that physiologically based in silico modelling approach facilitates a science-based comparison and read-across on the possible risks posed by food-borne DNA reactive agents.

REFERENCES

- [1] Witz, G., Biological interactions of alpha,beta-unsaturated aldehydes. *Free Radic Biol Med* 1989, 7, 333-349.
- [2] Golzer, P., Janzowski, C., Pool-Zobel, B. L., Eisenbrand, G., (E)-2-hexenal-induced DNA damage and formation of cyclic 1,N²-(1,3-propano)-2'-deoxyguanosine adducts in mammalian cells. *Chem Res Toxicol* 1996, 9, 1207-1213.
- [3] Janzowski, C., Glaab, V., Mueller, C., Straesser, U., *et al.*, Alpha,beta-unsaturated carbonyl compounds: induction of oxidative DNA damage in mammalian cells. *Mutagenesis* 2003, 18, 465-470.
- [4] Canonero, R., Martelli, A., Marinari, U. M., Brambilla, G., Mutation induction in Chinese hamster lung V79 cells by five alk-2-enals produced by lipid peroxidation. *Mutat Res* 1990, 244, 153-156.
- [5] EFSA, Minutes of the 26th plenary meeting of the scientific panel on food additives, flavourings, processing aids and materials in contact with food. <http://www.efsa.europa.eu/en/events/event/afc071127-m.pdf>. 2007.
- [6] EFSA, Genotoxicity Test Strategy for Substances belonging to Subgroups of FGE.191: Statement of the Panel on Food Contact Materials, Enzymes, Flavourings and Processing Aids (CEF). <http://www.efsa.europa.eu/en/scdocs/doc/854.pdf>. 2008.
- [7] Adams, T. B., Gavin, C. L., Taylor, S. V., Waddell, W. J., *et al.*, The FEMA GRAS assessment of alpha,beta-unsaturated aldehydes and related substances used as flavor ingredients. *Food Chem Toxicol* 2008, 46, 2935-2967.
- [8] JECFA, Evaluation of certain food additives and contaminants: Sixty-first report of the Joint FAO/WHO Expert Committee on Food Additives. http://whqlibdoc.who.int/trs/WHO_TRS_922.pdf. 2004.
- [9] JECFA, Evaluation of Certain Food Additives: sixty-third report of the Joint FAO/WHO Expert Committee on Food Additives. http://whqlibdoc.who.int/trs/WHO_TRs_928.pdf. 2005.
- [10] JECFA, Evaluation of certain food additives and contaminants : fifty-fifth report of the Joint FAO/WHO expert committee on food additives. http://whqlibdoc.who.int/trs/WHO_TRS_901.pdf. 2001.
- [11] NTP, NTP Technical Report on the Toxicology and Carcinogenesis Studies of *trans*-Cinnamaldehyde (Microencapsulated) (CAS NO. 14371-10-9) in F344/N Rats and B6C3F1 Mice (Feed Studeis). http://ntp.niehs.nih.gov/ntp/htdocs/lt_rpts/tr514.pdf. 2004.
- [12] Blakemore, W. M., Thompson, H. C., Trace Analysis of Cinnamaldehyde in Animal Feed, Human-Urine, and Wastewater by Electron-Capture Gas-Chromatography. *J Agric Food Chem* 1983, 31, 1047-1052.
- [13] Adams, T. B., Cohen, S. M., Doull, J., Feron, V. J., *et al.*, The FEMA GRAS assessment of cinnamyl derivatives used as flavor ingredients. *Food Chem Toxicol* 2004, 42, 157-185.
- [14] EFSA, Flavouring Group Evaluation 214: alpha,beta-Unsaturated aldehydes and precursors from chemical subgroup 3.1 of FGE.19: Cinnamyl derivatives. Scientific Opinion of the Panel on Food Contact Materials, Enzymes, Flavourings and Processing Aids (CEF). <http://www.efsa.europa.eu/en/scdocs/doc/880.pdf>. 2009.
- [15] Peters, M. M., Caldwell, J., Studies on *trans*-cinnamaldehyde. 1. The influence of dose size and sex on its disposition in the rat and mouse. *Food Chem Toxicol* 1994, 32, 869-876.
- [16] Kiwamoto, R., Rietjens, I. M. C. M., Punt, A., A physiologically based in silico model for *trans*-2-hexenal detoxification and DNA adduct formation in rat. *Chem Res Toxicol* 2012, 25, 2630-2641.
- [17] Adams, T. B., Gavin, C. L., Taylor, S. V., Waddell, W. J., *et al.*, The FEMA GRAS assessment of alpha,beta-unsaturated aldehydes and related substances used as flavor ingredients. *Food Chem Toxicol* 2008, 46, 2935-2967.
- [18] Boyland, E., Chasseau.Lf, Enzymes Catalysing Conjugations of Glutathione with Alphabeta-Unsaturated Carbonyl Compounds. *Biochemical Journal* 1968, 109, 651-&.
- [19] Eisenbrand, G., Schuhmacher, J., Golzer, P., The influence of glutathione and detoxifying enzymes on DNA damage induced by 2-alkenals in primary rat hepatocytes and human lymphoblastoid cells. *Chem Res Toxicol* 1995, 8, 40-46.
- [20] Delbressine, L. P., Klippert, P. J., Reuvers, J. T., Seuttler-Berlage, F., Isolation and identification of mercapturic acids of cinnamic aldehyde and cinnamyl alcohol from urine of female rats. *Arch Toxicol* 1981, 49, 57-64.
- [21] Pietruszko, R., Crawford, K., Lester, D., Comparison of substrate specificity of alcohol dehydrogenases from human liver, horse liver, and yeast towards saturated and 2-enoic alcohols and aldehydes. *Arch Biochem Biophys* 1973, 159, 50-60.
- [22] Stout, M. D., Jeong, Y. C., Boysen, G., Li, Y., *et al.*, LC/MS/MS method for the quantitation of *trans*-2-hexenal-derived exocyclic

- 1,*N*²-propanodeoxyguanosine in DNA. *Chem Res Toxicol* 2006, *19*, 563-570.
- [23] Schuler, D., Budiawan, B., Eder, E., Development of a ³²P-postlabeling method for the detection of 1, *N*²-propanodeoxyguanosine adducts of 2-hexenal in vivo. *Chem Res Toxicol* 1999, *12*, 335-340.
- [24] Rezaei, M., Harris, T. M., Rizzo, C. J., Stereoselective synthesis of the 1,*N*²-deoxyguanosine adducts of cinnamaldehyde. A stereocontrolled route to deoxyguanosine adducts of α,β -unsaturated aldehydes. *Tetrahedron Lett* 2003, *44*, 7513-7516.
- [25] Kiwamoto, R., Spenkeliink, A., Rietjens, I. M., Punt, A., An integrated QSAR-PBK/D modelling approach for predicting detoxification and DNA adduct formation of 18 acyclic food-borne α,β -unsaturated aldehydes. *Toxicol Appl Pharmacol* 2015, *282*, 108-117.
- [26] Kiwamoto, R., Spenkeliink, A., Rietjens, I. M. C. M., Punt, A., A physiologically based in silico model for *trans*-2-hexenal detoxification and DNA adduct formation in human including interindividual variation indicates efficient detoxification and a negligible genotoxicity risk. *Arch Toxicol* 2013.
- [27] Potter, D. W., Tran, T. B., Rates of ethyl acrylate binding to glutathione and protein. *Toxicol Lett* 1992, *62*, 275-285.
- [28] Csanady, G. A., Filser, J. G., A physiological toxicokinetic model for inhaled propylene oxide in rat and human with special emphasis on the nose. *Toxicological sciences : an official journal of the Society of Toxicology* 2007, *95*, 37-62.
- [29] Johanson, G., Filser, J. G., A physiologically based pharmacokinetic model for butadiene and its metabolite butadiene monoxide in rat and mouse and its significance for risk extrapolation. *Arch Toxicol* 1993, *67*, 151-163.
- [30] Brown, R. P., Delp, M. D., Lindstedt, S. L., Rhomberg, L. R., Beliles, R. P., Physiological parameter values for physiologically based pharmacokinetic models. *Toxicol Ind Health* 1997, *13*, 407-484.
- [31] DeJongh, J., Verhaar, H. J., Hermens, J. L., A quantitative property-property relationship (QPPR) approach to estimate in vitro tissue-blood partition coefficients of organic chemicals in rats and humans. *Arch Toxicol* 1997, *72*, 17-25.
- [32] Kirman, C. R., Gargas, M. L., Deskin, R., Tonner-Navarro, L., Andersen, M. E., A physiologically based pharmacokinetic model for acrylamide and its metabolite, glycidamide, in the rat. *Journal of toxicology and environmental health. Part A* 2003, *66*, 253-274.
- [33] van de Kerkhof, E. G., de Graaf, I. A., Groothuis, G. M., In vitro methods to study intestinal drug metabolism. *Current drug metabolism* 2007, *8*, 658-675.
- [34] Punt, A., Paini, A., Boersma, M. G., Freidig, A. P., *et al.*, Use of physiologically based biokinetic (PBK) modeling to study estragole bioactivation and detoxification in humans as compared with male rats. *Toxicological sciences : an official journal of the Society of Toxicology* 2009, *110*, 255-269.
- [35] Schuler, D., Eder, E., Detection of 1,*N*²-propanodeoxyguanosine adducts of 2-hexenal in organs of Fischer 344 rats by a ³²P-post-labeling technique. *Carcinogenesis* 1999, *20*, 1345-1350.
- [36] Jeffrey, P., Burrows, M., Bye, A., Does the Rat Have an Empty Stomach after an Overnight Fast. *Lab Anim* 1987, *21*, 330-334.
- [37] Sweeney, L. M., Kirman, C. R., Gargas, M. L., Carson, M. L., Tardiff, R. G., Development of a physiologically-based toxicokinetic model of acrylamide and glycidamide in rats and humans. *Food Chem Toxicol* 2010, *48*, 668-685.
- [38] Assimakopoulos, S. F., Thomopoulos, K. C., Patsoukis, N., Georgiou, C. D., *et al.*, Evidence for intestinal oxidative stress in patients with obstructive jaundice. *Eur J Clin Invest* 2006, *36*, 181-187.
- [39] Potter, D. W., Tran, T. B., Apparent rates of glutathione turnover in rat tissues. *Toxicol Appl Pharmacol* 1993, *120*, 186-192.
- [40] Sapienza, P. P., Ikeda, G. J., Warr, P. I., Plummer, S. L., *et al.*, Tissue distribution and excretion of ¹⁴C-labelled cinnamic aldehyde following single and multiple oral administration in male Fischer 344 rats. *Food Chem Toxicol* 1993, *31*, 253-261.
- [41] Yuan, J. H., Dieter, M. P., Bucher, J. R., Jameson, C. W., Toxicokinetics of cinnamaldehyde in F344 rats. *Food Chem Toxicol* 1992, *30*, 997-1004.
- [42] Zhao, H., Xie, Y. H., Yang, Q., Cao, Y., *et al.*, Pharmacokinetic study of cinnamaldehyde in rats by GC-MS after oral and intravenous administration. *J Pharmaceut Biomed* 2014, *89*, 150-157.
- [43] Cocchiara, J., Letizia, C. S., Lalko, J., Lapczynski, A., Api, A. M., Fragrance material review on cinnamaldehyde. *Food Chem Toxicol* 2005, *43*, 867-923.
- [44] Guth, S., Habermeyer, M., Baum, M., Steinberg, P., *et al.*, Thermally induced process-related contaminants: The example of acrolein and the comparison with acrylamide: Opinion of the Senate Commission on Food Safety (SKLM) of the German Research Foundation (DFG). *Molecular nutrition & food research* 2013.
- [45] Frederick, C. B., Potter, D. W., Chang-Mateu, M. I., Andersen, M. E., A physiologically based pharmacokinetic and pharmacodynamic model to describe the oral dosing of rats with ethyl acrylate

and its implications for risk assessment. *Toxicol Appl Pharmacol* 1992, *114*, 246-260.

[46] Yuan, J., Bucher, J. R., Goehl, T. J., Dieter, M. P., Jameson, C. W., Quantitation of cinnamaldehyde and cinnamic acid in blood by HPLC. *Journal of analytical toxicology* 1992, *16*, 359-362.

[47] Nath, R. G., Chung, F. L., Detection of exocyclic 1,*N*²-propanodeoxyguanosine adducts as common DNA lesions in rodents and humans. *Proceedings of the National Academy of Sciences of the United States of America* 1994, *91*, 7491-7495.

[48] Chaudhary, A. K., Nokubo, M., Reddy, G. R., Yeola, S. N., *et al.*, Detection of endogenous malondialdehyde-deoxyguanosine adducts in human liver. *Science* 1994, *265*, 1580-1582.

[49] EFSA, Flavouring Group Evaluation 214: alpha,beta-Unsaturated aldehydes and precursors from chemical subgroup 3.1 of FGE.19: Cinnamyl derivatives¹, Scientific Opinion of the Panel on Food Contact Materials, Enzymes, Flavourings and Processing Aids (CEF). 2009.

SUPPORTING INFORMATION

Cinnamaldehyde PBK/D model equations

(1) Uptake from GI cavity

The uptake of cinnamaldehyde from the intestinal cavity into the small intestine compartment was described by a first-order process as follows:

$$\begin{aligned} dAGI/dt &= -K_a * AGI \\ \text{InitAGI} &= \text{DOSE} \end{aligned}$$

where

AGI	Amount of cinnamaldehyde remaining in GI cavity (μmol)
K_a	Linear uptake rate (/h)
DOSE	Amount of cinnamaldehyde administered in a rat (μmol)

(2) Slowly perfused tissue, richly perfused tissue and fat

Amount cinnamaldehyde in slowly perfused tissue, richly perfused tissue or fat compartment was described as follows:

$$\begin{aligned} dAT_i/dt &= QT_i * (CA - CVT_i) \\ CT_i &= AT_i / VT_i \\ CVT_i &= CT_i / PT_i \end{aligned}$$

where

AT_i	Amount of cinnamaldehyde in a tissue (μmol)
QT_i	Blood flow into a tissue (L/h)
CA	Concentration of cinnamaldehyde in arterial blood perfusing a tissue ($\mu\text{mol/L}$)
CVT_i	Concentration of cinnamaldehyde in venous blood leaving a tissue ($\mu\text{mol/L}$)
CT_i	Concentration of cinnamaldehyde in a tissue ($\mu\text{mol/kg}$)
VT_i	Volume of a tissue (kg)
PT_i	Tissue/blood partition coefficient of cinnamaldehyde

(3) Liver

Amount cinnamaldehyde in the liver (AL, μmol) is described as follows:

$$\begin{aligned} dAL/dt &= QL * CA + QSi * CVSi - (QL + QSi) * CVL - (\text{eq.1} + \text{eq.2} + \text{eq.3} + \text{eq.4} + \text{eq.5} + \text{eq.6}) + \text{eq.14} \\ CL &= AL / VL \\ CVL &= CL / PL \end{aligned}$$

where

QL	Blood flow into the liver (L/h)
QSi	Blood flow into the small intestine (L/h)
CVSi	Concentration of cinnamaldehyde in venous blood leaving the small intestine ($\mu\text{mol/L}$)
CVL	Concentration of cinnamaldehyde in venous blood leaving the liver ($\mu\text{mol/L}$)
CL	Concentration of cinnamaldehyde in the liver ($\mu\text{mol/L}$)
PALDL	Liver/blood partition coefficient of cinnamaldehyde

Amount cinnamaldehyde oxidized to carboxylic acid enzymatically in the liver (AMLCA, μmol) is described to follow Michaelis-Menten equation:

$$dAMLCA/dt = V_{S_{\max, L_{CA}}} * CVL / (K_{m, L_{CA}} + CVL) \quad \text{----- eq. 1}$$

where

$V_{S_{\max, L_{CA}}}$	Scaled V_{\max} for enzymatic oxidation of cinnamaldehyde in the liver ($\mu\text{mol/h}$)
$K_{m, L_{CA}}$	K_m for enzymatic oxidation of cinnamaldehyde in the liver (μM)

Amount cinnamaldehyde reduced to cinnamyl alcohol in the liver (AMLAO, μmol) is described to follow Michaelis-Menten equation:

$$dAMLAO/dt = V_{S_{\max, L_{AO}}} * CVL / (K_{m, L_{AO}} + CVL) \quad \text{----- eq. 2}$$

where

$V_{S_{max,L_{AO}}}$ Scaled V_{max} for enzymatic reduction of cinnamaldehyde in the liver ($\mu\text{mol/h}$)
 $K_{m,L_{AO}}$ K_m for enzymatic reduction of cinnamaldehyde in the liver (μM)

Amount cinnamaldehyde metabolized in liver to GSH conjugation by GSTs ($\text{AMLAG}_{\text{GST}}$, μmol) is described by a two substrate ping-pong model:

$$\frac{d\text{AMLHG}_{\text{GST}}}{dt} = \frac{V_{S_{max,L_{GST}}} * \text{CVL} * \text{CLcGSH}}{(K_{m,L_{GST_G}} * \text{CVL} + K_{m,L_{GST}} * \text{CLcGSH} + \text{CLcGSH} * \text{CVL})} \quad \text{----- eq.3}$$

where

$V_{S_{max,L_{GST}}}$ Scaled V_{max} for enzymatic conjugation of cinnamaldehyde in the liver ($\mu\text{mol/h}$)
 CLcGSH Concentration of GSH in the liver cytosol ($\mu\text{mol/kg}$)
 $K_{m,L_{GST}}$ K_m toward cinnamaldehyde for enzymatic conjugation of cinnamaldehyde in the liver (μM)
 $K_{m,L_{GST_G}}$ K_m toward GSH for enzymatic conjugation of cinnamaldehyde in the liver (μM)

Amount cinnamaldehyde chemically bound in liver to GSH ($\text{AMLAG}_{\text{chem}}$, μmol) is described as following:
 $\frac{d\text{AMLAG}_{\text{chem}}}{dt} = k_{\text{GSH}} * \text{CVL} * \text{CGSH}_{\text{LC}} * \text{VL} \quad \text{----- eq.4}$

where

k_{GSH} Second order rate constant of cinnamaldehyde binding to GSH ($/\mu\text{mol/h}$)
 VL Volume of the liver (kg)

Amount cinnamaldehyde protein adducts in liver (AMLAP , μmol) is described as following:

$$\frac{d\text{AMLAP}}{dt} = k_{\text{GSH}} * \text{CVL} * \text{CPROL} * \text{VL} \quad \text{----- eq.5}$$

where

CPROL Concentration of protein reaction sites in the liver ($\mu\text{mol/kg liver}$)

The formation of DNA adduct in the liver ($\text{AMLDA}_{\text{form}}$) was described as following:

$$\frac{d\text{AMLDA}_{\text{form}}}{dt} = k_{\text{DNA}} * \text{CVL} * \text{CdGL} * \text{VL} \quad \text{----- eq.6}$$

where

k_{DNA} Second order rate constant of aldehyde binding to 2'-dG ($/\mu\text{mol/h}$)
 CdGL Concentration of 2'-dG in the liver ($\mu\text{mol/kg liver}$)

CdGL was calculated to be 1.36 $\mu\text{mol/kg liver}$ using the average molecular weight of nucleotides (330 g/mol) and reported concentration of DNA in a rat liver (1.8 g/kg liver).

Amount of DNA adduct in liver (AMLDA , μmol) is described by subtracting elimination of DNA adduct from the formation:

$$\frac{d\text{AMLDA}}{dt} = \text{eq.6} - \text{AMLDA} * (\ln 2 / T_{1/2})$$

where

$T_{1/2}$ Half-life of DNA adduct in the liver (h)

Amount of GSH present in the liver cytosol (AMGSH_{LC} , μmol) is described by zero-order synthesis and reduction by first-order elimination due to turnover and depletion by aldehyde:

$$\begin{aligned} \frac{d\text{AMGSH}_{\text{LC}}}{dt} &= \text{GSYN}_{\text{L}} * \text{VL} * 0.9 - (\text{eq.3} + \text{eq.4} + k_{\text{L_GLOS}} * \text{AMGSH}_{\text{LC}}) \quad \text{----- eq.7} \\ \text{Init AMGSH}_{\text{LC}} &= \text{InitGSH}_{\text{L}} * \text{VL} * 0.9 \\ \text{CGSH}_{\text{LC}} &= \text{AMLcGSH} / \text{VL} \end{aligned}$$

where

GSYN_{L} Rate of GSH synthesis in the liver ($\mu\text{mol/h}$)
 $k_{\text{L_GLOS}}$ First-order rate of GSH turnover in the liver ($/\text{h}$)
 $\text{InitGSH}_{\text{L}}$ Initial concentration of GSH in the liver ($\mu\text{mol/kg liver}$)

When eq.7 gave negative values, the value zero was used as the amount of GSH in the liver cytosol.

(4) Small intestine

The amount cinnamaldehyde in small intestine tissue, (ASi , μmol) is described as follows:

$$\begin{aligned} \frac{d\text{ASi}}{dt} &= \text{QSi} * (\text{CA} - \text{CVSi}) + \text{Ka} * \text{AGI} - (\text{eq.8} + \text{eq.9} + \text{eq.10} + \text{eq.11} + \text{eq.12}) + \text{eq.15} \\ \text{CSi} &= \text{ASi} / \text{VSi} \\ \text{CVSi} &= \text{CSi} / \text{PSi} \end{aligned}$$

where

CSi	Concentration of cinnamaldehyde in the small intestine ($\mu\text{mol/L}$)
VSi	Volume of the small intestine (kg)
PSi	Small intestine/blood partition coefficient of cinnamaldehyde

Amount cinnamaldehyde enzymatically oxidized carboxylic acid (AMSiCA, μmol) in the small intestine is described by Michaelis-Menten equation:

$$d\text{AMSiCA}/dt = V_{s_{\max, \text{Si}_{\text{CA}}}} * \text{CVSi} / (K_{m, \text{Si}_{\text{CA}}} + \text{CVSi}) \quad \text{----- eq. 8}$$

where

$V_{s_{\max, \text{Si}_{\text{CA}}}}$	Scaled V_{\max} for enzymatic oxidation of cinnamaldehyde in the small intestine ($\mu\text{mol/h}$)
$K_{m, \text{Si}_{\text{CA}}}$	K_m for enzymatic oxidation of cinnamaldehyde in small intestine (μM)

Amount cinnamaldehyde reduced to cinnamyl alcohol in the small intestine (AMSiAO, μmol) is described to follow Michaelis-Menten-equation:

$$d\text{AMSiAO}/dt = V_{s_{\max, \text{Si}_{\text{AO}}}} * \text{CVSi} / (K_{m, \text{Si}_{\text{AO}}} + \text{CVSi}) \quad \text{----- eq. 9}$$

where

$V_{s_{\max, \text{Si}_{\text{AO}}}}$	Scaled V_{\max} for enzymatic reduction of cinnamaldehyde in the small intestine ($\mu\text{mol/h}$)
$K_{m, \text{Si}_{\text{AO}}}$	K_m for enzymatic reduction of cinnamaldehyde in the small intestine (μM)

Amount cinnamaldehyde metabolized in small intestine to GSH conjugation by GSTs (AMSiAG_{GST}, μmol) is described by a two substrate ping-pong model:

$$d\text{AMSiHG}_{\text{GST}}/dt = \frac{V_{s_{\max, \text{Si}_{\text{GST}}}} * \text{CVSi} * \text{CSicGSH}}{(K_{m, \text{Si}_{\text{GST}_G}} * \text{CVSi} + K_{m, \text{Si}_{\text{GST}}} * \text{CSicGSH} + \text{CSicGSH} * \text{CVSi})} \quad \text{----- eq. 10}$$

where

$V_{s_{\max, \text{Si}_{\text{GST}}}}$	Scaled V_{\max} for enzymatic conjugation of cinnamaldehyde in the small intestine ($\mu\text{mol/h}$)
CSicGSH	Concentration of GSH in the small intestine cytosol ($\mu\text{mol/kg}$)
$K_{m, \text{Si}_{\text{GST}}}$	K_m toward cinnamaldehyde for enzymatic conjugation of cinnamaldehyde in the small intestine (μM)
$K_{m, \text{Si}_{\text{GST}_G}}$	K_m toward GSH for enzymatic conjugation of cinnamaldehyde in the small intestine (μM)

Amount cinnamaldehyde chemically bound in small intestine to GSH (AMSiAG_{chem}, μmol) is described as following:

$$d\text{AMLAG}_{\text{chem}}/dt = k_{\text{GSH}} * \text{CVSi} * \text{CGSH}_{\text{SiC}} * \text{VSi} \quad \text{----- eq. 11}$$

where

k_{GSH}	Second order rate constant of aldehyde binding to GSH ($1/\mu\text{mol/h}$)
VSi	Volume of the small intestine (kg)

Amount cinnamaldehyde protein adducts in small intestine (AMSiAP, μmol) is described as following:

$$d\text{AMSiAP}/dt = k_{\text{GSH}} * \text{CSiL} * \text{CPRO}_{\text{Si}} * \text{VSi} \quad \text{----- eq. 12}$$

where

C_{PRO_{Si}} Concentration of protein reaction sites in the small intestine ($\mu\text{mol/kg}$ liver)

Amount of GSH present in small intestine cytosol (AMGSH_{SiC}, μmol) is described in the same way as in the liver:

$$\begin{aligned} d\text{AMGSH}_{\text{SiC}} &= \text{GSYN}_{\text{Si}} * \text{VSi} * 0.9 - (\text{eq. 10} + \text{eq. 11} + k_{\text{GLOS}_{\text{Si}}} * \text{AMGSH}_{\text{SiC}}) \quad \text{----- eq. 13} \\ \text{Init AMGSH}_{\text{SiC}} &= \text{InitGSH}_{\text{Si}} * \text{VSi} * 0.9 \\ \text{CGSH}_{\text{SiC}} &= \text{AMSicGSH} / \text{VSi} \end{aligned}$$

where

GSYN _{Si}	Rate of GSH synthesis in small intestine ($\mu\text{mol/h}$)
$k_{\text{GLOS}_{\text{Si}}}$	First-order rate of GSH turnover in small intestine (/h)
InitGSH _{Si}	Initial concentration of GSH in small intestine ($\mu\text{mol/kg}$ small intestine)

As was the case in the liver, the value zero was used as the amount of GSH in the small intestine cytosol when eq.13 gave negative values.

(5) Venous blood and arterial blood

Concentration of cinnamaldehyde in venous blood (CV) and in arterial blood (CA, both in $\mu\text{mol/L}$) was described as follows:

$$\begin{aligned} dAV/dt &= QF*CVF + (QL+QSi)*CVL + QR*CVR + QS*CVS - QC*CV \\ CV &= AV/(VA+VV) \\ CV &= CA \end{aligned}$$

where

AV	Amount of cinnamaldehyde in venous blood (μmol)
QF	Blood flow into fat (L/h)
CVF	Concentration of cinnamaldehyde in venous blood leaving fat ($\mu\text{mol/L}$)
QR	Blood flow into richly perfused tissue (L/h)
CVR	Concentration of cinnamaldehyde in venous blood leaving richly perfused tissue ($\mu\text{mol/L}$)
QS	Blood flow into slowly perfused tissue (L/h)
CVS	Concentration of aldehyde in venous blood leaving slowly perfused tissue ($\mu\text{mol/L}$)

Cinnamyl alcohol PBK/D submodel equations

(1) Slowly perfused tissue, richly perfused tissue and fat

Amount cinnamyl alcohol in slowly perfused tissue, richly perfused tissue or fat compartment was described as follows:

$$\begin{aligned} dAohTi/dt &= QT_i*(CohA-CVohTi) \\ CohTi &= AohTi/VT_i \\ CohVT_i &= CohTi/PohTi \end{aligned}$$

where

AohTi	Amount of cinnamyl alcohol in a tissue (μmol)
CohA	Concentration of cinnamyl alcohol in arterial blood perfusing a tissue ($\mu\text{mol/L}$)
CohVTi	Concentration of cinnamyl alcohol in venous blood leaving a tissue ($\mu\text{mol/L}$)
CohTi	Concentration of cinnamyl alcohol in a tissue ($\mu\text{mol/kg}$)
PohTi	Tissue/blood partition coefficient of cinnamyl alcohol

(3) Liver

Amount cinnamyl alcohol in the liver (AohL, μmol) is described as follows:

$$\begin{aligned} dAohL/dt &= QL*CohA + QSi*CohVSi - (QL+QSi)*CohVL + eq.2 - eq.14 \\ CohL &= AohL/VL \\ CohVL &= CohL/PohL \end{aligned}$$

where

QL	Blood flow into the liver (L/h)
QSi	Blood flow into the small intestine (L/h)
CohVSi	Concentration of cinnamyl alcohol in venous blood leaving the small intestine ($\mu\text{mol/L}$)
CohVL	Concentration of cinnamyl alcohol in venous blood leaving the liver ($\mu\text{mol/L}$)
CohL	Concentration of cinnamyl alcohol in the liver ($\mu\text{mol/L}$)
PohL	Liver/blood partition coefficient of cinnamyl alcohol

Amount cinnamyl alcohol oxidized to cinnamaldehyde enzymatically in the liver (AohMLCA, μmol) is described to follow Michaelis-Menten equation:

$$dAohMLCA/dt = V_{s_{max, L_OH}} * CVL / (K_{m, L_OH} + CVL) \quad \text{----- eq. 14}$$

where

$V_{s_{max, L_OH}}$	Scaled V_{max} for enzymatic oxidation of cinnamyl alcohol in the liver ($\mu\text{mol/h}$)
K_{m, L_OH}	K_m for enzymatic oxidation of cinnamyl alcohol in the liver (μM)

(4) Small intestine

Amount cinnamyl alcohol in small intestine tissue, (AohSi, μmol) is described as follows:

$$\begin{aligned} dAohSi/dt &= QSi*(CohA -CohVSi) + eq.9 - eq.15 \\ CohSi &= AohSi/VSi \end{aligned}$$

Chapter 5

$$\text{CohVSi} = \text{CohSi}/\text{PohSi}$$

where

CohSi Concentration of cinnamyl alcohol in the small intestine ($\mu\text{mol/L}$)
 PohSi Small intestine/blood partition coefficient of cinnamyl alcohol

Amount cinnamyl alcohol enzymatically oxidized to cinnamaldehyde (AohMSiCA, μmol) in the small intestine is described by Michaelis-Menten equation:

$$d\text{AohMSiCA}/dt = V_{s_{\text{max,Si_OH}}} * \text{CohVSi} / (K_{m,\text{Si_OH}} + \text{CohVSi}) \quad \text{----- eq.15}$$

where

$V_{s_{\text{max,Si_OH}}}$ Scaled V_{max} for enzymatic oxidation of cinnamyl alcohol in the small intestine ($\mu\text{mol/h}$)
 $K_{m,\text{Si_OH}}$ K_m for enzymatic oxidation of cinnamyl alcohol in the small intestine (μM)

(5) Venous blood and arterial blood

Concentration of cinnamyl alcohol in venous blood (CohV) and in arterial blood (CohA, both in $\mu\text{mol/L}$) was described as follows:

$$d\text{AohV}/dt = QF * \text{CohVF} + (QL + Q\text{Si}) * \text{CohVL} + QR * \text{CohVR} + QS * \text{CohVS} - QC * \text{CohV}$$

$$\text{CohV} = \text{AohV} / (VA + VV)$$

$$\text{CohV} = \text{CohA}$$

where

AohV Amount of cinnamyl alcohol in venous blood (μmol)
 CohVF Concentration of cinnamyl alcohol in venous blood leaving fat ($\mu\text{mol/L}$)
 CohVR Concentration of cinnamyl alcohol in venous blood leaving richly perfused tissue ($\mu\text{mol/L}$)
 CohVS Concentration of cinnamyl alcohol in venous blood leaving slowly perfused tissue ($\mu\text{mol/L}$)



CHAPTER 6

General Discussion and Future Perspectives

This thesis aimed at examining dose-dependent detoxification and DNA adduct formation of DNA reactive α,β -unsaturated aldehydes using physiologically based in silico modelling, in order to safety assessment of these aldehydes used as food flavouring agents. In this chapter, the results of the thesis will be first summarized, followed by a general discussion including future perspectives for important aspects raised in the course of study. At the end of this chapter, an overall conclusion will be provided.

6.1 Summary of the results

α,β -Unsaturated aldehydes are widely distributed in the environment, and the diet is one of the major exposure routes for humans. Various α,β -unsaturated aldehydes are present in fruits, vegetables, spices, or processed products containing these items as natural constituents [1]. Many of the aldehydes have a unique odour representing the smell of the commodities, and for this reason the aldehydes are often used as added food flavouring agents. Because of the α,β -unsaturated aldehyde moiety the β carbon in the molecule becomes electron deficient and the aldehydes react with electron rich molecules including DNA via Michael addition [2]. The formation of DNA adducts raises a concern for genotoxicity, while the formation of DNA adducts may not be significant at low doses relevant for dietary exposure in vivo because of adequate detoxification. The thesis therefore aimed at determining dose-dependent detoxification and DNA adduct formation of food-borne α,β -unsaturated aldehydes by using a physiologically based in silico modelling approach in order to contribute to the safety assessment of these aldehydes used as food flavourings.

Physiologically based kinetic/dynamic (PBK/D) models were developed to simulate ADME (absorption, distribution, metabolism and excretion)(i.e. kinetics) as well as DNA adduct formation by the aldehydes (i.e. dynamics). In **Chapter 2 and 3**, rat and human PBK/D models were developed for the compound *trans*-2-hexenal, a model dietary α,β -unsaturated aldehyde used to investigate dose-dependent detoxification and DNA adduct formation, and to examine interspecies differences. The kinetic parameters for detoxification were collected by performing in vitro incubations using relevant rat or human tissue fractions. The PBK/D models revealed that at the estimated daily intake (EDI) i.e. 0.04 mg/kg bw, *trans*-2-hexenal is detoxified predominantly via GST-mediated conjugation with GSH in rat, while the reduction to 2-hexen-1-ol was the major pathway in human. Despite this interspecies difference in the detoxification, interspecies differences in the maximum DNA adduct levels in the liver were predicted to be limited. At the EDI, DNA adduct formation was predicted to be 0.01 adducts/ 10^8 nt in rat and 0.008 adducts/ 10^8 nt in human. These levels were 3 orders of magnitude lower than the natural background levels of structurally similar exocyclic 1, N^2 -propanodeoxyguanosine adducts present in disease free human liver (i.e. 6.8–110 adducts/ 10^8 nt) [3, 4].

The human PBK/D model was subsequently used to examine the impact of interindividual variation in *trans*-2-hexenal detoxification on DNA adduct formation in a human population. The parameters for detoxification were measured for 11 individuals to define the variation in aldehyde oxidation, reduction and conjugation with GSH and subsequently to simulate the distribution of DNA adduct formation in the population as a whole by performing Monte Carlo simulations. At the EDI, the maximum amount of DNA adducts in the liver was predicted to be 0.007 adducts/ 10^8 nt for the 50th percentile and 0.039 adducts/ 10^8 nt for the most sensitive persons (the 99th percentile). At a high intake level of 0.178 mg/kg bw (the 95th percentile of the dietary intake), DNA adduct formation was predicted to be 0.18 adducts/ 10^8 nt for the 99th percentile. These values were all well below the natural background levels of structurally similar exocyclic 1,N²-propanodeoxyguanosine adducts present in disease free human liver (i.e. 6.8–110 adducts/ 10^8 nt) [3, 4]. Based on these results, it was concluded that *trans*-2-hexenal in the diet may not significantly increase the DNA adduct levels in the liver compared to the background in both rats and humans including the most sensitive persons.

The objective of **Chapter 4** was to extend the rat PBK/D model developed for *trans*-2-hexenal to other α,β -unsaturated aldehydes that may be used as food flavourings, to examine DNA adduct formation at low doses relevant for human dietary exposure and to facilitate group evaluation. Considering the large number of the aldehydes of interest, the efficiency to collect chemical specific detoxification parameters was increased by applying a QSAR (quantitative structure-activity relationship) approach. Eighteen acyclic α,β -unsaturated aldehyde flavouring agents without 2- or 3-alkylation, and with no more than one conjugated double bond were selected as model compounds. Six of these 18 aldehydes were selected as the training set to define QSAR models to estimate kinetic parameters for detoxification of the other 12 aldehydes in the test set. Among the 18 aldehydes, 2-propenal (acrolein) was predicted to induce the highest number of DNA adducts in rat liver due to the lowest efficiency for oxidation and conjugation with GSH. The maximum DNA adduct formation by the 18 aldehydes was between 10^{-10} – 10^{-2} adducts/ 10^8 nt at their respective EDI as food flavourings. These levels are at least two orders of magnitude lower than the natural background levels of structurally similar DNA adducts (i.e. 6.8–110 adducts/ 10^8 nt). Based on these outcomes it was concluded that the DNA adduct formation by all 18 aldehydes when used as flavourings is negligible.

Unlike many α,β -unsaturated aldehydes for which in vivo data on genotoxicity and carcinogenicity are absent, cinnamaldehyde has been tested not to be genotoxic or carcinogenic in vivo [5]. The aim of **Chapter 5** was to examine DNA adduct formation by cinnamaldehyde using physiologically based kinetic/dynamic (PBK/D) modelling, and to compare these DNA adduct levels to those predicted for the 18 other food-borne α,β -unsaturated aldehydes in Chapter 4 for read-across. The cinnamaldehyde PBK/D models were developed based on kinetic parameters obtained by performing in vitro incubations with relevant tissue fractions. The model performance was evaluated, revealing that the kinetics of cinnamaldehyde such as time-dependent

cinnamaldehyde blood concentrations observed in vivo [6, 7] were overall adequately predicted. The PBK/D models revealed DNA adduct formation due to oral exposure to cinnamaldehyde in human to be lower than in rat because of efficient oxidation. In rats, cinnamaldehyde was shown to induce higher DNA adducts per exposure dose than 6 out of the 18 food borne acyclic α,β -unsaturated aldehydes, indicating these 6 aldehydes may also test negative for genotoxicity and carcinogenicity at high dose levels. At the highest cinnamaldehyde dose that was tested negative for carcinogenicity in vivo and tested negative, the model predicted formation of 79 DNA adducts/ 10^8 nt in rat. This value is at least three orders of magnitude higher than the PBK/D model based predictions of DNA adduct formation by the 18 other food-borne aldehydes at their respective EDI. These results corroborate the conclusion obtained in Chapter 4 that for all these 18 α,β -unsaturated aldehydes DNA adduct formation at doses relevant for human dietary exposure does not raise a safety concern. This chapter furthermore illustrates that physiologically based in silico modelling facilitates a science-based comparison and read-across on the possible risks posed by food-borne DNA reactive agents.

6.2 General discussion and future perspective

The results of the present thesis can be discussed in a wider perspective also focussing on what would be topics of interest to include and consider in future studies. The topics that are relevant to discuss in some more detail in this respect include:

- performance and need for further refinement of the PBK/D models,
- aldehyde toxicity and DNA adduct formation in the gastrointestinal (GI) tract,
- application of the integrated QSAR-PBK/D modelling to a wider range of α,β -unsaturated aldehydes,
- implication of the results obtained in this thesis for safety assessment, and
- future possibilities of PBK/D modelling for genotoxic agents in general.

Performance and need for further refinement of the PBK/D models

In order to draw conclusions that are relevant for in vivo situation from PBK/D model outcomes, it is important to ensure that the PBK/D models adequately simulate the behaviour of the compounds of interest in vivo. For this reason evaluation of a PBK/D model by comparing predictions with in vivo data is a crucial step in the model development to determine whether major determinants and/or process that are essential for describing the system behaviour have been adequately identified and characterized [8]. In this section the overview of the PBK/D model performance developed in this thesis is presented, as well as discussions on uncertainties that may have been present in the PBK/D models developed in this thesis.

The performance of the rat PBK/D models was evaluated by comparing the predictions on DNA adduct formation with in vivo data in Chapter 2 and 4. The predicted values for

trans-2-hexenal matched well with the data reported by Schuler and Eder [9], with a maximum difference of 4-fold. The overestimation in the DNA adduct formation was remarkable when the predictions were compared with the data reported by Stout et al [10]: the maximum difference reached 9,717-fold in Chapter 4. DNA adduct formation was overestimated up to 947-fold also for 2-butenal (crotonaldehyde) in Chapter 4 compared to the data reported by Budiawan and Eder [11]. The overestimation in the DNA adduct levels compared to certain *in vivo* studies [11, 12] may be attributed to the feeding status of the animals used in the *in vivo* studies. The assumption of the PBK/D models was the complete absorption of administered aldehyde at once. The rats used in the study by Stout et al. [12] were not fasted before the dosing, indicating that a part of the aldehydes may have reacted with thiol or other reactive protein residues of the food matrix thus being excreted in faeces without being absorbed. The binding of α,β -unsaturated aldehydes with food residues present in the GI lumen is supported by the fact that 15 to 28% of acrolein was excreted in faeces in Sprague-Dawley rats upon oral exposure to 2.5 to 15 mg acrolein/kg bw [13]. It should be furthermore noted that a part of the aldehydes may not have been absorbed due to severe damage to the mucosal tissue of the GI tract caused by extremely high concentration of *trans*-2-hexenal or crotonaldehyde reaching their LD₅₀ (780 mg/kg bw for *trans*-2-hexenal and 206 mg/kg bw for 2-butenal) [12].

The performance of the cinnamaldehyde PBK/D model was thoroughly examined in Chapter 5. The predicted time-dependent cinnamaldehyde concentrations in blood were compared with data obtained from rats exposed to cinnamaldehyde via gavage or intravenous (iv) injection. The predicted values were within 10-fold of the *in vivo* data, except for the peak concentrations (C_{max}) that occurred immediately after the dosing. The overestimation in C_{max} was bigger upon oral administration than after iv injection, reaching up to 48-fold and 545-fold compared to the data reported by Yuan et al. [6] and Zhao et al. [7] respectively. The tendency to overestimate the C_{max} especially upon oral exposure implies that the description of cinnamaldehyde oral administration could be improved. This may be done taking some of the following considerations into account.

In all the PBK/D models developed in this thesis, the aldehyde uptake in the small intestine was described to follow a first-order reaction:

$$dAGI/dt = -K_a * AGI$$

where AGI is the amount of aldehyde remaining in GI cavity (μmol) and K_a is the first-order rate constant (/h). The value of K_a was set to be 5 (/h) regardless of the aldehyde studied, representing a swift absorption of the compound. In practice, however, the absorption may already occur before the aldehyde reaches the small intestine upon gavage. Frederick et al. [14] developed a PBK model for ethyl acrylate, an α,β -unsaturated ester (Figure 6.1). In this model the absorption is described to occur already in the forestomach, glandular stomach, duodenum and finally in the small intestine assuming gavage administration. The gut lumen was divided into two phases: vehicle (i.e. oil phase) and lumen contents (i.e. aqueous gel of food matter). The ester was

described to be transported from the vehicle to the lumen contents before the absorption to the gut wall. The effect of inclusion of such an oral dosing model on the predicted cinnamaldehyde blood concentrations and subsequent DNA adduct formation can be evaluated by including these equations in the PBK/D model for cinnamaldehyde in rat developed in Chapter 5. The schematic diagram of this oral dosing model is presented in Figure 6.1, and the model equations and the parameters used in the model are attached at the end of this chapter as supplementary information. The parameters to describe the transportations from vehicle to lumen contents (K_{GUT}) and from lumen contents to gut walls (K_{AB}) may vary for each chemical. The parameters defined for ethyl acrylate by Frederick et al. [14] are applied in this chapter to obtain an idea about whether the inclusion of such an oral dosing model could improve the cinnamaldehyde PBK/D model performance.

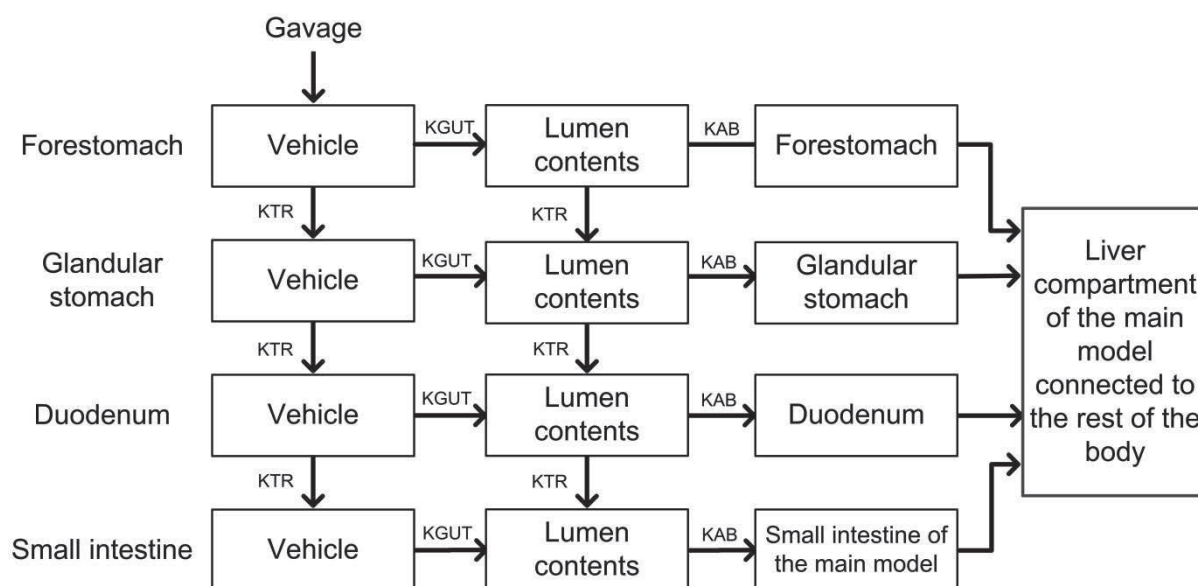


Figure 6.1 The schematic diagram of the oral dosing model derived from Frederick et al. [14]. The arrows represent the movement of an aldehyde.

Figure 6.2 shows the predicted cinnamaldehyde levels in blood upon oral administration of 250 or 500 mg cinnamaldehyde/kg bw in rats. These figures demonstrate that the prediction (solid lines) matches better with the observed data (circles) if the oral dosing model is included. The overestimations in the C_{max} of up to 17-fold and 450-fold compared to the data obtained by Yuan et al. [6] and Zhao et al [7], respectively, were lowered to 6-fold and 48-fold with the inclusion. In addition, the inclusion of the oral dosing model also improved the prediction on T_{max} , the timing when C_{max} occurs. The T_{max} was between 0.3-2.0 hours at 250 mg/kg bw and 2.0-3.9 hours at 500 mg/kg bw in vivo [6, 7]. The predicted T_{max} was 0.01 hour (36 second) after the gavage without the oral dosing model, and the inclusion of the oral dosing model delayed this timing to 0.9 hour at 250 mg/kg bw and 1.3 hour at 500 mg/kg bw. While the inclusion of the oral administration model improves the model performance on cinnamaldehyde kinetics, its influence

on the predictions on DNA adduct formation seems to be limited. The inclusion altered the predicted values for DNA adduct formation by cinnamaldehyde from 0.065 to 0.085 adducts/ 10^8 nt at its EDI and from 79 to 76 adducts/ 10^8 nt at 200 mg/kg bw, indicating the conclusions obtained in Chapter 5, stating that DNA adduct formation by the 18 α,β -unsaturated aldehydes at doses relevant for human dietary exposure does not raise a safety concern, will not be influenced.

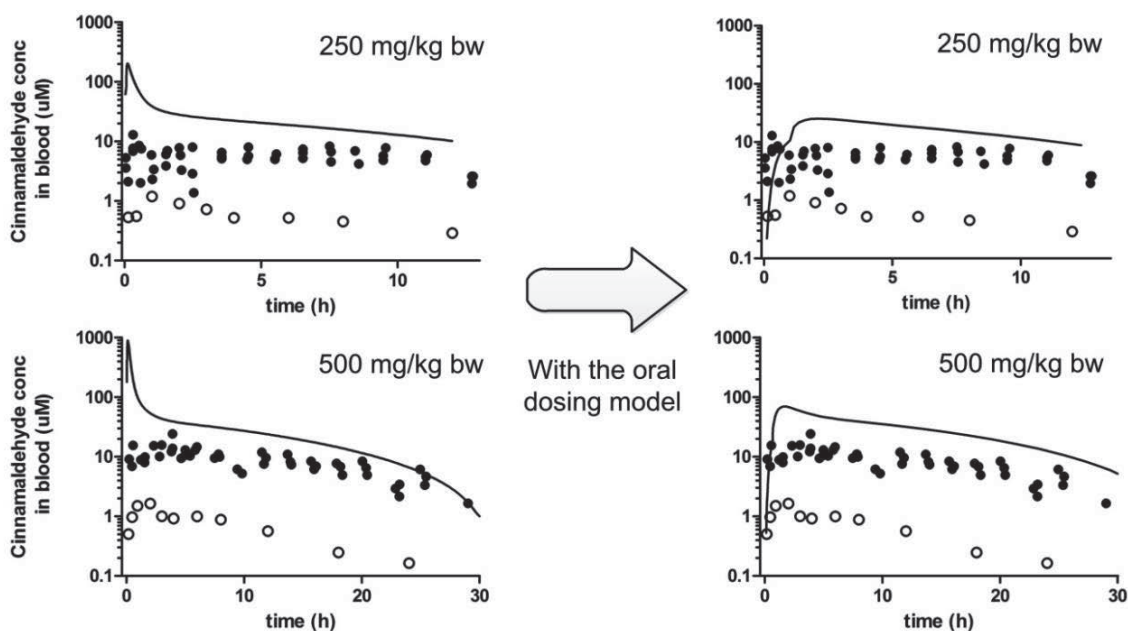


Figure 6.2 Performance of the rat cinnamaldehyde PBK/D model developed in Chapter 5 without (two figures on the left) or with (two figures on the right) the oral dosing model. The solid lines represent the predicted cinnamaldehyde levels in blood in rats upon oral administration of 250 or 500 mg cinnamaldehyde/kg bw. The circles represent the in vivo data reported by Yuan et al. [15] (closed circles) or by Zhao et al. [7] (open circles).

In order to see whether the description of the aldehyde uptake caused the remarkable overestimation in DNA adduct formation by *trans*-2-hexenal or 2-butenal (crotonaldehyde) in Chapter 2 and 4 as described above, the influence of the inclusion of the oral dosing model on DNA adduct level predictions for *trans*-2-hexenal was also examined (Table 6.1). The predicted DNA adduct formation is still 155 and 2,030-fold higher compared to the in vivo data reported by Stout et al. [12] or by Budiawan et al. [11], respectively, while the model performance is further improved deviating only up to 2.6-fold when the DNA adduct levels are compared with the data reported by Schuler and Eder [9]. This further supports that the remarkable overestimation in DNA adduct formation is possibly due to the differences in the experimental design of the three in vivo studies [9, 11, 12] such as the animal fasting status discussed already above.

Altogether, the inclusion of the oral dosing model is recommended where the time-dependent kinetics of the α,β -unsaturated aldehydes are the model outcomes of interest, however, the inclusion may not be necessary to predict DNA adduct formation in the liver because

of the limited influence of the submodel. The oral dosing model, if it would be included, could be refined to a further extent to describe especially the transportation from vehicle to gut contents and the absorption of the chemical of interest in each compartment, which may vary depending on the compound.

Table 6.1 Comparison of the PBK/D model predicted DNA adduct levels with in vivo data.

In vivo reference	Compound	Dose and time of the measurement	Observed values	Predicted values (Prediction/ in vivo data)	
				without the oral dosing model	with the oral dosing model
Budiawan and Eder [11]	2-butenal (crotonaldehyde)	200 or 300 mg/kg bw, 20h	2.9 and 3.4 adducts/10 ⁸ nt	1240 and 3220 adducts/10 ⁸ nt (428 and 946-fold)	437 and 739 adducts/10 ⁸ nt (151 and 217-fold)
Stout et al. [12]	<i>trans</i> -2-hexenal	200 or 500 mg/kg bw, 24 h	0.2 and 0.099 adducts/10 ⁸ nt	94 and 962 adducts/10 ⁸ nt (470 and 9717-fold)	65 and 195 adducts/10 ⁸ nt (325 and 1970-fold)
Schuler and Eder [9]	<i>trans</i> -2-hexenal	200 or 500 mg/kg bw, 48 h	16 and 179 adducts/10 ⁸ nt	61 and 625 adducts/10 ⁸ nt (3.8 and 3.5-fold)	42 and 127 adducts/10 ⁸ nt (2.6 and 0.7-fold)

In addition to uncertainties in the PBK/D model descriptions on the aldehyde absorption, there may be some uncertainties related to the parameters that were incorporated in the models. The half-life of DNA adducts ($T_{1/2}$) that represented the DNA repair efficiency is one of such parameters. In this thesis a half-life of 38.5 hours was applied for all compounds to describe the elimination of DNA adducts due to DNA repair. The value was derived from an in vivo study using male F344 rats [9], where the reduction in DNA adducts of *trans*-2-hexenal in the liver was followed after the dosing. However the elimination kinetics may vary depending on the compound. A shorter half-life of less than 3 hours has been observed for 4-hydroxy-2-nonenal in vitro [16], and moreover DNA repair kinetics may be biphasic consisting of a shorter half-life, reported to be as short as 15 min, which then slows down to a half-life of 48 hours [17, 18]. Such biphasic kinetics in DNA repair or chemical dependent variation in DNA adduct half-lives is not accounted for in this thesis. The parameter for DNA repair for each aldehyde could potentially be derived in vitro by incubating plasmid DNA substrates containing DNA adducts of interest in cell-free extracts of, for instance human cells that possess NER (nucleotide excision repair) mechanism, and by measuring the time-dependent elimination of the DNA adducts [16].

Aldehyde toxicity and DNA adduct formation in the GI tract

With the PBK/D models that were evaluated to be adequate, dose-dependent DNA adduct formation by different food-borne α,β -unsaturated aldehydes was predicted in the liver. The liver was selected as the organ of interest because several in vivo studies have reported DNA adduct formation in this organ [9, 11, 12]. These in vivo data were considered to be more reliable to

evaluate the PBK/D model performance than data in the first contact organs because no corrosion has been observed in liver due to the exposure to the aldehydes [12]. Also, the natural background levels of structurally similar DNA adducts are available for liver [3, 4], which were included in this thesis as reference values for evaluation of the significance of the DNA adduct levels formed by dietary aldehydes.

It should be noted, however, that the concentrations of the aldehydes may be higher in the organs that have a direct contact with the aldehydes following oral intake such as the stomach. In rats, the most pronounced toxicity has been observed in forestomach upon single oral exposure to extremely high doses of aldehydes. Stout et al. [12], for example histologically analysed the toxicity of *trans*-2-hexenal in the first contact organs following single administration of 50, 200 or 500 mg/kg *trans*-2-hexenal by oral gavage. Necrotic lesions accompanied by inflammation were predominant in the forestomach. The damage to the glandular stomach was clearly present but minor compared to the forestomach, and there were no significant lesions observed in the livers. Schuler and Eder [9] measured the DNA adducts formed by *trans*-2-hexenal in different organs using a ^{32}P post-labelling technique. The highest amount was observed in the forestomach, followed by the liver at 200 and 500 mg *trans*-2-hexenal/kg bw. The DNA adduct levels in colon and duodenum were lower than in the liver. These results suggest that in rats upon gavage administration of an extremely high dose of *trans*-2-hexenal reaching its LD₅₀ (780 mg/kg bw for male rats), the toxicity is most pronounced in the forestomach.

Long-term carcinogenicity studies have suggested forestomach or blood cells to be affected in rats by different α,β -unsaturated aldehydes. Occurrence of neoplasms in the forestomach increased due to the aldehyde exposure in a sub-chronic study for 2-propenal (acrolein) [19] and in a 2-year feeding study for *trans,trans*-2,4-hexadienal [20]. In these rodent studies 2-propenal was dissolved in 0.5% methylcellulose and administered by gavage for 14 weeks and *trans,trans*-2,4-hexadienal was dissolved in corn oil and deposited to the forestomach directly using a tube. In both studies an increase in hyperplasia was observed only in the forestomach and not in the glandular stomach or the liver. In 2-year studies for cinnamaldehyde and citral, the aldehydes were microencapsulated and provided in the feed [5, 21]. The microencapsulation was applied in these studies to prevent the spontaneous evaporation or oxidation of the aldehydes. Development of neoplasms was not observed in any of the organs in the study for cinnamaldehyde. Higher numbers of malignant lymphomas were observed in female rats receiving citral, which may have been related to exposure to citral [21]. The inconsistency in the experimental designs of the animal studies on aldehyde administration, such as dosing method (gavage or mixed in feed), form of aldehydes (with or without microencapsulation) and vehicle solution (corn oil, water or methylcellulose), makes the interpretation of the study outcomes problematic. Considering no toxicity was observed in forestomach when cinnamaldehyde and citral were encapsulated and mixed in feed, it may be concluded that the carcinogenicity observed in the forestomach for 2-propenal and *trans,trans*-2,4-hexadienal may have been caused by

extremely high concentrations of aldehyde directly deposited in the first contact organ, the forestomach in case of rats, as the results of local tissue irritation [22] as also pointed out by JECFA in their evaluation report for 2,4-hexadienal [23]. If this is the case, the toxicity observed in the forestomach in such animal studies does not represent the toxicity in humans because exposure of the forestomach is irrelevant for the human exposure situation with respect to exposure levels as well as organ.

Although the forestomach is not a relevant target organ in human, overall GI organs including the stomach and small intestine may be the target for toxicity in human. It is therefore still of interest to examine what DNA adduct levels could be expected in the rat GI tract. In order to investigate the DNA adduct formation in these organs, the theoretical distribution of the aldehydes in the GI tract can be simulated using the oral dosing model described in the previous section. According to the rat *trans*-2-hexenal PBK/D model coupled with the oral dosing model, *trans*-2-hexenal concentrations are the highest in the glandular stomach, followed by in the forestomach, duodenum, small intestine and then in the liver. The AUCs (areas under the curve) obtained from the time-dependent *trans*-2-hexenal concentration change in the GI organs are summarized in Table 6.2. The AUCs in the glandular stomach are in general three orders of magnitude higher than in the liver. At 0.04 mg/kg bw, the EDI of *trans*-2-hexenal, the AUC in the glandular stomach (1.6 $\mu\text{M}\cdot\text{h}$) was 533-fold higher than in the liver (0.003 $\mu\text{M}\cdot\text{h}$). Based on these AUCs, DNA adduct formed in the glandular stomach can be estimated to be 0.53 adduct/ 10^8 nt from the predicted DNA adduct amount in the liver (0.001 adduct/ 10^8 nt) at this level of exposure, assuming a linear relationship between AUC in an organ and DNA adduct levels formed. Assuming the natural background levels of structurally similar DNA adducts in the glandular stomach is the same as in the liver (6.8-110 adducts/ 10^8 nt) [3, 4], the DNA adduct formation in the glandular stomach due to *trans*-2-hexenal in the diet is an order of magnitude lower and therefore may still be negligible. Furthermore, it should be noted that the oral administration model used in this chapter does not include aldehyde metabolism in the forestomach, glandular stomach and duodenum, which may further reduce the aldehyde levels in the GI tract if included. To further determine the aldehyde distribution and DNA adduct formation in the GI tract, it is recommended to obtain parameters to describe metabolism and transportation of specific aldehydes of interest in the GI organst to refine the oral dosing model.

Table 6.2 AUC values ($\mu\text{M}\cdot\text{h}$) of *trans*-2-hexenal predicted by the rat *trans*-2-hexenal PBK/D model coupled with the oral dosing model

Dose (mg/kg bw)	Forestomach	Glandular stomach	Duodenum	Small intestine	Liver
0.04	0.78	1.6	0.07	0.009	0.003
500	4325	16021	1653	583	81

Application of the integrated QSAR-PBK/D modelling to a wider range of α,β -unsaturated aldehydes

This thesis demonstrated that the integrated QSAR-PBK/D modelling approach remarkably accelerated group evaluation of structurally similar aldehydes. In Chapter 4, QSAR models were developed for kinetic parameters based on the experimentally derived kinetic data on 6 compounds to predict the kinetic parameters for 12 other compounds, meaning the time and labour required to collect those chemical specific parameters were reduced to one third to develop PBK/D models for 18 compounds. The PBK/D models were shown to contribute to the safety evaluation of this large group of aldehydes by providing insights in the amount of DNA adducts formed at low doses relevant for dietary exposure, without performing animal experiments. Furthermore, the PBK/D models developed for the 18 aldehydes enabled to rank the compounds depending on their dose-dependent DNA adduct formation. This provides useful information to select aldehydes that represent the worst case within the group. Selecting such representative compounds contributes to a reduction, replacement, and refinement (3R) of animal studies because in vivo studies may not need to be performed for all compounds within a group but only for the worst case analogue to conclude on the safety of the group of structurally similar chemicals. Taking a group evaluation strategy, EFSA selected trans-2-hexenal, 2-octenal and trans-2-cis-6-nonadienal as representatives of the acyclic α,β -unsaturated aldehydes without 2- or 3-alkylation, and with no more than one conjugated double bonds for the further genotoxicity and carcinogenicity testing. The selection was based on chain length, lipophilicity and the results of an unpublished (Q)SAR [24], but the consideration on the detoxification kinetics seems to be lacking in the selection process. The PBK/D modelling approach applied in this thesis indicated that 2-propenal would represent the worst case in the group. This result illustrates the importance to take not only the reactivity with DNA but also overall kinetics of the compounds into account when a group evaluation strategy is applied for DNA reactive compounds.

The structures of dietary α,β -unsaturated aldehydes vary more than the variation between the 18 aldehydes that were examined in this thesis as presented in Table 1.1 in Chapter 1. To reach conclusions on a larger group of compounds than the 18 aldehydes, the integrated QSAR-PBK/D modelling approach is recommended to be applied to other dietary α,β -unsaturated aldehydes that were not examined in this thesis. To this end, an applicability domain first needs to be defined, and a sufficient number of aldehydes should be selected for a training set to develop statistically significant and robust QSAR models to define biochemical parameters such as K_m and V_{max} for the metabolism by performing in vitro experiments [25]. The PBK/D models developed based on QSAR estimated parameters will facilitate to select a compound in a subgroup or a subgroup from the entire group of α,β -unsaturated aldehydes used as food flavourings that represents the worst case analogue, taking crucial information such as detoxification efficiencies, reactivity with DNA and exposure levels into account.

In the following text several molecular descriptors that may be considered to model aldehyde metabolism or reactivity with DNA are discussed, since they provide possible parameters to be used for QSARs in future studies. For the chemical reaction of the aldehydes with DNA or with GSH, the important determinants to be considered are the energy value of the lowest unoccupied molecular orbital (E_{LUMO}) and the LUMO density at the reaction site within the molecule based on the frontier molecular orbital theory [26]. E_{LUMO} parameterizes the ability of an electrophilic compound to accept electrons. A molecule with a low E_{LUMO} value tends to show a high reactivity with electron rich molecules. Increasing LUMO density at the reaction atom makes it easier for the electrophilic site of the molecule, the β carbon in the case of α,β -unsaturated aldehydes, to accept electrons from a donor. The hard and soft acid and base (HSAB) theory has also been used to profile the reactivity of the aldehydes with nucleophilic substances [27]. Based on the HSAB theory, hard electrophiles react with hard nucleophiles i.e. DNA rather than soft nucleophiles i.e. GSH, protein. Hardness of a molecule (η) can be calculated from the energy levels of LUMO and HOMO (highest occupied molecular orbital) ($\eta = [E_{\text{LUMO}} - E_{\text{HOMO}}]/2$). The HSAB parameters are related to the ease with which electron redistribution occurs during the formation of covalent adducts, which in turn, is related to the rate of the adduct forming reaction. The molecular electrophilicity index (ω) is another comprehensive measure of electrophilicity, which is calculated from E_{LUMO} and E_{HOMO} ($\omega = [E_{\text{HOMO}}^2 + 2E_{\text{HOMO}}E_{\text{LUMO}} + E_{\text{LUMO}}^2]/[4(E_{\text{LUMO}} - E_{\text{HOMO}})]$).

The values of these descriptors of some aldehydes are listed in Table 6.3 together with the second-order rate constants with DNA (k_{DNA}) or with GSH (k_{GSH}) when available. The k_{DNA} obtained in in vitro studies decreased in the following order: trans-2-hexenal (1.6×10^{-7} / $\mu\text{M}/\text{h}$, Chapter 1) > 2,4-hexadienal (7.6×10^{-8} / $\mu\text{M}/\text{h}$, MSc thesis of Y. Wulansary) > cinnamaldehyde (1.6×10^{-8} / $\mu\text{M}/\text{h}$, Chapter 5). The order cannot be explained by E_{LUMO} , ω or by η , but may be explained by the higher LUMO density at the β carbon of trans-2-hexenal compared to that of 2,4-hexadienal or cinnamaldehyde. Nevertheless, the number of the compounds is too small to determine what is the most important determinant to quantitatively describe the reactivity of the aldehydes with DNA, but the increased tendency with increased LUMO density on the β carbon suggests that this LUMO density could be one of the important molecular descriptors to be considered when QSARs are made for k_{DNA} . The experimentally derived k_{GSH} decreased in the following order: 2,4-hexadienal (2.3×10^{-3} / $\mu\text{M}/\text{h}$, MSc thesis of Y. Wulansary) > cinnamaldehyde (6.6×10^{-4} / $\mu\text{M}/\text{h}$, Chapter 4) > trans-2-hexenal (5.8×10^{-4} / $\mu\text{M}/\text{h}$, Chapter 1), which could not be explained by any of the parameters listed in Table 6.3. Again the number of compounds to be compared should be increased to draw any conclusions, but it may be already considered that other descriptors than those listed in Table 6.3, such as steric hindrance [28] may be important determinants for aldehyde reactivity with GSH.

Table 6.3 The molecular descriptors of α,β -unsaturated aldehydes from different subgroups.

Compound	Structure	$E_{\text{LUMO}}^{a,b}$ (eV)	LUMO density at C- β^b	$\omega^{b,c}$ (eV)	$H^{b,d}$ (eV)	k_{DNA} (/ $\mu\text{M}/\text{h}$)	k_{GSH} (/ $\mu\text{M}/\text{h}$)
<i>trans</i> -2-hexenal		-0.17	0.40	2.7	5.1	1.6×10^{-7}	5.8×10^{-4}
<i>trans, trans</i> - 2,4-hexadienal		-0.66	0.25	2.9	4.4	7.6×10^{-8}	2.3×10^{-3}
<i>trans, trans</i> - 2-ethyl-2-hexenal		-0.13	0.39	2.6	4.9	NA ^d	NA
<i>trans, trans</i> - -3-ethyl-2-hexenal		-0.13	0.39	2.6	4.9	NA	NA
citral		-0.17	0.39	2.5	4.7	NA	NA
cinnamaldehyde		-0.83	0.20	3.1	4.3	1.6×10^{-8}	6.6×10^{-4}

^aenergy value of LUMO. ^b E_{LUMO} and E_{HOMO} were obtained using MOPAC Interface version 13.0 run on ChemBio 3D Ultra version 13.0.0.3015 (both PerkinElmer, Massachusetts). ^celectrophilicity index. ^dhardness. ^enot available

For enzyme-mediated detoxification of α,β -unsaturated aldehydes, this thesis revealed that within the acyclic α,β -unsaturated aldehydes without 2- or 3-alkylation, and with no more than one conjugated double bond, increasing bulkiness of the molecule decreases K_m of ALDH-mediated oxidation. Also, the increased bulkiness was shown to increase the GST-mediated conjugation efficiencies with GSH. These findings are in agreement with the findings reported in literature. A decrease in K_m was observed with increasing chain length for ALDH-mediated oxidation of 2-alkenals in human cells [29], and an increased specificity constant (k_{cat}/K_m) was reported for mammalian cytosolic GST with increasing hydrophobicity of 4-hydroxy-2-alkenals [30]. More data on a wider variety of α,β -unsaturated aldehydes are required to establish quantitative relationships between the structures and kinetic parameters for metabolism such as V_{max} and K_m .

Implication for safety assessment

For the safety assessment on the use of α,β -unsaturated aldehydes as food flavourings, JECFA applied the TTC (toxicological threshold of concern) approach and the exposure resulting from the level of use as flavouring for each aldehyde [23, 31, 32]. When the exposure level of an aldehyde was above the TTC, which was the case for cinnamaldehyde, in vivo carcinogenicity test results were examined [32] to conclude on its safety in use. The Expert Panel of FEMA has

referred to the low amount of use of the aldehydes as food flavouring agents when affirming their GRAS (generally recognized as safe) status, using the same TTC approach as applied by JECFA [33, 34]. In the EU, because of the absence of a safe level of exposure, genotoxic compounds are not allowed to be intentionally added to foods. Compounds for which positive in vitro genotoxicity data exist, which is the case for α,β -unsaturated aldehydes, require follow up in vivo studies to exclude the concern about genotoxicity and carcinogenicity. With the implementation of the EU regulation for food flavouring agents (Regulation (EU) No. 872/2012) the use of most of α,β -unsaturated aldehydes and their related compounds have been suspended since the enforcement of the regulation in 2013.

This inconsistency in the safety evaluation by JECFA and FEMA on one hand and EFSA on the other highlights the urgent need for better safety assessment methods, to allow harmonized and ideally quantitative evaluation of the safety and/or risks connected to exposure to low levels of genotoxic compounds. This thesis presented the use of physiologically based in silico modelling as a powerful and useful tool to contribute to the safety evaluation of food-borne DNA reactive agents. Using PBK/D models detoxification and DNA adduct formation were simulated for a number of aldehydes at low exposure doses, at which levels an increase in DNA adducts above background levels cannot be easily detected in in vivo experimental studies. In order to examine whether the predicted increase in DNA adduct levels due to exposure to the α,β -unsaturated aldehydes in the diet is significant, reference values are needed. In Chapter 2, 3 and 4, the predicted adduct levels were compared with the natural background levels of structurally similar exocyclic 1, N^2 -propanodeoxyguanine adducts (Figure 6.3 B and C for the structures). The structurally similar exocyclic 1, N^2 -propanodeoxyguanine adducts are present in the liver as background in disease-free human livers because some α,β -unsaturated aldehydes such as 2-butenal (crotonaldehyde) and malondialdehyde are formed endogenously due to lipid peroxidation in vivo. The natural background level of exocyclic 1, N^2 -propanodeoxyguanine adducts has been determined to be 6.8-110 adducts/ 10^8 nt based on two studies where the DNA adduct levels of 2-butenal and malondialdehyde were examined in human livers [3, 4]. In Chapter 5, the formation of DNA adducts by cinnamaldehyde used as a food flavour agent was used for a comparison, because cinnamaldehyde is known not to be genotoxic or carcinogenic in vivo despite the fact that it induces formation of exocyclic 1, N^2 -propanodeoxyguanine adducts in vitro [35]. The structure of the DNA adducts formed by cinnamaldehyde is presented in Figure 6.3D.

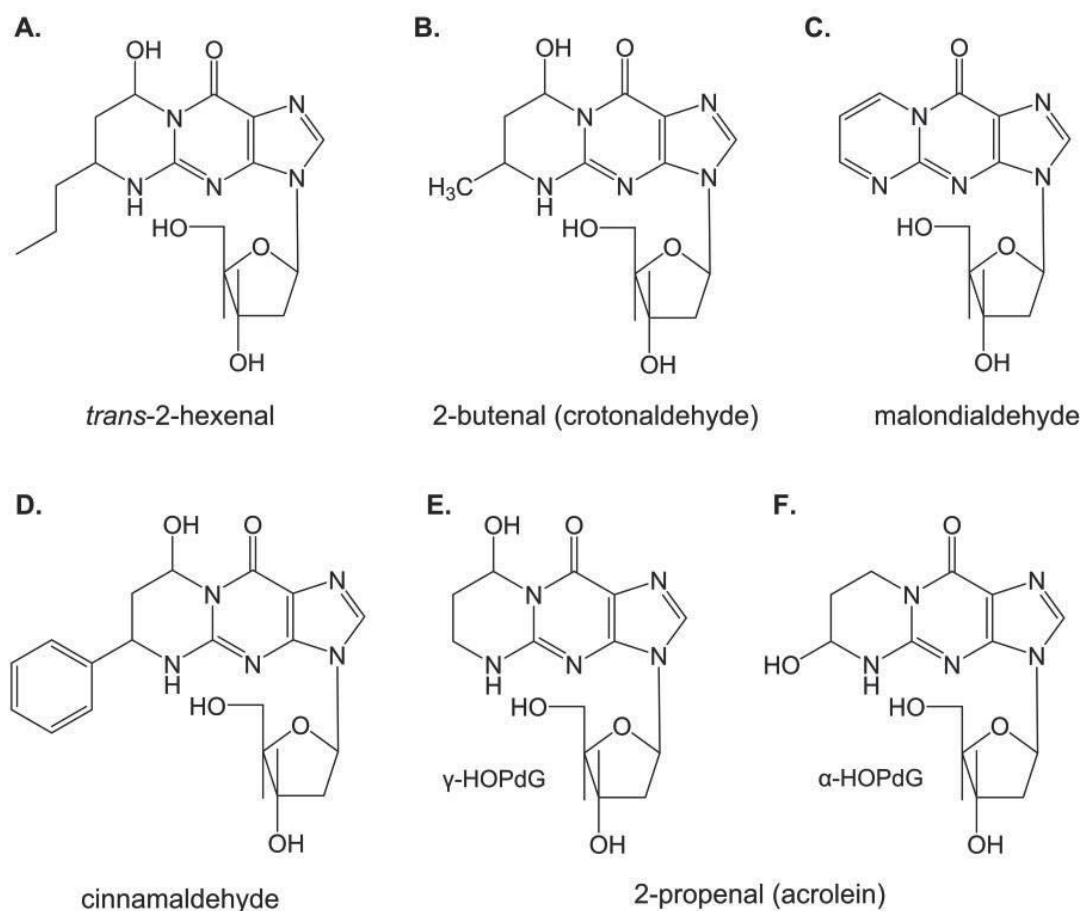


Figure 6.3 The structures of exocyclic 1, N^2 -propanodeoxyguanosine adducts formed by *trans*-2-hexenal (A), 2-butenal (crotonaldehyde) (B), malondialdehyde (C), cinnamaldehyde (D) or by 2-propenal (acrolein) (E and F).

The dose-dependent DNA adduct formation defined for the 18 aldehydes in this thesis provides a good starting point for read-across between the structurally related α,β -unsaturated aldehydes. The DNA adducts, namely exocyclic 1, N^2 -propanodeoxyguanine adducts formed by α,β -unsaturated aldehydes disrupt base pairing within duplex DNA, which may result in mutations [36]. It is important to be aware that the comparison of the DNA adduct levels is based on the assumption that each adduct has similar mutagenic and carcinogenic potency, while mutation potencies may not be the same for all the aldehydes. For example, γ -HOPdG, an exocyclic 1, N^2 -propanodeoxyguanine adduct of 2-propenal (acrolein) (Figure 6.3E) induced $\leq 1\%$ G to T and G to A base substitutions in HeLa and xeroderma pigmentosum complementation group A cells, whereas the α -HOPdG adduct, the regioisomeric guanine adduct of 2-propenal (Figure 6.3F) induced 10% base substitutions, primarily G to T transversions [36]. The aldehydes with longer chain length than 2-propenal are known to form γ -propanoguanine adducts [37] and therefore the high mutation potency as reported for the α -HOPdG adducts of 2-propenal is not expected. Nevertheless it is still recommended to determine the mutation frequency for each dietary as well

as endogenous aldehyde to allow for an even better safety assessment based on comparison of the DNA adduct levels induced by the α,β -unsaturated aldehydes and background DNA adduct levels.

The PBK/D model based predictions on dose-dependent DNA adduct formation elucidated that 2-propenal would be the most reactive aldehyde of the 18 aldehydes studied in DNA adduct formation (Chapter 4). If an in vivo study would still be performed despite the negligible levels of DNA adducts predicted to be formed for the 18 aldehydes at their EDIs, 2-propenal is recommended to be selected to represent the worst case in this group of acyclic α,β -unsaturated aldehydes. 2-Propenal could be seen as a compound of the highest concern also because of the increased mutation potency of the α -HOPdG adducts, which can be formed by 2-propenal but not by the other aldehydes as described in the previous paragraph. Considering the low LD₅₀ (26 mg/kg bw) and high volatility (269 Torr) of 2-propenal, administration of high doses of pure 2-propenal by gavage is not practical but the aldehyde needs to be microencapsulated and mixed in feed to achieve a stable long-term feeding without resulting in high mortality [22]. Further PBK/D studies are needed to examine to what extent 2-propenal also represents a worst case for other dietary α,β -unsaturated in other subgroups including for example 2- or 3- alkylated aldehydes, 2,4-dienals and cyclic aldehydes.

Future possibilities of PBK/D modelling for genotoxic agents in general

The ultimate goal of physiologically based in silico models developed for DNA reactive compounds is not limited to predicting DNA adduct formation but to predict further steps in the development of tumours. A tumour development is a multi-step process, which is often described to be divided into three phases: initiation, promotion, and the final stage progression. The first steps are reversible thus the formation of DNA adduct does not per se cause a tumour. A useful strategy to model chemical induced carcinogenicity would be to construct mathematical equations based on multistage carcinogenesis models reported by Luebeck et al.[38], as previously suggested by Punt et al. [39] and Paini [40]. Luebeck et al. described that a four-stage model that they could predict the epidemiological data on the age-specific incidence of colorectal cancers among the US population. The four-stage model consisted of two rare mutations in adenomatous polyposis coli (APC) genes, followed by high-frequency events in the conversion of a normal cell into an initiated cell that expands clonally to give rise to an adenomatous polyp, and subsequently by a transition of a preinitiated stem cell into an initiated cell capable of clonal expansion. To use this multi-stage model it is crucial to parameterize the frequency of the first two rare mutations for each chemical. The parameterisation could be achieved in vitro by exposing human cell lines to a chemical with or without bioactivation to quantify the mutation frequency in the APC genes including P53 and K-ras.

6.3 Conclusions

This thesis presented an alternative approach for the current methods relying on animal experiments for the safety evaluation of genotoxic compounds using α,β -unsaturated aldehydes as model compounds. Physiologically based in silico models were developed for 18 α,β -unsaturated aldehydes to define dose-dependent detoxification of these aldehydes and to obtain insights in DNA adduct formation at low doses relevant to human dietary exposure to these compounds. DNA adduct formation by the 18 aldehydes was negligible at their estimated levels of use as food flavourings compared to the natural background levels of structurally similar exocyclic 1, N^2 -propanodeoxyguanosine adducts present in disease free human liver. The same conclusion for the 18 aldehydes was obtained by comparing the DNA adduct levels with that of cinnamaldehyde that is known to test negative for genotoxic and carcinogenic in vivo even at high dose levels. Overall, the results indicated that the DNA adduct formation by the 18 α,β -unsaturated aldehydes as food flavourings are negligible and do not raise a safety concern at their levels of intake resulting from their use as food flavourings.

In addition, this thesis illustrated that physiologically based in silico models provide a very useful and powerful tool to facilitate a group evaluation and read-across for food-borne DNA reactive agents. The application of QSAR models to predict kinetic parameters to build PBK/D models strongly accelerated the development of the PBK/D models of the group of 18 compounds. PBK/D models furthermore enabled comparison of DNA adduct formation by the 18 aldehydes for which in vivo data are limited or even absent, with data on DNA adduct formation for a structurally related compound, cinnamaldehyde, which is known not to be genotoxic or carcinogenic in vivo. Altogether this thesis presented physiologically based in silico modelling as an approach to test relevance of positive in vitro genotoxicity results by DNA reactive compounds in vivo without using animal experiments.

REFERENCES

- [1] Feron, V. J., Til, H. P., de Vrijer, F., Woutersen, R. A., *et al.*, Aldehydes: occurrence, carcinogenic potential, mechanism of action and risk assessment. *Mutat Res* 1991, 259, 363-385.
- [2] Witz, G., Biological interactions of alpha,beta-unsaturated aldehydes. *Free Radic Biol Med* 1989, 7, 333-349.
- [3] Nath, R. G., Chung, F. L., Detection of exocyclic exocyclic 1,*N*²-propanodeoxyguanosine adducts as common DNA lesions in rodents and humans. *Proceedings of the National Academy of Sciences of the United States of America* 1994, 91, 7491-7495.
- [4] Chaudhary, A. K., Nokubo, M., Reddy, G. R., Yeola, S. N., *et al.*, Detection of endogenous malondialdehyde-deoxyguanosine adducts in human human liver. *Science* 1994, 265, 1580-1582.
- [5] NTP, NTP Technical Report on the Toxicology and Carcinogenesis Studies of *trans*-Cinnamaldehyde (Microencapsulated) (CAS NO. 14371-10-9) in F344/N Rats and B6C3F1 Mice (Feed Studies). http://ntp.niehs.nih.gov/ntp/htdocs/lt_rpts/tr514.pdf. 2004.
- [6] Yuan, J. H., Dieter, M. P., Bucher, J. R., Jameson, C. W., Toxicokinetics of cinnamaldehyde in F344 rats. *Food Chem Toxicol* 1992, 30, 997-1004.
- [7] Zhao, H., Xie, Y. H., Yang, Q., Cao, Y., *et al.*, Pharmacokinetic study of cinnamaldehyde in rats by GC-MS after oral and intravenous administration. *J Pharmaceut Biomed* 2014, 89, 150-157.
- [8] Kirman, C. R., Gargas, M. L., Deskin, R., Tonner-Navarro, L., Andersen, M. E., A physiologically based pharmacokinetic model for acrylamide and its metabolite, glycidamide, in the rat. *Journal of toxicology and environmental health. Part A* 2003, 66, 253-274.
- [9] Schuler, D., Eder, E., Detection of 1,*N*²-propanodeoxyguanosine adducts of 2-hexenal in organs of Fischer 344 rats by a ³²P-post-labeling technique. *Carcinogenesis* 1999, 20, 1345-1350.
- [10] Stout, M. D., Jeong, Y. C., Boysen, G., Li, Y., *et al.*, LC/MS/MS method for the quantitation of *trans*-2-hexenal-derived exocyclic 1,*N*²-propanodeoxyguanosine in DNA. *Chem Res Toxicol* 2006, 19, 563-570.
- [11] Budiawan, Eder, E., Detection of 1,*N*²-propanodeoxyguanosine adducts in DNA of Fischer 344 rats by an adapted ³²P-post-labeling technique after per os application of crotonaldehyde. *Carcinogenesis* 2000, 21, 1191-1196.
- [12] Stout, M. D., Bodes, E., Schoonhoven, R., Upton, P. B., *et al.*, Toxicity, DNA binding, and cell proliferation in male F344 rats following short-term gavage exposures to *trans*-2-hexenal. *Toxicol Pathol* 2008, 36, 232-246.
- [13] Parent, R. A., Caravello, H. E., Sharp, D. E., Metabolism and distribution of [2,3-¹⁴C]acrolein in Sprague-Dawley rats. *Journal of applied toxicology* : *JAT* 1996, 16, 449-457.
- [14] Frederick, C. B., Potter, D. W., Chang-Mateu, M. I., Andersen, M. E., A physiologically based pharmacokinetic and pharmacodynamic model to describe the oral dosing of rats with ethyl acrylate and its implications for risk assessment. *Toxicol Appl Pharmacol* 1992, 114, 246-260.
- [15] Yuan, J., Bucher, J. R., Goehl, T. J., Dieter, M. P., Jameson, C. W., Quantitation of cinnamaldehyde cinnamaldehyde and cinnamic acid in blood by HPLC. *Journal of analytical toxicology* 1992, 16, 359-362.
- [16] Choudhury, S., Pan, J., Amin, S., Chung, F. L., Roy, R., Repair kinetics of *trans*-4-hydroxynonenal-induced cyclic 1,*N*²-propanodeoxyguanine DNA adducts by human cell nuclear extracts. *Biochemistry* 2004, 43, 7514-7521.
- [17] Spencer, W. A., Singh, J., Orren, D. K., Formation and differential repair of covalent DNA adducts generated by treatment of human cells with (+/-)-anti-dibenzo[a,l]pyrene-11,12-diol-13,14-epoxide. *Chem Res Toxicol* 2009, 22, 81-89.
- [18] Episkopou, H., Kyrtopoulos, S. A., Sfikakis, P. P., Fousteri, M., *et al.*, Association between transcriptional activity, local chromatin structure, and the efficiencies of both subpathways of nucleotide excision repair of melphalan adducts. *Cancer Res* 2009, 69, 4424-4433.
- [19] NTP, Technical report on the comparative toxicity studies of allyl acetate, allyl alcohol, and acrolein. Administered by gavage to F344/N rats and B6C3F1 mice. http://ntp.niehs.nih.gov/ntp/htdocs/st_rpts/tox048.pdf. 2006.
- [20] NTP, NTP Technical Report on the Toxicology Toxicology and Carcinogenesis Studies of 2,4-Hexadienal in F344/N Rats and B6C3F1 Mice (Gavage Studies). http://ntp.niehs.nih.gov/ntp/htdocs/lt_rpts/tr509.pdf. 2003.
- [21] NTP, NTP Technical Report on the Toxicology Toxicology and Carcinogenesis Studies of Citral (Microencapsulated) (CAS No.5392-40-5) in F344 Rats and B6C3F1 Mice (Feed Studies). http://ntp.niehs.nih.gov/ntp/htdocs/lt_rpts/tr505.pdf. 2003.

- [22] Hebert, C. D., Yuan, J., Dieter, M. P., Comparison of the Toxicity of Cinnamaldehyde When Administered by Microencapsulation in Feed or by Corn-Oil Gavage. *Food and Chemical Toxicology* 1994, 32, 1107-1115.
- [23] JECFA, Evaluation of certain food additives and contaminants: Sixty-first report of the Joint FAO/WHO Expert Committee on Food Additives. http://whqlibdoc.who.int/trs/WHO_TRS_922.pdf. 2004.
- [24] EFSA, List of alpha, beta-Unsaturated Aldehydes and Ketones representative of FGE.19 substances for Genotoxicity Testing. Statement of the Panel on Food Contact Materials, Enzymes, Flavourings and Processing Aids(CEF). 2008.
- [25] OECD, Guidance Document on the Validation of (Quantitative) Structure-Activity Relationships [(Q)SAR] Models. 2007.
- [26] Fukui, K., Yonezawa, T., Nagata, C., Shingu, H., Molecular Orbital Theory of Orientation in Aromatic, Heteroaromatic, and Other Conjugated Molecules. *J Chem Phys* 1954, 22, 1433-1442.
- [27] LoPachin, R. M., Gavin, T., Molecular mechanisms of aldehyde toxicity: a chemical perspective. *Chem Res Toxicol* 2014, 27, 1081-1091. 1081-1091.
- [28] Schwobel, J. A. H., Wondrousch, D., Koleva, Y. K., Madden, J. C., *et al.*, Prediction of Michael-Type Acceptor Reactivity toward Glutathione. *Chem Res Toxicol* 2010, 23, 1576-1585.
- [29] Klyosov, A. A., Kinetics and specificity of human liver aldehyde dehydrogenases toward aliphatic, aromatic, and fused polycyclic aldehydes. *Biochemistry* 1996, 35, 4457-4467.
- [30] Danielson, U. H., Esterbauer, H., Mannervik, B., Structure-Activity-Relationships of 4-Hydroxyalkenals in the Conjugation Catalyzed by Mammalian Glutathione Transferases. *Biochemical Journal* 1987, 247, 707-713.
- [31] JECFA, Evaluation of Certain Food Additives: sixty-third report of the Joint FAO/WHO Expert Committee on Food Additives. http://whqlibdoc.who.int/trs/WHO_TRs_928.pdf. 2005.
- [32] JECFA, Evaluation of certain food additives and contaminants : fifty-fifth report of the Joint FAO/WHO expert committee on food additives. http://whqlibdoc.who.int/trs/WHO_TRS_901.pdf. 2001.
- [33] Adams, T. B., Gavin, C. L., Taylor, S. V., Waddell, W. J., *et al.*, The FEMA GRAS assessment of alpha,beta-unsaturated aldehydes and related substances used as flavor ingredients. *Food Chem Toxicol* 2008, 46, 2935-2967.
- [34] Adams, T. B., Cohen, S. M., Doull, J., Feron, V. J., *et al.*, The FEMA GRAS assessment of cinnamyl derivatives used as flavor ingredients. *Food Chem Toxicol* 2004, 42, 157-185.
- [35] Rezaei, M., Harris, T. M., Rizzo, C. J., Stereoselective synthesis of the 1,*N*²-deoxyguanosine adducts of cinnamaldehyde. A stereocontrolled route to deoxyguanosine adducts of α,β -unsaturated aldehydes. *Tetrahedron Lett* 2003, 44, 7513-7516.
- [36] Sanchez, A. M., Minko, I. G., Kurtz, A. J., Kanuri, M., *et al.*, Comparative evaluation of the bioreactivity and mutagenic spectra of acrolein-derived alpha-HOPdG and gamma-HOPdG gamma-HOPdG regioisomeric deoxyguanosine adducts. *Chem Res Toxicol* 2003, 16, 1019-1028.
- [37] Douki, T., Ames, B. N., An HPLC-EC assay for for 1,*N*²-propano adducts of 2'-deoxyguanosine with with 4-hydroxynonenal and other alpha,beta-unsaturated aldehydes. *Chem Res Toxicol* 1994, 7, 511-518.
- [38] Luebeck, E. G., Moolgavkar, S. H., Multistage carcinogenesis and the incidence of colorectal cancer. *Proceedings of the National Academy of Sciences of the United States of America* 2002, 99, 15095-15100.
- [39] Punt, A., Systems toxicology, Research Proposal for Veni Vernienwingsimpuls grant. 2011.
- [40] Paini, A., Generation of in vitro data to model dose dependent in vivo DNA binding of genotoxic carcinogens and its consequences : the case of estragole. *PhD thesis* 2012.
- [41] Brown, R. P., Delp, M. D., Lindstedt, S. L., Rhomberg, L. R., Beliles, R. P., Physiological parameter values for physiologically based pharmacokinetic models. *Toxicol Ind Health* 1997, 13, 407-484.
- [42] Poulakos, L., Kent, T. H., Gastric emptying and and small intestinal propulsion in fed and fasted rats. *Gastroenterology* 1973, 64, 962-967.

SUPPORTING INFORMATION**Supporting information 6.1.** Physiological and biochemical parameters used in the oral dosing model

Description	Value	Reference
Blood flow to tissue (fraction of the cardiac output, %)		
QFSc (forestomach)	0.3	[14]
QGSc (glandular stomach)	1.0	[14]
QDUOc (duodenum)	1.6	[14]
QSIc (small intestine)	11.8	[41]
Volume (fraction to the body weight, %)		
VFSc (forestomach)	1.6	[14]
VGSc (glandular stomach)	0.47	[14]
VDUOc (duodenum)	0.34	[14]
VSIc (small intestine)	1.2	[41]
Transportation rate of the gut contents down the gastric tract (/h)		
KTR1 (forestomach to glandular stomach)	0.7	[42]
KTR2 (glandular stomach to duodenum)	0.7	[42]
KTR3 (duodenum to small intestine)	7	[42]
Transfer rate from vehicle to the lumen contents (KGUT, /h) and from lumen contents to the gut wall (KAB, /h)		
Exposure dose of 50 mg/kg bw or lower		
KGUT1 (forestomach)	0.35	[14]
KGUT2 (glandular stomach)	9	[14]
KGUT3 (duodenum)	10	[14]
KGUT4 (small intestine)	10	[14]
KAB1 (forestomach)	0.35	[14]
KAB2 (glandular stomach)	9	[14]
KAB3 (duodenum)	10	[14]
KAB4 (small intestine)	10	[14]
Exposure dose higher than 50 mg/kg bw		
KGUT1 (forestomach)	0.20	[14]
KGUT2 (glandular stomach)	2.50	[14]
KGUT3 (duodenum)	5.00	[14]
KGUT4 (small intestine)	10	[14]
KAB1 (forestomach)	0.20	[14]
KAB2 (glandular stomach)	2.50	[14]
KAB3 (duodenum)	5.00	[14]
KAB4 (small intestine)	10	[14]

Supporting information 6.2. Equations for the oral dosing model made based on the study by Frederiek et al. [14]

(1) forestomach compartment

$$dAOFS/dt = -AOFS*(KGUT1+KTR1)$$

$$\text{Init AOFS} = \text{dose}$$

where

AOFS Amount aldehyde in vehicle oil in the forestomach (μmol)

$$dALFS/dt = AOFS*KGUT1 - ALFS*(KTR1+KAB1)$$

where

ALFS amount aldehyde in the lumen contents in the forestomach (μmol)

KGUT1 transfer rate of the aldehyde from vehicles to the lumen contents (/h)

KTR1 transportation rate of the gut contents from forestomach to glandular stomach (/h)

KAB1 transfer rate of the aldehyde from the lumen contents to the gut wall (/h)

$$dAFS/dt = ALFS*KAB1 - QFS*CVFS$$

$$CFS = AFS/VFS$$

$$CVFS = CFS/PRALD$$

where

AFS amount aldehyde in the forestomach (μmol)

QFS blood flow into the forestomach (L/h)

CVFS concentration of aldehyde in venous blood leaving the forestomach ($\mu\text{mol/L}$)

CFS concentration of aldehyde in the forestomach ($\mu\text{mol/L}$)

VFS volume of the forestomach (kg)

PRALD tissue/blood partition coefficient of aldehyde

(2) glandular stomach compartment

$$dAOGS/dt = AOFS*KTR1 - AOGS*(KGUT2+KTR2)$$

where

AOGS amount aldehyde in vehicle in the glandular stomach (μmol)

KGUT2 transfer rate of the aldehyde from vehicles to the lumen contents (/h)

KTR2 transportation rate of the gut contents from glandular stomach to duodenum (/h)

$$dALGS/dt = AOGS*KGUT2 + ALFS* KTR1 - ALGS*(KTR2+KAB2)$$

where

ALGS amount aldehyde in the lumen contents in the glandular stomach (μmol)

KAB2 transfer rate of the aldehyde from the lumen contents to the gut wall (/h)

$$dAGS/dt = ALGS*KAB2 - QGS*CVGS$$

$$CGS = AGS/VGS$$

$$CVGS = CGS/PRALD$$

where

AGS amount aldehyde in the glandular stomach (μmol)

QGS blood flow into the glandular stomach (L/h)

CVGS concentration of aldehyde in venous blood leaving the glandular stomach ($\mu\text{mol/L}$)

CGS concentration of aldehyde in the glandular stomach ($\mu\text{mol/L}$)

VGS volume of the glandular stomach (kg)

(3) Duodenum compartment

$$dAODUO/dt = AOGS*KTR2 - AODUO*(KGUT3+KTR3)$$

where

AODUO amount aldehyde in vehicle in the duodenum (μmol)

KGUT3 transfer rate of the aldehyde from vehicles to the lumen contents (/h)

KTR3 transportation rate of the gut contents from duodenum to small intestine (/h)

Chapter 6

$$dALDUO/dt = AODUO*KGUT3 + ALGS*KTR3 - ALDUO*(KTR3+KAB3)$$

where

ALDUO amount aldehyde in the lumen contents in the duodenum (μmol)
KAB3 transfer rate of the aldehyde from the lumen contents to the gut wall (/h)

$$dADUO/dt = ALDUO*KAB3 - QDUO*CVDUO$$

$$CDUO = ADUO/VDUO$$

$$CVDUO = CDUO/PRALD$$

where

ADUO amount of aldehyde in the duodenum (μmol)
QDUO blood flow into the duodenum (L/h)
CVDUO concentration of aldehyde in venous blood leaving the duodenum ($\mu\text{mol/L}$)
CDUO concentration of aldehyde in the duodenum ($\mu\text{mol/L}$)
VDUO volume of the duodenum (kg)

(4) small intestine compartment

$$dAOSI/dt = AODUO*KTR3 - AOSI*KGUT4$$

where

AOSI amount of aldehyde in vehicle in the small intestine (μmol)
KGUT4 transfer rate of the aldehyde from vehicles to the lumen contents (/h)

$$dALSI/dt = AOSI*KGUT4 + ALDUO*KTR3 - ALSI*KAB4$$

where

ALSI Amount aldehyde in the lumen contents in the small intestine (μmol)
KAB4 transfer rate of the aldehyde from the lumen contents to the gut wall (/h)



CHAPTER 7

Summary

Various α,β -unsaturated aldehydes are present in fruits, vegetables, spices, or processed products containing these items as natural constituents [1] or as added food flavouring agents. Because of the α,β -unsaturated aldehyde moiety the β carbon in the molecule becomes electron deficient and the aldehydes react with electron rich molecules including DNA via Michael addition [2]. The formation of DNA adducts raises a concern for genotoxicity, although formation of DNA adducts may not be significant at low doses relevant for dietary exposure in vivo because of adequate detoxification. The thesis therefore aimed at determining dose-dependent detoxification and DNA adduct formation of food-borne α,β -unsaturated aldehydes by using a physiologically based in silico modelling approach in order to contribute to the safety assessment of these aldehydes used as food flavourings.

Chapter 1 of this thesis introduced occurrence, metabolism, genotoxicity and carcinogenicity, and regulatory status of dietary α,β -unsaturated aldehydes as the basic background information of the compounds. Also, the uncertainty in the evaluation of genotoxicity at low exposure doses, a challenge for the safety evaluation of these flavouring compounds, the use of PBK/D (physiologically based kinetic/dynamic) models for DNA reactive compounds, and the aim and overall objectives of the thesis were described.

In **Chapter 2 and 3**, rat and human PBK/D models were developed for the model compound *trans*-2-hexenal. The kinetic parameters for detoxification were collected by performing in vitro incubations using relevant tissue fractions. The PBK/D models revealed that at the estimated daily intake (EDI) i.e. 0.04 mg/kg bw, *trans*-2-hexenal is detoxified predominantly via GST-mediated conjugation with GSH in rats, while the reduction to *trans*-2-hexen-1-ol was the major pathway in humans. Interspecies differences in the maximum DNA adduct levels in the liver were predicted to be limited. At the EDI, DNA adduct formation was 0.01 and 0.008 adducts/ 10^8 nt in rat and human, respectively. These levels were 3 orders of magnitude lower than the natural background levels of structurally similar exocyclic 1, N^2 -propanodeoxyguanosine adducts present in disease free human liver (i.e. 6.8–110 adducts/ 10^8 nt) [3, 4]. In Chapter 3, the human PBK/D model was subsequently used to examine the impact of interindividual variation in *trans*-2-hexenal detoxification on DNA adduct formation in the human population. The parameters for detoxification were measured for 11 individuals to define the variation in the parameters and subsequently the distribution of DNA adduct formation in the population was simulated by Monte Carlo simulations. At a high intake level of 0.178 mg/kg bw (95th percentile of the dietary intake), DNA adduct formation was predicted to be 0.18 adducts/ 10^8 nt for the 99th percentile of the population. This value was well below the natural background levels of structurally similar exocyclic 1, N^2 -propanodeoxyguanosine adducts (6.8–110 adducts/ 10^8 nt) [3, 4]. Based on these results, it was concluded that *trans*-2-hexenal in the diet may not significantly increase the DNA adduct levels in the liver in rats, or in humans including the most sensitive persons.

The objective of **Chapter 4** was to extend the rat PBK/D model for *trans*-2-hexenal to

other α,β -unsaturated aldehydes that may be used as food flavourings and to facilitate a group evaluation. Considering the large number of the aldehydes of interest, a QSAR (quantitative structure-activity relationship) approach was applied to collect chemical specific detoxification parameters. Eighteen acyclic α,β -unsaturated aldehyde flavouring agents without 2- or 3-alkylation, and with no more than one conjugated double bond were selected as the aldehydes of interest. Six of the 18 aldehydes were selected as the training set to define QSAR models to estimate the kinetic parameters for detoxification of the other 12 aldehydes in the test set. Among the 18 aldehydes, 2-propenal (acrolein) was predicted to induce the highest number of DNA adducts in rat liver due to the lowest catalytic efficiency for oxidation and conjugation with GSH. DNA adduct formation by the 18 aldehydes was predicted to be between 10^{-10} – 10^{-2} adducts/ 10^8 nt at their respective EDI as food flavourings. These levels are at least two orders of magnitude lower than the natural background levels of structurally similar DNA adducts (i.e. 6.8–110 adducts/ 10^8 nt). Based on these outcomes it was concluded that the DNA adduct formation by all 18 aldehydes when used as flavourings is negligible.

Unlike many α,β -unsaturated aldehydes for which in vivo data on genotoxicity and carcinogenicity are absent, cinnamaldehyde has been shown not to be genotoxic and to test negative in a long term carcinogenicity study in vivo [5]. The aim of **Chapter 5** was to examine DNA adduct formation by cinnamaldehyde and to compare these DNA adduct levels to those predicted for the 18 aldehydes in Chapter 4. The cinnamaldehyde PBK/D models revealed that in rats, cinnamaldehyde was shown to induce higher DNA adducts per exposure dose than 6 out of the 18 food borne acyclic α,β -unsaturated aldehydes, indicating these 6 aldehydes may also test negative for genotoxicity and carcinogenicity at high dose levels. At the highest cinnamaldehyde dose that tested negative for genotoxicity and carcinogenicity in vivo, the model predicted a formation of 79 DNA adducts/ 10^8 nt in rat. This value is at least three orders of magnitude higher than the predicted DNA adduct formation by all 18 other food-borne aldehydes at their respective EDI. These results corroborate the conclusion obtained in Chapter 4 that for all 18 α,β -unsaturated aldehydes DNA adduct formation at doses relevant for human dietary exposure does not raise a safety concern.

Chapter 6 of the thesis presented general discussions and future perspectives on different topics raised based on the results obtained in this thesis. For instance, a consideration was given on possible aldehyde toxicity in the GI tract where concentrations of aldehydes may become higher than in the liver. An oral dosing model that has been developed to describe kinetics of an α,β -unsaturated ester ethyl acrylate in the GI tract [6] was added to the rat *trans*-2-hexenal PBK/D models developed in this thesis. The results obtained from this tentative model indicated that *trans*-2-hexenal concentrations may be higher especially in the glandular stomach than in the liver, but DNA adduct formation in the GI organs would still not be of concern assuming the background levels of structurally similar DNA adducts in these organs to be comparable to the liver. Chapter 6 further presented general discussions and future perspectives on the performance

of the PBK/D models developed in this thesis and how it could be improved, on the application of the integrated QSAR-PBK/D modelling to the other food-borne α,β -unsaturated aldehydes and important molecular determinants to be considered for the QSAR development, on implication of the results obtained in this thesis for the safety evaluation of the use of α,β -unsaturated aldehydes as added food flavourings, and on PBK/D modelling for genotoxic agents in general.

In conclusion, this thesis presented an alternative approach for the current methods relying on animal experiments for the safety evaluation of genotoxic compounds, focussing on α,β -unsaturated aldehydes. Physiologically based in silico models were developed for 18 α,β -unsaturated aldehydes, and the model outcomes indicated that the DNA adduct formation by the 18 α,β -unsaturated aldehydes as food flavourings is negligible and does not raise a safety concern at their levels of intake resulting from their use as food flavourings. Higher levels of exposure is not likely to occur due to the self-limiting use of flavouring agents, with higher exposure leading to off-flavours. In addition, this thesis illustrated that physiologically based in silico models provide a very useful and powerful tool to facilitate a group evaluation and read-across for food-borne DNA reactive agents. The application of QSAR models strongly accelerated the development of the PBK/D models of the group of 18 compounds. PBK/D models developed for the group of compounds supported read-across from an aldehyde which is known not to be genotoxic or carcinogenic in vivo to other aldehydes, by allowing comparison of dose-dependent DNA adduct formations. Altogether this thesis presented physiologically based in silico modelling as an approach to test relevance of positive in vitro genotoxicity results by DNA reactive compounds in vivo without using animal experiments.

REFERENCES

- [1] Feron, V. J., Til, H. P., de Vrijer, F., Woutersen, R. A., *et al.*, Aldehydes: occurrence, carcinogenic potential, mechanism of action and risk assessment. *Mutat Res* 1991, 259, 363-385.
- [2] Witz, G., Biological interactions of alpha,beta-unsaturated aldehydes. *Free Radic Biol Med* 1989, 7, 333-349.
- [3] Nath, R. G., Chung, F. L., Detection of exocyclic 1,*N*²-propanodeoxyguanosine adducts as common DNA lesions in rodents and humans. *Proceedings of the National Academy of Sciences of the United States of America* 1994, 91, 7491-7495.
- [4] Chaudhary, A. K., Nokubo, M., Reddy, G. R., Yeola, S. N., *et al.*, Detection of endogenous malondialdehyde-deoxyguanosine adducts in human liver. *Science* 1994, 265, 1580-1582.
- [5] NTP, NTP Technical Report on the Toxicology and Carcinogenesis Studies of *trans*-Cinnamaldehyde (Microencapsulated) (CAS NO. 14371-10-9) in F344/N Rats and B6C3F1 Mice (Feed Studeis). http://ntp.niehs.nih.gov/ntp/htdocs/lt_rpts/tr514.pdf. 2004.
- [6] Frederick, C. B., Potter, D. W., Chang-Mateu, M. I., Andersen, M. E., A physiologically based pharmacokinetic and pharmacodynamic model to describe the oral dosing of rats with ethyl acrylate and its implications for risk assessment. *Toxicol Appl Pharmacol* 1992, 114, 246-260.



Appendices

List of Abbreviations

ADH	alcohol dehydrogenase
ALDH	aldehyde dehydrogenase
AR	aldose reductase
bw	body weight
CE	catalytic efficiency
DAD	diode array detection
DMSO	dimethyl sulfoxide
EDI	estimated daily intake
EFSA	European Food Safety Authority
FEMA	Flavor and Extract Manufacturers Association
GI	gastrointestinal
GSH	reduced glutathione
GST	glutathione S-transferase
Hex-GSH	<i>trans</i> -2-hexenal GSH conjugates
Hex-PdG	<i>trans</i> -2-hexenal exocyclic 1, <i>N</i> ² -propanodeoxyguanine adducts
HOMO	highest occupied molecular orbit
JECFA	The Joint FAO/WHO Committee on Food Additives
LC/MS/MS	liquid chromatography tandem mass spectrometry
LUMO	lowest unoccupied molecular orbit
MR	molecular refraction
NAD ⁺	oxidized β-nicotinamide adenine dinucleotide phosphate
NADPH	reduced β-nicotinamide adenine dinucleotide phosphate
NOAEL	no observed adverse effect level
NOEL	no observed effect level
nt	nucleotides
PBK/D	physiologically based kinetic/dynamic
QSAR	quantitative structure-activity relationship
SC	sensitivity coefficient
TFA	trifluoroacetic acid
UPLC	ultraperformance liquid chromatogram
2'-dG	2'-deoxyguanosine

Samenvatting

Verschillende α,β -onverzadigde aldehydes zijn van nature aanwezig in fruit, groenten, kruiden of als toegevoegde smaakstoffen in bewerkte producten. α,β -Onverzadigde aldehydes kunnen door hun structuur reageren met elektronenrijke moleculen, zoals eiwitten en DNA, volgens een Michael-additie. Door deze reactiviteit is er zorg dat deze stoffen in vivo genotoxisch zijn, ook al is de vorming van DNA adducten mogelijk minimaal bij lage doses via de voeding door voldoende detoxificatie. Om meer inzicht te krijgen in de relevantie van DNA adductvorming bij lage doseringen en om bij te dragen aan de risico-evaluatie van deze stoffen in de voeding, richtte dit proefschrift zich op het onderzoeken van dosis-afhankelijke detoxificatie en DNA adductvorming van α,β -onverzadigde aldehydes met behulp van fysiologisch gebaseerde in silico modellen.

Hoofdstuk 1 van dit proefschrift introduceerde het voorkomen van α,β -onverzadigde aldehydes in de voeding, het metabolisme, de genotoxiciteit en carcinogeniciteit en de stand van zaken met betrekking tot regelgeving als basis achtergrondinformatie van de stoffen. Ook werden onzekerheden in de evaluatie van genotoxiciteit bij lage doseringen, de uitdagingen in de veiligheidsevaluatie van deze smaakstoffen, het gebruik van PBK/D (fysiologische gebaseerde kinetische/dynamische) modellen voor DNA-reactieve stoffen en het globale doel van het proefschrift beschreven.

In **Hoofdstuk 2 en 3** werden PBK/D modellen voor de rat en de mens ontwikkeld voor de modelstof *trans*-2-hexenal. De kinetische parameters voor detoxificatie werden verzameld door in vitro incubaties uit te voeren met weefsselfracties die betrokken zijn bij het metabolisme. De PBK/D modellen lieten zien dat bij een geschatte dagelijkse inname (i.e. EDI) van 0,04 mg/kg lichaamsgewicht, GST-gemedieerde conjugatie met glutathion (GSH) de belangrijkste metabole route was in ratten, terwijl reductie naar *trans*-2-hexen-1-ol de voornaamste route was in de mens. Ondanks deze verschillen in metabolisme waren de onderlinge verschillen tussen ratten en mensen wat betreft de maximum DNA adductniveaus in de lever beperkt. DNA adductvorming was 0,01 adducten/ 10^8 nt in de rat en 0,008 adducten/ 10^8 nt in de mens bij de EDI. Deze niveaus waren 3 ordes van grootte lager dan de natuurlijk achtergrondniveaus van structureel gelijke exocyclische 1, N^2 -propanodeoxyguanosine adducten die aanwezig zijn in ziektevrije humane levers (i.e. 6,8-110 adducten/ 10^8 nt). In hoofdstuk 3 is het humane PBK/D model achtereenvolgens ook gebruikt om de invloed te onderzoeken van interindividuele variatie in *trans*-2-hexenal detoxificatie op DNA adductvorming in de menselijke populatie. De parameters voor detoxificatie van 11 individuen werden gemeten om de variatie in de parameters te bepalen. Vervolgens werd de distributie van DNA adductvorming in de populatie nagebootst door Monte Carlo simulaties. Bij een hoog innameniveau van 0,178 mg/kg lichaamsgewicht (95e percentiel van de dieetinname) zou de DNA adductvorming 0,18 adducten/ 10^8 nt zijn voor het 99e percentiel van de populatie. Deze waarde ligt ver beneden de natuurlijk achtergrondniveaus van structurele

gelijke exocyclische 1,*N*²-propanodeoxyguanosine adducten (6,8-110 adducten/10⁸ nt). Gebaseerd op deze resultaten werd geconcludeerd dat *trans*-2-hexenal in voeding DNA adductniveaus niet aanzienlijk verhoogt in de lever van de rat of de mens, inclusief de meest gevoelige personen.

Het doel van **Hoofdstuk 4** was het PBK/D model voor *trans*-2-hexenal in de rat uit te breiden naar andere α,β -onverzadigde aldehydes die gebruikt worden als smaakstoffen in voeding. Om PBK/D modellen te kunnen maken voor een grote groep stoffen is gebruik gemaakt van zogenaamde QSARs (kwantitatieve structuur-activiteitsrelaties) om de parameters voor detoxificatie te verzamelen. Achttien acyclische α,β -onverzadigde aldehyde smaakstoffen zonder 2- of 3-alkylatie en met niet meer dan één samengestelde dubbel-bond werden geselecteerd als de meest relevante aldehydes. Zes van de 18 aldehydes werden geselecteerd als de proefset (training set) om QSAR modellen te definiëren die de kinetische parameters voor detoxificatie van de andere 12 aldehydes in de proefset (test set) schatten. Van de 18 aldehydes zou 2-propenal (arcolein) het hoogste aantal DNA adducten in de rattenlever induceren. Dit werd veroorzaakt door de laagste catalytische efficiëncy voor oxidatie en GSH conjugatie. DNA adductvorming door de 18 aldehydes was tussen de 10⁻¹⁰ en 10⁻² adducten/10⁸ nt bij de respectievelijke EDI als smaakstoffen. Deze niveaus zijn ten minste twee ordes van grootte lager dan de natuurlijke achtergrondniveaus van structureel gelijke DNA adducten (i.e. 6,8-110 adducten/10⁸ nt). Op basis van deze uitkomsten werd geconcludeerd dat de DNA adductvorming door alle 18 aldehydes, bij gebruik als smaakstoffen, te verwaarlozen is.

In tegenstelling tot de meeste α,β -onverzadigde aldehydes waarvoor in vivo genotoxiciteits- en carcinogeniciteitsdata ontbreken, zijn deze data wel aanwezig voor cinnamaldehyde. Deze stof blijkt niet genotoxisch te zijn en is negatief getest in een langlopende carcinogeniciteitsstudie. Het doel van **Hoofdstuk 5** was de DNA adductvorming door cinnamaldehyde te onderzoeken en de verkregen DNA adductniveaus te vergelijken met de niveaus die voorspeld werden voor de 18 aldehydes in hoofdstuk 4. Uit deze vergelijking kwam naar voren dat cinnamaldehyde in ratten meer DNA adducten induceerde per blootstellingsdosis dan 6 van de 18 acyclische α,β -onverzadigde aldehydes, wat indiceert dat deze 6 aldehydes waarschijnlijk eveneens negatief zullen zijn voor genotoxiciteit en carcinogeniciteit bij hoge doseringen. Bij de hoogste cinnamaldehydedosis die negatief was voor genotoxiciteit en carcinogeniciteit in vivo, voorspelde het model een vorming van 29 DNA adducten/10⁸ nt in de rat. Deze waarde is minstens drie ordes van grootte hoger dan de voorspelde DNA adductvorming door alle 18 andere voedselgedragen aldehydes bij hun respectievelijke EDI. Deze resultaten bevestigen de conclusie die in hoofdstuk 4 is verkregen dat voor alle 18 α,β -onverzadigde aldehydes DNA adductvorming, bij de voor menselijk voeding relevante doseringen, geen reden tot zorg geven.

Hoofdstuk 6 van dit proefschrift presenteerde de algemene discussies en toekomstperspectieven over verschillende behandelde thema's gebaseerd op de in dit proefschrift verkregen resultaten. Zo is bijvoorbeeld een afweging gemaakt over mogelijke aldehyde toxiciteit

in het maag-darmstelsel waar concentraties van aldehydes hoger kunnen worden dan in de lever. Een oraal doseringsmodel dat is ontwikkeld om de kinetiek te beschrijven van een α,β -onverzadigde ester ethyl acrylaat in het maag-darmstelsel werd toegevoegd aan het *trans*-2-hexenal PBK/D model in de rat dat in dit proefschrift is ontwikkeld. De verkregen resultaten uit dit proefmodel toonden aan dat *trans*-2-hexenal concentraties vooral in de glandulaire maag mogelijk hoger zijn dan in de lever, maar dat DNA adductvorming in de gastro-intestinale organen nog steeds geen reden tot zorg zouden zijn, er van uitgaand dat de achtergrondniveaus van structureel gelijke endogene DNA adducten in deze organen vergelijkbaar zijn met de lever. Hoofdstuk 6 biedt verder algemene discussies en toekomstperspectieven ten aanzien van het resultaat van de PBK/D modellen die in dit proefschrift zijn ontwikkeld en hoe dat resultaat nog verbeterd zou kunnen worden, over de toepassing van de geïntegreerde QSAR-PBK/D modellering op de andere α,β -onverzadigde aldehydes die gebruikt worden in de voeding en belangrijke moleculaire determinanten die werden overwogen voor QSAR ontwikkeling, over de implicatie van de verkregen resultaten in dit proefschrift voor de veiligheidsevaluatie van α,β -onverzadigde aldehydes die als smaakstoffen aan voedsel worden toegevoegde, en over het gebruik van PBK/D modellering voor genotoxische stoffen in het algemeen.

Concluderend heeft dit proefschrift een alternatieve benadering voor de huidige methodes voor veiligheidsevaluatie van genotoxische stoffen gepresenteerd, die niet steunt op dierproeven. Voor 18 α,β -onverzadigde aldehydes zijn PBK/D modellen ontwikkeld en de modeluitkomsten toonden aan dat de DNA adductvorming door de 18 α,β -onverzadigde aldehydes te verwaarlozen is en geen reden tot zorg zijn voor de veiligheid bij innameniveaus kenmerkend voor gebruik als voedselsmaakstoffen. Hogere blootstellingsniveaus liggen niet voor de hand gezien het zelfbeperkend gebruik van smaakstoffen, waarbij hogere blootstelling leidt tot een onaangename smaak. Bovendien illustreerde dit proefschrift dat PBK/D modellen voorzien in een zeer nuttig en krachtig instrument om een groepevaluatie te faciliteren and read-across voor DNA- reactieve stoffen uit te voeren. De toepassing van QSAR modellen versnelde de ontwikkeling van de PBK/D modellen voor de groep van 18 stoffen. De PBK/D modellen ondersteunden read-across van een aldehyde waarvan bekend is dat deze in vivo niet genotoxisch of carcinogeen is naar de andere aldehydes, door vergelijking van dosisafhankelijke DNA adductvorming. Alles bijeen genomen presenteerde dit proefschrift PBK/D modellering als een benadering om de in vivo relevantie van positieve in vitro genotoxiciteitsresultaten bij DNA-reactieve stoffen te onderzoeken zonder dierproeven te gebruiken.

Acknowledgments

I would like to express my gratitude to people who supported me to accomplish this achievement.

First of all, my gratitude goes to my co-promoter and supervisor Ans. Your guidance, critical comments and enthusiasm for science encouraged me to carry on further. I also appreciate your friendliness. For a short discussion I could just drop by to your office, and you were always there for me although you were busy with tons of different tasks. This friendliness of you did not change since when I was your MSc thesis student, and throughout your supervision for my PhD project even during your maternity leave. Your support was not only about scientific topics but also personal things. I really appreciate the trust that you had on me, and your courage to take me from Japan as the first PhD in your career!

My gratitude also goes to my promoter Ivonne. Your constructive comments and ability to capture critical problems in no time often saved me from heading toward nowhere. You are incredibly efficient and at the same time a dedicated hard-working person. No matter where you were, you always immediately replied to my emails. This was very much appreciated especially during the last stretch of the PhD project. I am also grateful that you manage such a lively atmosphere at the Division of Toxicology with such a wonderful colleagues around.

I would like to thank all my colleagues in the Division of Toxicology, where I have spent wonderful four years as a PhD. My buddy Bert, thanks a lot for your dedicated work, as well as “gezellige” conversations sharing lots of personal interest. I would like to express my appreciation to Irene, Gré and Lidy for helping me out for administrative things that I had no clues what to do otherwise. Thank you Laura, Hans, Sebas, Marélie, Jochem, Nico, Ans Soffers, Letty and Tinka for your technical input and great talks with so many jokes that we’ve had together. My PhD colleagues (Wasma, Myrto, Hequn, Samantha, Barae, Rung, Erryana, Rozaini, Jonathan, Nacho, Myrthe, Jaime, Henrique, Karsten, Arif, Sophie, Justine, Abdul, Amer, Si, Agata, Marcia, Sunday, Alicia, Suzanne, Nynke, Linda, Merel, Marije, Sourav, Alá, Elise, Niek), and David, the other Laura and Judith! I had so much fun with you guys chatting during coffee breaks, having lunch or drinks. I could just forget time and chat with you forever....Thank you so much for the unforgettable memories that I could make with you for the last four years. I will miss you a lot. Thank you Rung and Myrthe for being there as my paranymphs (or clowns). I would also like to thank all MSc students for filling the department with laughter. Quan, Douwe, Ye, Yennie, thanks a lot for your interest and contributions to my project.

I also would like to thank my dear friends who supported me. Without you my life would be tasteless without joy. Wasma and Lisa, thanks a lot for your continuing friendship. For the last nine years you have become the great assets of my life. Agata, what a fun we can have together! We actually do not have so much in common but somehow we always end up chatting for hours. My Dutch course friends Anna, Lina, and Agnes, our Dutch may not have improved as much as we had hoped for but still our conversations in English brightened my life up. My friends from

MSc study, especially Milkha, Dilek, Ana, Saulo, Ferdie, Phabbie and Jenny. Without you my life in the Netherlands would have been so boring that I did not even consider staying here this long. Thanks a lot for helping starting my life in Wageningen and your continuing friendship. My Japanese friends that I met in the Netherlands, Yuki-san, Etsuko-san, Makoto, Rumiko-san and Shimojo-san, Keina-san and Iida-san, Seiko-san and Tomita-san, Aki-san, Hiroe-san and Noriko-san. With you my life in the Netherlands feels a lot easier with jokes that can be shared only among Japanese, and let's not forget great foods that we enjoy together. It was especially important for me to share the feeling when the devastating earthquake happened in Japan in 2011. Thank you for your presence in the Netherlands. I would like to thank all my friends from Japan. Sachiko, not only you but your family always makes me feel warm and happy. Riko-chan, Hatto, Kawaguchi, Wakana-chan, Delawary-chan, my friends from the University of Tokyo, and my ex-colleagues at the Ministry of Agriculture, Forestry and Fisheries Japan, I would like to thank for your continuing friendship via emailing, skyping, and by having short but intensive chat during my holidays in Japan.

Most importantly, I would like to thank my family in Japan and in the Netherlands. Otou-san and Okaa-san, you have been having a difficult time for the last few years. I appreciate that you still wish me the best and happiness in the Netherlands. I truly owe this achievement to your patience. Onii-chan and Megumi-san, thank you so much for being there for our parents. Mijn lieve schoonfamilie in Nederland, vooral Bert, Irma, Babs, Borre en Fir. Bedankt voor een grote liefde en steun. Ik ben heel blij dat ik familie van jullie ben geworden. Last but not least, mijn lieve schat Tjibbe! Jij hebt mij enorm gesteund de laatste jaren. We hebben samen al veel dingen meegemaakt, soms iets ontzettend moois en soms iets minder leuks. Ik kan altijd voelen hoe groot jouw liefde voor mij is en ik kan je er nooit genoeg voor bedanken. Ik vertrouw je, houd van je, en ik kijk uit naar onze gelukkige toekomst samen.

May 2015
Reiko Kiwamoto

Carriculum Vitae

Reiko Kiwamoto was born on 16 March 1979 in Orange County in the U.S. She grew up Tsukuba-city, Japan until she finished her secondary education. She did her BSc in agriculture (biological production science course) at the University of Tokyo (Tokyo, Japan) and the first MSc in Department of Biotechnology at the Graduate School of Agricultural and Life Sciences, the University of Tokyo (Tokyo, Japan). During this MSc study she successfully developed a new method to isolate and culture VNC (viable but non-culturable) bacteria from sea water as a part of her MSc thesis at the Laboratory of Molecular and Cellular Breeding.



After the first MSc, she worked at the Ministry of Agriculture, Forestry and Fisheries of the Japanese government (Tokyo, Japan) as a technical official for 7 years. She worked mostly at the Food Safety and Consumers Affairs Bureau of the Ministry and was involved in risk communication between the government and consumers, and establishment and implementation of the food education law. She was also involved in making the Japan's international policies related to food safety and animal and plant health dealt in WTO (World Trade Organisation), Codex and different bilateral schemes. While working for the Ministry she completed her MSc in Food Safety at Wageningen University (Wageningen, The Netherlands with the scholarship offered by the Japanese government. For this MSc she performed her thesis at Division of Toxicology on the topic of detoxification of estragole in HepG2 cells, human hepatocarcinoma cell line. She subsequently finished her internship in Dutch National Institute for Public Health and Environment (RIVM) on the topic of risk-benefit comparison of isoflavones on human health.

From February 2011, she started her PhD project presented in this thesis, which was funded by the Division of Toxicology, Wageningen University. Apart from the project, she was a co-organizer of the international PhD excursion to the UK of Division of Toxicology that took place in 2013. She was also a member of the research/equipment committee of the Division. During the four-year she followed a number of postgraduate courses in toxicology required for registration as a European Toxicologist.

List of Publications

Kiwamoto R., Rietjens I.M.C.M., Punt A.

A physiologically based in silico model for *trans*-2-hexenal detoxification and DNA adduct formation in rat. *Chem. Res. Toxicol.* **2012**, 25(12):2630-41.

Kiwamoto R., Spenkeliink A., Rietjens I.M.C.M., Punt A.

A physiologically based in silico model for *trans*-2-hexenal detoxification and DNA adduct formation in human including interindividual variation indicates efficient detoxification and a negligible genotoxicity risk. *Arch. Toxicol.* **2013**, 87(9):1725-37.

Kiwamoto R., Spenkeliink A., Rietjens I.M.C.M., Punt A.

An integrated QSAR-PBK/D modelling approach for predicting detoxification and DNA adduct formation of 18 acyclic food-borne α,β -unsaturated aldehydes. *Toxicol. Appl. Pharmacol.* **2015**, 282(1):108-17.

Al-Subeihi A.A., Alhusainy W., Kiwamoto R., Spenkeliink B., van Bladeren P.J., Rietjens I.M.C.M., Punt A.

Evaluation of the interindividual human variation in bioactivation of methyleugenol using physiologically based kinetic modeling and Monte Carlo simulations. *Toxicol. Appl. Pharmacol.*

In press

Kiwamoto R., D. Ploeg, Rietjens I.M.C.M., Punt A.

Dose-dependent DNA adduct formation by cinnamaldehyde and other food-borne α,β -unsaturated aldehydes predicted by physiologically based in silico modelling. **Submitted**

Overview of Completed Training Activities

Discipline specific activities

Ecotoxicology, Wageningen University (2011)
General toxicology, Wageningen University (2011)
Laboratory animal science, PET (2011)
Risk assessment, PET (2012)
Immunotoxicology, PET (2012)
Organ toxicology, PET (2012)
Mutagenesis and carcinogenesis, PET (2012)
Pathobiology, PET (2013)
Molecular toxicology, PET (2013)
Reproductive toxicology, PET (2014)

Meetings

First Joint German-Dutch Meeting of the Societies of Toxicology, Dusseldorf, Germany (2012)
(poster presentation)
Dutch Society of Toxicology (NVT) annual meeting, Zeist, The Netherlands (2013)
(poster presentation)
18th international conference on In Vitro Toxicology, Egmond aan Zee, The Netherlands (2014)
(oral presentation)

General courses

Scientific publishing, WGS (2011)
VLAG PhD week, VLAG (2011)
Scientific writing, WGS (2012)
Philosophy and Ethics of Food Science and Technology, WGS (2014)

Optional activities

Preparing PhD research proposal (2011)
Participation in the PhD excursions to Switzerland and Italy, Division of Toxicology Wageningen University (2011)
Organisation of and participation in the PhD excursion to UK, Division of Toxicology Wageningen University (2013)
Attending scientific presentations, Division of Toxicology Wageningen University (2011-2015)

The research described in this thesis was financially supported by Division of Toxicology, Wageningen University.

Financial support from Wageningen University for printing this thesis is gratefully acknowledged.

Layout: Reiko Kiwamoto and Ferdinand van Nispen, Citroenvlinder-dtp.nl, Bilthoven, The Netherlands

Printing: GVO drukkers en vormgevers B.V./Ponsen & Looijen, Ede, The Netherlands

Cover design: Toni and Reiko

Reiko Kiwamoto, 2015

